

Final Report

Design of a Cost-Effective
Stratospheric Aerosol Injection
System

Group 22



Final Report

Design of a Cost-Effective Stratospheric Aerosol Injection System

by

Group 22

to obtain the degree of Bachelor of Science
at the Delft University of Technology,

Student number:	Atiqah AHMAD TARMIZI	4531671
	Menno BOOGAARD	4548558
	Nout VAN DEN BOS	4551206
	Pere DURAN DUKOR	4566580
	Thomas HUNTER	4567250
	Nikki KAMPHUIS	4572637
	Sam LAM	4554507
	Jingyi LU	4532554
	Rick VAN TATENHOVE	4534395
	Thomas R. VERDUYN	4552695

Project duration: April 23, 2019 – July 4, 2019

Thesis committee:	Dr. S. J. Hulshoff	Principal Tutor
	Dr. ing. S. G. P. Castro	Tutor
	Ir. J. Steiner	Tutor

Contents

List of Figures	v
List of Tables	vi
Nomenclature	vii
1 Executive Overview	2
1.1 Problem Context and Solution Direction	2
1.2 Final Design	3
1.3 Design Integration in Society	5
2 Introduction	7
I Problem Context and Solution Direction	8
3 Mission Description	9
4 Requirements	10
4.1 Project Requirements	10
4.2 Technical Requirements	10
5 Sustainable Development Strategy	11
5.1 Social Sustainability	11
5.2 Technical Sustainability	12
5.2.1 Aircraft Design	12
5.2.2 Payload Design	12
5.2.3 Operational Sustainability	12
6 Functional Analysis	13
6.1 Functional Breakdown Structure	13
6.2 Functional Flow Diagram	13
6.3 Conclusion	13
7 Market Analysis	17
7.1 Added Value of SAI	17
7.2 Comparable products	18
7.2.1 New Aircraft Designs	18
7.2.2 Lighter Than Air Balloons	18
7.2.3 Existing High-Altitude Aircraft	18
7.2.4 Existing Tanker/Bomber Aircraft	19
7.2.5 Alternatives	19
7.3 Market Share Analysis	19
7.4 Market Segmentation	20
7.5 SWOT Analysis	20
7.6 Ceres Performance Comparison	21
8 Operations & Logistics Concept Description	22
8.1 Description	22
8.2 Selected Airports	22
8.3 Ground Handling and Logistics	24
9 Sensitivity Analysis	26
9.1 Uncertainty Margins	26
9.2 Sensitivity of MTOW and Fuel Weight	27
9.3 Sensitivity of the Operational Cost and Total Cost	28
9.4 Sensitivity With Respect to Cruise Altitude	28
10 Risk Assessment	30
10.1 Project Risks	30
10.2 System Risks	32
10.3 Other Risks	35

II	Final Design	37
11	Verification and Validation Procedures	38
11.1	Verification	38
11.1.1	Code Verification	38
11.1.2	Errors and Discrepancies	39
11.2	Validation	39
11.3	Integration of Verification and Validation	39
11.4	Results Discussion	40
12	Trade Off of Concepts	41
12.1	Initial Trade Off	41
12.1.1	Trade Criteria & Weights	41
12.2	Quantitative Trade Off	43
12.2.1	Evaluated Concept Description	43
12.2.2	Trade Method	43
12.2.3	Trade Criteria & Weights	43
12.2.4	Scoring Method	44
12.2.5	Trade Summary Table	44
12.2.6	Trade-off Sensitivity Analysis	45
12.3	Discussion and Results	45
13	Ceres Characterisation	46
13.1	Design Drivers	46
13.2	Aerodynamic Design	46
13.2.1	Lift Characteristics	46
13.2.2	Planform Design	51
13.2.3	Aeroelasticity Analysis	55
13.2.4	Fuselage	58
13.3	Propulsion Design	59
13.4	Mass Estimation	68
13.5	Flight Profile Determination	70
13.6	Stability and Control	76
13.6.1	Empennage	76
13.6.2	Control Surface	79
13.6.3	Dynamic Stability Coefficient Determination	81
13.6.4	Dynamic Stability Analysis	84
13.7	Payload Optimisation and Layout	86
13.7.1	Environmental Impact	86
13.7.2	Costs	86
13.7.3	Optimal Payload	86
13.7.4	Payload Burner	87
13.7.5	Payload Power	89
13.8	Structural Design	89
13.9	Systems and Internal Layout	95
13.9.1	Communication System	95
13.9.2	Electrical System	97
13.9.3	Hydraulic System	98
13.9.4	Fuel Systems	99
13.9.5	Internal Layout	100
13.10	Final Design Characteristics	100
14	Impact Assessment	103
14.1	Financial Impact Assessment	103
14.1.1	Method	103
14.1.2	Manufacturing & Acquisition	104
14.1.3	Maintenance & Operations	105
14.1.4	Total Program Costs	106
14.1.5	Verification & Validation	106
14.2	Environmental Impact Assessment	107
14.2.1	Emissions Quantification	107
14.2.2	Noise Assessment	110
15	Resource Allocation	112
15.1	Contingency Management	112
15.2	Mass and Balance Budget and Breakdown	113
15.3	Cost Budget and Breakdown	114
15.4	Power Budget and Breakdown	114
15.5	Compliance to requirements	115

III	Design Integration in Society	119
	16 Reliability, Availability, Maintainability and Safety Analysis	120
	16.1 Reliability	120
	16.2 Maintainability	120
	16.3 Availability	121
	16.4 Safety	121
	17 Production Plan	123
	18 Project Design and Development Logic	125
	18.1 Detailed Design and Optimisation	125
	18.2 Manufacturing and Testing	126
	18.3 Timeline	126
	19 Conclusion and Recommendations	128
	19.1 Conclusion	128
	19.2 Recommendations	129
IV	Appendices	133
	A GasTurb Inputs	134
	B DATCOM Input & Output	134
	C Task Distribution	138

List of Figures

5.1	Information Path in the Design Group.	11	13.12	The Engine Thrust over Weight and SFC as a Function of BPR at Sea Level.	64
6.1	First Level of the Functional Flow Diagram.	13	13.13	Engine Thrust over Weight and SFC as a Function for BPR at Cruise Altitude.	64
6.2	Second Level of the Functional Flow Diagram.	15	13.14	Thrust and SFC as a Function of T_4 at Sea Level.	65
6.3	Third Level of the Functional Flow Diagram.	15	13.15	Thrust and SFC as a Function of T_4 at Cruise Altitude.	65
6.4	Fourth Level of the Functional Flow Diagram.	16	13.16	Compressor Map for the LPC.	65
8.1	World Map of the Airport Locations, with the Achievable Range from each Airport.	23	13.17	Compressor Map for the HPC.	65
8.2	Example Schematic of the Fuelling System used in Paris-Charles de Gaulle Airport.	24	13.18	Altitude, Total Weight (Red), Fuel Used (Yellow) and Payload On-board (Blue), Velocities and SFC for the Mission Profile created.	73
8.3	Diagram representing the Work Flow Necessary to get Sulphur Granules from Storage to the Aircraft.	25	13.19	Lift Coefficient, L/D and Engine Parameters for the Ceres Mission Flight Profile.	74
9.1	MTOW and Fuel Weight, versus Error in OEW and Altitude.	27	13.20	Map of the Rate of Climb versus Altitude and Velocity	75
9.2	MTOW and Fuel Weight, versus Error in Thrust and Altitude.	27	13.21	Parameters Affected by the Tail Arm.	77
9.3	Total and Operational Costs, versus Error in OEW and Payload Mass.	28	13.22	Relation between Horizontal Tail Arm and Fuselage+Tail Weight.	77
9.4	Total and Operational Costs, versus Error in Thrust and Payload Mass.	28	13.23	Loading Diagram of the Ceres Aircraft.	78
9.5	MTOW and Total Cost, versus Altitude.	29	13.24	Range of Centre of Gravity.	78
9.6	MTOW and Fuel Weight, versus C_{D0}	29	13.25	Scissor Plot showing Stability and Controllability.	78
11.1	Total lines committed since the Midterm.	40	13.26	Zero-Lift Drag versus Wing Twist and Dihedral.	82
11.2	Coverage percentage of each model.	40	13.27	C_{l_β} versus Wing Twist and Dihedral.	82
13.1	Sweep Coefficients as a Function of Aspect Ratio and Taper Ratio.	49	13.28	Zero-Lift Drag versus Tail Twist and Dihedral.	82
13.2	Oswald Efficiency versus the Cruise Mach Number.	50	13.29	C_{l_β} versus Tail Twist and Dihedral.	82
13.3	Calculated Oswald (e_{calc}), and Mach Number Correction (ke_M), compared with the Oswald Efficiency for A320 Aircraft (e_{320}) [55].	50	13.30	Rendering of Modelled Ceres Aircraft.	83
13.4	Wing Penalty Function as a Function of the Wing Sweep in Degrees and the Design Lift Coefficient. The Plot shows the Constrained Condition where $A = 13$ and $M_{dd} = 0.78$	53	13.31	Drag Polar from Digital DATCOM.	84
13.5	Wing Penalty Function as Function of the Wing Sweep in Degrees and the Design Lift Coefficient. The Plot shows the Unconstrained Condition where $A = 24$ and $M_{dd} = 0.78$	53	13.32	Fleet Size in Year 1 versus the Payload Mass per Aircraft.	86
13.6	Wing Penalty Function as a function of the wing aspect ratio and lift coefficient. The plot shows the constrained case where the sweep angle is set to 26°	54	13.33	Total Fuel Burned after one Year versus the Payload Mass per Aircraft.	86
13.7	Wing Penalty Function as a function of the wing aspect ratio and lift coefficient. The plot shows the constrained case where the sweep angle is set to 0°	54	13.34	$f_3(x)$ with varying Weights.	87
13.8	Wing Penalty Function in the $\Lambda_w - \hat{C}_L$ Space for the Fokker 100, where $A = 8.43$	55	13.35	Required Combustor Inlet Area versus Mach Number.	88
13.9	Wing Penalty Function in the $\hat{C}_L - A_w$ Space for the Fokker 100.	55	13.36	Example of a NACA Duct from the Boeing 737-800	89
13.10	Thrust Lapse with Altitude.	63	13.37	Airfoil with Spars.	89
13.11	Differences in SFC over Altitude.	63	13.38	Sensitivity of Torsional Stiffness to Wing and Spar Thickness.	90
			13.39	Flight Envelope	91
			13.40	Vertical Shear Diagram.	91
			13.41	Bending Moment Diagram.	92
			13.42	Bending Stress over the Wing Span.	92
			13.43	Wing Deflection Diagram.	93
			13.44	Validation of the Wing Deflection.	94
			13.45	Communication Flow Diagram for the Aerosol Injection System to meet Specifications.	96
			13.46	Diagram for the Electrical System On-board of Ceres Mission Aircraft.	97
			13.47	Diagram for the Hydraulic System On-board of Ceres Mission Aircraft.	98
			13.48	Fuel System Layout.	100
			13.49	Visualisation of the Internal Layout of Ceres Aircraft.	100
			13.50	Three View Drawing of the Ceres Aircraft (Dimensions in m).	102
			15.1	Mass Contingency Management.	113
			15.2	Cost Contingency Management.	113
			15.3	Mass Breakdowns.	114

17.2	Assembly of Ceres Aircraft.	123
17.1	Parts and Sub-Assemblies of Ceres Aircraft.	124
18.1	Development Logic of the Detailed Design Phase.	126
18.2	Development Logic of the Manufacturing and Testing Phase.	127
18.3	Post DSE Gantt-Chart.	127
A.1	GasTurb Inputs	134
B.1	List of DATCOM Inputs and Outputs	138

13.9	Engines Available Proven to be Feasible for Operation at a Cruise Altitude of 20km	61
13.10	EJ200 Engine Specifications	62
13.11	Table of Validation Data for the Fuselage Weight Estimation	68
13.12	Table of Validation Data for the Wing Weight Estimation	69
13.13	Table of Validation Data for the Empennage Mass Estimation of Airbus A320-200	69
13.14	Weights, Inertial Position, and Velocity of Key Points in the Mission Flight Profile	72
13.15	Design Parameters of the Horizontal Tail and Vertical Tail	76
13.16	Required Vertical Tail Surface Area	79
13.17	Control Surfaces Parameters	80
13.18	Range of Deflection Angles for the Control Surfaces	80
13.19	DATCOM Results	82
13.20	Characteristics of the Eigenmotions	85
13.21	Verification of Eigenmotion Parameters	85
13.22	Specific Values for Sulphur Melting	89
13.23	Velocity and Load Factor Limits	91
13.24	Verification Bending Stiffness and Torsional Stiffness	93
13.25	Recapitulative table of the materials and properties which can be used	95
13.26	Final Design Parameters	101

List of Tables

1.1	Mass and Balance Recapitulative Table	5
4.1	List of Stakeholder Requirements	10
7.1	SWOT Diagram of a New SAI System	21
7.2	Performance Comparison of SAI Concepts	21
8.1	List of Selected Airports and Corresponding Diversions	23
9.1	Uncertainty Margins in Weight Estimations	26
9.2	Uncertainty Margins in Several Parameters	26
10.1	Risk Map of the Project Risks Before Mitigation	31
10.2	Risk Map of the Project Risks After Mitigation	32
10.3	Risk Map of the System Risks Before Mitigation	34
10.4	Risk Map of the System Risks After Mitigation	35
10.5	Risk Map of the Other Risks Before Mitigation	36
10.6	Risk Map of the Other Risks After Mitigation	36
12.1	Trade-off of Concepts	43
12.2	Quantitative Trade-off of Concepts	44
12.3	Sensitivity Analysis of the Quantitative Trade-off	45
13.1	Trade-off of wing airfoil selection for conventional concept	47
13.2	NASA SC(2)-0712 Characteristics at $Re = 1 \times 10^6$	47
13.3	Validation of Oswald Efficiency	50
13.4	List of Assumptions Made for the Planform Design	53
13.5	List of airfoil properties used during aeroelastic analysis which are assumed or based on literature	56
13.6	Aeroelastic speeds for the Ceres aircraft for an aspect ratio of 13. The divergence speed is well below the speed shown below	57
13.7	Verification and validation using SAGA and NeoCASS numbers. The aeroelastic speed values from the SAGA report are compared with self-obtained numbers.	58
13.8	The results of the aeroelastic speeds compared to the results shown in the SAGA report.	58

14.1	Chosen Parameters in the Preliminary Cost Model Based on Roskam's Method	104
14.2	R&D Costs of the Ceres Aircraft	105
14.3	Breakdown of the Manufacturing and Acquisition Costs for the Ceres Aircraft Per Unit	105
14.4	Operating Costs Roskam Method for the Ceres Aircraft	106
14.5	Breakdown of the Total Costs for the Ceres Aircraft	106
14.6	GWP and RF Values for Each Pollutant in the Chemical Equations	107
14.7	Computation of CO ₂ Equivalent for the Infrastructure of the System	108
14.8	Summary of the Total Emission and Environmental Impact due to Fuel Burnt During Operations	109
14.9	Breakdown of the Waste and Recycling Percentage of Large Sections of the Aircraft	110
15.1	Mass and Balance Recapitulative Table	114
15.2	Recapitulative Table of the Costs	114
15.3	Electrical System Power Budget Breakdown in the Take-off Condition	115
15.4	Electrical System Power Budget Breakdown in the Cruise Condition	115
15.5	System Requirements	115
15.6	Aerodynamics and Flight Performance Requirements	116
15.7	Payload Requirements	116
15.8	Flight Profile Requirements	116
15.9	Structural Requirements	117
15.10	Propulsion Requirements	117
15.11	Control Requirements	118
C.1	Task Distribution	139

Nomenclature

Abbreviations

<i>M&A</i>	Manufacturing & Acquisition
<i>M&O</i>	Maintenance & Operation
<i>R&D</i>	Research & development
AC	Alternative Current
ACARS	Aircraft Communications Addressing And Reporting System
ADF	Automatic Direction Finder
ADI	Attitude Direction Indicator
ADS-B	Automatic Dependent Surveillance - Broadcast
AFP	Automated Fibre Placement
AFR	Air to Fuel Ratio
AHP	Analytic Hierarchy Process
APU	Auxiliary Power Unit
ATZ	Aerodrome Traffic Zone
BPR	Bypass Ratio
CAD	Computer Aided Design
CEF	Cost Expansion Factor
CFD	Computational Fluid Dynamics
CFRP	Carbon Fibre Reinforced Polymer
CG	Centre of Gravity
DatCom	Data Compendium
DC	Direct Current
DLM	Doublet Lattice Method
DLR	German Aerospace Centre
DME	Distance Measuring Equipment
DOC	Direct Operational Cost
DSE	Design Synthesis Exercise
EAS	Equivalent Airspeed
EASA	European Union Aviation Safety Agency
EI	Environmental Impact
EPNL	Effective Perceived Noise Level
ESA	European Space Agency
EU	European Union
FEM	Finite Element Method
GHG	Green House Gas
GTP	Global Temperature increase Potential
GWP	Global Warming Potential
HLA	Hybrid Lift Airships
HLD	High Lift Devices
HPC	High Pressure Compressor
HSI	Horizon Situation Indicator
ICAO	International Civil Aviation Organization
IDE	Integrated Development Environment
IDG	Integrated Drive Generator
ILS	Instrument Landing System
IOC	Indirect Operational Cost
IPCC	Intergovernmental Panel on Climate Change
LCA	Life Cycle Assessment
LPC	Low Pressure Compressor

LTA	Lighter Than Air
M&A	Manufacturing and Acquisition
M&O	Maintenance and Operation
MAC	Mean Aerodynamic Chord
MLW	Maximum Landing Weight
MNS	Mission Need Statement
MTOW	Maximum Take Off Weight
MTTM	Mean Time To Maintain
MZFW	Maximum Zero Fuel Weight
NASA	National Aeronautics and Space Administration
NDB	Non-Directional Beacon
OEI	One Engine Inoperative
OEW	Operational Empty Weight
OSHA	Occupational Safety and Health Standards
POS	Project Objective Statement
PPI	Production Price Index
PTU	Power Transfer Unit
R&D	Research and Development
RAMS	Reliability, Availability, Maintainability and Safety Analysis
RF	Radiative Forcing
RNAV	Area Navigation
SAI	Stratospheric Aerosol Injection
SH	Stakeholder
SLS	Static Sea Level
SM	Stability Margin
SWOT	Strength, Weaknesses, Opportunities and Threats
TMA	Terminal Control Area
TOP	Take-Off Parameter
TPM	Technical Performance Level
TRL	Technology Readiness Level
UK	United Kingdom
UN	United Nations
USA	United States of America
UVLM	Unsteady Vortex Lattice Method
VFR	Visual Flight Rules
VHF	Very High Frequency
VOR	VHF Omnidirectional Range

Other Symbols

α	Angle of attack	°
$\alpha_{lift=0}$	Zero lift angle of attack	°
α_{stall}	Stall angle of attack	°
$\bar{\eta}_0$	Overall efficiency of the engine	-
\bar{c}	Chord length	m
$\bar{x}_{a.c}$	x location of the aerodynamic centre	m
$\bar{x}_{c.g}$	x location of the centre of gravity	m
β	Compressibility correction coefficient	-
δ	Relative ambient pressure	Pa
δ_0	Total pressure ratio	-
δ_e	Elevator deflection	°
δ_r	Rudder deflection	°
$\delta_{e_{max}}$	Maximum elevator deflection	°
$\delta_{r_{max}}$	Maximum rudder deflection	°

\dot{m}_f	Fuel flow rate	kg/s	h_f	Fuselage height	m
η	Efficiency coefficient	-	L_F	Enthalpy of Fusion	kJ/mol
η_h	Elevator efficiency	-	l_f	Fuselage length	m
γ	Heat capacity ratio	-	l_t	Tail arm	m
λ_{opt}	Optimal taper ratio	-	M^*	Critical Mach number	-
μ_T	Power plant weight over take-off thrust	kg/N	m_{burner}	Burner mass	kg
μ_{lg}	Landing gear fraction	-	M_{dd}	Drag divergence Mach number	-
μ_{resf}	Fuel reserve fraction	-	$m_{sulphur}$	Sulphur mass	kg
ρ	Air density	kg/m ³	n_{ult}	Ultimate load factor	-
τ	Corrected thrust lapse	-	p_{tot}	Total pressure	Pa
θ_0	Total temperature ratio	-	q	Dynamic pressure	Pa
$\tilde{C}_{L_{max}}$	Reference aircraft maximum lift coefficient	-	R_{eq}	Lost fuel	kg
Γ	Di/anhedral angle	°	S_h	Horizontal tail surface	m ²
Λ	Sweep angle	°	s_{tO}	Take-off distance	m
$\Lambda_{c/4}$	Quarter chord sweep angle	°	S_v	Vertical tail surface	m ²
$\Lambda_{h,50}$	Mid chord sweep angle of the horizontal tail	°	S_w	Wetted surface	m ²
$\Lambda_{v,50}$	Mid chord sweep angle of the vertical tail	°	s_{cruise}	Cruise distance	m
Ω	Twist angle	°	$S_{exposed}$	Exposed wing surface	m ²
A_w	Wing aspect ratio	-	s_{fl}	Field length	m
A_{inlet}	Inlet area	m ²	T_4	Turbine inlet temperature	K
b_e	Elevator span	m	$T_{1/2}$	Time to half amplitude	s
b_h	Horizontal tail span	m	t_{cruise}	Cruise time	s
b_r	Rudder span	m	T_{tot}	Total temperature	K
b_{vt}	Vertical tail span	m	TR	Temperature ratio	-
C	Specific Heat	kJ/(kgK)	V_a	Approach velocity	m/s
C_D	Aircraft drag coefficient	-	V_D	Dive speed	m/s
C_L	Aircraft lift coefficient	-	W_f	Fuselage weight	kg
C_l	Airfoil lift coefficient	-	W_G	Gross weight	kg
C_m	Aircraft moment coefficient	-	W_h	Horizontal tail weight	kg
C_r	Wing root chord	m	W_v	Vertical tail weight	kg
C_{D_0}	Zero lift drag coefficient	-	W_{box}	Wingbox weight	kg
C_{D_c}	Compressibility drag coefficient of the wing	-	W_{fix}	Weight of the fixed components of the body group	kg
C_{D_p}	Profile drag coefficient of the wing	-	$W_{LE\&TE}$	Leading and trailing edge weight	kg
C_{L_a}	Aircraft lift slope coefficient	-	W_{MTO}	Maximum take-off weight	kg
$C_{l_{\delta A}}$	Aileron roll control power	-	W_{pay}	Payload mass	kg
$C_{l_{des}}$	Airfoil design lift coefficient	-	$W_{penalties}$	Weight penalties	kg
C_{L_h}	Horizontal tail lift coefficient	-	W_{rib}	Rib weight	kg
$C_{L_{land}}$	Landing aircraft lift coefficient	-	W_{uc}	Undercarriage weight	kg
$C_{L_{max}}$	Aircraft maximum lift coefficient	-	W_{wing}	Wing weight	kg
$C_{l_{max}}$	Airfoil maximum lift coefficient	-	y_{eng}	y location of the engine	m
$C_{L_{to}}$	Take-off lift coefficient of the aircraft	-	A	Aspect ratio	-
C_{m_0}	Airfoil zero lift moment coefficient	-	b	Wing span	m
$C_{m_{\delta_e}}$	Elevator induced moment coefficient	-	C_{L_A-h}	Tail-less aircraft lift coefficient	-
$C_{m_{a.c}}$	Moment coefficient about the aerodynamic centre	-	D	Drag	N
D_f	Fuselage diameter	m	L	Lift	N
d_f	Fuselage diameter	m	M	Mach Number	-
e	Oswald efficiency factor	-	RC	Climb rate	m/s
F_{prop}	Propulsive function	-	S	Wing surface	m ²
F_{SL}	Sea level static thrust	N	SFC	Specific fuel consumption	g/(kN s)
F_{vt}	Vertical tail force	N	T	Thrust	N
g_0	Gravitational acceleration	m/s ²	t/c	Thickness to Chord ratio	-
H_e	Energy Height	m			

Preface

This report forms the concluding report of the series for the *Design Synthesis Exercise*. It is the final part of the major of the undergraduate degree in Aerospace Engineering at Delft University of Technology. This challenging task puts the studies in perspective allowing for the application of all skills learned during the Bachelors degree in a team initiative.

During 11 weeks of painstaking work, a group of 10 students tackle a challenge of their choice. Following the initiative of Dr. Steven Hulshoff and Wake Smith, the group designed a system capable of delivering 3 Tg of SO₂ in the stratosphere at an altitude of 20 km. An estimation of the financial and environmental cost of operating such a fleet of aircraft formed part of the task and resulted in the *Ceres* mission. Readers whose interest lie in the design method and design rundown are referred to Part II. Particular attention was paid to the modelling of the aerodynamic and propulsion modelling as well as the flight profile determination which can be seen in Section 13.2, Section 13.3 and Section 13.5, respectively. Finally, the cost and environmental impact models are found in Chapter 14.

Finally, we, Group 22, would like to thank our supervisor Dr. Steven Hulshoff and our two coaches Dr. ir. Saullo G.P. Castro and ir. Julia Steiner for always supporting our group and guiding us throughout the designing phase. Furthermore, we would also like to thank Wake Smith, Jeremy Snow, and Donald Bingaman for providing us support and wisdom with their knowledge and previous research on the topic. We would also like to show our gratitude to Delft University of Technology, and the Faculty of Aerospace Engineering specifically, for providing us with the necessary facilities and to the involved teaching assistants who were always supportive and helpful.

*Group 22
Delft, May 2019*



Executive Overview

1.1. Problem Context and Solution Direction

One of the greatest challenges that humanity faces in the upcoming decades is to reduce the emission of greenhouse gases (GHG). A direct consequence of these emissions is the increase in global temperature. Although action has begun to limit GHG, due to the uncertainties in climate prediction, this situation may evolve to be less fortunate than anticipated. If this happens, the designed system would be ready to counteract the strongest effects of climate change. It, however, does not constitute a solution to reduce emissions, but only an emergency measure which is able to temporarily curb the increase in global temperature.

This report which details the design of this geo-engineering method, focuses on the measure to inject aerosols into the stratosphere. The aerosols would be injected in clouds of crystallised sulphur dioxide to reflect part of the incoming sunlight.

The objective of this project was to design a fleet of aircraft which is capable of delivering 3 Tg of sulphur dioxide in the stratosphere at the height of operations. The name of this system is Ceres, named after the goddess of agriculture and fertility. The Mission Need Statement (MNS) and Project Objective Statement (POS) derived from this are the following:

1. MNS: If the reduction in GHG does not yield the required decrease in temperature, Project Ceres would be deployed as an emergency measure to further decrease the temperature.
2. POS: Design a cost-effective and feasible aircraft fleet, which demonstrates stratospheric sulphur injection as an emergency measure to satisfy the MNS.

The mission was characterised by the number of **stakeholders** involved which are listed below. In combination with the aforementioned statement, a set of technical and non technical requirements were created.

SH1: Delft University of Technology	SH4: UN/ Individual governments
SH2: Dr. Ir. Steven Hulshoff	SH5: General population of Earth
SH3: Mr. Wake Smith	SH6: Aircraft Manufacturers

The first phase of the Design Exercise was used to determine the design philosophy which the development would follow. This includes a **sustainability development strategy** which addresses both social and technical sustainability. The main takeaway from this study was that the mission should aim to minimise its impact socially, environmentally, and financially. It therefore uncovered design drivers such as the maximisation of the specific characteristics of the propulsion system as well as optimising the operation of the aircraft for minimum fuel burn, and as a result emissions. Moreover, it was decided to minimise the use of composite materials as its impact is very large due to the production methods and manufacturing methods are energy intensive.

This was followed by a short functional analysis which detailed how the system was to operate in order to comply to the requirements. This allowed to evaluate the added value of such a system with respect to other concepts of not only stratospheric aerosol injection systems but also other measures to complement the reduction of emissions of GHG.

Market Analysis Large scale systems like Ceres are only realistic if they add value to comparable and existing methods. The main added value of the product was found to be that it is a readily available and a feasible temporary emergency measure to help decrease the temperature if a reduction in emissions does not yield

sufficient results with respect to global temperatures. It was also found that to design a new aircraft would be the most economical and feasible option to inject aerosol in the stratosphere [56]. Due to the complexity of the impact of aerosol injection, which fell beyond the scope of this research, it was possible or desired to produce a return on investment as it would need to quantify and compare expenses to environmental impact, both primary and secondary.

Operations & Logistics Concept Description In order to satisfy the primary requirement of Ceres, formulated as the injection of 0.2 Tg of aerosol in the first year increasing to 3 Tg by the fifteenth year, an operation plan was devised. The operation plan was constituted around the selection of operating bases, primarily civilian airports, and their respective alternate airports in order to inject the aerosol around the 30°N, 15°N, 30°S and 15°S latitudes.

Additionally, the operational plan describes the necessary operation schedules and fleet numbers to meet the requirements. Aircraft were found to need to operate close to 24 h per day during 250 operational days per year. In order to meet the aerosol injection requirement of the 15th year, a fleet of 180 aircraft was needed. This implied a delivery interval of 1.5 months per aircraft for the first 7 years after which the delivery interval was decided to be decreased to 23 days.

Finally, each aircraft would have a cycle time of 5.8 h, consisting of a flight time of 4.6 h, 1.0 h of turn around time, and 0.2 h of taxiing time. Margins were given in order to account for delays and cancelled flights. This ensured the Ceres mission would operate at its highest possible efficiency.

Sensitivity Analysis Designs for stratospheric flight were found to be extremely sensitive to parametric changes. A set of key parameters were selected with which the sensitivity analysis was conducted. One of the key parameters was the Operational Empty Weight (OEW). A change of 10% from the calculated class II weight estimated results in a 39% OEW increase, which in turn increases the MTOW by 24%.

Additionally, the sensitivity of thrust in the cruise condition was evaluated. It was chosen due to the T/W increasing more than tenfold from the cruise to the ground condition, thus scaling the error more than tenfold. For a 600 N thrust error, the MTOW grew to unfeasible values. A lower bound was taken for thrust value at 20 km, resulting in a feasible design allowing for a 7.5 % error in thrust prediction.

Finally, cost was evaluated due to its influence on the feasibility of the design of the Ceres aircraft. Cost was found to scale similarly to MTOW, and as such, total cost scaled proportionally with OEW margins and altitude. Increasing these margins beyond 10% yielded a cost exceeding the stakeholder requirements.

Technical Risk Technical risk assessment contributed to the feasibility of the design due to risk scaling proportionally with cost. Situations may arise during development, flight testing, and operations with risks present. Therefore, risks were categorised depending on their nature, whether they were project (PTR), system (STR), and other (OTR) related risks. Each risk was categorised and solutions were proposed to mitigate the risk.

One major risk identified involved the misinterpretation around the purpose of the Ceres mission. This can be addressed by stating a clear mission need statement, where it is conveyed that the Ceres mission was developed specifically as a temporary emergency measure to help gap a potential latency in temperature decrease following the reduction of GHG emissions. Active risk management was identified to be crucial for the success of the Ceres mission as well as education about the benefits and drawbacks of using such a measure. This is to be combined with risk management ensuring control over project costs financially, environmentally, and socially.

1.2. Final Design

The design was driven by a number of parameters, some of which have been mentioned above. The main design drivers were aerodynamic and propulsion performance as well as feasibility. As such, these parts were detailed to a greater extent. Various concepts for the design of a new aircraft were considered and shown below, however, based on the maturity of the concepts as well as their aerodynamic performance, the aircraft was chosen to be an aircraft with a conventional layout operating at subsonic speeds.

Concept 1: A conventional wing layout with a conventional fuselage flying at subsonic speeds.

Concept 2: A conventional wing layout with a conventional fuselage flying at supersonic speeds.

Concept 3: A tandem configuration with a conventional fuselage layout.

Concept 4: A flying wing or blended wing body concept.

The aircraft is required to operate at an altitude where the air density is only 7% of the sea level value. These very constraining flight conditions require that the lifting surfaces be heavily optimised, which was done in the aerodynamic design. The climb performance was found to be critical as the aircraft would fly at conditions close to stall conditions. This led to the selection of an airfoil, the NASA SC(2)-0712, which was the most suitable for Ceres' cruise conditions. This drove the selection of the planform to provide sufficient performance. This performance consisted of the maximum lift coefficient and the aeroelastic behaviour. The first was quantified using the Philips-Alley method and the latter using Torenbeek [91]. The final wing was optimised for minimum weight as well as sufficient performance. The driving constraints for the planform were buffeting and aeroelasticity, which yielded an aspect ratio of 13. This wing design was complemented by an aerodynamic fuselage design which aimed at minimising drag, which was achieved using an iterative procedure with constraints on internal volume to accommodate for the payload.

The structural design of the wing was done in parallel with the aeroelastic study to ensure that the structure concurred with the expected interaction between aerodynamic and the wing. This structural design of the Ceres aircraft analysed the loads on the aircraft in different load cases and designed a structure that is capable of handling these loads. Much attention was given to the wing in particular as it is the most critical component of the aircraft. To increase feasibility, a conventional wing structure was chosen, with spars at 20% and 60% of the chord. The spar and skin thicknesses were chosen based on aeroelastic requirements and the number of stringers was chosen based on the stress analysis in the most critical load case. The materials used in the wingbox are aluminium alloys and Carbon Fibre Reinforced Polymers (CRFP). Due to an undesirable environmental impact, the use of CFRP was limited to the wingbox. The material selected in the rest of the aircraft structural components was the Aluminium 7075 alloy.

As mentioned previously, the propulsion system was a design driver of the system. This is a result of the air density being 7% of the sea level value. Consequently, the thrust of the engine drops off gravely, particularly for high bypass ratio engines which are most commonly found on commercial aircraft. The most efficient design to fulfil the mission would have required the use of five F118 engines. However, they are no longer produced and the risk of having reliability issues linked to the use of military engines, 6 EJ200s were chosen. This enables the design to operate at limited throttle settings which increases the durability of the engines and gives a thrust design margin which renders the design more feasible. These engines still have a significant drop off in performance as their cruise thrust is about 6% of their sea level thrust, they however constituted the best design solution to fulfil the mission of delivering payload at 20 km.

To be able to verify the feasibility of the design, an accurate estimation of the mass of all of the components of the aircraft was done. The mass was first broken down in fuel weight, payload weight, and operational empty weight. The first two items were optimised for, using minimisation of fuel burn and cost, which is discussed below. The mass estimation consisted in estimating the mass of the components of the operational empty weight. In order to do so, a method had to be found to be able to determine the mass of components based on performance parameters determined as in the paragraphs above. To do so, the group implemented Torenbeek's method of mass estimation, which consists in a set of semi empirical relations. This was complemented by other analytical methods when uncertainties were found to be too significant. This also allowed to compute the CG of the operational empty weight as well as of the fully loaded aircraft which was necessary to determine the stability and control characteristics of the aircraft. The values are summarised in Table 1.1.

The Ceres aircraft is required to remain stable and controllable during the entire flight. As a result, taking the current parameters obtained so far, tail surfaces were sized as per the requirements. In addition to this, the dynamic stability of the aircraft was determined. This was verified using the digital DATCOM method. This resulted in the aircraft to be determined to be stable but the motion damping for the short period in particular was computed to be uncomfortably long. This is thus an area which should be further studied in the future to remedy this characteristic.

Table 1.1: Mass and Balance Recapitulative Table

Parameter	Value [kg]	x location from nose [m]
Fuel	13468	28.96
Payload	9700	18
OEW	27928	28.95
<i>Propulsion</i>	<i>6000</i>	<i>26.34</i>
<i>Fuselage</i>	<i>5079</i>	<i>20.59</i>
<i>Wing</i>	<i>9793</i>	<i>28.96</i>
<i>Vertical Tail</i>	<i>933</i>	<i>39.52</i>
<i>Horizontal Tail</i>	<i>2133</i>	<i>39.52</i>
<i>Gear</i>	<i>1018</i>	<i>22.75</i>
<i>Systems</i>	<i>1018</i>	<i>22.75</i>
MTOW	51096	26.9

Flight Profile Optimisation As previously mentioned, the flight profile for the Ceres mission was required to be optimised for both cost and environmental impact. This meant in this case to minimise fuel burn which constitutes the main part of the emissions in an aircraft's life but also a great part of the operating costs. This most optimal flight profile was found by using the established non-dimensional discrete time calculator. Subsequently, a detailed flight profile with fuel burn was found by using the SUAVE software. This was then verified and improved by an analytical model which optimised the flight profile for minimum fuel burn. When compared to SUAVE, the minimum fuel burn climb occurs at unsteady speeds which contrasts with the output from SUAVE. This was used to tune SUAVE with more precise combinations of steady speed segments. This flight profile discretisation led to the conclusion that the aircraft should start to disperse the sulphur dioxide at an atmosphere of 19.5 km. This enabled to cut significantly the climb time which enables to save both fuel and flight time. The final flight time is 4.6 h and the fuel burned is 10.5 t if not diverted.

Payload Optimisation The second step of the optimisation process led to the determination of the most optimal payload. Previous research had stated that 10 t of sulphur was the optimal value, it was however determined that taking both cost and environmental impact into account, the optimal for this type of aircraft was 9250 kg. In order to estimate the cost, the number of aircraft in the fleet to satisfy the requirement was taken. Similarly, fuel burn was taken to estimate the environmental impact. This was done as cost models and environmental models have very high uncertainties, in contrast to the parameters taken. This optimisation was taken for the first year of operation due to the high probability of the mission running for a limited amount of time.

Once all these design parameters were sized, it was possible to determine the internal layout of the electrical, hydraulic and fuel system. The most important aspect of these systems was the determination of the electrical power budget as it was of utmost importance to determine if an external source of power was necessary to melt the sulphur to enable the combustion of the latter. It was found that the electrical power provided by the engine's Integrated Drive Generators (IDG). This system will also provide power to the hydraulic and fuel pumps. The fuel was also chosen to be positioned in the wings to create relief, which was beneficial having settled for a high aspect ratio.

1.3. Design Integration in Society

Financial Impact The financial impact assessment of Ceres was divided into the Research & Development (R&D), Manufacturing & Acquisition (M&A) and Maintenance & Operations (M&O) costs. These values were approximated by making use of Roskam's cost method[74]. This method relies on aircraft and specifications, and takes into account the three aforementioned aspects. The R&D cost were estimated to be in the range of \$1.92-3.32B, taking into account that the design does not require the development of new engines. Both the expected value and the high estimate were below the specified budget of \$4.48B. For M&A a budget of \$112.9M per aircraft was assigned. For this segment a manufacturing cost of \$107.45M per aircraft was found, meaning that the requirement was met. This estimation did assume a cost of \$5M per engine and resulted in a total fleet manufacturing cost of \$19.34B. Finally, the M&O costs were covered. These cost consisted of the direct- and indirect operating cost. The given requirement only mentioned the direct operating

costs and was specified at \$44.8M per aircraft per year. A DOC requirement was met and a value \$43.52M was obtained. For M&O a total annual cost per aircraft of \$69.92M was found, resulting in a total of \$86.61B for 15 years of operations.

Environmental Impact Three methods were used to quantify the environmental impact of the Ceres fleet of aircraft. The first was obtained by computing the global warming potential which results in an estimate in equivalent CO_2 . The second method which was used was the Radiative Forcing. This was implemented due to the fact it is the standard used by the IPCC, the authority on climate change. The last method used to determine environmental impact was also the method which yields the least amount of uncertainty and was the computation of the fuel burned during a flight. This was obtained by doing a numerical integration of the fuel consumption over the entire flight based on the thrust setting and SFC. These three numbers enabled a full reproducibility of the results. It is thus expected that the Ceres fleet of aircraft will contribute approximately 232–1065 Mt of CO_2e (equivalence) in total during the 15 years in which the system will be phased in. The radiative forcing will be 3.69×10^{-8} – 6.07×10^{-13} W/m². The range is very large and represents the difference between the theoretical value for a clean combustion versus the expected value based on the performance of other aircraft. The impact of the Ceres fleet of aircraft was found to be approximately 0.029% of the worldwide fuel consumption and 0.23% of all Jet-A consumption.

Lastly, in order to study the feasibility of the aircraft, a production plan was developed. The aircraft will be divided in different components. The different components are designed to be manufactured in batches and assembled in a production line. The assembly of the aircraft has the following sequence. Firstly, the cabin will be assembled along with the installation of the electrics, insulation, piping and valves for the dispersion and combustion system. Subsequently, the nose and the tail cone will be attached. The vertical tail, main wing and landing gear will be attached simultaneously to the fuselage structure. The internal layout for the cockpit and the wiring for the flight control are then installed along with the systems for payload delivery.

These elements described in this executive overview allowed to devise and design a concept for a fleet of aircraft which is can deliver 3 Mt of sulphur dioxide at an altitude of 20 km. In order to further improve the design, additional studies have to be made regarding stability, addressing the issue of the low dampening of motions but also the speed stability which was found to be occur when the estimate of C_{D_0} was too low. More accurate models also have to be developed both regarding propulsion and aerodynamics as they were found to be the most critical aspect of performance of the design.

Introduction

One of the potentially greatest challenges that humanity faces in the upcoming decades is global warming. The main cause for this is the continuous increase in emissions of greenhouse gases (GHG). Therefore, measures must be taken to reduce these emissions. In case climate changes evolve to be less fortunate than anticipated, geo-engineering methods could be used to counteract the strongest effect of climate change while GHG emissions are being reduced. In recent times, many initiatives have sought to capture greenhouse gas emissions or to manage the solar radiation of the Earth. However, the former is currently impractical and the latter is highly discouraged. Indeed, both do not provide an adequate and sustainable solution to climate change nor are those solutions to counteract the effects of climate change. Rather, these geo-engineering methods should only be considered, if and only if, unexpected adverse effects of climate change must be counteracted while greenhouse gas emissions are being reduced. One of the explored geo-engineering methods covered in this report is one that manages the incoming solar radiation. Examples of such countermeasures using solar radiation management are the deployment of mirrors in space, cirrus cloud thinning and stratospheric aerosol injection. The report will focus on the last, presenting a concept for the aircraft and its deployment. Therefore, the aim of this project is to provide a possible measure that would be used to counteract the strongest effects of climate change in case uncertainty in temperature rise creates a disastrous situation. Preferably, there will be no need to use Ceres, since an operational fleet of aircraft would result in additional emissions and possible unforeseen adverse effects. However, when the positive effect of SAI outweighs these extra emissions it could prove beneficial to use as an emergency measure. The name of this system is Ceres, named after the goddess of agriculture and fertility.

The Ceres mission aims to deliver aerosol into the stratosphere. The reasoning is to form clouds of crystallised aerosol which will cover the Earth and enable the scattering and reflection of sunlight. Just as there exist various solutions to manage solar radiation, various ways to deliver aerosol into the stratosphere exist and have been considered. However, many lack feasibility or efficiency. As such, Ceres explores the use of a fleet of aircraft that have been optimised for the stratospheric aerosol injection mission. An operational scenario is formulated in order to ensure that all requirements are met. Extensive cost analysis studies as well as secondary environmental impact assessment are conducted in order to quantify the cost, both financially and environmentally for the implementation of an airborne stratospheric aerosol injection.

The report starts off with an introductory part. In Part I, the mission is first described. This is followed by Chapter 4 which describes the technical requirements as well as the requirements which are linked to the nature of the project. Chapter 5 describes the ways in which sustainable development has been taken into account during the design of Ceres. From this, it is possible to explore the functions which must be satisfied by the operations and the aircraft which help determine design constraints and boundaries, as shown in Chapter 6. This is followed by Chapter 7 in which the alternatives for stratospheric aerosol injection are described and the Ceres mission is put into perspective in a market analysis. Chapter 8 discusses the Ceres operational and logistics concept. Part I is closed by Chapter 10 in which the risks and their respective mitigations of Ceres are shown. The following Part II explores the design of the Ceres aircraft by describing how verification and validation are implemented in Chapter 11. The various aircraft concepts are then compared against one another in Chapter 12. The design is then conducted in Chapter 13 by focusing on a number of design aspects. Finally, Part III explores various aspects regarding the implementation of Ceres and the following steps of the development. First, a RAMS analysis is done in Chapter 16. This is followed by a production plan in Chapter 17. Chapter 18 describes the project design and development logic as well as the Gantt Chart of the activities to conduct following this design exercise. Conclusions and recommendations can then be found in Chapter 19.

I

Problem Context and Solution Direction

Part Introduction

This opening part details the problem as it was posed to the group ten weeks ago. This is followed by a description of the main goals of the report which are identified and described. These define the desired outputs of the Design Synthesis Exercise.

A market analysis is then presented which was conducted in order to assess and evaluate possible shortcomings of competitors. The relation and comparison between the latter and the designed aircraft is explored and evaluated. Finally, this part of the report concludes with a description of the operation and logistic concept description. This latter description introduces various design parameters which are then expanded upon in the design part of the report which follows.

3

Mission Description

Although actions have been taken already regarding the reduction of GHG emissions, uncertainties in climate and atmospheric models may not be able to accurately predict the consequences of this reduction in emissions. More specifically, due to latency and feedback mechanisms in various ecosystems, it is probable that the rise in global temperature is not slowed down sufficiently or stopped altogether. The Ceres mission would then help curb the increase in global temperature by means of a geo-engineering process called stratospheric aerosol injection (SAI) in combination with the reduction of GHG. Ceres thus represents by no means a solution to climate change, global warming or GHG emissions but solely a temporary emergency measure if the evolution of global temperature was observed to be less fortunate than predicted. This is to be achieved by injecting aerosols into the stratosphere (for better longevity) close to the latitudes situated at 15° and 30° North and South. The aerosols will then diffuse over higher latitudes due to atmospheric currents away from the original injection position. The resulting spread of aerosol particles will mimic the observed cooling effect of sulphates from volcanic eruptions. These particles will reflect part of the sunlight back into space.

The most economical method to inject aerosols into the stratosphere would consist in a fleet of aircraft.^[57] This creates challenges, since aircraft that have flown as high as the stratosphere (≥ 20 km) have carried relatively light payloads such as cameras. Meanwhile Ceres would be required to carry efficiently a payload of multiple tons. Consequently, it would need to climb with the optimum payload weight to the mission altitude. More specifically, the fleet would be required to deliver 3 Tg/yr of SO₂ according to the user requirement at the height of operations. Based on these facts, the aircraft, operation plan, and fleet size were designed. Its cost and secondary environmental impact were also estimated and quantified.

A general description of the project is given by the Mission Need Statement (MNS) and the Project Objective Statement (POS).

1. MNS: If the reduction in GHG does not yield the required decrease in temperature, Project Ceres would be deployed as an emergency measure to further decrease the temperature.
2. POS: Design a cost-effective and feasible aircraft fleet, which demonstrates stratospheric sulphur injection as an emergency measure to satisfy the MNS.

The MNS and POS determine the general direction of the project and therefore influence trade-offs of different design aspects. This is an important baseline for the remainder of the project.

Requirements

The mission is defined by a series of constraints which are presented as technical and non technical requirements. This chapter builds upon the requirements which were explored in one of the previous reports [32]. It first presents the requirements inherent to the report and then Section 4.2 explores the technical requirements of the Ceres mission and aircraft.

4.1. Project Requirements

This section presents the requirements resulting from the objective of the project as well as the requirements related to the functioning of the Design Synthesis Exercise.

The requirements can be identified by a stakeholder to which they belong as well as a number which creates a unique call which can be referred to. These stakeholders as well as their requirements can be observed below and in Table 4.1, respectively. Along with the requirements, a distinction is made between the types of requirements to show how much these influence the design of the concept and the aircraft. It can either be '*non-driving*', '*driving*', '*key*' or '*killer*'. The requirements where no mention is made are non-driving.

SH1: Delft University of Technology

SH2: Dr. Ir. Steven Hulshoff

SH3: Mr. Wake Smith

SH4: UN/ Individual governments

SH5: General population of Earth

SH6: Aircraft Manufacturers

Table 4.1: List of Stakeholder Requirements

Requirement	Statement	Type
REQ-SH1-01	Each member of group 22 shall have both a managerial and technical contribution.	
REQ-SH1-02	Group 22 shall give updates in the form of reports, presentations and other applicable means of communication.	
REQ-SH1-03	Each member of group 22 shall work at least 8 hours per day, from Monday through Friday.	
REQ-SH1-04	Group 22 shall be a representative of TU Delft at the Symposium, thus they shall behave as such.	
REQ-SH2-01	The SAI system shall be deployable in the next 15 years.	
REQ-SH2-17	The project shall include a summary of the secondary environmental effects of the complete system.	
REQ-SH2-18	All system components shall have an end of life plan.	
REQ-SH3-04	The project shall provide a detailed market analysis.	
REQ-SH3-05	The project shall focus on the design of the system.	
REQ-SH4-01	The SAI system shall provide a temporary cooling effect to Earth.	
REQ-SH4-02	The SAI system shall not impair individual countries.	
REQ-SH4-03	The system shall have evaluable limited direct environmental impacts.	key
REQ-SH4-04	The aircraft shall provide a quantifiable effect on the global temperature within the first 5 years.	
REQ-SH4-05	The effect of the aircraft shall be evaluated on a yearly basis.	
REQ-SH4-06	The local impact of SAI shall be quantifiable and limited.	
REC-SH4-07	The execution of the project shall be promoted globally.	
REQ-SH5-01	The emission of the payload shall have no direct medical consequences.	
REQ-SH5-03	SAI system shall be funded by using the current budget for global temperature control.	
REQ-SH6-01	The aircraft shall have a development time of less than 10 years.	
REC-SH6-05	The responsibilities of each community member shall be clarified and agreed upon by the community.	
REC-SH6-03	The ownership of the products shall be clarified and agreed upon by the community.	
REQ-SH6-06	The production of the aircraft shall not endanger the health of the employees.	

4.2. Technical Requirements

The technical requirements can be found in the previously mentioned report [32]. These were divided in stakeholder, system and subsystem requirements. For conciseness, the driving, key and killer requirements will be assessed in a compliance matrix in Section 15.5.

Sustainable Development Strategy

Sustainable development is a wide ranging topic which includes the study and consideration of many aspects of Ceres. In this discussion of its strategy, the technical and social aspect of the mission are explored to determine which actions would be taken to reduce negative environmental impact and improve the technical and social sustainability.

5.1. Social Sustainability

Project Sustainability This aspect concerns the social well-being of Ceres' stakeholders and users. Here, the social sustainability is discussed with respect to the employees, customers and community. Throughout this DSE, the Sustainability Officer is responsible for addressing and improving the social well-being of the group members. It is necessary to monitor the number of hours being spent on the project in order to minimise the risks related to stress, fatigue and frustration. This is complemented by an even distribution of work which prevents the rise of conflicts. Moreover, these tasks should be verified to have realistic deadlines for similar reasons as previously mentioned. Lastly, sufficient breaks should be allocated in order to allow for mental rest which would otherwise impede productivity. In order to ensure a fair division of tasks and communication in the group, an N^2 Chart was created which presents the information path in the group as shown in Figure 5.1.

Aerodynamics	CL, CD, L/D, Vcruise, Mcruise, Climb perf.	Aero Forces	M, V	Cl, CD, CL, CM	M, V, T	Risk related to dep.	L/D, D		L/D, Geometry, Location	
V, Disp. range, Disp. time, A inlet	Flight Performance	Flight profile, Flight envelope		Mission profile, Flight envelope	T/W, OEW/MTOW, Take-off Thrust	Risk related to dep.	Fuel cons., Flight time	Mission Profile	Operating cost	Vcruise, Flight profile
l/c, AR, Mass breakdown and location, CG	l/c, AR, Mass breakdown and location, LG	Structures	Aircraft layout	Mass breakdown, CG location, MTOW	MTOW, Mass budget	Risk related to dep.	Materials and mass, Manufacturing and production method	MTOW, OEW	Location, Geometry, Mass, CG, Cost	MTOW, Manufacturing method
V, Disp. range, Disp. time, A inlet	V, Disp. range, Disp. time, A inlet, Tank size, Mburner, Mtank	MBurner, Mtank, Payload Mass, Size of Tank Size of Burner	Payload	Location of Payload, Mass of Payload	Cruise Velocity	Risk related to dep.	Corosivity, EI of Payload	Mpay Disp	Mass and size of system, V, Disp. range, Disp. time, cost	Estimated cost
Req. control surfaces, Surface areas, Flap location and size		Control surfaces information		Control		Risk related to dep.		CG range,	Stability and control	Estimated cost
	Thrust and SFC	Mass budget (as based on Thrust)		Engine Thrust for 1 engine out	Propulsion	Risk related to dep.	SFC, Engine type (manufacturing)	Engine Selection	Cost	Engine cost
Mitigation of specific risk	Mitigation of specific risk	Mitigation of specific risk	Mitigation of specific risk	Mitigation of specific risk	Mitigation of specific risk	Risk Manager	Mitigation of specific risk	Risk map	Mitigation of specific risk	Mitigation of specific risk
	Fuel consumption objective				Fuel Consumption Objective	Risk related to dep.	Sustainability Officer	EI	EI	
					Risk Mitigation			Project Manager	Scheduling	Budget
L/D, Dimensions and weights	Flight envelope, Flight profile, Required range	Mass budget, Size and dimension	Mass and power budget, Dimensions and locations, range, V	Control characteristics, CG range achievable, Dimensions and locations of subsystems	Mass Budget, Power Budget, T required	Risk related to dep.	Design information	Mission fulfillment	System Engineer	Overall cost of dep.
Cost budget	Cost budget	Cost budget	Cost budget	Cost budget	Cost budget	Risk related to dep.		Estimate of cost and budget	Estimate of cost and budget	Business Manager

Figure 5.1: Information Path in the Design Group.

System Social Sustainability During the operation of the fleet of aircraft and the design of the aircraft, it must be ensured that the **customer** is taken into account in relation to the toxicity of the aerosol (sulphur dioxide) used. A safe handling procedure must be determined in order to create a safe working environment.

This will be executed according to the standards covering handling, storage, first-aid measurements and protective clothing set by the sulphur supplier as well as those set by OSHA ¹. This should also cover the handling of the aircraft during flight which must not be straining on the pilot relative to other aircraft of general aviation. Lastly, maintenance of the fleet must be considered to ensure sustainability. As such, the operation costs, both environmental and financial, should be minimised as well as the productivity, which should be maximised.

Ceres' most affected stakeholder would be the general **community**. Sulphur dioxide has a distinct smell which would cause trouble for the community. As a result, the dispersion rate should not be too excessive. Moreover, the pollution due to emissions and noise should be minimised. This resulted in a number of airports which would be chosen to be spread worldwide. Finally, the flammable payload means that in case of an emergency or catastrophic failure, the aircraft should be able to land far from population to prevent disasters.

5.2. Technical Sustainability

To guarantee a sustainable technical design of the aircraft and its operations, various aspects must be kept in mind during the design.

5.2.1. Aircraft Design

Ceres' requirement to be designed to minimise costs while limiting the secondary environmental impact is the basis for decisions made within the various departments.

The **propulsion** department focused on optimising the engine for the highest thrust-to-weight ratio as well as the lowest specific fuel consumption (SFC). By optimising these parameters, it was ensured that the correct engines were chosen for the mission. This is of utmost importance considering that the engines are the main contributor of pollution, both in terms of emissions and noise. Due to performance impacts, biofuels are not used [30]. An assessment of the direct environmental impact of the operation of the aircraft is explained in more detail in Chapter 14. The noise was also considered and assessed in the same chapter. This was coupled with a flight profile optimisation which minimised fuel burn.

Similarly, to minimise the impact of **structures** and **manufacturing**, specific materials and manufacturing and assembling methods were chosen as is discussed in Chapter 17. Here, as justified in Section 13.8, specific alloys were chosen. Not only have they been used throughout the aerospace industry for many years. They also have a more limited environmental impact compared to CFRP structures. Only for specific areas, such as the wingbox, CFRP is used as the high loads mean that the weight savings outweigh the environmental impact. Quantification of the environmental impact of the used materials is further discussed in Section 14.2.

Finally, the last department which has taken sustainable development into account is the team specialising on the **aerodynamic** design. This was optimised for the mission and aimed at getting optimal lift-over-drag while MTOW was minimised in order to facilitate climb to an altitude of 20 km and to cruise at this altitude. As such, particular attention was paid to the design of the planform and the fuselage. This was done to ensure that most conditions the aircraft would operate were feasible or close to optimal.

5.2.2. Payload Design

The **payload** was also designed and optimised for the mission. This optimisation method and process as well as result can be observed in Chapter 13. This involved taking the performance of a specific aircraft optimised for a certain payload mass and comparing all designs. The direct environmental impact of sulphur injection falls beyond the scope of this project but has been shortly described in Chapter 7.

5.2.3. Operational Sustainability

Due to the operations of the SAI system, over time the system produces GHGs, thus increasing the amount of pollutants in the atmosphere. However, the goal of the SAI system is to result a temperature reduction by injecting sulphur-dioxide into the stratosphere. As such, the impact of the SAI system shall result in a **net** temperature reduction when GHG emissions of the system are taken into account. The quantification of the environmental impact of operating the Ceres aircraft fleet and infrastructure are discussed in detail in Section 14.2.

¹https://www.osha.gov/laws-regs/oshact/section_6

Functional Analysis

Functional analysis is a tool to understand the design problem to be solved. The main objective is to establish a basis for the SAI system to be designed. In Section 6.1 the functional breakdown structure is discussed, while Section 6.2 shows the functional flow diagram.

6.1. Functional Breakdown Structure

In the functional breakdown structure the functions of Ceres are grouped together based on similarities. The mission need statement has been taken as the starting point of the diagram: 'Temporarily cool the Earth by injecting aerosols into the stratosphere [34].'

Fulfilling the mission as stated previously is seen as the main function of Ceres. Subsequently, the mission was split up into three parts: the operation of Ceres, the support of Ceres, and the end of the mission. By means of general knowledge of systems engineering [38] [70], these three functions have been broken down into five levels of depth. On the next page the functional breakdown structure is shown. The first level of functions is shown in red, the second in blue, the third in green, the fourth in yellow, and the fifth in purple.

6.2. Functional Flow Diagram

In the functional flow diagram the functions of the systems are structured in a different way than in the functional breakdown structure. In this diagram, functions of Ceres are ordered by their sequence of execution. The functions in the functional breakdown structure were analysed for connections and the flow diagram was established using these functions as a baseline. The functional flow diagram contains one level less than the functional breakdown structure.

The first level is presented in blue in Figure 6.1. This level includes the support, operation, and end of the Ceres mission. Next, the second level of depth is shown in red in Figure 6.2 and in turn the third is shown in green in Figure 6.3. Note that the fourth level shown in Figure 6.4 of the diagram only describes a few functional blocks in more detail.

6.3. Conclusion

From the functional analysis diagrams it appears that the Ceres system is different from other systems in some ways. This is due to the SO₂ injection during flight, requiring functions of the system such as on ground sulphur handling and sulphur combustion. Additionally, the system must be able to reach 20 km altitude with a heavy payload, uncommon in aviation.

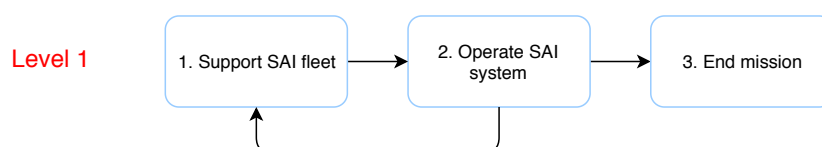


Figure 6.1: First Level of the Functional Flow Diagram.

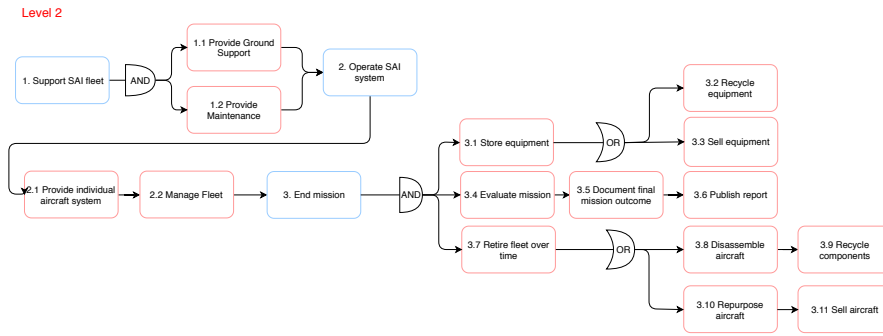


Figure 6.2: Second Level of the Functional Flow Diagram.

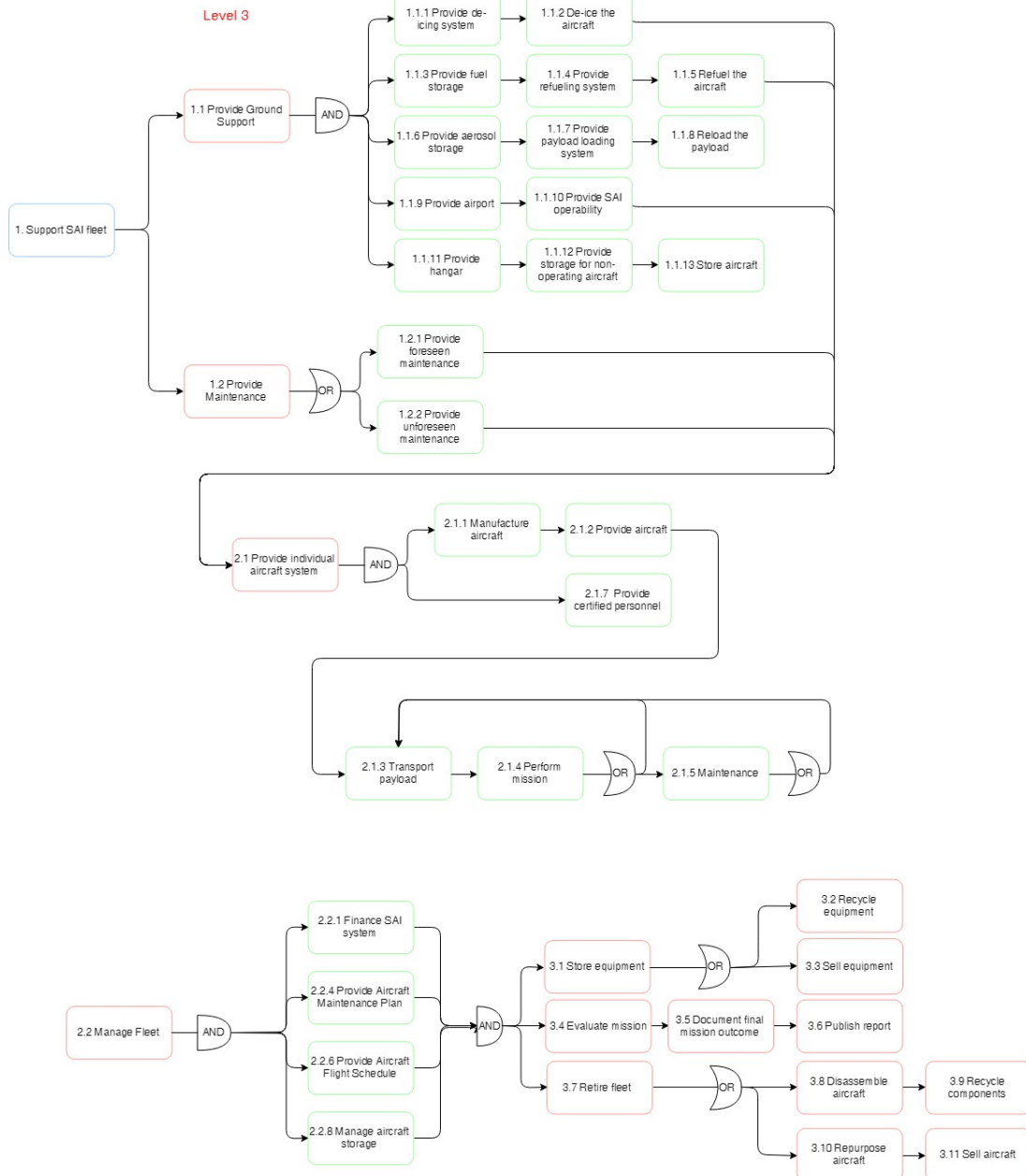


Figure 6.3: Third Level of the Functional Flow Diagram.

Level 4

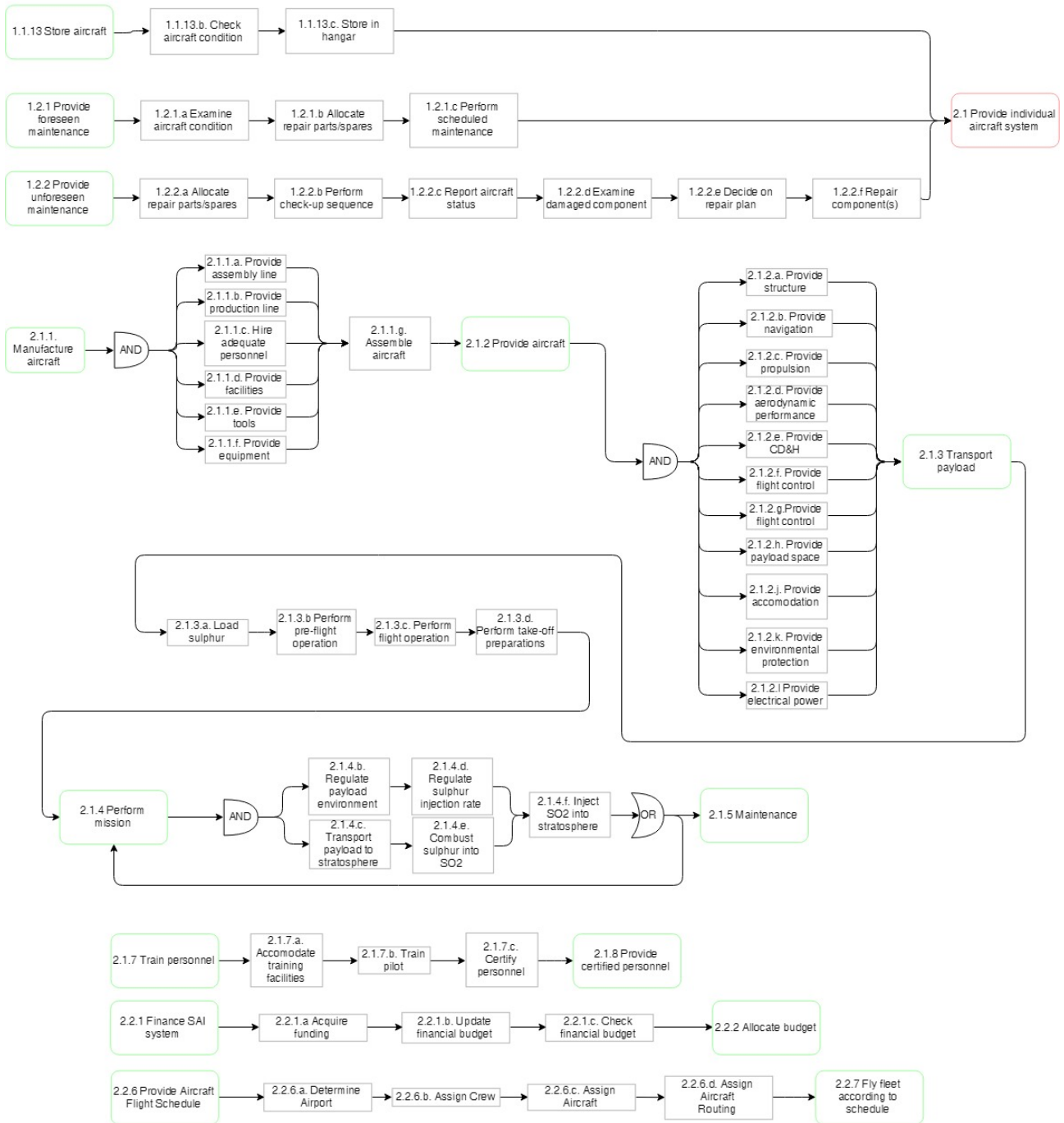


Figure 6.4: Fourth Level of the Functional Flow Diagram.

Market Analysis

It is necessary to conduct a market analysis to understand the position that Ceres has with respect to other SAI solutions. The role of Ceres would be to compensate for unforeseen latency between the reduction of GHG emissions and a reduction in global temperature to sustainable levels. Due to the mission requirements, the functions that the fleet of aircraft must fulfil and its role, it is possible that the Ceres system would represent a very large investment. It is thus necessary to conduct a market analysis which shows the feasibility of the project. Initially, the added value of SAI is discussed, after which other methods to inject aerosols into the stratosphere are compared to the Ceres fleet of aircraft. The market share analysis and market segmentation both aim to show the feasibility of such a project. Finally, a SWOT-analysis was performed to indicate the strengths and weaknesses of SAI.

It must be noted that the quantification of the impact of the aerosol for the environment falls beyond the scope of the DSE, moreover due to the nature of the mission which is not aimed at yielding commercial profit, a return on investment was not conducted.

7.1. Added Value of SAI

A system like Ceres must only be considered and deployed if its added value is superior to alternative actions or measures. If the added value, i.e. limiting effects of climate change due to less fortunate predictions, does not justify the high environmental and financial cost linked to the creation and operation of this fleet of aircraft, Ceres must not be used.

Thus, the main added value of SAI is that, in the case of unexpected significant environmental changes, it will provide a readily deployable and cost-effective method in counteracting these changes on a global scale while GHG emissions are being reduced. As stated before, it gives no permanent solution to global warming or greenhouse gasses by any means. The idea behind SAI is to provide an emergency system to combat unexpectedly negative outcome of climate change effects while GHG emissions are being reduced.

By injecting a significant amount of sulphur dioxide into the stratosphere, Ceres aims at reflecting a part of the incoming sunlight into space. This results in a lower amount of energy being absorbed by the Earth's atmosphere and thus a lower temperature. The benefit of injecting the aerosol directly into the stratosphere, as opposed to injecting into lower atmospheric layers, is that the aerosol stays effective for a longer period. The injected sulphur will stay effective for around 1 to 2 years in the stratosphere as opposed to only a week in the troposphere. Besides, injecting the sulphur into lower layers of the atmosphere could cause additional harm to human health, which is kept to an absolute minimum in the stratosphere [14].

J. McClellan et al. (2012) give a rough approximation of the impact of SAI on a global scale. They estimate that 1 Mt (1 megaton or 1 billion kilograms) of stratospheric injected sulphur would result in a change of 1 W/m^2 received solar flux [57]. Another research conducted by U. Niemeier et al. (2011) shows an estimated decrease of 0.31 W/m^2 per megaton [94]. For the Ceres system 3 Mt of sulphur is planned to be injected once a fully operational fleet is established. This comes down to a decrease of 3 W/m^2 in the most favourable case and around 1 W/m^2 in the most reserved case on a global scale. Using 1360.8 W/m^2 as a reference value, this means the proposed Ceres system will result in a 0.07–0.22 % decrease of the total solar flux received at Earth [50]. The dependency of the temperature on the change in solar flux is roughly $0.75 \text{ K/(W/m}^2)$ [18]. Resulting in a temperature reduction of 0.75–2.25 °C. In the case that global emissions are not being reduced sufficiently to decrease the temperature rise, which results in adverse effects to the environment, SAI could be used.

One important part of the Ceres project is that a new type of aircraft is specifically designed for this type of injection mission. There have been other plans for using aircraft for SAI missions proposed, however, these suggestions use existing military aircraft or cargo aircraft. The problem with military aircraft is that they cannot carry enough payload to the correct altitude, which would require a very extensive fleet size. For

cargo aircraft, the main concern is that they cannot reach the desired altitude of 20 km. In both cases, the aircraft must first be modified to be able to bring a decent amount of sulphur to the desired altitude, which would be sub-optimal for operations. In general, the existing options are high payload - low altitude or low payload - high altitude aircraft, while this mission calls for a high payload - high altitude design. Another research of J. McClellan shows that designing a new aircraft for SAI is indeed the cheapest option compared to the other methods to inject aerosol into the stratosphere [56]. Which other methods and products could be used for aerosol injection is elaborated on in the following section.

7.2. Comparable products

Applications of SAI are scarce and, as such, reference data is hard to come by. Very few aircraft or other measures have specifications that allow them to achieve high altitude with a heavy payload. As a result, the next subsections will discuss possible designs that are investigated that could work for SAI.

7.2.1. New Aircraft Designs

The most obvious existing competitor is probably also a conventional aircraft. J. McClellan et al. investigated a large number of possible aircraft designs for aerosol injection [56]. Out of this investigation, it became clear that the most cost-effective method (in terms of total cost) would make use of smaller aircraft with an initial estimate of 10 000 kg of aerosol on board. Only a system designed to inject 5 Tg/yr at a specific altitude range would be more cost-effective with larger aircraft. The least costly option to inject 1 Tg/yr to altitude at 20 km would cost a total of 0.9 billion USD per year. The cheapest option for Ceres' goal of injecting 3 Tg/yr in the stratosphere at 20 km would cost a total of 2 billion USD per year. Note that the total cost does not exactly scale with the amount of aerosol. This is because of the significant research and development costs of roughly 6 billion USD [56] for the mission of Ceres.

7.2.2. Lighter Than Air Balloons

The use of lighter than air (LTA) balloons could be considered a comparable method to aircraft. These balloons also have difficulties associated with the high altitude and large payload required.

One compelling option would be to transport aerosols to a tethered balloon via the tether (pipe). Pumping aerosols to altitude appears to be a cheaper option than many transportation alternatives. Davidson et al. show a tethered balloon aerosol injection system will have a total cost an order of magnitude smaller than its closest competitors. The major problem concerning this design is that with current material technology, a tether strong enough cannot be designed. [19]

J. McClellan et al. investigated the option of hybrid LTAs called Hybrid Lift Airships (HLA) which also generate some aerodynamic lift [56]. These do tend to be able to carry heavier payloads compared to LTAs without aerodynamic lift, which is of high importance for aerosol injection. HLAs do still struggle with higher altitudes, moreover these types of aircraft are relatively slow causing mission duration to increase when the correct dispersion rate needs to be achieved.

J. McClellan et al. estimate that using this method to deposit 1 Tg/yr at 20 km altitude would cost 1 billion USD per year.

7.2.3. Existing High-Altitude Aircraft

In an inquiry into space tourism, the following four aircraft were investigated as alternatives to orbital flights while still reaching high altitudes [82]. These aircraft at least satisfy the service ceiling requirement, but other aspects still need to be investigated.

- Lockheed SR-71 Blackbird
- Lockheed U-2
- Martin/General Dynamics RB-57F Canberra
- Scaled Composites Proteus

The existing high-altitude aircraft all have similar service ceilings of more than 60 000 ft (\approx 18 km). Other similarities include payload sizes of the order of magnitude of 2000 kg and the purpose of these aircraft. The first three listed aircraft are all reconnaissance aircraft and the Proteus can be used for various payloads like

a radar. This difference in payload nature and mass makes these aircraft in their current state not optimised for SAI. The most important difference is that these four aircraft have high endurance (around 10 hours) at altitude whereas for SAI only requires high payload mass ($\approx 10\,000\text{kg}$). For all but the Proteus aircraft, the total fuel capacity is close to $10\,000\text{kg}$ (the same as the optimal payload size suggested by J. McClellan et al. [56]). The to be designed aircraft will not need endurance but climbing with a heavy payload also requires a lot of fuel. As a result, these aircraft are not directly usable for SAI when their fuel capacity is replaced by aerosol.

7.2.4. Existing Tanker/Bomber Aircraft

Tanker & bomber aircraft have very similar mission profiles to Ceres. They climb with heavy payload (tanker fuel or missiles), deposit the payload and descend back down for the next mission. This could make tanker aircraft good reference designs for Ceres. Abundant refuelling aircraft exist and many of them are based on regular commercial aeroplanes whilst others are specifically designed as tankers. The payload (including fuel) masses of these aircraft vary depending on their size and size of aircraft they service. The service ceilings of these refuelling tankers are all not as high as the required $20\,000\text{m}$ aerosol injection altitude.

An aircraft with payload mass $\approx 10\,000\text{kg}$ is needed, which only leaves some smaller military aircraft capable of carrying bombs and in some cases also refuelling. Larger aeroplanes in this category are usually purely tanker aircraft but do not fly as high as these military aircraft. One drawback of these smaller military bombers/tankers that can also fly rather high ($\geq 40\,000\text{ft}$), is that they are built for combat and not for the most efficient climb to altitude, which Ceres does need to be. In order to make these aircraft fast enough, they are equipped with high thrust engines which are not the most efficient. This does help to increase the service ceiling. The following aircraft are possible reference aircraft with enough payload capacity but still too low service altitude.

- McDonnell Douglas F/A-18 Hornet
- Lockheed S-3 Viking
- LTV A-7 Corsair II
- Vickers Valiant
- Blackburn Buccaneer

In order to adapt the payload size and service altitude to the values needed for Ceres, the flight performance characteristics need to be adjusted. This will probably include changes to the propulsion system, aerodynamics and wing geometry, whilst the payload placement needs to be reconsidered too.

7.2.5. Alternatives

Rockets were investigated too by J. McClellan et al. as a means to inject aerosols into the stratosphere [56]. Based on their estimation this method would cost close to one thousand times as much as regular aircraft making it unfeasible.

Another researched alternative is to use guns to shoot shells with 70kg of aerosol which is released in the stratosphere. This method would cost roughly 140 times as much as the aircraft and HLA based systems would. The cost of the method using guns does scale quite closely with a bigger or smaller amount of injected aerosol. Still it cannot be considered a close competitor to Ceres.

7.3. Market Share Analysis

Geo-engineering methods like SAI are a relatively young branch of engineering. As of now not a lot of companies and governments have invested in it on a larger scale. The total scale of the SAI system considered is defined by its requirement of 3Tg/yr . Based on the requirement and fleet size, a financial scale in the order of magnitude $\text{€}50\text{B}$ (development, manufacturing and operating cost) is required. However, a cost analysis conducted during the design phase resulted in a required budget of close to a $\text{€}100\text{B}$ for the full 15 years of operation. This is based on a fleet of 180 operational aircraft, which will be elaborated on in later sections of this report. Again it is emphasised that the Ceres system is by no means a solution to greenhouse gas emissions. However, in the case that the emissions and climate change get to a critical point, a fleet of newly designed aircraft will be the better option compared to the alternatives. In the additional years won by SAI,

emissions should be further reduced. In recent times the focus to counter global warming is larger than ever, for example, the UN proposed a global approach to oppose this problem [95]. Over the last 6 years, the EU spent more than 1 billion euros on the climate, and it is increasing its budget for climate change year by year and has a target of spending 25 % of their total expenditure on climate objectives [24]. Larger amounts of money invested in climate come from countries' individual investments. For example, a country as small as the Netherlands reserved 4 billion euros on economic and environmental affairs in 2019, while the USA have spent 40 billion USD on energy and environment in 2015¹[97]. This indicates that there is a market for large-scale projects like SAI in the case of catastrophic changes in the environment. In this market a full share can be obtained by Ceres. As of now, no other large-scale geo-engineering projects are ongoing and Ceres aims at completely filling up this market in the scenario where it is required. When the system goes into development it is likely to be the only one in its class and thus would obtain the full market share. Since the project takes such extensive funding and development, it is highly unlikely that another similar system will be developed once Ceres is operating. Thus, it is most likely that only one system will be operating, though the size of the system can differ by the given requirements.

7.4. Market Segmentation

Market segmentation was done to get a better indication of what different groups of potential customers exist. For SAI, the market can be split up in two buyer groups: individual countries and larger international organisations. Individual countries would want SAI to counter the adverse effects of global warming within their own borders while GHG emissions are being reduced. World-leading nations can provide a large enough budget on just one project, thus e.g. USA, Russia, the UK or Germany can be seen as potential customers. However, climate change happens on a global scale, so cooperation between countries can be expected. Potential international organisations which would be interested in this system are the EU and UN since further global warming can cause even greater adverse effects on the environment, possibly resulting in political instability, which both organisations want to avoid. In the end, both groups have minimising the effect of climate change as their main goal and since it is likely that both groups will provide around the same amount of funding, they can be approached as one marketing group.

7.5. SWOT Analysis

In order to evaluate the potential success of designing a new SAI system, its internal (strengths and weaknesses) and external (opportunities and threats) aspects were compared with the present market below and summarised in Table 7.1. Based on analysis of the current market, one can conclude that new aircraft offer the strongest prospect of being a successful SAI platform.

The strengths of applying aircraft to inject aerosols are primarily the cost-effectiveness and the wide range of possible reference designs. When a new SAI system needs to be designed, aircraft are likely to be the cheapest option based on the analysis from McClellan et al. [56]. Moreover, data from many reference aircraft is available to aid in the design process.

Potential weaknesses may include the magnitude of the effect of SAI. As mentioned in [32], 3 Mt of SO₂ injected will only decrease the solar flux by 0.22 %. Maintaining public support for SAI with this apparent small effectiveness may prove difficult. Even if this 0.22 % does have a significant impact to counteract the global temperature increase, the public still needs to be convinced that investing in SAI is worthwhile.

Opportunities in the market of global warming include the public and political interest of countering this problem. As mentioned in Section 7.3, governments have large budgets available to oppose global warming. When it is shown that SAI is a cost-effective method to achieve that goal, financial support from governments could become available to fund the development and execution of the SAI system.

As mentioned earlier, the threat of public distrust in SAI needs to be prevented actively. This can be done by showing that small solar flux changes that can be achieved by SAI are still effective to oppose a global temperature increase. This can be complemented by education on geo-engineering and climate control which displays the goal and outcomes of such methods.

¹<https://www.rijksoverheid.nl/onderwerpen/prinsjesdag/miljoenennota-en-rijksbegroting>

Table 7.1: SWOT Diagram of a New SAI System

	Helpful	Harmful
Internal	Strengths	Weaknesses
	Many references Low cost	Small effect
External	Opportunities	Threats
	Political interest Financial support	Limited public support

7.6. Ceres Performance Comparison

With the current design and the issues faced during the process, Ceres can be compared more accurately to the closest competitor out of presently considered concepts for SAI. This competitor is the tethered balloon concept. This comparison is described in Table 7.2 based on the most important mission characteristics. The start-up time should not be neglected as an important factor considering that any SAI program may be cancelled after a few years. It is thus essential to have a concept that can be started up in the lowest amount of time.

Table 7.2: Performance Comparison of SAI Concepts

Characteristic	CERES		Tethered Balloon	
	Pros	Cons	Pros	Cons
Feasibility	Relies on Existing Technology	High Altitude	Easy Transportation	Tether Material
Cost	Low Initial Cost	High Operating Cost	Cheap Operation	-
Environmental Impact	Overall Minimised EI	Operations Emission	Low Operating Emission	-
Start up Time	High TRL	Production of Fleet	Low TRL	No Airports Needed
Market Share	No Current Competitors	Available References	No Proven Operating Competitor	No Reference Designs

Operations & Logistics Concept Description

The goals of Project Ceres greatly influence the operations and logistics concept. Two main goals are to disperse 0.2 Tg of aerosols after the first year and to disperse 3 Tg of aerosols each year from year fifteen onward. Other elements which influence the operations and logistics concept are the feasibility, technology readiness level, the initial costs, and optimal injection location.

This chapter elaborates on the operations and the logistics of Project Ceres. First, a description is given of the general operations, such as the number of flights per day, the fleet size over the years, and et cetera. Then the airports that are going to be used are shown. Finally, the ground operations are elaborated upon.

8.1. Description

Due to the constraint of 250 operational days per year, there will be five operational days per week. This leaves 10 additional off days, which are to be determined by each airport, based on local holidays. In order to maximise the use of the operational days, they will be as close to 24 hours as possible. In the two non-operational days, maintenance will be performed. The fleet size has a buffer of 10 %, in case immediate maintenance is necessary, or additional aircraft are necessary due to delays due to weather conditions. The two non-operational days are also used as an additional buffer in case there are more delays than can be caught up by using the reserve aircraft.

From Section 13.7, the maximum payload mass was determined to be 9.7 t. However, the requirement of 0.2 Tg SO_2 in year one can be met with less payload per aircraft. This results in a cycle time of 5.8 hours, including a flight time of 4.6 hours, a turnaround time of 1 hour, and taxiing of 0.2 hours. From this, it was determined that there are four flights on every operational day. This leaves room for small delays each day, while cancelled flights will be caught up by reserve planes or in the two buffer days. Departures and arrivals will be undertaken from the same airport. This will reduce the risk of the mission not being able to be executed in case one of the two airports in use is unavailable. In addition, operating from more airports will drive the costs up which is undesired since they are to be minimised.

From the operation plan and buffers required, a fleet size of twelve aircraft in year one was determined. In order to deliver the payload necessary in year fifteen, a total of 180 aircraft are necessary, including the spares. It is of utmost importance to keep the costs of the initial phase low, as there is a possibility that Project Ceres will be cancelled during this phase. Due to this, it was chosen that the fleet size will not be increased with the same amount every year. The first seven years, eight aircraft will be produced every year, whereas, from year eight, sixteen aircraft will be produced every year, resulting in 180 aircraft at the start of year fifteen. This requires a delivery interval of 1.5 months for the first 7 years and a delivery interval of 0.75 months from thereon. The decrease in the delivery interval is achieved by increasing the number of work shifts.

It was chosen that the aircraft should be manually controlled, as opposed to unmanned flight. This is because both the costs and certification are in favour of manned flight. While the total estimated costs for unmanned flight are significantly lower than that for manned flight, this does not consider the certification regulations. Furthermore, the costs at the start of operations are lower, 120 million dollars for crew training in the first year against 1 billion dollars for software development for the unmanned option. This is more important as it is essential to keep the initial costs low. Finally, the current technology readiness level of unmanned flight is not feasible for such a large-scale operation. Therefore, it was chosen to design the aircraft for manned flight.

8.2. Selected Airports

In the first year, the fleet is to operate from four airports, whereas in year fifteen, the fleet is to operate from eight airports. Several requirements constrained the location of the airports.

The fleet of aircraft has to be able to take off in 2500 m or less, based on a sea level equivalent. Only airports which have a runway length of 2500 m or more were selected, as to not further constraint the take-off length. Another requirement was that the payload must be delivered at the following latitudes: 30°N, 15°N, 15°S or 30°S. Due to this requirement, airports that were near these latitudes were selected. The chosen airports are listed in the Table 8.1. This table presents the location of the airport, ICAO identification code, latitudinal position and the runway length. The distance from the airport to the actual latitude is abridged during the climb phase, as during this part no payload is dispersed. This limits the cruise range necessary, and in turn reduces the fuel burn. Airports such as SBBR, GMAD, FNMO and HHAS do not have certified CAT II ILS systems. Depending on weather conditions these airports may need to be recertified in their CAT II ILS categories according to the Stakeholder requirements.

Table 8.1: List of Selected Airports and Corresponding Diversions

Airport	ICAO	Position [°]	Runway [m]	Distance to Delivery [km]	Alternate ICAO	Distance [km]
Houston	KIAH	29.8 N	2750	22.2	KHOU	37.19
Brasilia	SBBR	15.8 S	3200	88.8	SBGO	163.80
Agadir	GMAD	30.4 N	3200	44.4	GMMX	195.02
Namibe	FNMO	15.2 S	2500	22.2	FNUB	151.00
Durban	FALE	29.9 S	3700	11.1	FQMA	320.00
Asmara	HHAS	15.2 N	2500	22.2	HHMS	65.35
Hangzhou	ZSHC	30.3 N	3400	33.3	ZSPD	165.11
Perth	YPPH	32 S	3444	222	YPEA	30.49

In Figure 8.1, the geographical position of the airports are shown. As can be seen, the airports are relatively spaced out across the globe. This is done mostly because the dispersion of SO₂ must be maximised. The circles in Figure 8.1 show a range of 3750 km which is the maximum range for the aircraft. The range necessary for the mission is 3400 km. From this range, the diversion possibilities were identified in order to comply with the diversion requirements. The alternate ICAO identifications and the flight distance are shown in Table 8.1.

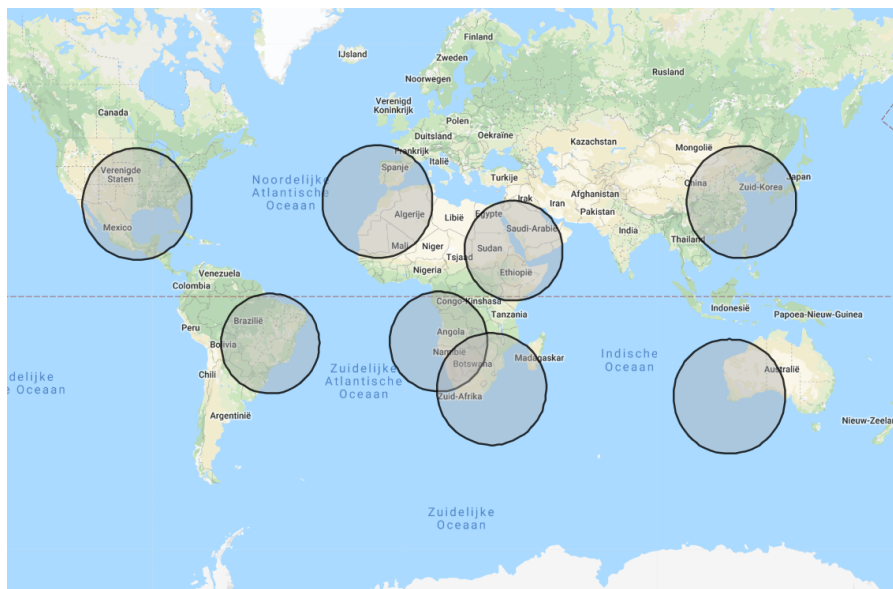


Figure 8.1: World Map of the Airport Locations, with the Achievable Range from each Airport.

The aircraft will first be operated from Asmara, Houston, Durban, and Brasilia in order to do a first assessment of the primary and secondary environmental impact of the entire Ceres system. Project Ceres will incorporate more airports when the fleet size at a single airport reaches 23, as this is deemed the maximum capacity per airport. This happens half-way through year 9, at this point the total fleet has 92 aircraft, just half-way of the eventual fleet size. The aircraft will be redistributed evenly across all eight airports, in order to keep the SO₂ distribution balanced as well. From thereon, the fleet size of each airport will increase until the goal of a 180 aircraft is reached.

8.3. Ground Handling and Logistics

The aircraft has a fuel mass of 13 479 kg as per Chapter 15. Aircraft refuelling will involve Jet A-1 fuels. These fuels are commonplace in current airport environments. Airport fuelling companies are compliant with AS5877 standard fuelling nozzles [63], as is the aircraft in this report. The consequence is such that no major changes in the airport infrastructure are required for fuelling of the aircraft for the Ceres Mission. Refuelling rates of up to 900 kg/min can be seen on airport premises, with averages around 650 kg/min. This means for 12 200 kg of fuel, a time span of roughly 19 minutes is required which combined with coupling and uncoupling extends to 25 minutes. Fuelling is done by the airport contracted company and is not up to the Ceres mission to plan personnel logistics. A schematic example of refuelling procedures is given in Fig. 8.2.

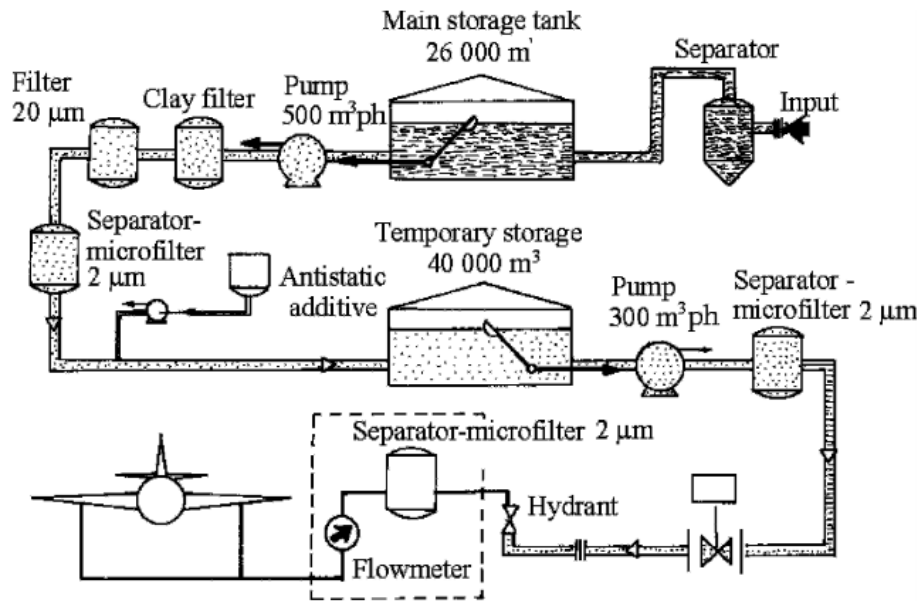


Figure 8.2: Example Schematic of the Fuelling System used in Paris-Charles de Gaulle Airport. [4]

A cargo mass of 9700 kg is chosen for the execution of the mission as per Section 13.7. Sulphur is taken on board in the form of sulphur pellets, and fed and liquefied for combustion within the sulphur dioxide burner as explained in Section 13.7. For this to be achieved, the aircraft must be loaded with sulphur on the airport premises.

The storage of sulphur occurs off-airport to reduce the impact of sulphur dust on airport personnel and aircraft corrosion due to hydrogen sulphide formation under the presence of humidity. These stockpiles of granular sulphur may be gathered and stored in an open environment, as is common practice in the sulphur granulation industry. Transport from stockpiles to silo conveyor belts is to occur with the means of wheel loaders, helping to keep the silos full at all times. Airport cleared, specialised sulphur pump trucks load the sulphur on-board by going underneath the silos and loading the necessary sulphur. The task of keeping the silo full as well as transporting the sulphur only requires one ground member.

The truck is specialised to allow for the pumping of sulphur from the truck tank onto the aircraft. The truck must be capable of pumping 9700 kg of sulphur in a similar time span as refuelling takes place. This requires a flow rate of 526.4 kg/min which combined with a pellet density around 1120 kg/m³ results in a flow rate of 0.47 m³/min. Pumps such as the Supavac SV280-V¹ are capable of pumping 0.5 m³/min. These pumps use the principle of under and over pressure to suck and pump material from a container into another container. The average sulphur flow speed is of 1.00 m/s, but due to the pumps suction and pumping cycles, this flow rates can double. The flow speed is kept low to reduce reinforcement in the tanks.

Once the truck arrives onto airport premises, the necessary security checks are performed. Once cleared, the truck goes towards the respective aircraft. The 100 mm coupling is attached to the aircraft and the

¹<https://www.supavac.com/products/sv280-v-heavy-duty-solids-pump/>

pumping begins. During refuelling and reloading, other actions may be performed which are relevant to the operation, such as crew changes, maintenance actions, and flight briefings. A representation of these procedures is given in Fig. 8.3.

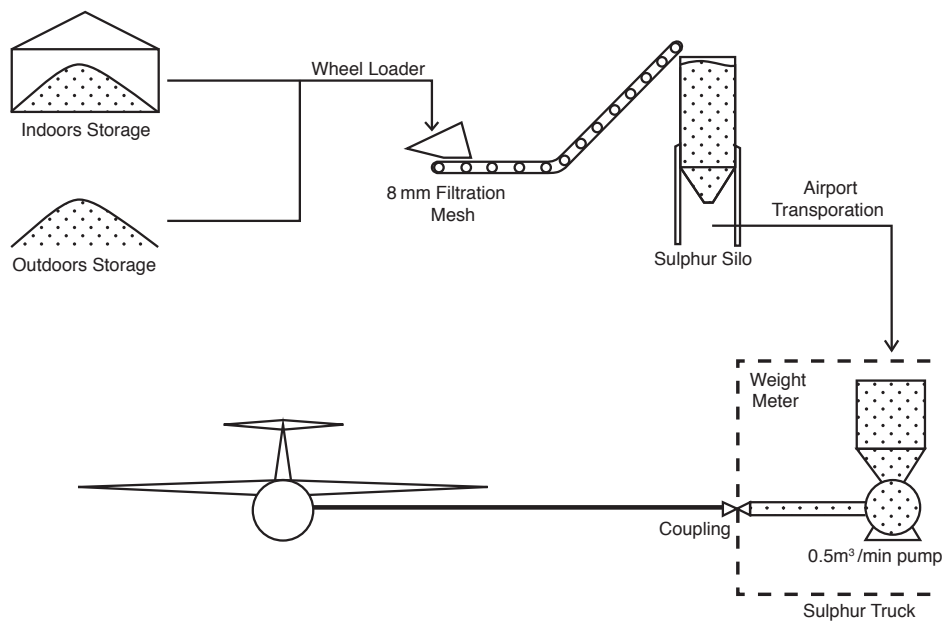


Figure 8.3: Diagram representing the Work Flow Necessary to get Sulphur Granules from Storage to the Aircraft.

For the operation to run smoothly it requires personnel on the ground delivering a steady flow of sulphur to the aircraft. Replenishment of sulphur into the silo requires an operator on the ground for the wheel loader. Additionally, the active maintenance and surveillance of sulphur storage and silo operation requires one more ground member. In addition, each truck delivering sulphur to the airport premises requires at least one driver. Assume each truck delivers an exact amount of payload to each aircraft. On the first year three aircraft will operate from four bases. Thus, at each base at least six ground personnel are required per shift. Assuming three shift per day of eight hours, then eighteen employed personnel are required. In the case two people are required per truck, then the total number goes to twenty-four employed people. In the fifteenth year, personnel requirements will go from 29 to 52 whether each truck is crewed by one or two employees respectively. In the case operations is well tailored, the requirement of one truck per aircraft can be reduced, as one truck will be able to attend different aircraft at different times. Additionally, the requirement of three people operating wheel loaders, silos and maintenance doubles due to the larger operation.

Sensitivity Analysis

In the Midterm Report [33], a sensitivity analysis was performed, which showed that the design will most likely be constraint by the thrust required, which was kept in mind during the design phase and mission profile design. During the design process, other drivers also became clear. In this design phase, there are still uncertainties in the models. The most important uncertainties which drive the design, are the uncertainty in OEW and the uncertainty in the thrust that the engines can deliver at altitude. Besides uncertainties from the design process, there are also uncertainties in the required mission profile. While the required cruise altitude was given to be 20 000 m, it might be that further research indicates that the optimal altitude for dispersion is actually higher. For further development of this project, it is interesting to determine how a change in altitude affects the design.

In this chapter, first, a summary is given of the possible error margins in the weight estimation methods, as well as the margin of the thrust values at altitude. Based on these values, as these uncertainties are driving for the design, a sensitivity analysis is conducted to see how they influence the feasibility of the design, characterised by MTOW, and the fuel weight. Aside from the feasibility and sustainability of Project Ceres, the cost is a very important factor. The sensitivity of the cost is analysed for uncertainties in the OEW and thrust deliverable at altitude, as well as payload mass per aircraft. This sensitivity analysis was performed after the design of the aircraft, and it is meant to show that this aircraft is still feasible and affordable if changes in the design or mission profile happen. Lastly, it will show how the cost and weight change if other cruising altitudes are required.

In Chapter 13, more in-depth sensitivity analyses are given for each subsystem, whereas this chapter focuses more on the sensitivity of the total system with respect to design drivers.

9.1. Uncertainty Margins

In this section, a brief overview is given of all the uncertainty margins in the current models, for the weight estimations and thrust and C_{D_0} estimation. Only these uncertainty margins are displayed here, as they have the largest impact on the design. In Chapter 13, each possible uncertainty margin is elaborated upon.

Table 9.1: Uncertainty Margins in Weight Estimations

Subsystem	Margin
Wing	$\pm 3.8\%$
Fuselage	$-11-1\%$
Tail	$\pm 10\%$
Landing gear	$+3-6\%$
Propulsion system	0%
Payload system	$\pm 30\%$

Table 9.2: Uncertainty Margins in Several Parameters

Parameter	Margin
Thrust per engine during cruise	3.93-4.51 [KN]
C_{D_0}	0.015-0.285 [-]

The uncertainty margins are shown in Table 9.1. As can be seen, the largest uncertainty margin is from the payload system, due to this being a modified version of an existing engine. However, the total weight of the payload system is relatively small, so it does not affect the design by that much. Furthermore, the weight estimation of the fuselage is shown to overestimate the weight. There is no uncertainty margin for the engines, as these are taken off the shelf, and their weights are already known. In the worst case scenario, the OEW would be 3.9% higher than estimated, according to the uncertainty margins. This number is on the low side, since the largest components of the aircraft have low to no uncertainty in weight estimation. Based on this number, and previously set contingencies[32], the safety margin for the OEW is set at 10%.

In Table 9.2, the uncertainty margins for C_{D_0} and the thrust per engine at cruise altitude are shown. The uncertainty margin in thrust is due to the uncertainty in spool speed. The uncertainty in C_{D_0} is due to differences in different estimation methods. For C_{D_0} , the most conservative method was chosen in order to size the aircraft, and it will still be feasible if the method turned out to be overly conservative. Furthermore, for the thrust, the lowest bound was taken as well. This bound is at a reduction in spool speed of 13 %. From this thrust with a lower spool speed, there still is a 9 % safety margin for the total thrust necessary.

This section has shown that even if the most important models were off by their maximum error, the aircraft can still perform the mission. The next section will show the effects on the design of these uncertainties.

9.2. Sensitivity of MTOW and Fuel Weight

Influence of OEW margin and altitude From Figure 9.1, it can be seen that both the MTOW and the fuel weight are very sensitive towards the error in OEW. Both MTOW and fuel weight show to increase exponentially with respect towards the uncertainty in OEW. This is due to the fact that if the OEW is underestimated, the OEW will increase, which will increase the drag, required lift, fuel weight, and so on, this will again increase the OEW, as e.g. larger wing surfaces are needed in order to provide enough lift. Eventually for the given mission and payload size, if the total weight estimation method is 10 % off, the OEW will increase with 39 %, the MTOW will increase with 24 %, and the fuel weight will increase with 21 %. This is due to the fact that the OEW needs to be reiterated again, until there are no discrepancies between the designs. This process is further elaborated upon in Section 13.4.

The fuel weight is also an indication of the total environmental impact of Project Ceres, as fuel burn is the largest contributor for this. Thus, Figure 9.1 also shows that for an increasing error in OEW, the environmental impact grows.

As high feasibility is one of the main design drivers, it is important that the design can undergo small corrections, without it being necessary to redesign the whole aircraft. And from this analysis, errors in OEW estimation can lead to large changes in design. Based on the previous section, a safety margin of 10 % is used, based on the aircraft with maximum payload and fuel. In Chapter 15, contingency management is elaborated upon in more detail.

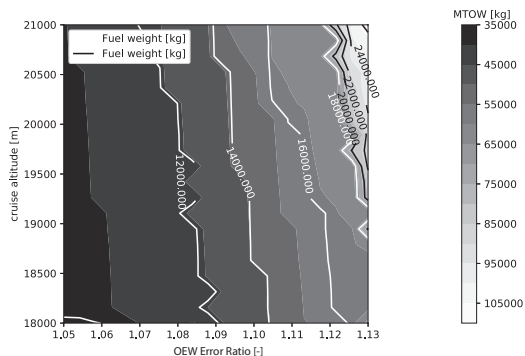


Figure 9.1: MTOW and Fuel Weight, versus Error in OEW and Altitude.

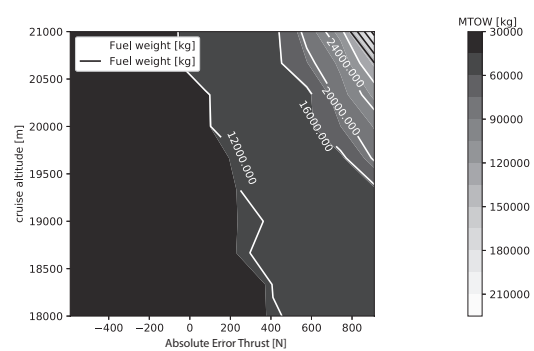


Figure 9.2: MTOW and Fuel Weight, versus Error in Thrust and Altitude.

Influence of thrust error and altitude From Figure 9.2, it can be seen that for an difference in thrust of smaller than 150 N, the MTOW and fuel weight stay relatively similar. This is clarified by the fact that there is a considerable margin in the thrust that can be delivered versus what is needed. Due to this, the number of engines stays the same for an error lower than roughly 150 N. However, for errors larger than this, the number of engines increases, and eventually for errors larger than 600 N, the MTOW diverges, as the increase in engines needed is not feasible. Figure 9.2 shows that while the calculated thrust at altitude is already conservative, it is still feasible until an error of 600 N per engine. If it turns out that the error is larger, then the engines need to be adjusted or new engines need to be selected.

The allowable error is variable with respect to the cruising altitude, as for certain altitudes, more engines are selected, which allows for a larger error per engine. For an error of larger than 600 N per engine, the

MTOW grows to an unacceptable extent, and it diverges for cruising altitudes of larger than 20.5 km. For even larger errors, the design diverges at lower altitudes. In Section 9.4, a more elaborate analysis of the influence of the cruise altitude is performed.

From this analysis, it was determined to use 6 EJ200 engines, instead of 4 F118 engines. 6 EJ200 engines weigh only 300 kg more, while providing more thrust. Next to this, the EJ200 is still being manufactured as well, and more data about it is available, making it the more feasible option. The lowest bound for the thrust value at 20 km is taken. With this lower bound, the aircraft is able to complete its mission with the thrust available at cruise altitude, up until a 7.5 % error. The engine selection will be more elaborated upon in Section 13.3.

Influence of C_{D_0} In Figure 9.6, the influence of C_{D_0} on the MTOW and fuel weight is shown. From this graph, it can be noted that having a lower C_{D_0} , would significantly reduce both the fuel weight and OEW. This is due to the large effect C_{D_0} has on both the thrust necessary and the fuel weight necessary. Due to the large influence of C_{D_0} on the design, the more conservative estimate of 0.285 is used for the design of the aircraft, in order to maximise the feasibility of the design.

9.3. Sensitivity of the Operational Cost and Total Cost

From Figure 9.3, it can be seen that as expected, both the operational and total costs increase with increasing OEW margin and altitude. From this it can also be seen that the total cost requirement is met at Ceres' design point. It was chosen to favour feasibility over costs, thus due to necessary margins, the cost requirement is just met. Increasing the safety margin even further than 10 %, will cause the costs to exceed the cost requirement. The relation with payload is even more complex. With more payload, the fleet size gets smaller, however, this is a discrete function. Another discrete function influenced by the payload mass is the number of engines. Both functions have a big influence on the cost, which is why the plot presents multiple kinks.

Similar results can be concluded from Figure 9.4. For larger errors in thrust, the costs increase. This is due to the fact the engines are the largest part of the acquisition cost and depreciation cost. Concluding from these plots, with the necessary margins, all cost requirements have been met.

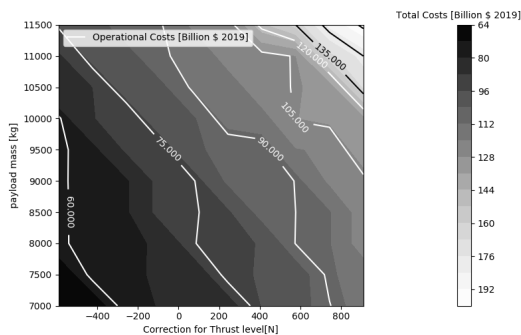


Figure 9.3: Total and Operational Costs, versus Error in OEW and Payload Mass.

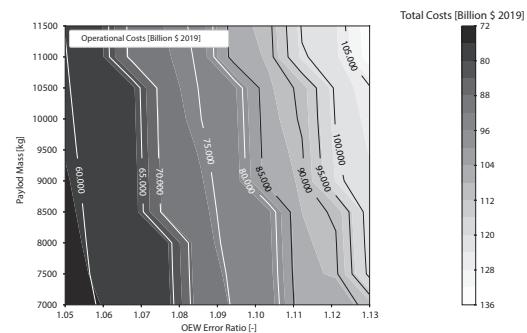


Figure 9.4: Total and Operational Costs, versus Error in Thrust and Payload Mass.

9.4. Sensitivity With Respect to Cruise Altitude

In this section, the sensitivity of the MTOW and the total cost are analysed for varying cruise altitude. From Figure 9.5, it can be seen that both the cost and the MTOW look like a step function. This is due to the number of engines needed to provide the necessary thrust. The range in altitude is taken as 18–21 km. 21 km is chosen as the upper limit, as this is the limit that would be possible to design for, based on the payload mass and required thrust levels, after this point, the MTOW diverges.

The design is still very feasible at 20 km, however, the number of engines, MTOW, and cost would reduce significantly if the cruise altitude were to be lowered by roughly 500 m. It is recommended that further research will be conducted about what the optimal dispersion height will be, as well as the effectiveness at lower altitudes. After this, a trade-off study can be made which compares flying at a lower altitude with

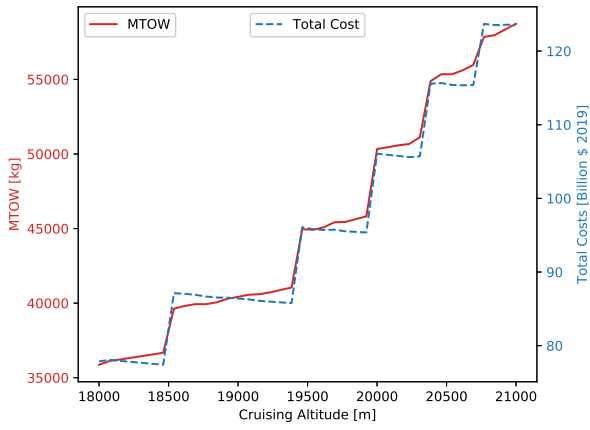


Figure 9.5: MTOW and Total Cost, versus Altitude.

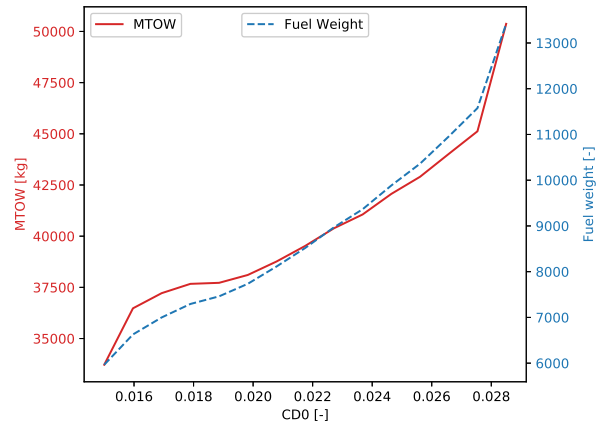


Figure 9.6: MTOW and Fuel Weight, versus C_{D0} .

more payload, versus flying at the optimal altitude with less payload. This way, the cost can be minimised.

Risk Assessment

This chapter identifies and ranks the risks that may occur in the development of Ceres. The risks are identified, assessed, analysed and handled. The scale of the consequences is discussed and visualised on a risk map.

The risks are categorised to project, system, and other risk assessment. Risks that affect the technical performance of the Ceres aircraft-based system are identified. Risks can be assessed based on their probability of occurrence and their consequences. Risks resulting in mission failure or the degradation in technical performance can be isolated by looking at the top-level requirements. Once the risks are assessed, a mitigation plan is conducted.

The consequences - catastrophic, critical, marginal, negligible - of the risks are defined in [68]. Additionally, the probability of occurrence is defined as frequent, reasonably probable, remote, extremely remote and extremely improbable and are defined qualitatively as: [53]

- Frequent - the risks is predicted to occur several times.
- Reasonably probable - during the entire cycle, the risks is anticipated to occur one or more times.
- Remote - the risks is an unlikely occurrence for individual aircraft but can occur several times in a fleet.
- Extremely remote - the risks is unlikely to occur during the entire operational time of the aircraft and fleet but still have to be considered possible.
- Extremely improbable - risks is not anticipated to happen during the entire lifetime of the aircraft and fleet.

10.1. Project Risks

The risks associated with the project are uniquely identified using **PTR**. In addition to affecting the technical performance of the project, the project risks also have a consequence on the project schedule because they will require an extensive reanalysis of the problem.

PTR1 When establishing interfaces between subsystems there is a likelihood of other subsystems failing or not meeting their own criteria: If the risk does occur, it can lead to mission failure as all subsystems need to run for the mission. This risk is very likely to happen as the design phase is done concurrently.

Mitigation: A data handling system can be established for the sharing of data with other departments. Hence, any interface done is based on the same parameters. Additionally, agreements can be made on the performance of the aircraft by establishing which subsystems are more crucial.

PTR2 Missing forces in the analysis of the structural characteristics: Improper analysis of the forces on the structure is catastrophic. For instance, not all failure modes are considered, and an aircraft can fail in these modes. However, this risk is unlikely as the forces an aircraft is subjected to can be extrapolated from existing flight designs.

Mitigation: All the forces applied to the structure are verified by other members in the team to ensure that no forces are missing. Moreover, the aircraft structural analysis can be checked in existing literature.

PTR3 Over simplification of calculations: This will have an impact on the technical performance as the aircraft can be under-designed. Simplifications and assumptions such as booms, using a gravity parameter of 9.81 m/s^2 at 20 km, and et cetera can result in a critical outcome of the design. However, the design of aircraft has been done numerous times and data can be extrapolated from existing flight

designs to ensure that the right equations are used so it is an unlikely event. This will affect the design choices such as the engines, payload weight and many more.

Mitigation: Similarly to PTR1, a data handling system can be established making sure that everyone uses the same set of equations. All assumptions and simplifications should also be documented. Furthermore, based on the level of simplifications and the design stage, appropriate safety factors are applied.

PTR4 Manufacturing and direct operating cost exceeds the specified amount: Exceeding the total costs can lead to a reduction in performance of the aircraft as some aspects of the aircraft need to be compromised. The effectiveness of the total project is influenced if the degradation of the performance leads to the aircraft being grounded. Without proper attention to costs, this can be a risk likely to occur. Even though it is not catastrophic for the total success of the mission, it can still be of critical influence.

Mitigation: Costs models have to be made as precise and detailed as possible and can be thoroughly validated and verified when finished. Further contingency values should be used during the design phase, such that a safety margin is present at all times with respect to the target value. When the budget is overshoot during the preliminary design phase, a redesign of the concept might be needed.

PTR5 Unstable gust response at 20 km: This risk is associated with the control and stability of the aircraft. If the stability of the aircraft is not considered properly at the altitude, stall is possible. This is catastrophic to the mission and it is reasonably probable to occur during the operational life of the aircraft.

Mitigation: Control and stability should be done properly. Verification and validation methods should be made to ensure that the aircraft is stable due to any response.

PTR6 Speed of aircraft falls below the stall limit / beyond the critical Mach number: The aircraft is cruising at high altitude and the margin of the minimum speed and maximum speed is narrow. If speed falls outside of the limits, stall can happen. This can lead to a catastrophic failure and likelihood is reasonably probable.

Mitigation: Speed analysis should be done properly for the project. Compromise on the design should also be done to ensure that the speed at which the cruise occurs is within the limits.

PTR7 Aeroelasticity: Due to the high aspect ratio of the wing, aeroelasticity can be a problem for the Ceres aircraft. At speeds within the flight envelope, the aircraft should not exhibit any static (torsional divergence) and dynamic (flutter) aeroelastic stability. The likelihood of this happening is reasonably probable and could be critical to the mission.

Mitigation: To mitigate torsional divergence, the wing should be reinforced and have a high enough stiffness so that the wing does not deflect under aerodynamic load which will result in the failure of the wing. Proper flutter analysis should be done with numerical simulation and wind tunnel testing. An initial analysis of the aeroelasticity was done in Section 13.2.3.

Table 10.1: Risk Map of the Project Risks Before Mitigation

Frequent			PTR1,PTR4	
Reasonably probable			PTR7	PTR2
Remote				PTR3, PTR5, PTR6
Extremely remote				
Extremely improbable				
Probability/ Consequences	Negligible	Marginal	Critical	Catastrophic

Table 10.2: Risk Map of the Project Risks After Mitigation

Frequent				
Reasonably probable				
Remote			PRT3, PRT4	
Extremely remote			PRT1, PTR5, PTR7	PRT2, PTR6
Extremely improbable				
Probability/ Consequences	Negligible	Marginal	Critical	Catastrophic

10.2. System Risks

The risks associated with the system are uniquely identified using **STR**. System risks also have a consequence on the costs and schedule because they have a direct correlation to the operating costs. Additionally, the failure of a component also delays the scheduling of the fleet.

STR1 Engine failure due to component failure: Engines that are used are most likely to be off-the-shelf engines, therefore, the occurrence can be extremely remote. The engines used are already implemented in existing airlines. The failure of the engine has a critical consequence as this can quickly escalate into a very complex situation. The severity is dependent on the number of engines.

Mitigation: To reduce the occurrence of this risk, each component of the engine and any interface with the engine should be analysed with great care. Any off-the-shelf engine used should have high reliability and must have been rigorously tested prior to use. A maintenance plan should also be devised. The best measures to avoid this risk are to use an off-the-shelf engine with high reliability and conduct regular maintenance.

STR2 Failure of injection system: The injection system is based on existing non-flight engineering data as the aircraft-based aerosol injection is not a widely researched topic. As such, the system has not been applied to any flight design yet. So, the occurrence is remote. The failure of the injection system has a marginal consequence as aircraft can return to base to repair the injection system. The risk will not result in failure of the mission.

Mitigation: This risk can be minimised by conducting a thorough R&D of the injection system. By performing validation and verification on the design the risk can further be reduced. By performing sufficient maintenance during operation, the likelihood of occurrence can be made marginal.

STR3 Failure of combustion system: The combustion system is based on existing non-flight engineering and it is applied on the aircraft-based aerosol injection system, the likelihood of the risk is remote. The risk has a critical severity on the mission because the aircraft is unable to perform the mission with a non-functional combustion system.

Mitigation: To minimise this risk, sufficient resources should be spent on maintenance of the combustion system during operations. Since the combustion system is still experimental, enough attention should be paid to the reliability at the start of operations to reduce the chances of failure.

STR4 Structures are unable to withstand extreme natural hazards: The most common natural hazards are thunderstorms (cumulonimbus clouds) which are associated with lightning, hail, and updrafts/downdrafts. It is a regular occurrence in the equatorial region; therefore, it is unavoidable. This risk is catastrophic as the fleet will be flying in the same region and the whole fleet will suffer the consequences of the thunderstorm if it is of unexpected magnitude.

Mitigation: Conventional aircraft also deal with the environmental factors, therefore enough information on the topic is available. By consulting weather forecasts the largest natural hazards can be avoided. Since the aircraft are designed for 250 operational days per year, on days with hazardous weather it can be decided to keep the aircraft grounded.

STR5 Leakage of sulphur due to material corrosion: Sulphur is the main payload of the aircraft hence it is important that the material must be compatible with the corrosive nature of sulphur. As a consequence of this risk, the degradation of the material of the payload holdings may result in a smaller

lifetime for the fleet which is thus critical. A thorough analysis of sulphur and the material should be done, as this occurrence is probable.

Mitigation: Avoidance of this risk can be done by performing research on the characteristics of sulphur to ensure the material used for the handling of the payload will be compatible with sulphur. The trade-off of the materials shall be done as the materials must comply with other requirements.

STR6 Fatigue failure: Majority of aircraft failures are linked to fatigue. The aircraft will need to be operational for a number of cycles and because of cyclic loading the aircraft will degrade due to fluctuating stress applied to it. The likelihood of this happening is remote as the fuselage is not pressurised, and the consequence is catastrophic.

Mitigation: Risk can be mitigated by scheduling frequent maintenance and inspection of the components of the aircraft that are subjected to cyclic loading. The fatigue failure mode should also be investigated in more depth.

STR7 Fuel leakage: Fuel leakage can happen due to an imperfection in the gas tank, or due to corrosion of the tank, or a factory defect, et cetera. This has a catastrophic consequence for the flight and subsequently, the mission due to fire or fuel tank explosion. The occurrence is remote as fuel leakage is common in the aviation industry and it usually goes unnoticed.

Mitigation: Fuel leakage can be prevented by having a proper maintenance plan and performing thorough inspection when the aircraft is on the ground. Materials for the fuel tank must be chosen wisely and any adverse reaction of the material and the fuel should also be researched.

STR8 Failure of an electrical component: The bus-bar is the central point for the distribution of the electrical power and failure of the electrical system could lead to a fire. Additionally, any short-circuited equipment can lead to electrical system failure. The likelihood of the risk happening is extremely remote but can lead to a critical situation.

Mitigation: If a fire is the resultant of the component failure, insulation should be properly installed with an appropriate fire extinguishing circuit, and redundancy should also be added. A secondary power system should also be applied into the aircraft system so that if the risk should occur critical components can still run.

STR9 Failure of instrumentation: Airspeed instrument failures originate from the slow icing over the pitot tube. Even with the heated pitot to prevent icing the contributions of the altitude, temperature and Mach at cruise prevent the melting of the ice which results in incorrect instrumentation values [65]. This is considered as a marginal consequence, as the situation can be avoided by not flying into icing conditions. Other instruments can fail, such as the HSI and ADI, but these instruments are usually backed-up with a zulu compass and standby ADI, respectively.

Mitigation: Risk mitigation has already been implemented by having heated pitot tubes. However, if risks do occur (which is likely), the pilot should be well informed of the risks of flying into known icing conditions and the certification status of the aircraft into known icing conditions. The pilot should generally aim to avoid any icing situations. Other instruments should be aided with a back-up, and basic standby instrumentation is required.

STR10 If operating speed of aircraft falls below the stall limit / beyond the critical Mach number: At high altitude, the stall speed is close to the minimum speed required for steady flight. If the speed falls below the stall limit, the aircraft will lose altitude and possibly drop a wing. This situation could easily deteriorate into a spin under wrong pilot inputs. Recovery could only occur by gaining airspeed, but this can prove to be difficult to tackle since there is also a constraint on the upper limit for the speed due to the critical Mach number limit. This is when the flow at some point on the airfoil is $M=1$. Beyond this point, the flow is separated and there is a formation of shockwaves. This will be catastrophic for the mission and the likelihood is reasonably probable.

Mitigation: Implementation of docile stall characteristics through an ample stall margin between the lifting surfaces and the balancing surfaces. Use of supercritical airfoils can reduce compressibility

effects during recovery. Stick-pusher systems may be required in the case docile stall characteristics cannot be achieved. Pilot training for abnormal situations may also be necessary.

STR11 Malfunctioning of control surfaces: The control surfaces are the ailerons, elevators and rudder. The malfunctioning of these control surfaces will lead to the degradation in the longitudinal and lateral controllability of the aircraft. This will be catastrophic especially at high-altitude and the likelihood of it occurring is remote.

Mitigation: The pilot can be trained to be aware of the situation and can be prepared on the recovery procedure if a control surface is not functioning.

STR12 Ignition of fuel vapour¹: Electrostatic charge build-up in the fuel can occur during refuelling and defueling and does not dissipate easily. The discharge of the electrostatic energy is capable of igniting the fuel vapour and can cause an explosion. This risk is catastrophic to the mission and the likelihood is reasonably probable.

Mitigation: Static dissipator additives can be added to the fuel to prevent any increase in conductivity during fuel handling. This will decrease the likelihood of the risk occurring.

STR13 Ineffective tail surface area: The Ceres aircraft will have a T-tail configuration. The risk associated with a T-tail is the possibility of a deep stall. At high angle of attack, the tail will be in the wake of the wing and therefore, the tail surface is ineffective. This can be catastrophic to the mission and the likelihood is remote as the aircraft will not be operating at high angle of attacks.

Mitigation: A stick-pusher system may be implemented to force a nose down motion to ensure that the T-tail does not enter a deep stall. Additionally, a stick-shaker can also be installed to warn the pilot of an impending stall. This will make the likelihood of the risk happening extremely remote.

STR14 One engine out: This is related to STR1 and is also overlapping with the project risks. A one engine out can originate from a component failure or even an object strike. This will influence on the yaw performance of the aircraft.

Mitigation: The design of the vertical tail and rudder deflection must accommodate for the most outward one engine out scenario. Pilot training should be done for this occurrence and the aircraft should also return to base.

STR15 Improper loading of sulphur and fuel: The improper loading of sulphur and the fuel could lead to a shift in the location of the centre of gravity. This will have an influence on the take-off and cruise performance as wrong settings will be used by the pilot. The likelihood is reasonably probable, and the consequence is critical as this might result in the aircraft stalling.

Mitigation: Ground handling should be improved for the loading of the payload and during refuelling to prevent the risk of the likelihood from happening. To warn the pilot of any impending stall condition, stall warning should also be installed.

Table 10.3: Risk Map of the System Risks Before Mitigation

Frequent				
Reasonably probable		STR9	STR2,STR3,STR5, STR15	STR1, STR12
Remote			STR14	STR4,STR6, STR7, STR10, STR11, STR13
Extremely remote			STR8	
Extremely improbable				
Probability/ Consequences	Negligible	Marginal	Critical	Catastrophic

¹ https://www.skybrary.aero/index.php/Refuelling_and_Defuelling_Risks

Table 10.4: Risk Map of the System Risks After Mitigation

Frequent				
Reasonably probable				
Remote		STR11		
Extremely remote	STR9	STR2, STR5, STR14, STR15	STR3,STR7	STR1, STR6, STR10, STR12, STR13
Extremely improbable	STR8		STR4	
Probability/ Consequences	Negligible	Marginal	Critical	Catastrophic

10.3. Other Risks

The risks associated with the project will be uniquely identified using **OTR**.

OTR1 Ceres is not marketed properly: Stratospheric aerosol injection is a geo-engineering method to limit the extremes of temperature. It is, however, not a solution to solve the growing issue of global warming and Ceres is not by any means a viable solution to combat the problem of increasing greenhouse gases. Aerosol injection is analogous to the emission of sulphur dioxide from a volcanic eruption which has a global cooling effect. However, due to the injection around the equator, there will be a more extreme temperature in the northern and southern hemisphere which can potentially accelerate the melting of the ice caps.[52] This risk is very likely to happen, and it has a marginal effect on the mission.

Mitigation: To make the concept of Ceres more approachable for the general public as an emergency measure in the case that the attempts of reducing GHG fail, extra resources could be spent on the marketing of the project. Additionally, in the marketing of Ceres, it should be stressed that SAI is not a solution and commencing of the project will only be considered if actions to limit GHGs evolved to be less fortunate than anticipated.

OTR2 Net CO₂ emission causes temperature rise: To inject a sufficient amount of sulphur dioxide into the stratosphere on an annual base, a large fleet of aircraft has to be constructed. The manufacturing and operating of such fleet results in an addition of the CO₂ emissions. Next to the fleet, there is also a scenario where new airports could be built. Such a process results in significant CO₂ emissions. As a result, it could be the case that the net CO₂ emissions turn out to be playing a larger role on the temperature increase than the injected SO₂ counters it. Considering the attention to sustainability in the design phase, the chance of positive net emissions is extremely remote. However, it will be catastrophic for the operations. Since a positive net emission defies the purpose of Ceres.

Mitigation: This risk can be minimised by appointing a sustainability officer in each phase of the design to assess the environmental influence of the specific design choices. During the assessment, the environmental aspects can get priority over the aircraft performance regarding certain design choices. An example of this could be to not build new airports due to emission reasons, and instead choosing for slightly less efficient aircraft design, such that net emissions are positive.

OTR3 Does not get approval from airports around latitudes: The injection of SO₂ is most effective when injected into ± 15 and ± 30 degrees latitude. The number of airports located close to these parallels is limited. As a result, it is important that Ceres gets approval for operating on the airports that are selected. Otherwise, aircraft located further from the parallels must be chosen. However, this requires a longer aircraft range and is thus undesired.

Mitigation: A method by which this risk is completely mitigated is constructing airports purely for Ceres. However, this can only be done if it is feasible from both an economical and environmental aspect, which is highly unlikely. To get approval from existing airports, Ceres must compete with conventional cargo and transport aircraft, which can pose some difficulties. A way to prevent this is by making sure that Ceres is an international collaboration between countries. When multiple countries are involved it is more likely that the aircraft will get permission to land and operate on the selected airports due to political reasons.

OTR4 Adverse effect of SAI on the ozone: It has been theoretically and numerically proven that a large quantities of sulphate aerosol injected in stratosphere can accelerate the hydroxyl catalysed ozone

destruction cycles[64]. This results in a significant depletion of the ozone. Moreover, there are many more uncertainties in the response of climate change to SAI. Other potential consequences of stratospheric aerosol injection are the melting sea ice, food depletion in the tropics, increase in the rate of sea level rise etc. This risk is reasonably probable to happen and is catastrophic.

Mitigation: According to [64], both the amount of sulphate aerosol and the dispersion rate influence the effect of SAI on the ozone. A more accurate climate model should be constructed to obtain the optimal payload dispersion strategy to minimise the aforementioned effects.

OTR5 Ceres has a smaller effect than expected: As of now, the effect of Ceres is only estimated with existing models. From volcanic activity, the effect of Ceres can be approximated. However, this is not completely comparable since the composition of the gases and emitted altitude differ largely from one another. If Ceres turns out to have a smaller effect than expected after the first few operating years, it is unlikely that the project will be put to a complete stop.

Mitigation: By constructing detailed models of the atmosphere and looking at the effect of SO₂ after volcanic activity. The effect of SO₂ can be determined as accurately as possible, which will prevent a smaller effect than expected from happening.

OTR6 Delay in production: From Chapter 8, the delivery interval for the first 7 years of operation is set to 1.5 months and from there on the delivery interval is set to 0.75 months. These were determined to comply with the requirement of delivering 3 Tg of SO₂ to an altitude of 20 km. With the delay in production, it will have a direct impact on the delivery time, thus the mission. The consequence is critical, and the probability of likelihood is remote.

Mitigation: By having the same workers performing the same task in the assembly line, the workers will gain experience, therefore, the effort and time needed for the task will decrease. With this tactic, the delay in production can be mitigated. Additionally, more workers can also be employed. Having spares of the aircraft is also beneficial and will make the consequence of the risk marginal.

OTR7 Moral hazards: Actions should be implemented to reduce the emission of greenhouse gases. The introduction of project Ceres could lead to wrong assumptions that it could be a solution to global warming. As a consequences, any effort of reducing greenhouse gases will stop, therefore, the culprit of climate change is not eliminated. The risk of it happening is reasonably probable and it is catastrophic.

Mitigation: The consequences of the project Ceres should be emphasised to the public to reduce the likelihood of this risk. The mitigation of this risk is also related to the mitigation of OTR1.

Table 10.5: Risk Map of the Other Risks Before Mitigation

Frequent		OTR1		
Reasonably probable			OTR8	OTR2, OTR7
Remote		OTR5	OTR3,OTR6	
Extremely remote				OTR4
Extremely improbable				
Probability/ Consequences	Negligible	Marginal	Critical	Catastrophic

Table 10.6: Risk Map of the Other Risks After Mitigation

Frequent				
Reasonably probable				
Remote	OTR1			
Extremely remote		OTR3,OTR5,OTR6		OTR2,OTR7
Extremely improbable				OTR4
Probability/ Consequences	Negligible	Marginal	Critical	Catastrophic

II

Final Design

Part Introduction

In this part, the reader will be walked through the various design steps which were taken in this Design Synthesis Exercise. First, the technical requirements to which the aircraft must comply to will be presented. These will enable to identify key design drivers. In order to converge towards a final design, the various explored concepts are presented. For each of the concepts, an initial sizing is conducted. From this, it is then possible to assess and quantify various performance parameters. Building on these latter numbers, a trade off has been performed whose results are presented below.

In a second phase, the preliminary sizing as well as the Class II sizing was conducted. The various methods used in this step will be presented with particular attention paid to the sections of the models used which were identified as design drivers. The emphasis of this report is put on methodology and reproducibility of results. This is stressed by the verification and validation which is integrated throughout the design process.

Finally, a sensitivity analysis of the various design parameters has been conducted which provides an additional degree of understanding of the effect of design parameters on the aircraft characteristics. This is concluded by a detailed description of the design of the Ceres aircraft, its dimensions and various notable properties and characteristics.

11

Verification and Validation Procedures

In this chapter, the verification and validation procedures are presented. Section 11.1, discusses the general procedure for verification of models. Similarly, Section 11.2 shows the same procedure for validation. Finally, the closing section shows the how verification and validation was integrated in the development and use of the models. For further details, in Chapter 13, the verification and validation of each model is reported upon in their respective section.

11.1. Verification

Verification is a key part of the development of models as it determines that ability of a model to reliably give results according to inputs. Moreover, this enables to then conduct validation which assesses the ability of a model to predict behaviour and represent reality. For both of these steps, it is necessary to determine which parts of the code should be verified and validated as well as which parameters. The latter is the most difficult to determine as it requires to find available information on potentially sensitive topics or some parameters are not directly measurable in reality. Not all models can be verified using the same tests. Thus, how each model was verified is presented throughout the design chapter of this report, Chapter 13, whereas this chapter elaborates on the general procedures.

11.1.1. Code Verification

The code verification was greatly facilitated with the use of an IDE for python 3.X which was used by the group. This enabled to prevent simple syntax errors and typing errors. This was combined by a cross checking method in which two members would check each others code, neither knowing about the topic of the model of the other. This time consuming step forced the creator of the model to document well their code as it is then necessary to explain where the relations came from or how certain derivations are done. This enabled the other person to then check the relations for typos or logical errors. Lastly, this method also had the benefit of allowing group members to have more overview on the project and the tasks at hand.

This error checking was complemented with the full integration of verification and version control using GitHub and Travis CI. This, however, will be detailed in Section 11.3.

11.1.2. Errors and Discrepancies

The errors and discrepancies were quantified and assessed when possible. Discrepancies were allowed to be within 5% when the models were documented with very high uncertainties. Otherwise, the error was not allowed to go above a 1% threshold. If it happened, the model was put to be read by another group member and if the error was still present then the model was changed to another model which was either more documented or could give consistent results.

11.2. Validation

This part was particularly difficult since data for aircraft which satisfy similar missions are rare if not non-existent. As a result, a key part of validation was to assess first the applicability of the model and second if it could predict the behaviour of other aircraft reliably. Since most of the models used apply to transport aircraft or are based on semi-empirical models, the first aspect was difficult to determine and relied on validating the outputs for a range of various aircraft which had similarities to the Ceres aircraft. These aircraft were mostly airlines as data is more widely available, ranging from the A320 to the Boeing 747. Other aircraft with high altitude capabilities were also used such as the U-2. In Chapter 18, it is outlined how validation which was outside the scope of DSE should be handled.

Handling of Errors The way in which errors were handled was considered on a case by case for the models. According to the level of detail of the model various levels of discrepancies were allowed. These values can be found in Section 15.1. If the model exceeded these values, either a new model was taken or the uncertainty was explicitly taken throughout the design to assess the level of uncertainty. This was also accompanied by taking a conservative estimate for the said parameter so that performance requirements could be met.

11.3. Integration of Verification and Validation

For models which only have a small influence on the design, and models that are very simplistic, the tools explained in Section 11.1 were deemed sufficient. However, for more complicated models and models for parameters that have a very large influence on the design, extra verification tools were used. Both unit tests and system tests were utilised. More system tests were used however, as errors that are usually detected by unit tests, were in Ceres' case already detected with the tools from Section 11.1. System tests encapture multiple models and check if the endresult is correct. Tests were made in python, by comparing the outcomes of the system, with more simplified models, or models which were verified in an earlier stage.

Github is used as a form of version control and synchronisation tool. Tests are always performed when someone pushes a new commit to Github, due to the implementation of Travis CI. Travis CI is a hosted continuous integration system, which installs the module of project Ceres as found on Github, and runs the code on a virtual machine. This also runs the tests, and Travis CI then returns a 'build passing' or a 'build failing', depending on whether the tests were passed or not. Next to this, Github was also integrated with Coveralls. This program reports the percentage of code which has been covered by tests, broken down for each folder, to each individual file. With this program, it is also possible to see exactly which lines in each file were covered and which were not.

At this moment, the build is passing, with a coverage of 59%. The coverage is not particularly high, however this is due to a variety of reason. Firstly, there are several old models, which are not used anymore and not tested as well, which drive down the coverage percentage. Secondly, several models were deliberately not tested in this manner as stated before, due to their simplicity and relatively low importance. Lastly, several tests that were conducted as mentioned in Chapter 13, were not implemented in the pytest. This is recommended to be done in the next design phase, as well as adding more tests.

A total of 112 models have been made, excluding sensitivity models and plotting tools. Of those 112 models, 32 have not been tested, due to the aforementioned reasons. The amount of lines committed over time can be seen in Figure 11.1. Several large models have been imported, such as SUAVE and DATCOM, which explains the large amount of lines committed. excluding DATCOM and SUAVE, the code consists of a total of 5901 relevant lines (i.e. without white lines). Models were categorised into their respective discipline, such as aerodynamics, or weight estimations etc. For each discipline their respective coverage is shown in Figure 11.2.

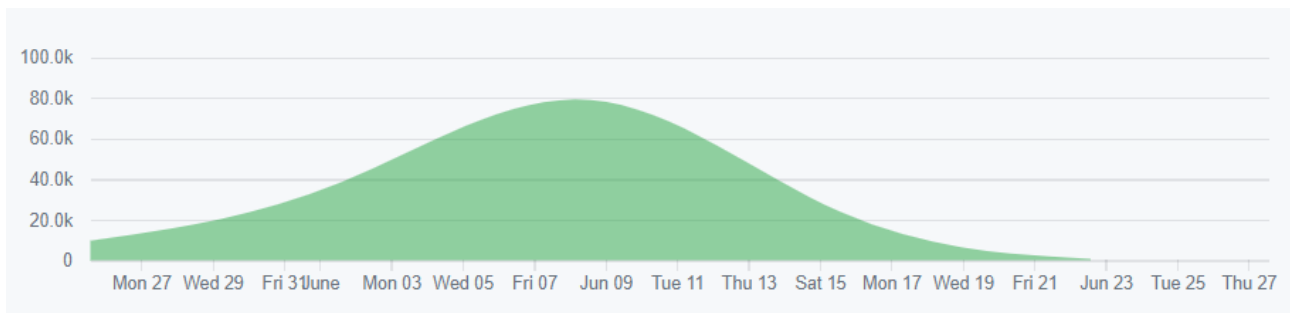


Figure 11.1: Total lines committed since the Midterm.

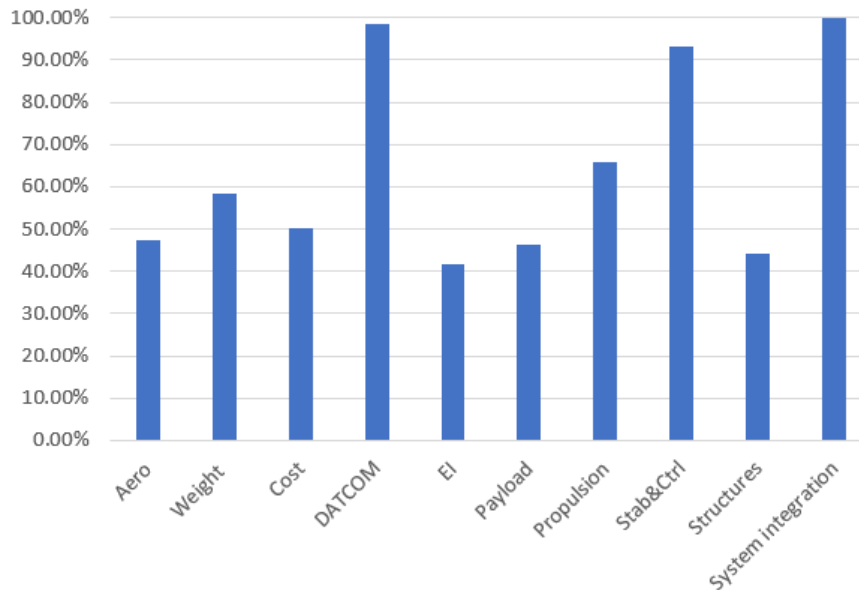


Figure 11.2: Coverage percentage of each model.

11.4. Results Discussion

All departments have successfully verified their computational models. A majority of the models has been verified by means of inspection and examining the trends. Aside from inspection other comparable models were used for comparison.

As for validation, most programs have been validated using the input data of reference aircraft. This resulted into discrepancies of a maximum of 10%, which can be argued by the assumptions of the model.

However, some departments did not manage to completely validate their programs. The validation of the eigenmotions and derivatives by the stability & control department was still beyond the scope of this report. Furthermore, no engine reference data was available, hence the propulsion department was not able to validate their models.

Trade Off of Concepts

The Trade-off of the possible concepts was performed in two stages. An initial qualitative trade-off was performed for four concepts as discussed in Section 12.1. Out of this trade-off two concepts remain which have been further investigated in more detail. Based on this detailed concept exploration a quantitative trade-off could be performed as described in Section 12.2. This resulted in one final concept which was designed as reported in Chapter 13 and discussed throughout this report.

12.1. Initial Trade Off

The following four design concepts were considered in the initial qualitative trade-off. This trade-off was performed in order to disqualify any concepts which are unfeasible before a detailed quantitative study on the remaining concepts can be performed.

Concept 1: A conventional wing layout with a conventional fuselage flying at subsonic speeds.

Concept 2: A conventional wing layout with a conventional fuselage flying at supersonic speeds.

Concept 3: A tandem configuration with a conventional fuselage layout.

Concept 4: A flying wing or blended wing body concept.

12.1.1. Trade Criteria & Weights

A trade-off was performed for the different concepts. The criteria and their associated weights, which are used for the trade-off, are listed below.

- Performance (8)
- Technology readiness level (TRL) (5)
- Research and development costs (4)
- Acquisition costs (3)
- Availability of models (3)

A heavy weight must be applied to performance as it is associated with the aircraft's ability to fulfil the mission. The aircraft must be able to reach an altitude of 20 km for the injection of aerosols, which requires optimal performance in cruise conditions at this altitude. Based on the reference aircraft of each concept, a preliminary qualitative analysis was conducted on its aerodynamic performance, structural performance etc. A weight of 8 is assigned to performance.

There is a correlation between performance and technology readiness level. The maturity of technology is achieved when a concept is proven through a series of successful missions. Additionally, to limit the occurrence of risks, the concept chosen should have a high TRL. Thus, a weight of 5 is given to TRL.

R&D costs are also important as those revolve around the conceptual, preliminary and detailed design. Specifically for Ceres, cost is a driving requirement, the R&D costs in particular. There is a possibility that Ceres can come to an abrupt stop due to any possible adverse climate feedback, so minimising the development cost is preferred. A weight of 5 is selected for R&D costs. Furthermore, acquisition cost is also listed as one of the criteria and takes into account the manufacturing cost. It is given a weight of 3.

Lastly, the availability of models is also given a weight of 3. With existing models of each concept, preliminary parameters can be used for sizing and verification purposes. Existing empirical models also help in weighing the 'availability of models' criterion.

All concept aspects were graded from 1 to 7, 1 being unacceptable and 7 being excellent. For this purpose, it is necessary to define what is 'unacceptable' and what is 'excellent' for each criterion. Firstly, performance is defined 'unacceptable' when a concept is virtually unable to fulfil the mission or its design is driven to the extent that it becomes unreasonable. Subsequently, 'excellent' performance means the con-

cept is able to perfectly fulfil the mission and has been done previously and proven to be successful as well as providing great opportunities for optimisation regarding environmental impact and costs.

The performance also takes into account the aerodynamic, structural, controllability and stability capabilities of the concepts. The conventional subsonic aircraft was given a score of 5 due to its proven performance in the current aviation industry. The ambiguity of its performance at 20 km resulted in a lower score than 'excellent'. Some supersonic conventional aircraft are able to cruise at 20 km but the behaviour of the injection system in the supersonic regime is not reliable. In addition noise and structural considerations lead to a score of 4. The tandem wing configuration has demonstrated excellent performance at high altitude but its performance specific to the mission is debatable which justifies the score of 5. The flying wing extremely lacks in stability and this poses a threat for the project leading to a score of 4.

The grading for the TRL is defined using ESA's TRL Handbook [96]. An excellent TRL is defined by ESA as the system being flight-proven through successful mission operations. On the contrary, an unacceptable TRL refers to a system for which only the basic principles are observed and reported.

A TRL score of 2 is given to the flying wing concept because it is proven feasible in theory but the implementation of the concept for a high-altitude mission is not found. Moreover, the found reference aircraft were outdated. A 6 is given to subsonic, supersonic and tandem wing aircraft because the configurations have shown their technology readiness. However, they have only demonstrated their capabilities and not been implemented in a mission operation similar to Ceres where high altitudes are reached.

R&D costs are deemed unacceptable when they exceed the budget as provided by the requirements and drive the design of Ceres to an unreasonable extent. R&D costs are favourable when low, implying little research and development time, which fit the mission background. Excellent acquisition costs indicate the costs being well within the budget as provided by the requirements, leaving sufficient margin for unforeseen costs. In contrast, unacceptable acquisition costs exceed the provided budget and drive the design to an unacceptable extent.

The conventional subsonic concept receives a score of 6 for R&D and acquisition costs because it is a widely known concept so R&D costs are low and subsequently, so are acquisition costs. The supersonic variant receives a lower score of 2 due to the complex nature of flying at supersonic speeds and the issues associated with it. Additionally, aerodynamic and propulsion design is complex resulting in a higher overall cost. The tandem wing is a modification of the conventional subsonic aircraft with an inclusion of an oversized canard thus the acquisition cost is low. However, there is still ample development needed to be done to ensure that the concept is feasible. Thus, a score of 4 is given for R&D costs and 5 for acquisition costs. A score of 2 is given to flying wing for both costs because the concept has not matured and there is still ongoing research and development on the concept.

The availability of models is defined as unacceptable when no models or literature on the concept are available at all. While excellent availability of models is defined as an extensive amount of accurate empirical relationships and literature available to the public. The available models should be of similarly sized aircraft with a similar mission altitude.

A grade of 5 is given to the conventional subsonic aircraft. There is literature on the initial sizing of the configuration and can be used for the further development of the concept. However, the majority of the existing aircraft under the conventional subsonic category lack the potential of flying at high altitude. The conventional supersonic concept receives a score of 4 due to the deviation of the estimation method compared to the conventional subsonic aircraft. Most conventional supersonic configurations do fly at an acceptable mission altitude but compared to conventional subsonic aircraft, available models are not as abundant. The flying wing receives a 1 due to the scarcity of existing configurations. A 4 is given to the tandem wing because methods used for conventional subsonic aircraft can be adapted with the addition of an oversized canard.

Based on the grading system of 1-7, the concepts are assessed and the scores are given in Table 12.1. The total score of each concept is calculated by multiplying the grades by the weight of the criterion and summing them.

Table 12.1: Trade-off of Concepts

Criterion Concept	Performance (8)	Acquisition Cost (3)	R&D Cost (4)	TRL (5)	Availability of Models (3)	Score (166)
Conventional Subsonic	Current standards (5)	Widely known (6)	Widely known (6)	Near proven (6)	Decent (5)	127
Conventional Supersonic	Large fuel consumption (4)	Complex (2)	Complex (2)	Near proven (6)	Lacking (4)	88
Tandem Wing	Good, but requires refinement (5)	Stability design (5)	Stability design (4)	Near proven (6)	Adapt known methods (4)	113
Flying Wing	Lacks stability (4)	immature concept (2)	immature concept (2)	Feasible in theory (2)	Scarce (1)	59



Based on the scores, it is apparent that the conventional supersonic aircraft and flying wing are not attainable concepts for Ceres. For that reason, these concepts are not discussed further for Ceres. This leaves the conventional subsonic aircraft and the tandem wing aircraft for the quantitative trade-off.

12.2. Quantitative Trade Off

This section describes the quantitative trade-off. First, an overview of the concepts to be traded off is given. Then a trade-off method is chosen and specified and finally the concepts are traded off.

12.2.1. Evaluated Concept Description

The designs to be evaluated in the quantitative section have been selected in Table 12.1. The two design concepts that are evaluated are the conventional subsonic and the tandem wing aircraft.

The conventional design consists of a highly loaded main wing with a tail section for stability purposes. This concentration of lift helps to achieve a very efficient wing, as it is not significantly influenced by other elements, apart from the wing-fuselage intersection. The ability to add high lift devices if necessary helps making the aircraft more controllable. The tandem wing design consists of two loaded wings, with a higher loading on the front wing. This spread out distribution has the possibility for performing with higher apparent aspect ratios compared to a conventional wing. A tandem wing aircraft has the probability of having high lift devices at the expense of weight, and being very front wing lift limited. A docile nose down stall occurs, which is an advantageous trait in the cruise condition, whilst having the probability of being dangerous at low altitudes when operating at high values of C_L .

12.2.2. Trade Method

The three main methods for trade-offs in systems engineering and engineering in general are the Analytic Hierarchy Process (AHP), graphical model comparison and the weighted criteria score. All three have their advantages and limitations which will be explored below.

In AHP a final judgement is then made based on this and the capacity to fulfil the original goals. It is not suitable for this trade-off as it would lead to a bias towards certain design aspects as they would be accounted for multiple times in the trade-off. The graphical model comparison is not suitable for this trade-off as it requires a mature design and developed tools which need to have been verified. The weighted criteria score enables to identify parameters which can be treated independently of each other, in opposition to the AHP. Moreover, this method does not require the development of specific tools which would require extra verification and validation. Weighted criteria score was thus chosen as the method with which the trade-off would be performed.

12.2.3. Trade Criteria & Weights

With a preliminary design of each concept, a quantitative trade-off between the conventional subsonic concept and the tandem wing concept can be performed. The top level criteria and their weights are listed below:

- Costs (9)
 - R&D cost (4)
 - Operation Cost (2)
 - Acquisition Cost (3)
- Environmental Impact (4)
 - Operational environmental impact (2)
 - CO₂ Ground segment environmental impact (2)
- Feasibility (15)
 - TRL (5)
 - Reliability (2)
 - Performance (8)
 - ◇ MTOW (5)
 - ◇ C_{D0} (2)
 - ◇ Payload (1)

According to the driving mission requirements, one of the most significant criteria for the selection of the concept is the cost. The cost components relevant to the quantitative trade-off are R&D costs, operation cost, and acquisition cost. The R&D costs is considered to be more important because in the early development stage of the new aircraft, a low R&D costs is more attractive to stakeholders for future execution. The acquisition cost is considered to be the second important since a number of aircraft is needed to perform the mission. The total project cost can be extremely costly if the acquisition cost per aircraft is high. The operation cost was weighed more for the design of more advanced versions of aircraft in the future.

With reference to the environmental impact, the fuel fraction and the amount of CO₂ emission is used to evaluate each concept with identical weight. The fuel fraction evaluates the efficiency of the fuel consumption. A more efficient fuel consumption is favourable for the sustainability development. The CO₂ emission obtained from the estimation model indicates the amount of CO₂ emission per operation cycle.

The feasibility of the concept is composed of the TRL, reliability and the performance. The TRL is considered to be significant because less development time and cost is favourable. A concept with a low TRL also increases the difficulty of the aircraft design in the next stage. The aircraft performance is evaluated in terms of MTOW and C_{D0} and payload. The MTOW and C_{D0} are considered to be the killer criteria because they both have an indirect influence on the cost and environmental impact.

12.2.4. Scoring Method

The method to score and compare the two concepts was chosen to be the following, the conventional concept would act as a baseline and as such scores a 1 in every category. From there, the score of the other concept is determined according to how much better or worse it performs with respect to the baseline. This is achieved by adjusting the score proportionally to the baseline based on the difference in performance as shown in the equation, where P is the characteristic being evaluated; $Score = \frac{P_i}{P_{baseline}}$.

12.2.5. Trade Summary Table

In each column in the trade summary table in Table 12.2, the criterion is stated, with its weight. The width of the columns are scaled to each weight. The concepts are stated in the first column, with the final score between brackets below. In the row of each concept, their respective scores are stated. As mentioned before, the conventional aircraft acts as a baseline, which is why the scores for the conventional aircraft are all equal to one.

Table 12.2: Quantitative Trade-off of Concepts

Concept \ Criterion	Feasibility				
	Reliability (2)	MTOW (5)	Performance		
			C _{D0} (2)	Pay-load (1)	TRL (5)
Conventional (1)	1	1	1	1	1
Tandem Wing (0.96)	1.1	1.02	0.9	1.01	0.9

Concept \ Criterion	Costs			Environmental Impact	
	R&D Cost (4)	Operation cost (2)	Cost per unit (3)	Operational EI (2)	Ground segment EI (2)
Conventional (1)	1	1	1	1	1
Tandem Wing (0.96)	0.9	0.96	0.94	1.02	0.99

	+ 10% or more		- 10% or more
	+ 0%-5%		- 5%-10%
	baseline		- 0%-5%

From Table 12.2 and Table 12.1, it was concluded that the conventional aircraft is the final concept, for

which further design iterations are to be made. From Table 12.1, which compared the different concepts in a qualitative manner, the conventional aircraft already appeared to have more advantages, as the higher score indicates. This was established again from Table 12.2, as the conventional aircraft had a higher score again.

12.2.6. Trade-off Sensitivity Analysis

Here, the sensitivity of the weight of the various criteria which entered the trade-off are evaluated in order to quantify the sensitivity of the decision to a change in tack for the problem. For example, when the focus switches from cost minimisation to environmental impact minimisation. The table below shows the change in the relative score of the tandem aircraft for an increase in the weight of the criterion of 10 % of its original value as shown in Table 12.2. A positive change in the value below is equivalent to the tandem aircraft scoring higher by the corresponding number of percentage points. From Table 12.3, it can be observed that no parameter changes the outcome of the trade-off significantly. This can be partly explained by the fact that there are few criteria in which one of the concept scores very poorly or much better than the other.

Additionally, the effect of removing criteria for the canard score has also been quantified. Removal of the cost category increased the score of the canard by 1.8 %. For this category, R&D costs contributed the most. Removal of the other two categories, performance and environmental impact, only further decreased the score of the canard.

Table 12.3: Sensitivity Analysis of the Quantitative Trade-off

Parameter	Reliability	MTOW	C_D	Payload	TRL	R&D Cost	Operational Cost	Cost per Unit	Operational EI	Other EI
Value [%]	0.10	0.11	-0.05	0.01	-0.11	-0.09	0.00	-0.02	0.043	0.02

12.3. Discussion and Results

In conclusion, a trade-off between subsonic conventional wing layout, supersonic conventional wing layout, tandem wing layout, and flying wing or blended wing body were performed qualitatively. Since these four concepts were selected based on their respective advantages of performance for Ceres mission, their performance scores are comparable. However, the conventional supersonic and flying wing concepts were proven to be more costly compared to the other two concepts due to the complexity of development and manufacturing. Besides, the availability of models of the flying wing concept is unacceptably low, which makes the concept unfavourable for further design. Thus, the conventional supersonic and flying wing concepts were rejected in the qualitative trade-off.

With an initial concept development done, a quantitative trade-off between subsonic conventional concept and tandem wing concept was performed. Driver design parameters such as MTOW, C_{D_0} , and cost were computed for both concepts. Although the tandem wing concept has a slightly lower MTOW resulting in larger payload capacity, C_{D_0} and cost are larger than those of the conventional concept.

Due to the generally better performance in both the qualitative and quantitative trade-offs, the conventional concept was selected for Ceres aircraft. In the following chapters, detailed aircraft designs based on the selected concept will be discussed.

Ceres Characterisation

This chapter presents the various methods used to design the aircraft which will fulfil the Ceres mission. It will first bring to light the various elements which have been identified to drive the design to a greater extent. This can be found in the opening section of the chapter. This is then followed by sections which detail the methods used for the sizing of the various elements of the aircraft. After this, the payload size and placement is elaborated upon, as well as the structural design of the wing and the internal systems and their placement. Finally, an overview is given of the final design characteristics.

13.1. Design Drivers

During the development of the aircraft, several design aspects were identified to be driving the design. Amongst these aspects, the main drivers are the aerodynamic and the propulsion related constraints. The former can be explained by the nature of the mission which requires flight at 20 km altitude. At this height, the air only has 7% of its sea level density. However, the aircraft relies on this air to produce lift and maintain flight at this altitude. The main issues faced in the aerodynamic design are related to the cruise conditions. First of all, the drag divergence Mach number significantly limits the design due to the high altitude and high cruise speed. Also, the high required maximum lift coefficient during cruise due to the thin atmosphere drives the aerodynamic design of Ceres heavily. These two constraints combined are known as the 'coffin corner' in which Ceres will be operating during cruise. This flight regime defines the challenging aerodynamic design of Ceres.

Similarly, the propulsion system relies on the same thin air to produce thrust. A jet engine that is provided with inlet air with lower density will have affected performance. In combination with the high cruise Mach number, this will have significant consequences for the propulsion system. The first part of this effect is a decrease in thrust compared to sea level conditions. As a result of this thrust lapse, the propulsion system needs to be designed for a much higher sea level thrust than the required value during cruise. This thrust lapse is quantified at about 5–10 % in Section 13.3. Furthermore, the engine efficiency, quantified by the specific fuel consumption (SFC), may be affected by a change in altitude and Mach number. Both these phenomena will heavily impact the required fuel mass, thus affecting the entire design of Ceres.

Since these two aspects make up the driving design elements of Ceres, they are performed with the highest priority. This means design considerations for aerodynamics and propulsion will be weighted more heavily compared to other aspects. The discussion of the aspects related to aerodynamics are discussed below, followed by propulsion.

13.2. Aerodynamic Design

13.2.1. Lift Characteristics

Due to the mission requirements, the aircraft is required to operate at very high altitude. However, the aerodynamic performance must be verified to comply with these requirements at all operating altitudes and flight conditions. Due to the high importance of the lift coefficient in particular, it is necessary to construct accurate and reliable models to be able to predict the performance of the aircraft. The lift coefficient determines the capacity of a certain wing geometry to generate lift. This was done in this subsection which details the various aerodynamic parameters and characteristics of the chosen aerofoil. When this information was coupled to models from DATCOM and the Philips Alley method[67], the maximum lift coefficient was obtained.

Reynolds number and Mach number range The Reynolds and Mach numbers were computed using the formulae provided below in Equation (13.1) and Equation (13.2). The inputs used for these relations are the ones encountered in the mission profile. The found range of operating conditions were Reynolds numbers

from 20×10^6 to 90×10^6 and Mach numbers from 0.1 to 0.72. This is due to the varying conditions in the span direction as well as the wide varying range of conditions during flight. The greatest changes in Equation (13.1) are in air density as well as air viscosity. The first was taken from the ISA model in accordance to regulations. The latter, was determined based on the engineering toolbox¹ for the range of altitudes from sea level to 20 km. The very large range of Reynolds numbers has numerous impacts most notably the boundary layer which becomes heavily turbulent and also larger. This was combined with high subsonic Mach numbers which induce compressibility effect in the flow. This can be partly estimated by the Prandtl Glauert correction factor $\beta = \frac{1}{\sqrt{1-M^2}}$ which is accurate up to $M = 0.7$ which is the chosen cruise velocity.

$$Re = \frac{\rho VL}{\mu} \quad (13.1) \quad M = \frac{V}{\sqrt{RT\gamma}} \quad (13.2)$$

Knowing this, it is possible to predict the three dimensional lift characteristics based off the measured characteristics of the aerofoil.

Airfoil characteristics Based on the characteristics of Ceres, three suitable supercritical airfoils were compared to determine the most suitable supercritical airfoil for Ceres. Hence, a trade-off was performed based on the following criteria and weights:

- M_{dd} should be above the maximum Mach number achieved during the whole mission. Additionally, it should be as high as possible. (5)
- Lift-to-drag ratio should be as high as possible at the designed lift coefficient. (4)
- Small C_{d_0} to minimised the parasitic drag (consists of the skin friction drag and pressure drag). (3)
- Small C_{m_0} to minimised the horizontal tail sizing for trim condition. (2)

The drag-divergence Mach number was weighted heavily (5) because the aircraft is flying near the transonic regime so flow separation and adverse pressure gradient should be avoided. The large increase of drag on the airfoil is potentially catastrophic. A weight of 4 was assigned to the lift-to-drag ratio as higher value improved the climb performance. The zero-lift-drag coefficient related to the parasitic drag was weighted 3 since it is only one of the two contributions of drag but also affects the thrust-to-weight ratio. Moreover, the zero-lift-drag also contains the drag interactions with horizontal tail, fuselage etc. Lastly, the pitching moment coefficient at zero angle of attack was given a weight of 2.

The criteria were graded on a scale of 1 to 3 and the total can be calculated by multiplying the grades by the weight and summing them.

Table 13.1: Trade-off of wing airfoil selection for conventional concept

Airfoil	M_{dd}	L/D	C_{d_0}	C_{m_0}	Total
Weight	5	4	3	2	
NASA SC(2)-0614	2	1	3	3	29
NASA SC(2)-0712	3	3	2	2	37
NASA SC(2)-0714	1	2	2	1	21

The final choice was the *NASA SC(2)-0712*, whose characteristics can be observed below in Table 13.2. Next, XFOil was used to determine the characteristics of the airfoil which are shown in Table 13.2.

Table 13.2: NASA SC(2)-0712 Characteristics at $Re = 1 \times 10^6$

(t/c)%	L/D	$C_{l_{des}}$	C_{d_0}	$C_{l_{max}}$	C_{m_0}	M_{dd}
12	90	0.55	0.007	1.7	-0.123	0.78

The software however has limitations regarding high Reynolds numbers as well as transonic Mach numbers [23, 36, 45]. The numbers obtained thus have very high uncertainties. To take into account high Reynold's number turbulence and compressibility, the DATCOM method was used which also has uncertainties[35]. However, it has been validated with existing aircraft.

3D lift characteristics To take into account the losses in lift performance due to the finite wing, two methods were used. The first was DATCOM, it was used to estimate the maximum lift coefficient as well as the

¹https://www.engineeringtoolbox.com/standard-atmosphere-d_604.html

gradient of the lift curve and the stall angle of attack. This was verified with XFLR5 which implements a section method of XFOIL as well as the Philips Alley Method. The latter has shown to fall within 1 % of CFD computations, which is consistent with DATCOM. The effects of Reynolds number and Mach number on the prediction of the maximum lift coefficient were also explored as most methods only take into account low Mach number stall as well as Reynolds numbers up to 1×10^6 . [46, 83, 99, 102]

An improvement to the two methods mentioned above is the possibility to implement the critical section method. This method is more widely used and has also shown to be accurate. It, however, requires to use more advanced CFD tools which represent a time investment which falls beyond the time constraints provided by the Design Synthesis Exercise. [83]

DATCOM The relations used as part of this *Data Compendium* (DATCOM) are shown below. They have been developed by the USAF as a stability and control prediction tool to be used both in preliminary design as well as the evaluation of engineering modifications to existing designs. It is based on statistical and semi-empirical relations. It however has limitations in the study of aircraft with low aspect ratios, twist and variable aerofoil sections as has shown Gudmundsson, in which his comparison with the wing of the SR22 Cirrus wing yielded an error of 11 %. [27, 35]

$$\begin{aligned} C_{L_{max}} &= C_{l_{max}} \cdot \frac{C_L}{C_l} + \Delta C_{L_{max}} \\ C_{L\alpha} &= \frac{2\pi A}{2 + \sqrt{4 + \left(\frac{A\beta}{\eta}\right)^2}} \cdot \left(\frac{S_{exposed}}{S}\right) \cdot F \\ \alpha_{stall} &= \frac{C_{L_{max}}}{C_{L\alpha}} + \alpha_{lift=0} + \Delta\alpha_{C_{L_{max}}} \end{aligned} \quad (13.3)$$

Philips-Alley method This method uses the relations below to estimate the $C_{L_{max}}$ of the aircraft. This method uses various coefficients to correct the airfoil lift coefficient to take into account twist, sweep and compressibility effects. It was here judged that this method was more complete as it is the only method which accurately predicts the behaviour of high-speed stall, or stall at high Mach numbers with an accuracy of 1 % with respect to CFD simulations for a range of taper ratios, aspect ratios and sweep angles [67]. The method is based on the lifting line theory in which the lift of a finite wing is estimated using a spanwise distribution of vorticity. When the Helmholtz vortex theorem was used in combination with the circulation theory of lift, the classical lifting line theory is obtained as formulated in Eq. (13.4). The unknown in this equation is $\Gamma(z)$; it can however be estimated with a sine only Fourier series. The coefficients of the series are obtained in well detailed methods as per Anderson [2]. This enables to compute both the lift coefficient and the induced drag. However, Philips in [67] describes a new method based on a simple change of variable $\alpha(\theta) - \alpha_{L0}(\theta) \equiv (\alpha - \alpha_{L0})_{root} - \Omega\omega(\theta)$ which enables to link lifting performance to twist and twist distribution which is not possible in the classical theory.

$$\frac{2\Gamma(z)}{V_\infty c(z)} + \frac{\tilde{C}_{L,\alpha}}{4\pi V_\infty} \int_{\zeta=-b/2}^{b/2} \frac{1}{z-\zeta} \left(\frac{d\Gamma}{dz}\right)_{z=\zeta} d\zeta = \tilde{C}_{L,\alpha} [\alpha(z) - \alpha_{L0}(z)] \quad (13.4)$$

Additional correction factors are then added to determine the maximum lift coefficient based on the effect of sweep, taper ratio and aspect ratio. This latter parameter is of utmost importance due to the peculiar operation conditions of the aircraft. This method yielded results which were within 1 % of the DATCOM method which is still sensible as the latter is evaluated to be accurate to an order of magnitude of 10 % as explained above. [27, 67]

$$\begin{aligned} C_{L_{max}} &= \left(\frac{C_L}{\tilde{C}_{L_{max}}}\right)_{\substack{\Omega=0 \\ \Lambda=0}} \kappa_{Ls} \kappa_{L\Lambda} (\tilde{C}_{L_{max}} - \kappa_{L\Omega} C_{L,\alpha} \Omega) \\ \kappa_{Ls} &= 1 + (0.0042 R_A - 0.068) (1 + 2.3 C_{L,\alpha} \Omega / \tilde{C}_{L_{max}}) \\ \kappa_{L\Lambda} &\cong 1 + \kappa_{\Lambda 1} \Lambda - \kappa_{\Lambda 2} \Lambda^{1.2} \end{aligned} \quad (13.5)$$

$$\kappa_{L\Omega} = \left[1 - \frac{C_L}{\tilde{C}_{L_{max}}} / \left(\frac{C_L}{\tilde{C}_{L_{max}}} \right)_{\Omega=0} \right] / \frac{C_{L,\alpha}\Omega}{\tilde{C}_{L_{max}}}$$

In Equation (13.5), Ω corresponds to the wing twist angle (here taken to be zero), Λ is the sweep angle, R_T is the taper ratio, R_A is the aspect ratio and the various κ values are taken from the plots shown below in Figure 13.1. As can be observed in the relations of Equation (13.5), the values of the lift coefficient ratios had to be determined. These were computed using the relations found in Equation (13.6)[67] and were compared to the values obtained in XFLR5. Since the discrepancy was less than 5%, the values taken were the ones from the paper as the uncertainty was quantified there.

$$\frac{C_L}{\tilde{C}_{L_{max}}} = \frac{\pi \sin(\theta_{max})}{2(1 + R_T)} \quad (13.6)$$

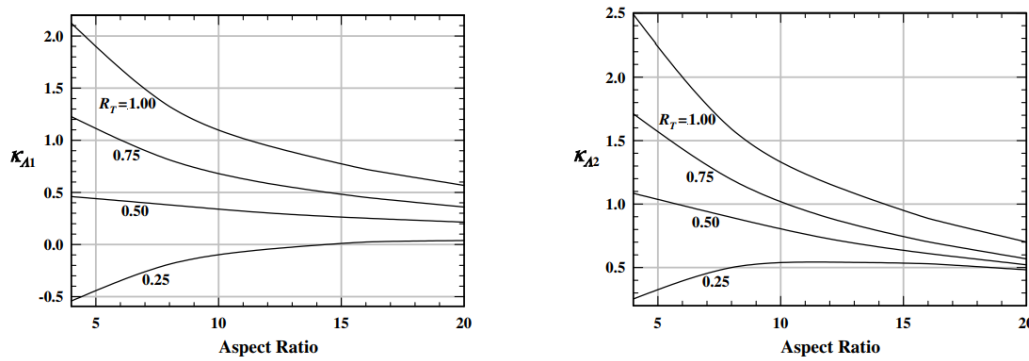


Figure 13.1: Sweep Coefficients as a Function of Aspect Ratio and Taper Ratio.

When the values for $C_{L_{max}}$ were obtained, it was possible to integrate this value into the design iterations to ensure that this upper bound on aerodynamic performance was respected. This was complemented with the verification and validation of the model as well as a sensitivity analysis of this coefficient and its conclusions.

Verification and Validation As mentioned above, the verification of the model from Philips and Alley was done using the DATCOM method. The discrepancy was within 1% for a $C_{L_{max}}$ value of 1.03. The validation was done using the values for the maximum lift coefficients for various aircraft with varying parameters which is recapitulated below. It must be noted that the limitation of the Philips Alley method is that it does not take into account the possibility for flaps. This nonetheless does not affect the Ceres aircraft as it does not have flaps. The lifting line model was validated using the data provided in [62]. From this book, it was possible to take the lift curves of existing aircraft (the 747 in the book from Obert [62]) and compare these with the modelled lift curve. The found discrepancy was approximately 10% which is coherent considering the assumptions made and the uncertainty of the methods.

Taper Ratio The taper ratio was optimised for the lift distribution of the wing, i.e. the taper ratio was chosen such that an elliptical lift distribution was approximated. The analytical relation provided by [55] in Equation (13.7) gives the optimal taper ratio. By establishing an elliptical lift distribution, the induced drag was minimised. Equation (13.7) shows that an optimal taper ratio for an unswept wing is equal to 0.45, where it decreases with increasing quarter-chord sweep.

$$\lambda_{opt} = 0.45e^{-0.0375\Lambda_{c/4}} \quad (13.7)$$

Oswald efficiency factor The Oswald efficiency factor affects the entire design, as it influences the aerodynamic efficiency, and thus the fuel burn. A method proposed by M. Nita [55] was used to determine the Oswald efficiency. This method is based on the wing characteristics, and takes into account the fuselage interaction, the zero-lift drag influence, and the influence of Mach number. Reynolds number was not taken into account, as the parabolic relation between C_D and C_L holds for $Re > 5e6$ [31].

$$e_{theo} = \frac{1}{1 + f(\lambda - \Delta\lambda) \cdot A} \quad (13.8)$$

A theoretical Oswald Efficiency factor of the wing was calculated using Equation (13.8), where $f(\lambda - \Delta\lambda)$ is a function from [55]. Based on this, the Oswald Efficiency of the aircraft was calculated using Equation (13.9), where K_{ef} , K_{eM} and $K_{e\Gamma}$ are penalties for the effects of wing-fuselage interaction, Mach number and di/anedral, respectively. Q represents the inviscid part, while P represents the viscous part. Formulas used to estimate the penalisations are shown in Equation (13.10). As described by Nita, Coefficients K , a_e and b_e are statistically determined, K is based on roughly 30 general aviation aircraft, while a_e and b_e are based on transport aircraft.

$$\begin{aligned} e &= \frac{K_{eM} \cdot K_{e\Gamma}}{Q + P\pi A}, \\ Q &= e_{theo} \cdot K_{ef}, \\ P &= K \cdot C_{D_0} \end{aligned} \quad (13.9)$$

$$\begin{aligned} K_{ef} &= 1 - 2\left(\frac{d_F}{b}\right)^2, \\ K_{eM} &= a_e \left(\frac{M}{M_{comp} - 1}\right)^{b_e} + 1, \\ K_{e\Gamma} &= \left(\frac{1}{\cos\Gamma}\right)^2 \end{aligned} \quad (13.10)$$

Since the method is fairly simple, verification was done by inspection. Validation is much more important, this was done by calculating the Oswald efficiency factor of several aircraft and comparing the results to their actual Oswald efficiency factors. The results are shown in Table 13.3, and as can be seen, the highest difference is 5.3%, deeming the method validated. A sensitivity analysis showed great sensitivity towards the Mach number at cruise, which is shown in Figure 13.2. This behaviour was validated by analysing the behaviour of the Oswald factor of an A320, as shown in Figure 13.3. From these plots, it was concluded that the cruise Mach number should not increase, as this causes a big decrease in Oswald efficiency.

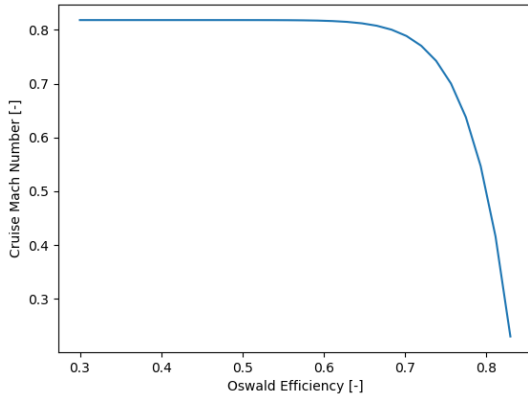


Figure 13.2: Oswald Efficiency versus the Cruise Mach Number.

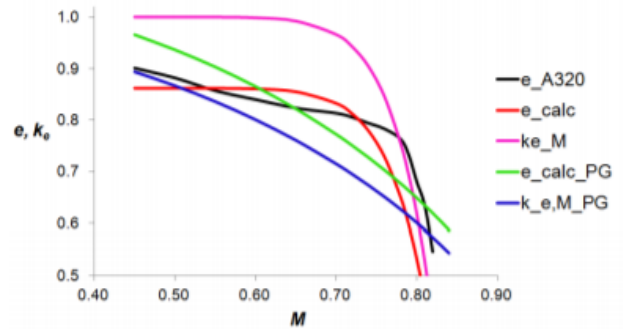


Figure 13.3: Calculated Oswald (e_{calc}), and Mach Number Correction (ke_M), compared with the Oswald Efficiency for A320 Aircraft (e_{320}) [55].

Table 13.3: Validation of Oswald Efficiency

Aircraft	Calculated [-]	Actual [-]	Difference [%]
A320	0.785	0.783	0.25
B737-800	0.697	0.66	5.3
Fokker F28-2000	0.802	0.818	1.9

Using the method above resulted in an Oswald Efficiency factor of 0.81. While some penalties do rely on statistics, these statistics are from transport aircraft and general aviation. It is expected that these coefficients still apply to Ceres' design, as it was shown that for various types of aircraft, with various $\frac{d_F}{b}$, this method obtained accurate results [55]. Furthermore, as stated earlier, it was assumed that the Reynolds number would not affect the Oswald factor.

13.2.2. Planform Design

From the Class I planform design based on statistical data, the wing planform was designed in more detail and consequently more selection variables were introduced to optimise the wing, not only for aerodynamic performance but also for minimum MTOW. Indeed, given the aerodynamic constraints of the aircraft, the objective of the planform design is to minimise the MTOW.

To achieve this goal, the method described in chapter 10 of Torenbeek [91] was used for the design of the detailed planform design which resulted in the selection of the design lift coefficient, span, taper ratio and sweep angle. Below, the method and its results will be elaborated in more detail.

Method In the search for the basic planform design, the *design* lift coefficient was introduced which is defined as shown Equation (13.11), where \hat{q} is the dynamic pressure at cruise condition corrected by 2 to 3% for the weight lost during climb and take-off.

$$\hat{C}_L = \frac{W_{MTO}}{\hat{q}S_w} \quad (13.11)$$

As details of the aircraft such as the weight fractions of various components of the aircraft were still unknown and varying, it was sub-optimal to define and directly minimise MTOW. As such, parameters were introduced to improve the approximations in the design and selection of the planform. The first parameter introduced was the wing penalty function, which is shown in Equation (13.12), where the propulsion function (F_{prop}) is defined as Equation (13.13).

$$WPF = \frac{\Phi_3 A_w \sqrt{A_w / \hat{C}_L}}{(\bar{t}/c)_w \cos^2 \Lambda_w} + \frac{\Phi_2}{\hat{C}_L} + F_{prop} \left(\frac{\check{C}_{D_p} + C_{D_c}}{\hat{C}_L} + \frac{\hat{C}_L}{\pi A \bar{e}} \right) \quad (13.12) \quad F_{prop} = \frac{R_{eq}}{\bar{\eta}_0 H/g} + \frac{\mu_T}{\bar{\tau} \delta} \quad (13.13)$$

Wing Penalty Function (WPF) consists of the wing and tail structure weight, engine weight required to balance the wing and horizontal tail and mission fuel weight required to balance the wing and horizontal tail along the mission range. Φ_1 and Φ_2 are constants based on statistical data that determine the wing and horizontal weight. Furthermore, the wing penalty function depends on the wing aspect ratio (A_w), lift coefficient (\hat{C}_L), mean thickness ratio (\bar{t}/c_w), the propulsion function (F_{prop}), the profile drag of the wing and horizontal tail (\check{C}_{D_p}), the compressibility drag (C_{D_c}) and the modified Oswald factor which assumes that the wing will be adapted to the final design lift coefficient by selecting optimal camber and wash-out distribution (\bar{e}). In this expression, it is assumed that the nacelle drag is negligible in the thrust loss. Instead, the nacelle drag area is considered in $C_{D_{p_{fix}}}$. Additionally, the propulsion function defined in Equation (13.13) depends on the mission fuel minus the lost fuel (R_{eq}), the overall efficiency of the engine ($\bar{\eta}_0$) and a jet fuel property (H/g). The last term of the propulsion function depends on the power plant weight over the take-off thrust (μ_T), corrected thrust lapse ($\bar{\tau}$) and the relative ambient pressure (δ). Alternatively, the second term can be defined as the power plant weight over the available cruise thrust.

Using this wing penalty function the expression of the MTOW is defined by Equation (13.14)[91].

$$W_{MTO} = \frac{W_{pay} + \sum W_{fix} + F_{prop} q (\check{C}_{D_p} S)_{fix}}{1 - (\mu_{resf} + \mu_{lg} + F_{wp})} \quad (13.14)$$

As can be remarked from Equation (13.14), minimisation of F_{WP} is equivalent to minimising the MTOW. This means that the terms in the numerator did not need to be known for the optimisation of the wing planform. As such, the MTOW was optimised by finding the minimum value for F_{WP} . While the resulting F_{WP} value from the resulting planform selection could be used to compute the MTOW using Equation (13.14), it was only used as an indication for minimum MTOW.

Optimal Thickness and Sweep Torenbeek shows that minimisation of wing penalty function directly from Equation (13.12) results in the optimal combinations of $(\bar{t}/c)_w$ and Λ_w values which are too high to be practical[91]. Thus, optimal combinations of $(\bar{t}/c)_w$ and Λ_w were limited to reasonable values for the compressibility drag during cruise.

The

These were found by adapting Korn's relation to the three-dimensional airfoils using simple sweep theory, which is shown in Equation (13.15).[91]

$$\overline{(t/c)}_w (\cos \Lambda_w)^2 = (\cos \Lambda_w)^3 (M^* - M_{dd} \cos \Lambda_w) - 0.115 \hat{C}_L^{1.5} \quad (13.15)$$

$$\cos \Lambda_w = 0.75 \frac{M^*}{M_{dd}} \quad (13.16)$$

Equation (13.16) holds for $M^* \leq 0.75 M_{dd}$. It can be remarked that the equation only depends on the critical Mach number and the drag-divergence Mach number of the airfoil. Using Equation (13.16) a half-chord sweep angle was selected before solving for the (maximum) thickness ratio using Equation (13.15).

Partial Optima Curves By taking the partial derivative of the expression for F_{WP} with respect to the selection variable, partial optima curves were found for the wing aspect ratio ($\partial F_{WP} / \partial A_w = 0$) and design lift coefficient ($\partial F_{WP} / \partial \hat{C}_L = 0$). They are defined by Equation (13.17) and Equation (13.18).

$$A_w = \hat{C}_L^{0.6} \left[\frac{2F_{prop}}{3\pi\check{e}\Phi_3} \{(\cos \Lambda_w)^3 (M^* - M_{dd} \cos \Lambda_w) - 0.11 \hat{C}_L^{1.5}\} \right]^{0.4} \quad (13.17)$$

$$\hat{C}_L = \sqrt{\check{C}_{D_p} \pi A_w \check{e}} \left(1 + \frac{0.5\Phi_3 A_w \sqrt{A_w \hat{C}_L}}{\check{C}_{D_p} F_{prop}} + \frac{\Phi_2}{\check{C}_{D_p} F_{prop}} \right)^{0.5} \quad (13.18)$$

Intersection of the two partial optima curves result in an aerodynamically unconstrained optimum planform design given a constant wing aspect ratio and drag-divergence Mach number. However, during design, both feasibility and practicality pose design requirements for the planform, which constrained the achievable design lift coefficient, sweep and aspect ratio. This also had to be considered in the planform selection.

Constraints In cruise conditions the aircraft may experience gust loads or be required to perform manoeuvres. As a result, dynamic aeroelastic behaviour may be experienced which leads to high-frequency instability such as shock waves and turbulence. This instability is referred to as buffeting and regulations dictate that this can only happen beyond a load factor of at least 1.30. In other words, a 30% margin is required from the initial buffet onset C_L and the C_L during cruise conditions[49, 91]. Since buffeting is difficult to predict during the early phase of the design, literature and statistical data of transonic airliners were consulted to approximate the lift coefficient for initial buffet onset.

Buffeting airfoil data of a similar second-generation supercritical airfoil was found and showed an initial buffet onset C_L of approximately 0.92.[6] Comparing the value from the airfoil to the buffeting onset boundary of four transonic airliners, it was concluded that the lift coefficient of the airfoil slightly overestimates the actual C_L buffet onset boundary.[62] As such, an uncertainty margin of 5% was used in addition to the minimum 30% margin² to take into account the usage of data of a similar but not identical airfoil and the small (statistical) sample size. As a result, the cruise (design) lift coefficient must not be higher than 0.6.

An additional driving constraint of the planform selection is the aeroelastic behaviour of the wing. An increase in aspect ratio results in a longer wing, therefore increasing the total deflection of the wing and structural loads. These reasons complicate the manufacture and cost of the aircraft and consequently decrease the feasibility of the design.

More importantly, a high aspect ratio means the aircraft is more prone to aeroelastic instability such as flutter, (aeroelastic) divergence and control reversal. Not taking into account the possible aeroelastic complications of high aspect ratio may result in catastrophic failure of the mission and loss of aircraft. This analysis of the aeroelastic behaviour is explained in Section 13.2.3 and resulted in a maximum wing aspect ratio of 13.

²<https://www.law.cornell.edu/cfr/text/14/25.251>

<https://www.easa.europa.eu/sites/default/files/dfu/CS-25%20Amdt%205.pdf>

It must be noted that at high sweep angles, the stall progression starts from the tips of the wing. Since the tips are aft of the wing, the centre of pressure will move forward, resulting in a pitch-up tendency during stall[91], consequently stalling the aircraft even further. To alleviate this pitch-up tendency, several measures can be explored. First, vortex generators can be used to delay local flow separation by obstructing the span-wise boundary layer flow and to re-energise the boundary layer, example of vortex generators are slats, shark fins, and vortilons.[11, 66] Additionally, wing twist can be applied to the wing such that the incidence angle is lower at the tips than at the root. Lastly, a combination of a stick-shaker³ and stick-pusher⁴ system can be used to warn the pilot of entering stall and allow the flight computer to safely drop the nose of the aircraft at a predetermined angle of attack.

Further discussion on aerodynamic devices to alleviate the pitch-up tendency is beyond the scope of this DSE report but shall be discussed more in-depth in the later stages of the design.

Finally, the last constraint is the optimum $C_{L_{climb}}$. However, it was determined that this constraint was not driving in the wing planform selection.

The list of assumptions used throughout the planform design is shown in Table 13.4.

Table 13.4: List of Assumptions Made for the Planform Design

Assumptions	
Engine data are acquired through GasTurb	
$M^* = 0.935$	
Total wing profile drag: $d_{w+h} = 1.25$ (typical value)	
$C_{Dc} = 0.0010$	
Shape factor for profile drag: $r_\phi = 3.0$	
Specific weight for predominantly aluminium wing: $\Omega_S = 210 \text{ N/m}^2$	
Modified Oswald factor: $\bar{e} = 0.85$	

Results From the method and assumptions, the resulting WPF contours (coloured ones) are shown in Figure 13.4 and Figure 13.5. The latter figure shows the contours with the constrained aspect ratio, while the former figure shows the contours for the unconstrained case. The figures also show the contours for constant thickness which were varied over various shades of grey.

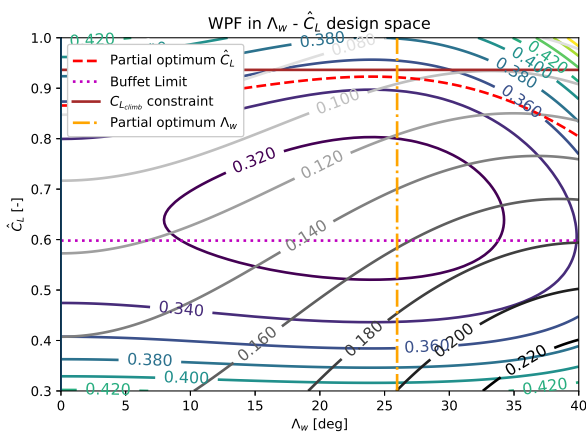


Figure 13.4: Wing Penalty Function as a Function of the Wing Sweep in Degrees and the Design Lift Coefficient. The Plot shows the Constrained Condition where $A = 13$ and $M_{dd} = 0.78$.

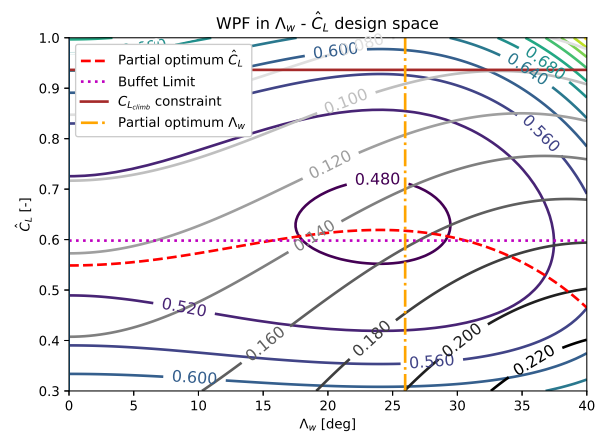


Figure 13.5: Wing Penalty Function as Function of the Wing Sweep in Degrees and the Design Lift Coefficient. The Plot shows the Unconstrained Condition where $A = 24$ and $M_{dd} = 0.78$.

Given $A = 24$, the aerodynamically optimal planform properties are shown as the intersection of the partial optimum curves in Figure 13.5. The intersection is near the innermost WPF contour, meaning that also near-minimum MTOW is achieved in this case. This results in $\hat{C}_L \approx 0.62$, $\Lambda_w \approx 26^\circ$ and $\bar{t}/c_w \approx 0.155$.

³https://www.skybrary.aero/index.php/Stall_Warning_Systems

⁴https://www.skybrary.aero/index.php/Stick_Pusher

As for the constrained optimum, the maximum achievable aspect ratio is constrained by the weight, manufacturability and most importantly the aeroelasticity. Indeed, aeroelastic analysis of the wing showed that the maximum achievable aspect ratio is at most 13. Moreover, the maximum achievable \hat{C}_L is constrained. Namely, according to regulations, a margin of at least 30% should be taken between cruise \hat{C}_L and initial buffet onset.[49] From these two driving constraints, the selected planform is $A_w = 13$, $\hat{C}_L = 0.60$, $\Lambda_w \approx 26^\circ$, and $t/c_w \approx 0.158$.

From Figure 13.4 it can be remarked that the selection of the wing planform based solely on aerodynamic criteria would have resulted in a sub-optimal solution if the buffet limit constraint is not considered, which was also concluded from section 10.6 of [91].

Sensitivity Analysis The effect of varying the aspect ratio for the $\Lambda_w - \hat{C}_L$ is shown in Figure 13.4 and Figure 13.5. It can be remarked that increasing the aspect ratio also displaces the partial optimum \hat{C}_L -curve towards minimum MTOW. However, as seen from the WPF values of the contours, it also results in a higher MTOW. Increasing the aspect ratio even further results in sub-optimal intersection point of the partial optimum \hat{C}_L -curve and partial optimum Λ_w -curve.

Moreover, Figure 13.6 and Figure 13.7 show the $\hat{C}_L - A_w$ design space for constant wing sweep. As can be remarked, the optimal aspect ratio does not result in minimum MTOW. In fact, opting for a lower aspect ratio benefits the MTOW greatly, i.e. the MTOW reduces by roughly 40% if the planform is selected for intersection of the optimal aspect ratio and design lift coefficient. However, this would result in poor aerodynamic performance of the aircraft at the service ceiling. Furthermore, higher aspect ratio means less constraining thrust requirement for propulsion, the ability to carry more payload and a more fuel-efficient aircraft.

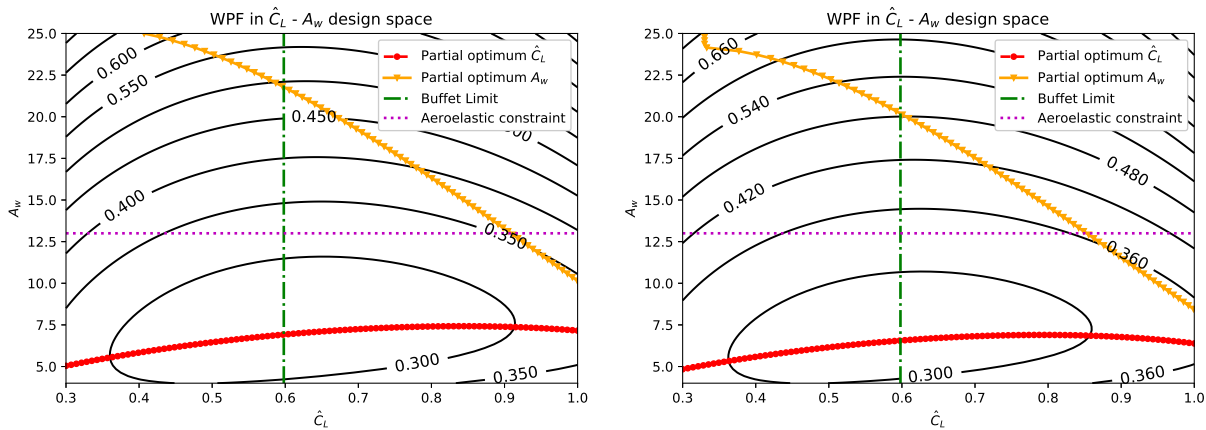


Figure 13.6: Wing Penalty Function as a function of the wing aspect ratio and lift coefficient. The plot shows the constrained case where the sweep angle is set to 26°

Figure 13.7: Wing Penalty Function as a function of the wing aspect ratio and lift coefficient. The plot shows the constrained case where the sweep angle is set to 0°

Verification and Validation For the verification of the code, the output of the functions were compared to values acquired by Torenbeek for an subsonic freighter aircraft in chapter 10 of [91]. Comparing the contours acquired by Torenbeek and the results shown in Figure 13.4 and Figure 13.5, it can be seen that the results are similar, implying that the algorithm to compute the wing penalty function is verified. However, Figure 13.6 shows the slope of the curve is significantly different than shown in Figure 10.12 of [91]. As such, additional verification of this part of the code must be performed in the future.

Torenbeek mentions that the accuracy of the wing penalty function is 1 to 2%.[91]

Furthermore, Torenbeek mentions that the quasi-analytical constants, i.e. θ_2 and θ_3 result in an uncertainty factor between 5 to 10% as these are partially based on statistics. To validate the acquired results, the contours acquired from a Fokker 100 were compared to the actual dimensions of the Fokker 100 planform. The results are shown in Figure 13.8 and Figure 13.9.

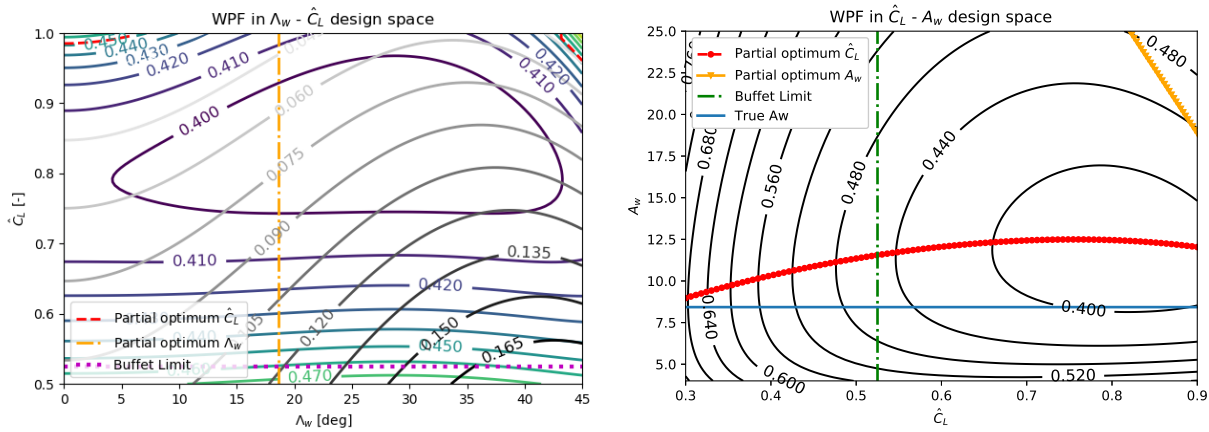


Figure 13.8: Wing Penalty Function in the $\Lambda_w - \hat{C}_L$ Space for the Fokker 100, where $A = 8.43$. Figure 13.9: Wing Penalty Function in the $\hat{C}_L - A_w$ Space for the Fokker 100.

In both figures, the lift coefficient buffet onset constraint is shown, which was found in literature to be 0.75 at a cruise Mach number of 0.74. From Equation (13.15), the resulting sweep angle amounted to 15.7° at the outboard mid-chord line. Compared to the actual value of 13.7° at the half-chord⁵, this resulted in an error of 14.4%. This difference can be explained by the contours in Figure 13.8 near the buffet limit. Namely, it shows that wing penalty function, or MTOW does not change significantly if less sweep is selected. In fact, less sweep is preferred as this improves the low-speed aerodynamic characteristics of the aircraft.

Moreover, given the true $\Lambda_{c/2}$, Figure 13.9 predicts the aspect ratio to be approximately 12.15. This is significantly different from the true aspect ratio of 8.43 (by 44.1%). This error may be explained by other driving constraints in the design of the Fokker 100 which were not considered in Figure 13.9. These constraints may have limited the acquirable maximum aspect ratio. Examples of these may be related to aeroelastic behaviour at high aspect ratios or handling characteristics at transonic speed. As mentioned before, an aircraft with high aspect ratio and sweep angle, may result in pitch-up tendency during stall as the stall progresses from the wing tips for a swept-back wing. Thus, it is likely that the maximum aspect ratio for the Fokker 100 is less than the aspect ratio determined from Figure 13.9.

To achieve the high aspect ratio of 13 for the Ceres aircraft, several solutions are available to alleviate the pitch-up tendency, e.g. a stick-shaker and stick-pusher system could be used in combination with vortex generators and wing twist. Further analysis and sizing on aerodynamic devices must be performed in later stages of the design to ensure that pitch-up tendency is avoided during nominal operations.

13.2.3. Aeroelasticity Analysis

Aeroelasticity deals with the behaviour of an elastic structure in an airflow where there is signification interaction between the two.' [41]. This definition has three elements. Firstly an elastic structure is needed, secondly there is an airflow over the structure and lastly and most importantly is the interaction between these two. The aircraft must not show (unstable) aeroelastic behaviour at the speeds within the flight envelope extended by 15% above the constraining speed in this diagram. The structure of an aircraft has two main relevant characteristics for aeroelasticity, namely the inertia and the elasticity. The interaction of the elastic component with the aerodynamic flow is known as static aeroelasticity or divergence. The interaction of the inertia, elasticity and aerodynamic flow is known as the dynamic aeroelasticity or flutter.

The first form of static aeroelasticity is torsional divergence. Divergence occurs when aerodynamic loads tend to increase the deformation of the wing continuously. With constantly increasing deflection, the stresses in the wing increase as well, ultimately leading to failure of the wing. The second form of static aeroelasticity is control reversal. Control reversal happens when the control of an aircraft reverse themselves, which causes pilots to give the wrong input. These two static forms of aeroelasticity will be analysed with an analytical approximation, which is proven to be accurate.[41]

The dynamic form of aeroelasticity is known as flutter, i.e. self-sustained oscillations arising from fluid-structure interactions. The flutter point is the point where damped oscillations result in unbounded oscillations.

⁵<https://booksite.elsevier.com/9780340741528/appendices/data-a/table-8/table.htm>

latory motion. As such, the operable region defined as the flutter envelope must be determined to prevent the aircraft from exiting this flutter envelope during service, which results in structural damage and failure.

To characterise the aeroelastic behaviour of the aircraft, a 2D-analysis, with two-degrees of freedom was performed on the airfoil section at 75 % of the span section. A simple model of the analysis is shown in [41]. Here the airfoil is suspended by two springs. This 2D analysis is sufficient for the early phases of the design. The purpose of this aeroelasticity analysis was to identify whether the aforementioned forms of aeroelasticity constraints are driving in the design, i.e. whether aeroelastic instabilities occur in the flight envelope and normal operations of the aircraft. Consequently, as an increased span of the aircraft results in poor aeroelastic properties, the subsequent analysis results in an upper limit constraint for the maximum achievable aspect ratio of the aircraft.

A list of all assumptions and values derived from literature are shown in Table 13.5.

Table 13.5: List of airfoil properties used during aeroelastic analysis which are assumed or based on literature

Assumptions	
x_θ	0.3
r_θ	0.4
e	0.4
C_{L_δ}	0.04186
$C_{M_{ac\delta}}$	-0.010

x_θ and r_θ were assumed to be 0.3 and 0.4, respectively, which were found in literature for airfoil analysis[87].⁶ However, in the future, these values can be altered and tweaked by mass balancing such that problematic aeroelastic behaviour is delayed. Furthermore, e , the eccentricity factor of the airfoil was set to be 0.4, acquired from a family of cambered airfoils in figure 6.24 from [78]. Furthermore, $C_{M_{ac\delta}}$ was assumed to be -0.010 and C_{L_δ} was computed using the procedure explained in chapter 12 of [77]. Other parameters such as the lift slope of the wing were already determined beforehand and discussed in previous chapters.

Static Aeroelasticity As discussed in [41], the divergence speed was found using Equation (13.19).

$$q \leq \frac{K_\theta}{C_{L_\alpha} e c S} \quad (13.19)$$

Where K_θ is the torsional stiffness, e is the eccentricity factor of the airfoil, c the chord length and S the reference area defined as $S = 2b$.

$$q_{\text{reversal}} = -\frac{C_{L_\delta} K_\theta}{C_{L_\alpha} C_{M_{ac\delta}} c S} \quad (13.20)$$

Next, the control reversal speed is defined by Equation (13.20), where C_{L_δ} is the change in the lift of the aircraft due to a deflection of the aileron and C_{L_α} is the change in lift due to a change in angle of attack. $C_{M_{ac\delta}}$ is the change in the aerodynamic moment due to tan aileron deflection.

Dynamic Aeroelasticity For the flutter speed, Pine's condition was used which is described in [41]. This condition describes the transition point where a convergent self-induced oscillation becomes divergent. This point was found using a quadratic formula which is shown in Equation (13.21), where Q is defined as shown in Equation (13.22).

$$Q_1, Q_2 = \frac{-C_1 \pm \sqrt{C_1^2 - 4C_2 C_0}}{2C_2} \quad (13.21) \quad Q = \frac{q S b C_{L_\alpha}}{K_\theta} \quad (13.22)$$

Additionally, C_0 , C_1 , and C_2 are dependent on the geometric and structural properties of the airfoil, see Equation (13.23), where x_θ is the displacement of the CG from the elastic axis (EA) and ω_w and ω_θ are the bending natural frequency and natural torsional frequency, respectively.

⁶<http://orbit.dtu.dk/files/3315978/ris-r-1663.pdf>

$$\begin{aligned}
C_2 &= (x_\theta + 2e)^2 \\
C_1 &= -2 \left[x_\theta + 2e + \left(\frac{w_h}{w_\theta} \right)^2 \left(x_\theta - 2e + 4e \frac{x_\theta^2}{r_\theta^2} \right) \right] \\
C_0 &= \left[1 - \left(\frac{w_h}{w_\theta} \right)^2 \right]^2 + 4 \frac{x_\theta^2}{r_\theta^2} \left(\frac{w_h}{w_\theta} \right)^2
\end{aligned} \tag{13.23}$$

From the above equations, the driving aeroelastic constraints were found for the given altitude and cross-sectional properties. The latter are consequently dependent on the structural properties of the wing such as the material, the cross-sectional bending and torsional stiffness. As such, by varying the feasible range of bending and torsional stiffnesses for the given aeroelastic constraints, the required skin thickness and shear web thickness were computed.

Lastly, the point before which unstable aeroelastic effects should not happen is dictated by regulations. Namely, CS 25.629, which states that unstable aeroelastic behaviour must happen at or beyond the highest of V_{dive} or 1.15 times V_c . This constraint is set to ensure that aeroelasticity does not pose any issues within the normal flight envelope.

Results The results of the aeroelasticity analysis are summarised in Table 13.6. It was concluded that the Ceres aircraft with an aspect ratio of 13 at its cruise altitude does not suffer from significant aeroelastic effects. In fact, aeroelastic effects become worse as the density increases, which is clearly shown by the table. While the aeroelasticity does not pose any problems at cruise altitude, it does pose a critical point at sea-level conditions, where the flutter speed is within normal flight envelope.

However, favourable flutter characteristics can be obtained by tweaking the mass distribution of the wing by shifting the position of various components in the wing group to acquire favourable bending and torsional natural frequencies.

Table 13.6: Aeroelastic speeds for the Ceres aircraft for an aspect ratio of 13. The divergence speed is well below the speed shown below

Altitude [m]	Divergence Speed [m/s]	Control Reversal speed [m/s]	Flutter speed [m/s]
0	351.56	394.1	299.8
11000	645.00	723.0	550.0
20000	1311.37	1470.05	1118.3

Verification and Validation For the verification of the aeroelasticity analysis, the results were compared with [9] using the parameters indicated in that report. Additionally, a bending and torsional stiffness of 0.00044 m^4 and $3.05 \times 10^6 \text{ N m/rad}$ were assumed, respectively. The results are shown in Table 13.7 and Table 13.8.

It can be remarked that while the in-house code has a relatively low mean discrepancy when compared to the results from NeoCASS, the deviation shows to be non-conservative and larger than the deviation SAGA[9] had. This may be due to used numbers which deviates from the numbers SAGA[9] used, resulting in larger discrepancies. For example, the bending and torsional stiffness were assumed as these values are unknown. Additionally, r_θ is unknown as well and was taken to be the same as shown in Table 13.5.

Furthermore, NeoCASS is a much more detailed module which takes the whole aircraft geometry, including engine position, as input to compute the structural and aeroelastic model.⁷ For instance, the wingbox dimensions computes and optimises locally while the in-house code assumes a constant skin and web thickness. The section-by-section optimisation of NeoCASS results in much more accurate approximations for the torsional and bending stiffness than the in-house code. Moreover, the engine positions are taken into account in NeoCASS, which significantly affects the output as x_θ and r_θ can be varied and optimised by shifting the longitudinal engine position.

Lastly, the in-house code uses a 'typical (airfoil) section' method, where the aeroelastic speeds are determined at 75% of the span. Thus, compared to NeoCASS, where the complete geometry of the aircraft is

⁷https://www.neocass.org/?Home_Documentation_Manuals_and_Tutorials

considered, it is clear that discrepancies in the between the results of the in-house code and NeoCASS are large.

Table 13.7: Verification and validation using SAGA and NeoCASS numbers. The aeroelastic speed values from the SAGA report are compared with self-obtained numbers.

Altitude [m]	Divergence Speed [m/s]	Control Reversal speed [m/s]	Flutter speed [m/s]	Flutter speed SAGA [m/s]	Flutter NeoCASS [m/s]
Take-off (sea-level)	228.3	283.6	194.7	185.3	187.4
13000	490.4	609.0	418.2	364.6	496.9
19000	787.0	977.0	671.2	533.9	628.5
19500	818.7	1016.9	698.2	553.8	598.0

For the validation of the aeroelastic speeds, actual flight tests have to be performed to determine the actual speeds at which unstable aeroelasticity starts. As such, the validation of the aeroelastic speeds are beyond the scope of this DSE report and the results should be validated in further design. Furthermore, detailed analysis using the semi-rigid wing model and CFD should be performed in the future to obtain higher certainty on the aeroelastic effects of the wing and resulting constraining aeroelastic speeds to ensure that the unstable dynamic and static aeroelastic behaviour occur outside the flight envelope.

Table 13.8: The results of the aeroelastic speeds compared to the results shown in the SAGA report.

	Divergence speed	Control Reversal speed	Flutter (own vs NeoCASS)	Flutter (SAGA vs NeoCASS)
mean discrepancy [%]	11.96	29.25	2.90	12.55
standard deviation [%]	8.17	9.42	11.82	9.51

13.2.4. Fuselage

The fuselage has been sized with regard to two of its functions, minimising the aerodynamic drag and carrying the payload and landing gear, whilst keeping the fuselage weight at a minimum. The former is crucial to sizing as the fuselage contributes to approximately 30% of the zero lift drag [26], while the latter is clearly essential for the successful completion of Ceres' mission. The following paragraphs elaborate on these two functions and size the fuselage accordingly.

Fuselage Diameter Requirements In order to carry the payload, the fuselage dimensions need to provide sufficient space, hence the total volume and dimensions of the sulphur tank and combustion engine had to be considered. The sulphur was decided to be transported in solid state as pellets, since molten sulphur has disadvantages such as extra weight due to advanced storage tanks, logistical and operational risks, and safety hazards. These pellets have a density of 1121.29 kg/m^3 ⁸ resulting in a required storage volume of 8.65 m^3 and a diameter of 2.25 m. Additionally, the combustion engine has a required inlet diameter of 0.64 m^2 .

In order to accommodate the 8.65 m^3 payload tank, sufficient space in the fuselage is required. Also, the bottom 20 % of the fuselage was reserved for plumbing or pumps required to transport the sulphur to the burner. The tank was designed to be cylindrical in shape and can be placed directly ahead of the tailcone of the fuselage, requiring minimum plumbing to transport the sulphur to the burner located at the tailcone of the fuselage.

Longitudinal Fuselage Dimensions Three factors influence the design of the longitudinal fuselage dimensions. The payload must be carried in the most compact way possible, the length must be sufficient for the tail arm, and the fuselage shape should minimise aerodynamic drag. The tail arm was discovered to be a driving factor for the fuselage design, as the total fuselage length was set by it. In order to reduce weight, the cabin length and fineness ratio were set as small as possible, while providing enough volume for the payload. As a result the tailcone became longer. The fineness ratios were traded based on their effect on the MTOW. Ultimately the combination which yielded minimum MTOW and sufficient volume was selected.

For the purpose of quantifying the effects of the fineness ratio, the fuselage weight and effect on C_{D_0} had to be computed. The fuselage weight estimation is elaborated on in Section 13.4. As for the effect on C_{D_0} , the friction coefficient method as presented in Equation (13.24) was used to calculate contribution of

⁸<https://suw.biblos.pk.edu.pl/downloadResource&mId=152405>

the fuselage [100]. The total wetted area has then been calculated using Torenbeek's method [91]. Results yielded a C_{D_0} fraction of 39%, coherent with the previously mentioned value of 30%.

$$C_{D_0} = C_{f_e} \frac{S_{w fus}}{S} \quad (13.24)$$

Design for minimal drag In order to ensure that the fuselage did not produce a disproportionate amount of drag with respect to the rest of the aircraft at cruise, the fuselage shape was compared to literature [76]. This model for zero lift drag coefficient prediction approximates the Squire-Young Formula as from [29]. The equation which is the base of the Squire-Young formula is shown in Equation (13.25) when compressibility is taken into account. The goal of this equation is to predict the far wake of a body and to simulate a true control volume momentum balance. Moreover, its major advantage is the possibility to account for compressibility and Reynolds numbers due to the integration of the development of the boundary layer. This is an accurate prediction method as has been discussed in said paper. In [76] Dodbele et al. discuss the iterative design of a fuselage for laminar flow, taking into account certain constraints. These mostly regard dimensions which should be respected. The relations, that this paper gives, allow to design for and estimate the C_{D_0} of the fuselage. The geometry satisfies the relations below, where x_m is the location of the widest part of the fuselage and x_i is the location of the inflection of the fuselage. This was however modified so that the shape only changed the shape of the nose section. This was done as the inflection occurs just after the widest section of the fuselage which is not located at the tail in this design. The F and G functions in Equation (13.26) are polynomials which can be found in [76].

$$c_d = 2 \left(\frac{\delta_{2,TE}}{c} \right) \left(\frac{U_{TE}}{U_\infty} \right)^{\frac{5+H_{12,TE}+(\gamma-1)M_\infty^2}{2}} \left(\frac{1 + \frac{\gamma-1}{2} M_\infty^2}{1 + \frac{\gamma-1}{2} M_{TE}^2} \right)^{\frac{1}{\gamma-1}}$$

where,

$$H_{12} = \frac{\delta_1}{\delta_2} \quad (13.25)$$

$$\delta_1 = \int_0^\infty \left(1 - \frac{\rho u}{\rho_e U_e} \right) dy$$

$$\delta_2 = \int_0^\infty \frac{\rho u}{\rho_e U_e} \left(1 - \frac{u}{U_e} \right) dy$$

$$r(x) = \left(\frac{1}{2f_r} \right) [r_n \quad F_1(x) + k_1 F_2(x) + G(x)]^{1/2}, \text{ for } x < x_m$$

$$r(x) = \left(\frac{1}{2f_r} \right) \{r_i + (1 - r_i) [k_1 F_1(x) + s_1 F_2(x) + G(x)]\}, \text{ for } x_m < x < x_i \quad (13.26)$$

$$r(x) = s_i x (1 - x^3) - s_1 x^2 (2x - 3)(x - 1) + x^2 (3x^2 - 8x + 6), \text{ for } x_i < x$$

This fuselage design showed that the fuselage C_{D_0} , due to its extended length, is just over 60% of the zero lift drag coefficient, with an approximate value of 0.026. This heavily contrasts the estimated 30% and as such was not taken as an input for other functions. It however enables the programme to converge towards a minimum of drag.

13.3. Propulsion Design

In this section the propulsion system is discussed. This system should provide the Ceres aircraft with sufficient thrust to perform the selected flight profile. This section looks into the available engine options and how they could be modified for better performance at cruise altitudes.

Method The main method to predict the thrust and SFC levels of the engine is by making use of the model GasTurb. It is a licensed model, constructed by a former MTU employee, that is specialised in analysing engine performance and optimisation of it⁹. The program requires engine specifications, such as bypass and

⁹<http://www.gasturb.de/the-original-author.html>

pressure ratios of the compressors and turbines as inputs. From this, it computes the desired parameters at each engine stage. This way an approximation of the thrust at higher altitude can be obtained. Before a detailed design is done, first an engine selection is made. This is done by making use of a simplified thrust scaling method, which is explained later in this section. When a suitable engine is found, it is looked into with more detail by making use of GasTurb.

Engine Selection In this section the method used to determine the most suitable engine is elaborated upon. The dispersion of the payload of the Ceres systems takes place at 20 km altitude. Since density and pressure at that altitude are significantly lower compared to sea-level, piston and propeller engines are not viable options. These type of engines, given that their technology readiness level are on a sufficient level, are either altitude or speed limited for these type of operations. Turboprop engines generate most of their thrust with the propeller which also makes them not suitable at high altitudes. The only viable options that remain are either turbojet or turbofan engines. Since turbofan engines in general have improved propulsive efficiencies and thrust levels, these will be the type of engine selected. [77]

From the initial sizing, a maximum required thrust value was obtained [33]. This thrust value corresponds to the required thrust to weight ratio for the different flight stages, assuming thrust scales with density. More advanced models were applied in this stage, which considered Mach number and ambient conditions. These models were obtained from [35]. The model starts by defining two ratios, θ_0 and δ_0 , which represent the total temperature and total pressure relative to sea level conditions. These values depend on the altitude and the Mach number of the aircraft.

$$\begin{aligned}\theta_0 &= \frac{T_{tot}}{T_0} = \frac{T}{T_0} \left(1 + \frac{\gamma - 1}{2} M^2 \right) \\ \delta_0 &= \frac{p_{tot}}{p_0} = \frac{p}{p_0} \left(1 + \frac{\gamma - 1}{2} M^2 \right)^{\frac{\gamma}{\gamma - 1}}\end{aligned}\quad (13.27)$$

To scale the thrust of the engines from S.L.S. conditions a series of empirical relations must be applied. For low-bypass engines using maximum thrust, Equation (13.28) must be used. A thrust ratio (TR) refers to the throttle ratio at which the engine theta break occurs depending on the design conditions. A TR of 1.0 is chosen. The first formula shown in Equation (13.28) shall be used when $\theta_0 \leq TR$, with the lower relation whenever the condition is not satisfied.

$$\begin{aligned}F &= F_{SL} \delta_0 \\ F &= F_{SL} \delta_0 \left[1 - \frac{3.5(\theta_0 - TR)}{\theta_0} \right]\end{aligned}\quad (13.28)$$

For low-bypass engines using military thrust, Equation (13.29) must be used. The above relation shall be used when $\theta_0 \leq TR$ with the lower relation whenever the condition is not satisfied.

$$\begin{aligned}F &= 0.6 F_{SL} \delta_0 \\ F &= 0.6 F_{SL} \delta_0 \left[1 - \frac{3.8(\theta_0 - TR)}{\theta_0} \right]\end{aligned}\quad (13.29)$$

Finally, for high-bypass engines, Equation (13.30) must be used. The above relation shall be used when $\theta_0 \leq TR$ with the lower relation whenever the condition is not satisfied.

$$\begin{aligned}F &= F_{SL} \delta_0 \left[1 - 0.49 \sqrt{M} \right] \\ F &= F_{SL} \delta_0 \left[1 - 0.49 \sqrt{M} - \frac{3(\theta_0 - TR)}{1.5 + M} \right]\end{aligned}\quad (13.30)$$

From the initial sizing [33], the thrust required for climbing at 500 fpm at the cruise height, as well as the thrust required for flying at the maximum design cruise speed were considered to be most critical. A

selection of possible engines is made based on their proven performance. Only engines that have been used close to or above the given altitude requirement of 20 km were considered as possible options. The selected engines with the relevant data are shown in Table 13.9. The relations mentioned above were applied onto the engines selected to check for the thrust they provide at altitude.

Table 13.9: Engines Available Proven to be Feasible for Operation at a Cruise Altitude of 20km

A/B	Name	S.L. Static Thrust [N]	Mass [kg]	SFC [kgN ⁻¹ s ⁻¹]	Cost [M\$ 2019]
False	F118-GE-101 ^a	75700	1429	18.63 · 10 ⁻⁶	-
	F137-RR-100/AE3007H ^b	36880	745	17.70 · 10 ⁻⁶	4.00
	EJ200 Mil. Power ^c	60000	1000	22.00 · 10 ⁻⁶	5.00
	F110-GE-100 Mil. Power ^d	73800	1800	21.10 · 10 ⁻⁶	7.12
	F100-PW-200 Mil. Power ^e	65270	1467	20.39 · 10 ⁻⁶	6.36
True	EJ200	90000	1000	49.00 · 10 ⁻⁶	5.00
	F110-GE-100	124600	1800	55.83 · 10 ⁻⁶	7.12
	F100-PW-200	106000	1467	70.81 · 10 ⁻⁶	6.36

^ahttps://janes.ihs.com/Janes/Display/jae_0560-jae_

^bhttps://janes.ihs.com/Janes/Display/jae_0755-jae_

^chttps://www.mtu.de/fileadmin/DE/7_News_Media/2_Media/Broschueren/Engines/EJ200.pdf

^dhttps://janes.ihs.com/Janes/Display/jae_0559-jae_

^ehttps://janes.ihs.com/Janes/Display/jae_0748-jae_

The engine was selected by choosing the option of which the overall weight was minimised. This is due to a proportionality between engine weight and overall cost. Additionally, maintenance costs increase proportionally to engine weight. This condition tends to drive the engine selection to the engine with the best thrust to weight ratio. This allows the model to provide the lowest engine cost possible for the aircraft.

A thrust requirement of 21.58 kN after performing analysis of the flight profile was obtained. This resulted in the lightest option being 6 EJ200 engines. These 6 engines will provide approximately 23.57 kN of maximum continuous thrust at cruising altitude. At sea level, this means a maximum continuous thrust of 360 kN is available, meaning that for take-off no thrust problems arise. The EJ200 being selected is a result of it having the highest thrust over weight ratio of the possible options. This is when the afterburner option was disregarded. The motivation to disregard the afterburner is due to fuel usage. Implementing an afterburner drastically increases the fuel consumption, and during operations it could only be useful at end of climb. However, then the additional required fuel would have to be carried during the prior part of the mission, further increasing the overall fuel usage. In the following section the design of the selected engine is explained in more detail.

The EJ200 is also regarded as the most feasible engine since its technology readiness level is high. The engine has a built in Engine Control and Monitoring Unit (ECMU), which allows for better testability and monitoring functions. Resulting in a lower maintenance time and improvement of the availability and operational reliability [25]. In the Eurofighter Typhoon, the engine has proven to be capable of reaching the desired altitude, whilst also being very reliable. In over 3,000 hours of intensive operations no engine replacements were necessary¹⁰. Furthermore, the engine is specifically designed to be fuel efficient, reliable and to allow for easy maintenance. With currently having more than a 1,000 engines delivered, the EJ200 has matured well and the engines are still fully in use. Meaning that, from a manufacturing point of view, the EJ200 is a realistic option. Furthermore the engine has roughly the same performance level after 1,400 running hours as a brand new engine and is capable of operating for more than a 1,000 flying hours without the need of unscheduled maintenance, which indicates that the engine is very reliable for a military engine. From a manufacturing standpoint the engine is also the better option. It was developed and manufactured in collaboration by Rolls-Royce, MTU, Avio and ITP¹¹. Making it a suitable organisation for collaboration in a Ceres project.

The cost aspect of the EJ200 is a bit more uncertain. By looking at the first 2 tranche deals and comparing the costs to the other engines, an estimate of 5 million USD was used for the engine costs. This lower-side estimate is made because only a conventional engine design is required, not depending on the most modern technologies. With the specified amount of engines required for the whole program, a deal covering

¹⁰https://rusi.org/sites/default/files/whr_1-15_maximising_european_combat_air_power_0.pdf

¹¹<https://www.eurofighter.com/the-aircraft>

a minimum of 1080 engines is needed. Resulting in a deal of approximately \$5.5B.

Engine Design Since a suitable engine had been selected, a more detailed look was taken into the design of the engine. This will cover engine specifications and compressor maps. Since it is desired to keep the feasibility of the project as high as possible, it was chosen to not make significant changes in the design of the engines. The EJ200 has proven to be capable of reaching 20 km altitude and proposed changes could unexpectedly result in degradation of performance at higher altitude. However, to determine the thrust lapse and the absolute thrust at altitude, the design drivers of the engine were looked into. To start this section off more details on the engine are given in Table 13.10¹². The thrust at 20 km and the turbine inlet temperature are both found using GasTurb. Finally a power off-take per engine of 50 kW is used, for powering of other on-board systems. During all computations, standard Jet A-1 fuel was assumed to be used. All the inputs and outputs used in GasTurb is found in Appendix A.

Table 13.10: EJ200 Engine Specifications

EJ200	Value	Unit
Thrust (SL)	60	kN
Thrust (20 km)	3.93	kN
Bypass ratio	0.4	-
LPC PR	4.2	-
Stages	3	-
HPR PR	6.2	-
Stages	5	-
Mass flow	77	kg/s
Length	4000	mm
Diameter	850	mm
Weight	1000	kg
Turbine Inlet Temperature	1650	K
Power Off-Take	50	kW

The thrust of 60 kN is static sea level thrust. When the altitude is increased the density will reduce and the thrust will too. By flying at a higher velocity, the amount of energy required to propel the air backwards also increases. Compared to static thrust this further results in a decrease, however, with less significance than the density. The most important part of the propulsion system for this mission is the thrust level and specific fuel consumption at higher altitudes. At 20 km the thrust can be as low as only 5 to 10 % of the static sea-level thrust. As mentioned previously the primary method for determining the thrust at different altitudes is GasTurb. From GasTurb both on- and off-design thrust values were obtained. On-design means that the input design specifications were used to determine the thrust at that given altitude, while off-design took the given inputs at a certain altitude and scaled those to other altitudes. An example of the differences between the two was that for on-design the pressure ratios are constant for the given input and for off-design they will vary. How the on- and off-design thrust scales with altitude is shown in Figure 13.10.

The engine selection code relies on the thrust scaling method from [35], also shown in the figure. Finally the thrust scaling with density is shown, since this was used in the early stages of the design for determining thrust values. From the figure it can be noticed that at lower altitudes there are relatively large differences. As the altitude is increased the thrust levels gradually come together. The most accurate thrust prediction is the off-design GasTurb one. It predicts 3.93 kN at 20 km at Ceres' cruise velocity of $M = 0.7$. GasTurb automatically differs the relative spool speed when working on off-design points. For the case at cruise only a relative spool speed of 87 % was used. Meaning that the engine could operate at even higher thrust levels. When corrected for the relative spool speed, such that the same relative speed at statics sea level conditions is achieved, a thrust of 4.51 kN is found. This lower spool speed is used to take into account the uncertainties that occur during the modelling engines at high altitude. The lower bound estimate of 3.93 kN is only 6.55 % of the EJ200's static sea-level thrust. The required thrust during cruise of 21.58 kN means that the engine thrust could be even lower than the estimation of 3.93 kN by 8 % and the aircraft would still be able to cruise at 20 km. Even in the most passive modelled case this lower thrust level of 3.61 kN would not be reached.

¹²https://www.mtu.de/fileadmin/DE/7_News_Media/2_Media/Broschueren/Engines/EJ200.pdf

In Figure 13.11 the change in SFC over the change in altitude is shown. This SFC is for maximum sustainable thrust and only the values for on- and off-design are used. Out of these the off-design is regarded as the leading value and the on-design point is there for a reference value. As can be seen in the figure the SFC first decreases after which it increases. The decrease in SFC is a result of the lower ambient temperature at higher altitudes, leading to a higher thermal efficiency. The SFC starts to increase rapidly in the off-design case above 10.5 km. This is a result of lower efficiencies of various engine components such as the compressors. These components tend to have a lower efficiency once the perceived Reynolds number decreases due to the lower density. For on-design the SFC stays roughly constant at 0.92 lbf/(lbf-hr), since no changes in efficiencies are taken into account.

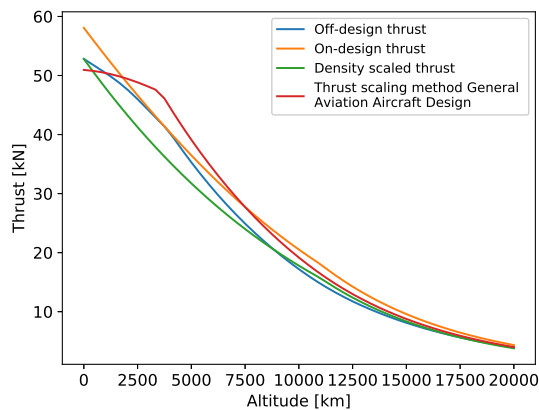


Figure 13.10: Thrust Lapse with Altitude.

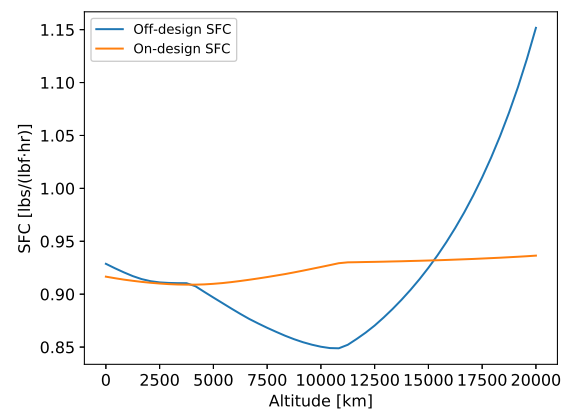


Figure 13.11: Differences in SFC over Altitude.

The design drivers considered for the EJ200 are the compressor pressure ratios, bypass ratio, and the temperature of the combustion gasses. The inlet area is not stated here because GasTurb derives the value from the inlet mass flow. As a result the inlet area is not considered as a separate parameter. However, when looked at the bypass ratio, the mass flow through the engine core is kept constant and by varying the BPR the outer part of the engine will thus increase. This will result in an increased mass flow and thus an increased inlet area. Since it is chosen not to change the engine too much from the original EJ200 design, the pressure ratios are fixed at their original values. This is also done considering that the engine is originally designed to have a sufficient surge limit to minimise the chance of engine stall. More on this will be explained later in this section.

Bypass Ratio As the bypass ratio (BPR) is increased, the engine will take in more air and the compressors will add more energy to the total air flow. However, as the fan increases in size, the total weight of the engine also increases. GasTurb has an integrated option that estimates the weight of the given engine. By making use of this function a plot is made showing how the engine thrust over weight ratio varies with BPR. This plot is shown in Figure 13.12 for static sea level conditions. In Figure 13.13 the same plot for cruising altitude is shown. The value for the thrust over weight does not completely correspond to the expected value of 6 N/kg at static sea level conditions. This is because the weight used in GasTurb, while obtaining the data, did not include the afterburner and thus relied on a lower engine weight. A correction is applied for this, taking into account the removed afterburner.

Another matter that should be noted is that GasTurb does not allow for manual changes in the BPR for off-design analysis. Resulting in the fact that these plots only could be made for on-design, meaning lower accuracy of the values found. However, the plots are still shown to get an idea of how the BPR influences the design. Again, when changing the BPR, the engine core is kept constant and only the outer fan size is increased. This will result in more air being given energy and thus in more thrust. Since more air is required to be accelerated by a smaller velocity difference, the engine will become more efficient and the SFC will reduce. From the plots it can be seen that this is actually the case at sea level. As the BPR increases the thrust over weight also increases and SFC decreases due to the more efficient design. For cruising conditions, however, a higher bypass ratio becomes less effective. There is still a slight increase in total thrust but the

thrust over weight of each engine is lower. Since the cruising altitude is of uttermost importance for this design a small BPR should be selected according to these results. However, it should be noted that in both figures the SFC goes down for an increase in BPR. Meaning that an increase in BPR could be beneficial for total fuel consumption. Another reason to keep the BPR low is that for this mission, feasibility is an important aspect. For high thrust, high bypass engines at high altitudes, the effectiveness is not proven. Of the selected engines the F137 (AE3007) has the highest bypass ratio of close to 5. This is already classified as a high bypass engine but numbers can go up to above 10 for engines such as the Rolls-Royce Trent 1000¹³. Since their efficiency at the specified cruise altitude is uncertain, those high-bypass engines were not considered for the engine selection.

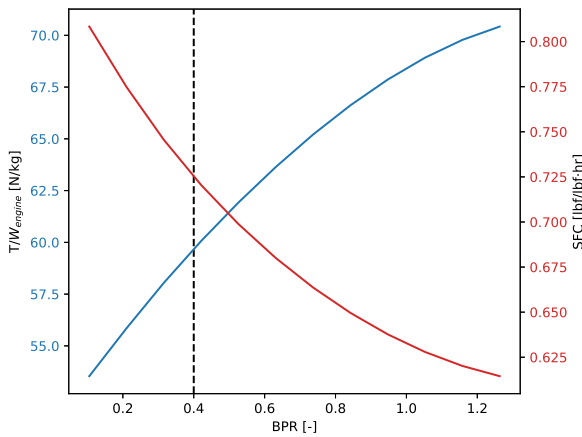


Figure 13.12: The Engine Thrust over Weight and SFC as a Function of BPR at Sea Level.

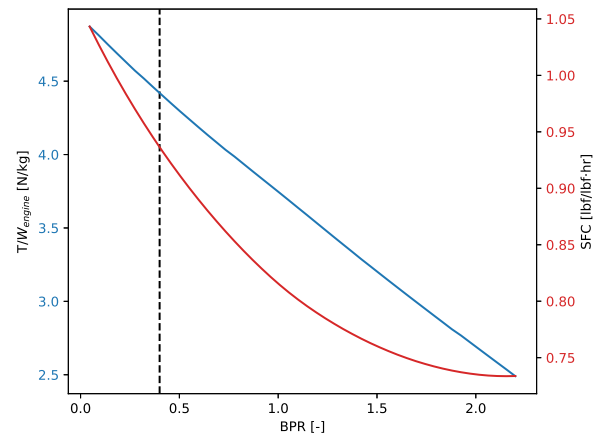


Figure 13.13: Engine Thrust over Weight and SFC as a Function for BPR at Cruise Altitude.

Turbine Inlet Temperature Another important design parameter considered is the turbine inlet temperature (T_4). This temperature is directly related to the energy given to the flow, and thus how much thrust the engines can generate. For now, a value of 1650 K during static sea level conditions is used. This value is found by reverse engineering of the EJ200 engine into GasTurb. During cruising conditions a T_4 of 1552.52 K was obtained using GasTurb. In Figure 13.14 and Figure 13.15 the changes in thrust and SFC against T_4 are shown. The first figure indicates the off-design case at sea level, while the second plot gives the results during cruise at altitude. In both plots the values on the y-axis are corrected for HPC spool speed.

In the off-design option in GasTurb the spool speed is allowed to vary. In order to be able to compare values for each different T_4 , the correction for the spool speed is taken into account. From the plots it can be concluded that at both conditions, the effect of the turbine inlet temperature stays roughly the same. A higher temperature results in more thrust and a lower SFC. This is mainly due to a higher thermodynamic efficiency resulting from a larger temperature difference between the ambient and turbine inlet temperature. Thus a T_4 as high as possible is desired. Nowadays, the limiting factor is mostly the material properties. The higher temperatures push the materials to their limits which increases wear and the risk of failure. It is shown that T_4 for newer engines increases with 19 K/yr, while the operating temperature of the materials increases with 5 K/yr, meaning that cooling methods also become more advanced [103].

Compressor Maps As mentioned before, the engines will operate in a low density environment, which can lead to a higher risk of compressor stall. Compressor stall occurs, in a multi-stage compressor, when the pressure of the incoming flow is too low compared to the flow pressure in later stages. A mild surge will cause a marginal drop in power for a short period of time. However, a full engine stall or engine surge will result in a negative airflow and complete loss of power in that engine. Since at higher altitudes the pressure is relatively low, the chance of engine stall or surge increases. By constructing compressor maps,

¹³<https://www.rolls-royce.com/products-and-services/civil-aerospace/airlines/trent-1000.aspx#section-overview>

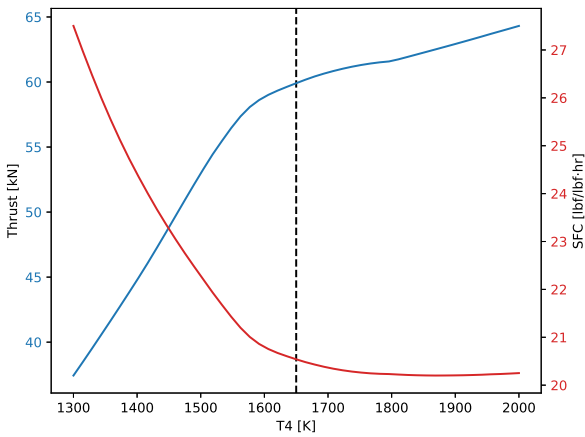


Figure 13.14: Thrust and SFC as a Function of T_4 at Sea Level.

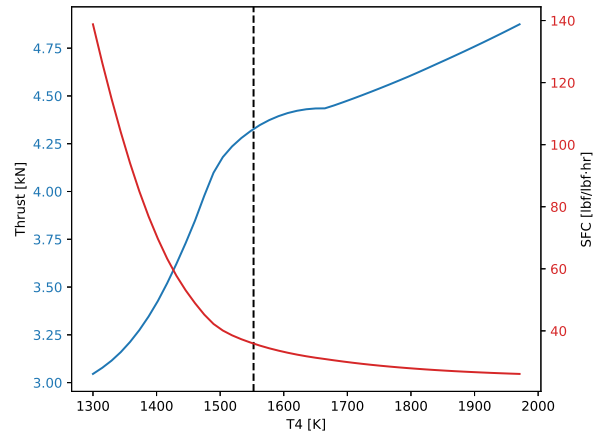


Figure 13.15: Thrust and SFC as a Function of T_4 at Cruise Altitude.

the risk of engine stall is analysed. The compressor map for the LPC and HPC are shown in Figure 13.16 and Figure 13.17, respectively.

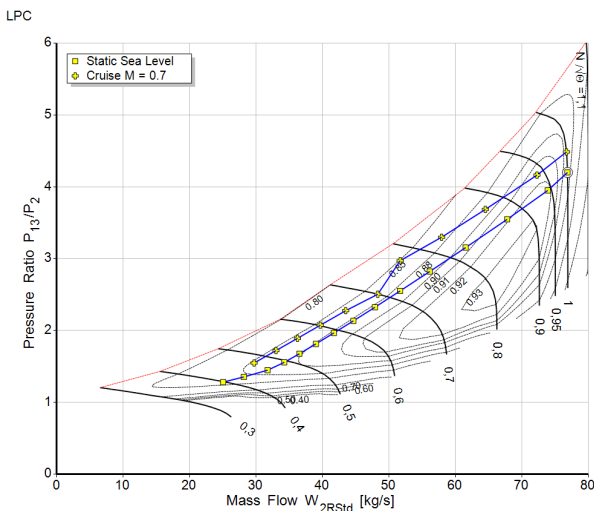


Figure 13.16: Compressor Map for the LPC.

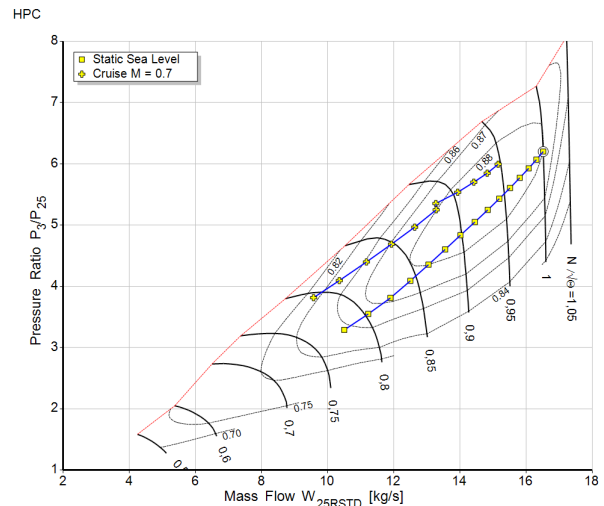


Figure 13.17: Compressor Map for the HPC.

On the x-axis the mass flow through the engine inlet corrected to S.L.S. conditions is plotted, while on the y-axis the pressure ratio over the LPC is shown. The vertical lines that curve to the left as the pressure ratio increases, indicate spool speeds. The spool speed is divided by the static sea level maximum value, resulting in a maximum value of 1. The regions covered in the background are efficiency regions, indicating the overall efficiency of the specific compressor. The red line indicates the surge line. Above this red line the chance of engine stall is increased and operating in this regime should be avoided at all times. The blue lines in each plot indicate the operating limits. In both cases the lowest line is the static sea level line and the upper line the one for cruise conditions at $M = 0.7$. Even though in both cases the line during cruise is closer to the surge line, under no condition the line is crossed. Assuming that GasTurb can make relatively accurate predictions on engine stall, the surge margin is further explained by the type of operations that the engine is designed for. The engine was specifically designed to have a sufficient surge margin and should not show problems during any stage of operations [69].

Engine Design Recommendations Now that the most important aspects of the design are covered, some recommendations are given to improve the overall design. The first main point of improvement of the EJ200 is removing the afterburner section. Since it is not planned to make use of the afterburner, it can as well be completely removed from the engine. An approximation of the weight saved by removing it, is made by

comparing the F110 and F118 engines and by using GasTurb. The F110 is an afterburning engine based on the F118. Apart from the afterburner the engines only have minor differences. When comparing the masses, a difference of roughly 320 kg is found¹⁴¹⁵. Since the total engine mass of the F110 is 1.8 that of the EJ200, the possible weight savings by linear scaling results in about 180 kg.

GasTurb includes an option for an engine weight estimation. By using the inputs of the EJ200 it estimates a standard mass of 1015.83 kg. Considering the actual mass of the engine, this is only a 1.58 % difference. By deselecting the afterburner option a new mass of 853.27 kg is obtained, meaning a mass saving of 162.56 kg. Taking into account the number of engines, this could result in a weight savings of around 950 kg, making up 1.88 % of the MTOW.

A second motivation for removing the afterburner is a reduction in maintenance time and costs. Now, even though the afterburner is not used, it still has to be monitored and checked during maintenance. Not having to inspect afterburners from the 6 engines per aircraft will add up over time. An argument to keep the afterburner section installed is that the engines are now only produced including the system. Removing it might require new nozzle design and changes in the manufacturing line. This could result in an increase in R&D and manufacturing costs. Finally the afterburner could be used in case of emergency, if the conditions allow for it.

For now it is recommended to keep the bypass ratio at a value of 0.4. As can be seen from Figure 13.13 the engine thrust over weight decreases for higher altitudes as the BPR is increased. The SFC, however, decreases for an increase in BPR. This holds for a BPR of up to 1.0. Depending on the importance of fuel consumption it, can be chosen to increase the BPR at costs of a slightly higher weight.

For the turbine inlet temperature a temperature as high as possible is required. Compared to the value used for the EJ200, T_4 for newer engines has increased by a fair amount. Turbine inlet temperatures in the most advanced turbofan engines can go up to more than 2000 K [103]. The most efficient design is achieved by maximising T_4 for continuous thrust. At higher altitudes a T_4 higher than 1675 K rapidly increases the thrust. However, more research should be done to see what values are achievable under these operation standards.

Finally, it is advised to look into more detail for compressor efficiency at higher altitude. When the Reynolds number drops below the critical value of $3.5 \cdot 10^5$, the efficiency of the compressor will decrease [88]. The perceived Reynolds number for the compressors is lower compared to that of the aircraft, since now the compressor fan blade chord length is used and not the wing chord length. This decrease in Reynolds number is mainly caused by the lower density at higher altitudes. By making use of wide chord fan blades a higher Reynolds number can be achieved, minimising the reduction in efficiency. Furthermore, by looking at the compressor maps and varying the spool speed, an optimal configuration can be found. The off-design points on GasTurb do take into account the lower efficiencies, however, study has shown that a newer method can be used to approximate these more accurately [88]. Applying this could result in a more accurate thrust prediction.

Engine Position In this section the method used to position the engines is elaborated. The engine placement is dependent on the number of engines needed. For each scenario, the engine positions are established.

Comparing the wing-mounted and the fuselage-mounted options, wing-mounted integration is preferred due to its benefits in reducing aerodynamic bending load on a wing, which is favourable especially for a long span wing. The engines are placed in front of the wing, as this makes sure that the airflow at the intake is less influenced by the pressure field of the wing. Furthermore, the engine can be mounted higher to the wing, such that the landing gear can be shortened, and in the case of an uncontained engine failure, the engine is less likely to damage the wing. Lastly, a forward engine placement is also beneficial from a aeroelastic point of view, as the distance between the elastic axis and the centre of gravity is reduced.

Similarly to the B-52, the engines are placed in pairs. This is due to the fact that it lowers the nacelle weights, and it gives a lower wetted surface area. Due to the large tail arm needed for a feasible horizontal tail surface of Ceres, the engines can be placed further out than previously established. For four engines, the engines will be placed at 35 % of the half-span, as there will be a supporting rib here, which makes it

¹⁴https://janex.ihs.com/Janes/Display/jae_0560-jae_

¹⁵https://janex.ihs.com/Janes/Display/jae_0559-jae_

easier to append nacelles here. If six or eight engines are needed, the additional engines will be placed at the beginning of the ailerons, as another structural enforcement will be present here.

One disadvantage of this engine placement compared to when podded individually is that the engines receive less air during take-off. This occurs because at take-off the engine sucks in air from all around the inlets. When the engines are placed closely together, the airflow of the two engines interfere with each other and result in a slightly lower air intake rate at take-off and low air speeds. At higher velocities the engines only take in the air directly in front of their respective inlets and do not suck in air from the sides. As a result, the shared nacelle will not have a significant influence on the engine performance during the critical operation phases. During take-off the engines are relatively strong, so a slight decrease in thrust is not a problem during this phase [62]. By carefully designing the nacelle shape, no additional aerodynamic disadvantages are added to the design. As mentioned above, the B-52 uses this principle by having eight engines paired in four pods. With a surface ceiling of more than 15 km and a cruise Mach number of 0.86, paired engines have been proven to work¹⁶. Finally it should also be noted that by pairing 2 engines on each side the risk of both engines failing when one fails is introduced.

The longitudinal position of the engines is determined such that the clearance needed from the wing is minimised. This results in a clearance of roughly 10 cm. This requires that the point at 45 % of the engine length, is at -20 % of the cord-length of the wing.

As stated previously it is found that six engines are required and their spacing (symmetric for each side of the wing) is determined. As explained above, two of the three engines on each side will be podded in pairs. The paired engines are placed relatively close to the fuselage at 35 % of the wing semispan. The third engine is placed further away from the fuselage at 75 % of the wing semispan. This is done to achieve wing bending relief and minimise the problems in case of engine failure. Furthermore, at these spots the ribs and ailerons are located in and on the wing, meaning that at those points the wing can take up more loads compared to other points.

Verification & Validation The output of the models used during the design of the propulsion system has, as every other model, to be validated and verified. First, the engine selection model is verified by comparing the amount of thrust required versus the number of engines the program outputs. If the non-afterburning version of the code is selected, the AE3007 is never selected. This behaviour is coherent with the thrust lapse that occurs due to its high bypass ratio. If the engine selection is fixed to the EJ200 and the payload mass is decreased from 9700 kg to 9500 kg, the programme decreases the required number of engines from 6 to 5. If the programme is allowed to choose whichever engine, it tends to select the F118 at 9700 kg payload mass, as the required number of engines is 4. On the other hand, as soon as the payload is decreased to 9500 kg, 5 EJ200's are selected as their overall mass is 5000 kg, which beats the 5716 kg if the F118 is selected. This behaviour is considered correct and beneficial for the design. Further, if the afterburner option is selected and the payload remains at 9700 kg, the engine requirement goes to 14 EJ200 A/B engines. This is due to a threefold increase in fuel consumption requiring a much larger fuel fraction. This in turn drives the MTOW up for a given payload mass, thus leading to 14 afterburning engines. This is coherent with what is expected and this part of the model is verified.

Apart from GasTurb, another engine performance program widely used in the aerospace sector is the Gas Turbine Simulation Program (GSP). This model originally was developed at the TU Delft and is further updated by the NLR. This program has been verified and validated in more detail than GasTurb. By comparing the two models, the use of GasTurb is justified. For a single spool turbojet, the differences between GasTurb and GSP range from 0.2 % thrust at conventional conditions up to 1.6 % for supersonic conditions at 8 km altitude [86]. The article further shows that, for conditions up to 8 km, the outputs of the two programs are always within 1.5 % for other parameters such as fuel flow and specific fuel consumption. For higher altitudes, no comparison is made. However, since there are a lot of uncertainties for estimating thrust at higher altitudes and the programs show great similarities at lower altitudes, it is assumed that the use GasTurb is validated.

In an attempt to further validate GasTurb at higher altitude, there has been contact with experts in the field of propulsion. Unfortunately no validation data was available to compare to at higher altitudes. However, it was mentioned that GasTurb is a validated program and should be, at least for lower altitudes, accu-

¹⁶ <https://www.boeing.com/defense/b-52-bomber/>

rate.

The GasTurb program relies on various detailed inputs, which are hard to acquire for existing engines. The second year course Power and Propulsion (AE2230-II) provides the required data and is thus used for verification purposes. Verification is done by taking the input data from the course and comparing the thrust and specific fuel consumption as output. The first engine that is compared has a twin spool configuration. When this is compared for the given Mach number and altitude, a difference of 2.45 % is found for the thrust level and 10.4 % for the SFC. The second engine used for the verification is a modified GE90 engine. For this engine the differences are larger. The thrust obtained from GasTurb is lower by 14.2 % and the SFC is higher by 18.9 %. The main reason for this is most likely the higher level of detail of the GasTurb program. It takes into account a lot more efficiencies and additional input parameters, which are likely to cause a difference in output.

Finally SUAVE is also used for verification and validation. SUAVE relies on a scaling method for determining the thrust. This means that a reference value for the thrust is needed and that the thrust at different altitudes and Mach numbers is computed by engine specifics. Further it also relies on the efficiencies mentioned above. By comparing the SFC outputs between GasTurb and SUAVE a difference of 8.35 % is found. Considering the number of differences between the models, this is within an acceptable range.

13.4. Mass Estimation

Fuselage In the first part of the Class II weight estimation, estimating the fuselage weight, a semi empirical estimation, the GD method, as described by Roskam [73] shown in Equation (13.31) was used, as it is specifically suitable for commercial transport airplanes. In this equation K_{inl} refers to how the engines are installed and is equal to 1 for the Ceres aircraft. Many other weight estimations have proven to be inadequate or too complicated for this stage of the design. The equation resulted in a final fuselage mass of 5079.6 kg.

$$W_f = 2 \cdot 10.43(K_{inl})^{1.42} (\bar{q}_D/100)^{0.283} (W_{TO}/1000)^{0.95} (l_f/h_f)^{0.71} \quad (13.31)$$

Verification & Validation The fuselage weight estimation was verified by checking its behaviour for increasing dimensions. The results of the verification were positive: increasing the dimensions of the fuselage led to higher weights. Additionally, the dimensions have also been set to zero and the estimation successfully resulted zero weight.

Furthermore, the results have been validated with results in Section 13.4 showing a comparison of fuselage weights according to the estimation in Equation (13.31) and the actual fuselage weight. Fractional difference in this context refers to the absolute difference between MTOW fractions. Data on fuselage weight fractions have been taken from [90]. The validation data show that the estimation adds 1 to 11 % to fuselage weight, which can be accounted for as the Equation (13.31) only relies on a few dimensional variables such as fuselage length and height. Moreover, the differences between MTOW fractions are small.

Table 13.11: Table of Validation Data for the Fuselage Weight Estimation

Aircraft	Actual Weight (N)	Estimated Weight (N)	Absolute Difference (%)	Fractional Difference (%)
McDonnell Douglas DC-9/10	49672	54901	11	1.28
Boeing 737-200	53841	54483	1	0.14
Airbus A300B/2	159620	166725	4	0.53

Wing Wing weight estimation was performed using Torenbeek's method [91]. The method separates the wing into the wingbox, ribs, and the leading and trailing edge curves including control and high lift devices. Moreover, the method includes relief factors for engines, fuel weight, and the wing structure itself to account for relief of the bending moment due to the lift. Finally penalties for fail safety measures, engines on the wing, and the fuselage connection were appointed. Equation (13.32) shows the final equation for wing weight estimation as well as the method to calculate the wingbox weight and the rib weight. Previously mentioned weight relief factors were incorporated in the wingbox calculations. Torenbeek's method

is semi-analytical since computations of the wingbox and rib weight depend on analytical relationships. However, leading and trailing edge weight computations, as well as weight penalties were based on empirical relationships. The method results in a final wing weight of 9.79 tonnes.

$$W_{wing} = W_{box} + W_{rib} + W_{LE \& TE} + W_{penalties}$$

$$W_{box} = I_{2t} n_{ult} R_{in} W_G \eta_{cp} b_{st} \frac{\rho g}{\bar{\sigma}_r} \left(1.05 \frac{R_{cant}}{\eta_t} + 3.67 \right) \quad (13.32)$$

$$W_{rib} = \rho g k_{rib} S \left(t_{ref} + \frac{t_r + t_t}{2} \right)$$

Verification & Validation The wing weight was verified by examining the wingbox and rib weights behaviour to changing certain variables, for example taper, aspect ratio, and sweep. According to theory, increasing the sweep, taper, and aspect ratio should lead to an increase in weight; the program successfully passed this test. Furthermore, the code blocks for weight penalties, relief factors, and leading and trailing edge weights have been tested as well for their main influence factors (e.g. the number of engines) from which followed that the code passed.

For validation of the method, a paper by Torenbeek on the method was used [89]. Table 13.12 shows a table which presents the method's results and actual wing weights. As shown in the table the discrepancy is approximately $\pm 4\%$. From these results it was concluded that the method is trustworthy.

Table 13.12: Table of Validation Data for the Wing Weight Estimation

Aircraft	Computed (kN)	Actual (kN)	Error (%)
Boeing 747-100	391.6	384.4	+1.9
Airbus A340	345.0	340.9	+1.2
Fokker F-28 Mk4000	32.02	33.28	-3.8
Cessna Citation II	5.950	5.730	+3.8

Empennage The empennage weight estimation was performed using Torenbeek's method [90]. The weight of the empennage is dependent on the surface area, half-chord sweep and the dive speed of the Ceres aircraft. The constant k_h is dependent on whether the tail is fixed or trimmable and k_v is dependent on the vertical location of the horizontal tail on the vertical tail. The resulting weight of the horizontal and vertical tail are 2132.7 kg and 932.7 kg, respectively.

$$W_h = k_h \cdot S_h \cdot \left(62 \cdot \frac{S_h^{0.2} \cdot V_D}{1000 \cdot \sqrt{\cos \Lambda_{h,50}}} - 2.5 \right) \quad (13.33) \quad W_v = k_v \cdot S_v \cdot \left(62 \cdot \frac{S_v^{0.2} \cdot V_D}{1000 \cdot \sqrt{\cos \Lambda_{v,50}}} - 2.5 \right) \quad (13.34)$$

Verification & Validation The verification of the weight estimation for the empennage was done by varying the parameters to see the response of the weight. As a result of increasing the surface area, the weight of the component increases. The increase rate was also inspected to ensure that the numbers do not overshoot.

It is stated in Torenbeek that the tail group contributes about 2-3% of the MTOW [90] but with the current T-tail configuration, the empennage represents 6% of the MTOW. This could be due to the larger horizontal tail surface higher loads from caused by it on the vertical tail structure. A320-200 parameters were used for the validation of the tail mass estimation with discrepancies shown in Table 13.13.

Table 13.13: Table of Validation Data for the Empennage Mass Estimation of Airbus A320-200

Tail Surface	Computed [kg]	Actual [kg]	Error [%]
Horizontal	704.44	625.0	+12.7
Vertical	445.44	463.0	-3.8

Landing Gear An initial weight estimation of the landing gear could be made with Torenbeek's method [90], using Equation (13.35) where $k_{uc} = 1.08$ for the selected high wing layout. The equation uses coefficients A through D from statistical data for the main and nose gear, which can be found in [90]. This gives a total landing gear mass of 1018 kilogram. [90] shows an error margin of 3–6 % for validation data.

$$W_{uc} = k_{uc} [A + B \cdot W_{TO}^{0.75} + C \cdot W_{TO} + D \cdot W_{TO}^{1.5}] \text{ [lbs]} \quad (13.35)$$

Burner and Sulphur Tank Next to the 9700 kg of sulphur pellets, the total payload mass consists of the sulphur burner and storage tanks. The mass of the burner was estimated with an empirical relation given by [84] in Equation (13.36). This equation uses a 2-step power law scaling for mass flows. The used burner is a modified Pratt & Whitney engine with an estimated mass of 462 kg and large uncertainty of $\pm 30\%$. For the storage tanks an external tank and a tank stored in the fuselage are considered. The first option would be easier to load, but it would lead to an increase in the parasitic drag and waste of fuselage space. Therefore the second option was chosen with the option to make the tank removable to speed up the reloading process. The sulphur was assumed to be stored in solid pellet form with a bulk density of 1121 kg/m^3 ¹⁷. The required volume with 5 % safety margin to store the 9700 kg of payload is 9.1 m^3 for an aluminium storage tank with a 3 mm skin. The tank has tube shape with circular end to fit into the fuselage. The mass of the storage tank was estimated to be 168 kg. [33]

$$m_{burner} = 1.6 \cdot (304 \cdot \dot{m}^{0.9})^{0.7} \text{ [kg]} \quad (13.36)$$

Convergence with initial estimate After the weight of each subsystem was known, a new estimate of the OEW and MTOW were made. A significant difference in MTOW over one iteration, would cause a difference in the required wing surface area and thrust etc. To address these discrepancies, a model was made to iterate the design in order to converge to a final solution. The model is based on the following principles:

An MTOW difference larger than 1 %, constitutes a new calculation of MTOW, required surface area, thrust, total range, and fuel fraction. From these requirements, the new subsystem sizes and weights were calculated following the procedures as explained in Section 13.4. These weights were then used to recalculate OEW and MTOW, which are checked to differ no more than 1 % from the old values.

13.5. Flight Profile Determination

The flight profile for the Ceres mission aircraft is found by the use of a non-dimensional discretised flight profile calculator for estimating fuel fractions. This provides an estimate for the fuel on-board for achieving the mission in the Class II iteration. This tool was developed in the Mid-Term report[33]. To expand and detail the flight profile further, SUAVE is chosen. This facilitates the development and verification of the numbers obtained in the Class II iteration which allow for an achievable mission profile.

Take-Off & Landing Calculations

The Ceres aircraft has a wing loading of 1776 N/m^2 and a thrust to weight of 0.759. Additionally, a maximum coefficient of lift of 1.03 during takeoff and landing is achievable.

Take-off performance is checked with the empirical relations provided by Roskam, volume 1 [74]. The equation is shown in Equation (13.37), where the TOP is empirically derived from statistics in Roskam and is equal to 0.2387 in metric units. Using the above given values, a takeoff distance of 673 m is estimated.

$$s_{to} = 0.2387 \left(\frac{W/S}{C_{L_{to}} \sigma T/W} \right) \quad (13.37)$$

The landing phase is checked using the method described in volume 1 of Roskam [74], the empirical relation between field length and approach velocity is used. Note, s_{fl} is equal to $\frac{s_l}{0.6}$. The relationships to calculate the limiting wing loading are given in Equation (13.38).

¹⁷ <http://www.anval.net/downloads/bulk%20density%20chart.pdf>

$$\begin{aligned}\overline{q}_{s0} &= \frac{W/S}{C_{L_{land}}} \\ V_a &= 1.3V_{s0} \\ s_{fl} &= V_a^2 \frac{0.3}{0.6} \left(\frac{1}{0.5144} \right)^2 \frac{1}{3.28}\end{aligned}\quad (13.38)$$

Using the above given values, and a maximum coefficient of lift of 1.03 in the landing configuration, a landing weight of 30 metric tonnes and assuming sea level conditions, a distance of 1558.5 m is obtained for landing distance. The highest airport of Project Ceres is FNUB at 5772 feet of altitude. Based on the mean high temperature in September at 28°, the equivalent pressure altitude is at 9005 feet. This equates to a density of 76% of sea level, thus the necessary landing distance increases to 2158 meters. Ceres' MLW to meet the 2500 m runway is 46.5 metric tonnes for sea level conditions and 35.5 metric tonnes at FNUB. Thus, both the takeoff and landing distance meet the requirements set for a 2500 m runway operation.

Flight Profile & Fuel Fraction Calculations

To calculate the necessary fuel fraction, the W/S and T/W are taken from the initial sizing. The flight profile is discretised in time to calculate the appropriate fuel fractions. The first step is calculating the climb performance from the initial climb altitude to the final cruise flight level.

For the climb phase, the aircraft will climb at its maximum ROC, to reduce the necessary time to get to altitude, thus increasing operational effectiveness. The rate of climb for an unsteady quasi rectilinear climb is given in Equation (13.39), and is derived by Ruijgrok [75].

$$RC = \frac{TV - DV}{W \left(1 + \frac{V}{g} \frac{\partial V}{\partial h} \right)} \quad (13.39) \quad V_{i+1} = V_i - \frac{\frac{\partial RC_s(V_i)}{\partial V}}{\frac{\partial^2 RC_s(V_i)}{\partial V^2}} \quad (13.40)$$

As per Ruijgrok [75], the rate of climb can be maximised by setting the derivative of steady rate of climb relative with velocity to zero in the energy height frame, $\left[\frac{\partial(RC_s)}{\partial V} \right]_{H_e} = 0$. To obtain RC_s , the above given formula must have $\frac{\partial V}{\partial h}$ set to 0.

To find the maximum climb rate, a function is written to find the solution to where $\frac{\partial RC_s}{\partial V} = 0$. The function consists of a Newton-Raphson method to find the highest potential rate of climb. The dependent variable is flight speed.

From this Newton-Raphson method, the rate of climb can be established. This in turn helps simulate the position of the aircraft per discretised time step. During climb, the aircraft is assumed to climb at its maximum thrust setting. With the knowledge of thrust, the fuel flow can be calculated as given in Equation (13.41).

$$\dot{m}_f = SFC \cdot T \quad (13.41) \quad \begin{aligned} \left(\frac{\dot{m}_f}{W} \right)_i &= SFC \left(\frac{T}{W} \right)_i \\ \left(\frac{\dot{m}_f}{W_0} \right)_i &= SFC \left(\frac{T}{W} \right)_i \frac{W_i}{W_0} \end{aligned} \quad (13.42)$$

Since the aircraft parameters are expressed non-dimensionally, the fuel consumption must also be expressed non-dimensionally. This is done by finding the mass fuel flow for a given weight using the thrust to weight at that time step. In order to relate the mass fuel flow to the initial starting weight, the T/W at time i must be corrected for the weight lost during time steps 0 to i .

With the ability to obtain flight speed, rate of climb and fuel consumption, the forward integration of the flight path for the climb can be given, as per Equation (13.43). Thrust to weight varies with fuel burn as well as density depending on the flight altitude. The ratio $\frac{W_i}{W_0}$ depends on the fuel burn during the climb, but is also influenced by the payload dispersion during the cruise.

During cruise, the thrust required to maintain a cruise velocity is not equal to the maximum available thrust. Thus, the T/W at cruise must be obtained by finding $\frac{C_D}{C_L}$ for the cruise condition. For maximum range, the coefficient of lift depends on the parasite drag. Thus, the drag to lift ratio can be found as per Equation (13.44). Thus, to obtain a mass flow rate, the T/W must be inserted in Equation (13.42).

$$\begin{aligned} \left(\frac{m_f}{W_0}\right)_{i+1} &= \left(\frac{m_f}{W_0}\right)_i + SFC \left(\frac{T}{W}\right)_i \frac{W_i}{W_0} \delta t \\ h_{i+1} &= h_i + RC_i \delta t \\ s_{i+1} &= s_i + V_i \delta t \end{aligned} \quad (13.43)$$

$$\begin{aligned} C_L &= \sqrt{\frac{C_{D0} \pi A e}{3}} \\ \frac{C_D}{C_L} &= \frac{C_{D0} + \frac{C_L^2}{\pi A e}}{C_L} \end{aligned} \quad (13.44)$$

SUAVE Flight Profile

Stanford's Aerospace Conceptual Design Environment, SUAVE is used throughout the analysis of the flight path for this aircraft. The programme is designed for various aircraft configurations, including electric flight and UAVs. Payload release was not modelled in SUAVE initially, thus it was added to assume the weight loss during cruise.

Table 13.14: Weights, Inertial Position, and Velocity of Key Points in the Mission Flight Profile

Segment	Gross Weight [kg]	Fuel Used [kg]	Payload Onboard [kg]
On Runway	51096.0	0	9700
Injection Initiation	46928.1	3691.54	9700
Top of Climb	44083.3	4933.56	8097.2
Top of Descent	30924.6	9995.01	0
Touchdown	30483.3	10436.3	0
Alternate Top of Descent	28709.8	12209.8	0
Alternate Touchdown	28641.6	12278.1	0

Segment	Altitude [m]	True Airspeed [m/s]	Distance Travelled [km]
On Runway	0	0	0
Injection Initiation	19507.2	206.548	598.30
Top of Climb	20000	206.548	999.04
Top of Descent	20000	206.548	3052.29
Touchdown	0	0	3402.12
Alternate Top of Descent	7620	169.767	3655.48
Alternate Touchdown	0	0	3749.5

The first step is creating the flight profile. Altitude, true airspeed, Mach number, equivalent airspeed, weights and SFC are given in Figure 13.18. The climb segment of the flight profile is formed from 17 discretised constant EAS & climb rate to help reduce the error due to a linear climb. In reality, the aircraft will perform a climb at a constant throttle setting and constant airspeed, but SUAVE experiences convergence problems when implementing such functions. The climb profile is discretised in height every 5000 ft. Error accumulation occurs more close to the service ceiling of 20km, due to a very shallow climb resulting in a prolonged time required to reach the service ceiling. Mission profile parameters are given in Table 13.14.

The thrust settings for the designed aircraft is shown in Figure 13.19. Thrust settings are restricted to 92.5% available power to increase engine longevity and reliability. This thrust limit is set by changing the performance on the 6 engine model, thus leaving a 7.5% performance margin in emergency situations. Aeroelastic behaviours do not limit the aircraft below a equivalent air speed of 240 knots.

Initiation of aerosol injection occurs at 19500 m. This is done to help increase the climb rate close to service ceiling and reduce the time required for the climb, as well as reducing the required range for the injection of the aerosol. This allows for a 66% increase in rate of climb at 19500 m for a similar thrust setting. Top of climb occurs when reaching 20000 m. The climb occurs at an indicated airspeed of 240 knots, switching to a Mach limited climb at 30000 ft. The mach limit is of Mach 0.7. The initial cruise Mach number is of 0.7, and no reduction in speed occurs as the upper bound for the optimal C_L for cruise is 0.70, and SUAVE predicts a cruise coefficient of lift of between 0.83 and 0.545.

Descent is performed Mach limited until 30000 ft. The descent occurs at Mach 0.7, at a descent rate of 2000 ft/min. After passing 30000 ft, a switch to EAS is performed, further increasing the descent rate to 2200 ft/min. In reality, the aircraft will descend at an idle mode and will not descend at a constant descent rate. Constant descent rate is used due to SUAVE's limitations. The flight profile does not account for the approach phase, where the indicated airspeed would be reduced from 240 knots to 180 knots for the ILS approach and a further reduction once fully established on the ILS and on short final. The flight profile

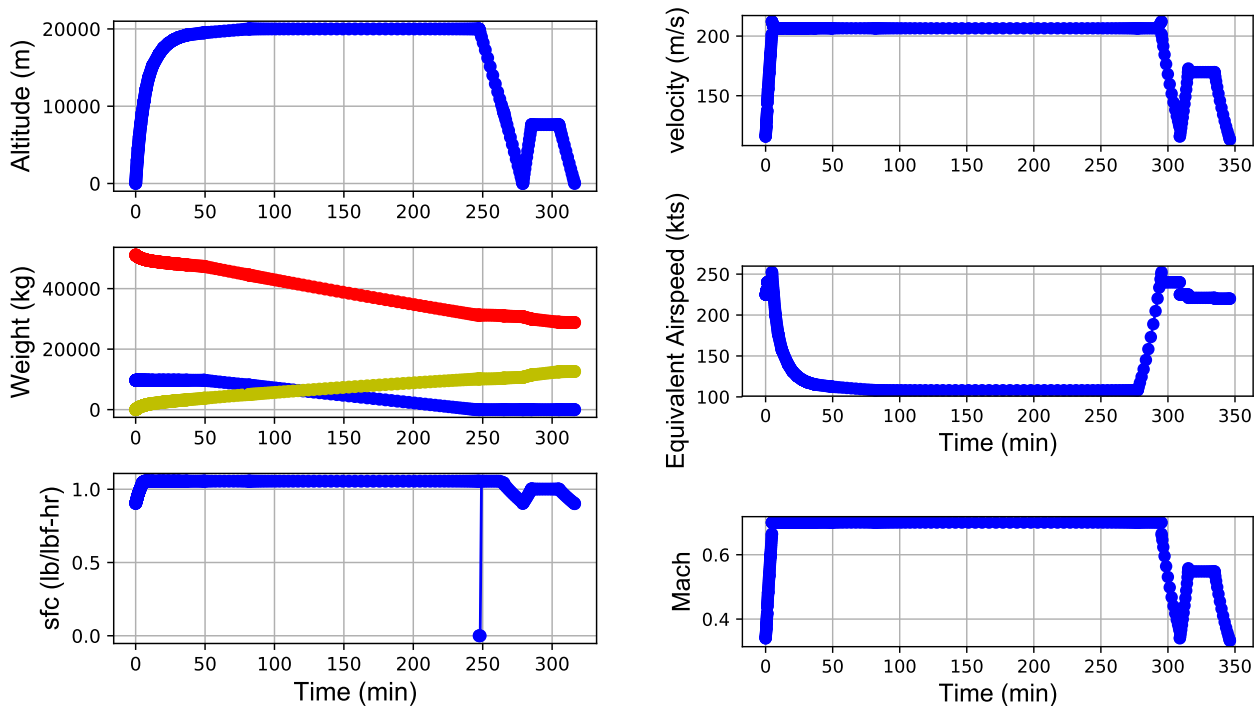


Figure 13.18: Altitude, Total Weight (Red), Fuel Used (Yellow) and Payload On-board (Blue), Velocities and SFC for the Mission Profile created.

does include the manoeuvres required to execute a diversion to the planned diversion airport. Initial climb rates include 20 m/s at a speed of 225 kts. Climb does not occur at full rate to help with controllability of a seriously overpowered aircraft due to the weight lost. This helps limit the thrust used and thus reduce workload and fatigue of the pilot flying. Cruise to the alternate occurs at 25 000 ft and accounts for at least 320 km, with a current projected alternate range of 350 km. This allows for contingency fuel in the range of 10 %, whereas 5 % is the upper bound in flight planning.

The aerodynamic performance for the designed aircraft is shown in Figure 13.19. The maximum observed coefficient of lift occurs at the peak of the climb or at the start of cruise. The maximum of this peak is 0.83. In addition, a peak in coefficient of lift is expected for takeoff and landing, in the magnitude of 0.9, due to a maximum lift coefficient around 1.03. The aircraft is speed stable below a coefficient of lift of 0.70, thus the aircraft is speed unstable for the first half of the flight. This calls for the use of autothrottles.

Assumptions in this flight profile is the proximity of the release zone to the airport. In reality politically and socially motivated reasons may push the zones further away from the airports over oceans. Additionally SUAVE computes parasitic drag coefficients in the order of 0.015. This differs from empirical estimates yielding a coefficient of 0.028. This can prove to be killer for the design but suave has shown to have good verification and validation results.

SUAVE Verification and Validation

Verification and validation of SUAVE has been performed previous to this report. *Trent Lukaczyk et al.*[92] proved SUAVE's consistency to performs accurate estimates for the performance of aircraft no matter if conventional or conceptual. Five verification and validation procedures were performed in order to verify and validate the program. Three cases of conventional aircraft were considered which were previously operational at the time of writing. These cases involved a B737, E190 and the Concorde. In the verification and validation of a B737 modelled within SUAVE for a 2950 nm mission, consistency within SUAVE and reality is observed, with fuel burn values predicted by SUAVE within 4 % of reality. SFC is also reflected to an accuracy within 3 % of reality with L/D values claimed to be within a few percent of reality. In the verification and validation of a E190 in terms of a payload range diagram, the accuracy of SUAVE was within 3 %. These findings aid in increasing the confidence behind the results obtained for the flight profile for the Ceres mission. Verification and validation on SUAVE at high altitude flight has not been performed, but is required to ensure feasible results. Nonetheless, no significant differences can be attributed to high altitude flight,

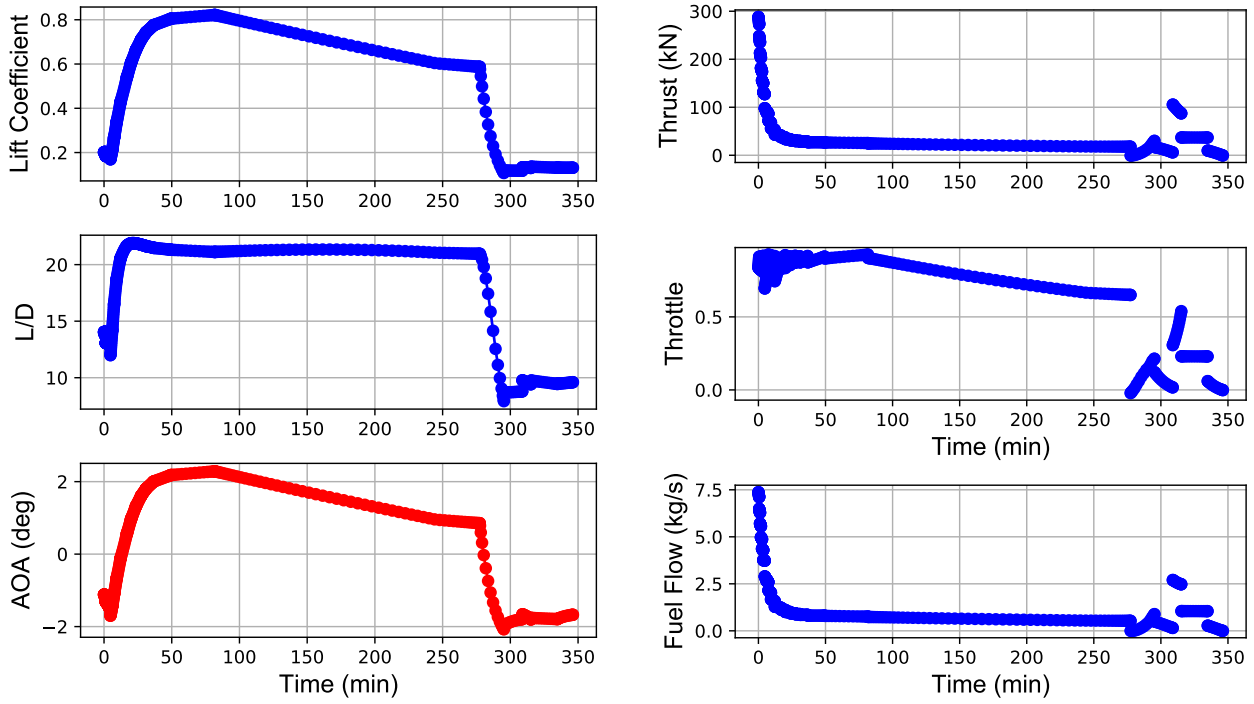


Figure 13.19: Lift Coefficient, L/D and Engine Parameters for the Ceres Mission Flight Profile.

except for the very low Reynolds number in the power plant due to the fan blade cord length.

Climb Optimisation for Minimum Fuel Burn

To complement and verify the flight profile analysis done using SUAVE, a separate and independent analysis was done using analytical relations. This was based on the method for minimum time to climb as expressed in [75]. The minimum time to climb was determined to be a very good approximation of the minimum fuel burn climb as the SFC was taken to be constant at the highest achievable value of the engines. Due to the assumption of constant SFC, a conservative estimate was taken which was the upper bound for this value of 26 g/(kN s) per engine. The code was run with multiple SFC values in order to ensure that this assumption still held. This means that the engines are modelled to function sub-optimally. The method was implemented as the mission is very sensitive to altitude and as such, it is of utmost importance to determine if the mission can be fulfilled.

The method bases the computation of the rate of climb on the equations of unsteady climb as shown below in Equation (13.45). It is necessary to thus determine the available power as well as the required power during the entire climb profile. In order to provide a conservative estimate for the climb, the flight profile is discretised and for each time step the highest climb rate is chosen for the current energy height at which the aircraft is situated. After this rate of climb was chosen, knowing both the thrust and SFC it is possible to deduce the mass reduction. This enables to reach the desired altitude and velocity the fastest possible taking into account various elements such as the fact that the C_L must be 0.9 times the value of $C_{L_{max}}$ at most or take the value for the optimal climb otherwise. This optimal lift coefficient is taken from the relation shown in Equation (13.46) where $K = \frac{1}{\pi A e}$ as per [75]. Moreover, the propulsion was modelled to give results which were underestimating the results observed in GasTurb. The modelling was done using a linear relation between sea-level thrust and air density.

$$\frac{dH_e}{dt} = \frac{P_a - P_r}{W} = RC_{steady} \quad (13.45)$$

$$C_L = \frac{1}{2K} \left[-\frac{T}{W} \pm \sqrt{\left(\frac{T}{W}\right)^2 + 12C_{D_\alpha}K} \right] \quad (13.46)$$

From these relations, it was possible to obtain the plot shown in Figure 13.20, where the blue line is the

optimal flight profile, the orange the stall speed and the dot is the final desired condition of cruise speed and altitude. The speed is represented in true airspeed. It must be noted that the rate of climb changes at every time step since more fuel is burned, the one showed here is thus the one at the latest iteration. This depicts very well the problem of flying at high altitudes as it shows that the performance of the aircraft is not bound by power at this stage but purely aerodynamics which limit the the rate of climb. This model predicts a climb time to 19.5 km of about 100 minutes. This is coherent with the results obtained with SUAVE.

The discrepancies arise from the drag estimations. It was observed that the zero lift drag estimation of SUAVE was about half of the one predicted by the models of the group. Since this drag is about half of the total drag, this explains the loss in performance shown in this model. It is also important to note that from Figure 13.20 it is clear that the most optimal climb does not occur at constant velocity or climb gradient for that matter. This could be potentially extremely straining for the pilot to operate multiple times a week. This could be automated or a simplified climb profile could be followed. The fuel burn and climb time was then also determined using Equation (13.47) and Equation (13.48), respectively [75].

It can be observed that the end of climb does not occur when the dot is reached but when the climb reaches 20 km as at this altitude the aerosol can be dispersed irrespective of speed. Finally, it can be observed in Figure 13.20 that there is a physical boundary for rate of climb, which was determined to originate from a Mach number at which the power available is limiting the velocity at which the aircraft can sustain flight. This is also due to the fact that the aircraft must have a high lift coefficient at the end of climb due to the high weight of the aircraft which leads to high induced drag.

$$W_f = \int_{H_{e1}}^{H_{e2}} \frac{m_{fuel}}{RC_{st}} dH_e \quad (13.47)$$

$$t = \int_{H_{e1}}^{H_{e2}} \frac{dH_e}{RC_{st}} \quad (13.48)$$

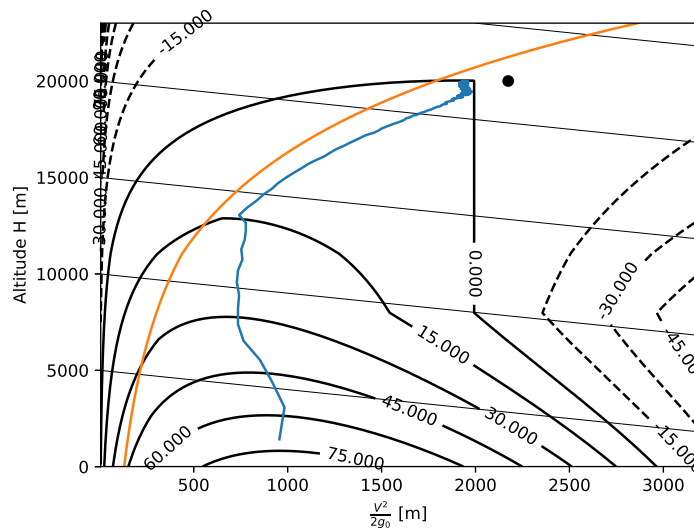


Figure 13.20: Map of the Rate of Climb versus Altitude and Velocity where the contours are constant Rate of Climb lines, the orange line the stall speed and the blue line the climb profile. The grey lines are lines of constant energy height.

It is thus preferable to start dispersing the payload at the altitude of 19.5 km as this will further decrease the weight of the aircraft and enable it to climb to the desired altitude where more of the dispersion can occur and be more effective. This would prevent an unnecessary amount of fuel burn only to be able to shed weight and reach the cruise altitude. This confirms the decision made to disperse the aerosol earlier. This makes that the total fuel burn is estimated to be 3.9 t for the climb up to 19.5 km. This represents a discrepancy of less than 10% with respect to the 3.6 t obtained with SUAVE. This thus serves as verification for this part of the model. It also serves to prove once again the sensitivity of the design to cruise altitude as it only takes about 35 minutes to reach an altitude of 19 km but it takes about 60 minutes to climb an

extra 500 m. In addition to this, a short sensitivity analysis was conducted to determine the theoretical ideal altitude to disperse payload. This was found to be approximately 19 km. This was found as releasing the aerosol earlier than this altitude yields a reduction in climb time of less than 10 minutes for 18.5 km compared to the mentioned altitude. Releasing the aerosol at the specified altitude yields a reduction in climb time of nearly an hour compared to releasing at 20 km.

Moreover, this can lead to improvements of the SUAVE model to be made more accurate. The SUAVE model takes values for climb segments which are constant airspeed and constant rate of climb. This model can thus enable to determine better predictions for the ideal climb velocity and rate of climb.

13.6. Stability and Control

13.6.1. Empennage

The horizontal tail and vertical tail of Ceres aircraft were designed and sized in terms of the aerodynamic and stability requirement. A list of tail design parameters is shown in Table 13.15. The detailed reasoning for the determination of each parameter will be discussed in the following paragraphs.

Table 13.15: Design Parameters of the Horizontal Tail and Vertical Tail

	$S [m^2]$	$A [-]$	$b [m]$	$\lambda [-]$	$\Lambda_{25} [^\circ]$	$l_t [m]$	$V [-]$
Horizontal Tail	49.3	8.7	20.7	0.348	31.5	27.3	1
Vertical Tail	26.0	1.3	5.8	0.646	39.0	27.3	0.043

Horizontal tail A T-tail configuration was chosen for the empennage. Due to the small and flat dimensions of the fuselage and the high wing, the configuration was desirable to mitigate the problem of the wing wake. The problem of the wake could be solved by applying a twist angle, but it was difficult to quantify the twist needed. With this configuration weight of the vertical tail was compromised because it must be heavily reinforced and stiff due to the weight of the horizontal tail. Deep-stall is one of the phenomena that might occur during flight, however, Figure 13.19 shows that the maximum angle of attack during operation does not exceed $\approx 2^\circ$. One of the disadvantages of the T-tail is that it is prone to flutter due to the pairing of the horizontal and vertical tail.

The selected airfoil for the horizontal tail is NASA SC(2)-0610. A supercritical airfoil was chosen to prevent any local shock formation. By having a thinner section hence lower thickness ratio, the Mach drag divergence of the tail is delayed. Additionally, a high sweep was applied to ensure that the horizontal tail will stall at a higher angle of attack. The sweep was determined by Equation (13.49). This took into account statistical data on the relation of the wing sweep and the horizontal sweep. Generally, the taper ratio of the horizontal tail is smaller than that of the wing, therefore, $\lambda = 0.348$ was chosen based on statistics. The sweep and taper ratio were kept constants for further calculations.

$$\Lambda_h \approx \Lambda_w + 5^\circ \quad (13.49) \quad l_{opt} = 1.4 \cdot \sqrt{\frac{4 \cdot \bar{c} \cdot S \cdot V_h}{\pi \cdot D_f}} \quad [77] \quad (13.50)$$

From the analysis of the static stability and controllability, the horizontal tail surface area was determined. Equation (13.50) was used for the preliminary value of the tail arm and was finalised by the mass balance method. With the T-tail configuration, it was assumed that the horizontal tail is not affected by the downwash of the main wing. Therefore, an incidence angle of 0° was applied.

Vertical Tail A symmetric airfoil was selected for the vertical tail to feature similar aerodynamic behaviour in both the positive and negative angle of attack. According to [93], for an aircraft flying at a high subsonic Mach number as Ceres aircraft, the thickness ratio of the vertical is usually 2% lower than that of the main wing. Thus, a commonly used vertical tail airfoil - NACA 0009 was chosen due to its low thickness ratio. The sweep angle of the vertical tail is commonly between 35° to 50° for a high-speed subsonic aircraft. 39° was selected for the vertical tail quarter chord sweep angle based on the reference heavy jet transport and cargo aircraft. In addition, a taper ratio of 0.311 was chosen for the vertical tail based on reference aircraft.

For a preliminary design parameter, the same tail arm was chosen for vertical tail as the horizontal tail. The tail arm was iterated and optimised in terms of the stability characteristics and the structural weight.

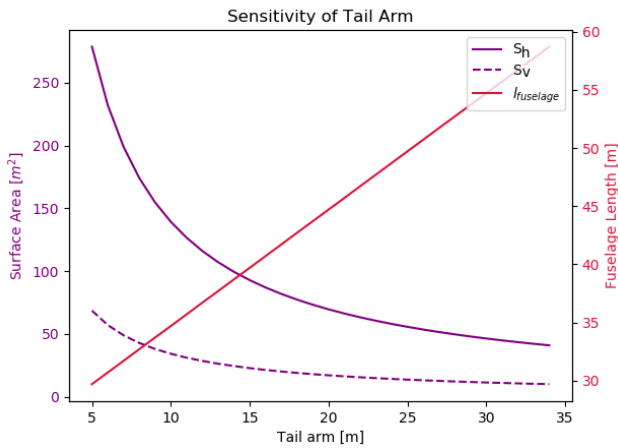


Figure 13.21: Parameters Affected by the Tail Arm.

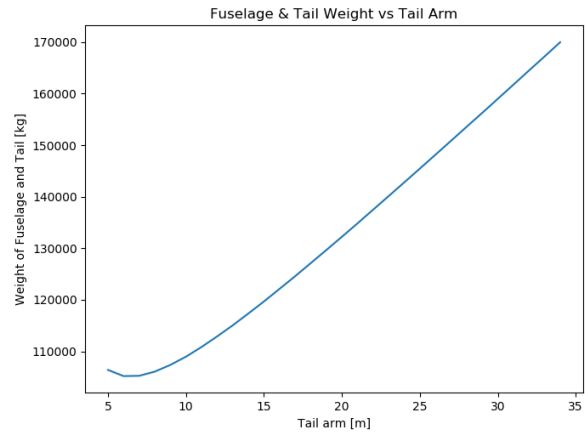


Figure 13.22: Relation between Horizontal Tail Arm and Fuselage+Tail Weight.

From Figure 13.21, it can be seen that the surface area of the empennage is affected by the tail arm to provide for stability. It is deduced that the fuselage length varies linearly with the tail arm. The tail arm is a constraining factor in the fuselage length. From the weight perspective, as can be seen in Figure 13.22, a tail arm of 6 m is the optimal length. However, this leads to an unacceptable surface area for the horizontal tail. Moreover, this optimal length is not chosen as the stability and controllability of the aircraft, which will be discussed in the following paragraphs, are more restricting on the length of the tail arm.

Longitudinal Stability and Controllability To size the horizontal tail, an analysis of the longitudinal stability is important. A scissor plot was generated to give the optimal area of the horizontal tail based on the maximum and minimum range of the centre of gravity. The sequence of the loading was initiated with the loading of the fuel and finalised with the payload and is visualised in Figure 13.23. By shifting the location of XLEMAC to $\pm 15\%$ of the fuselage length, the CG range diagram was plotted based on the most forward and most aft location of centre of gravity.

Equations used for the stability and controllability curves are given by Equation (13.51) and Equation (13.52), respectively. The stability equation was deduced by looking at the stick-fixed static stability and the neutral point position. A stability margin of 0.05 was set during design to ensure that the centre of gravity is always located in front of the neutral point. The controllability equation was derived for trim condition at which the aircraft moment coefficient is null.

$$\frac{S_h}{S} = \frac{1}{\frac{C_{L\alpha_h}}{C_{L\alpha_{A-h}}} \left(1 - \frac{d\epsilon}{d\alpha}\right) \frac{l_h}{\bar{c}} \left(\frac{V_h}{V}\right)^2} (\bar{x}_{c.g} - \bar{x}_{a.c} - S.M) \quad \frac{S_h}{S} = \frac{1}{\frac{C_{L_h}}{C_{L_{A-h}}} \frac{l_h}{\bar{c}} \left(\frac{V_h}{V}\right)^2} (\bar{x}_{c.g} + \frac{C_{m_{a.c}}}{C_{L_{A-h}}} - \bar{x}_{a.c}) \quad (13.52)$$

The scissor plot is depicted in Figure 13.25 and is superimposed with Figure 13.24 to find the optimal ratio for the horizontal tail surface area. The ratio that was chosen for $\frac{S_h}{S}$ is 0.18. This was chosen in order to comply with the longitudinal stability and controllability requirement. This ratio, however, is not the optimal ratio and was selected based on the fact that the centre of gravity shift during dispersion at 20 km, where the longitudinal stability is critical, is limited and does not vary drastically. With this ratio, the tail arm was determined to be 27.3 m.

Lateral Stability and Controllability For the sizing of the vertical tail, constraints in terms of the lateral stability and controllability must be imposed on. Two critical conditions for sizing are one engine inoperative (OEI) and crosswind landing.

According to the CS25 requirements, the aircraft shall remain stable and controllable with one engine inoperative at minimum control velocity, which is 1.13 times the stall speed, with a small sideslip angle and maximum rudder deflection angle. Therefore, the yawing moment generated from the vertical force should be larger than or equal to the moment due to asymmetric thrust as demonstrated by Eq. (13.53). As mentioned in Section 13.3, two inboard engines are integrated together. There is a possibility that two

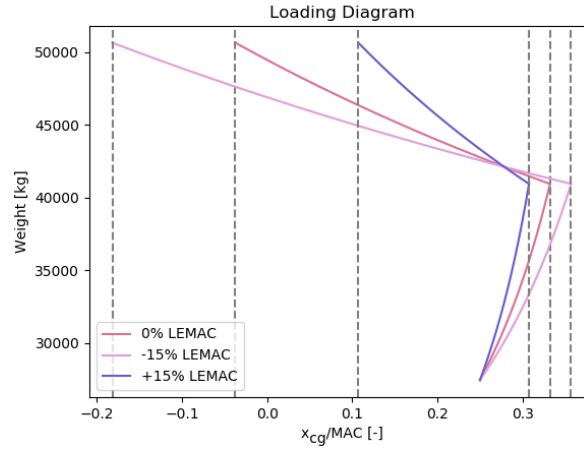


Figure 13.23: Loading Diagram of the Ceres Aircraft.

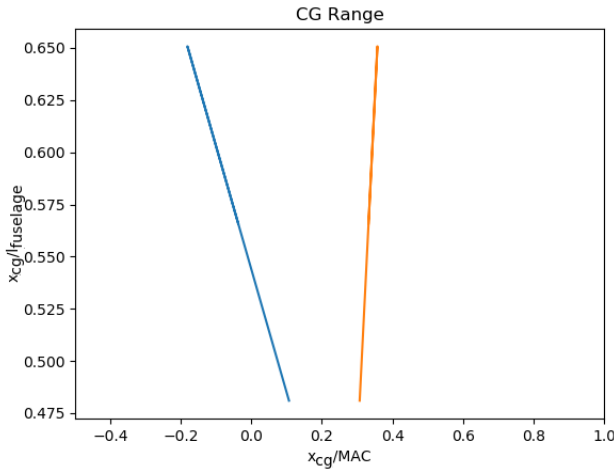


Figure 13.24: Range of Centre of Gravity.

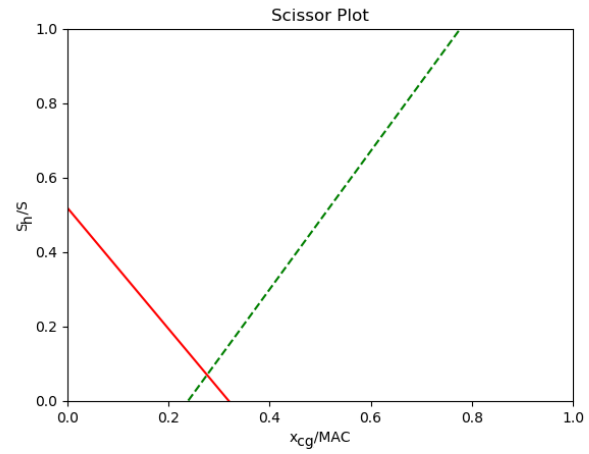


Figure 13.25: Scissor Plot showing Stability and Controllability.

inboard engines fail simultaneously. However, the spanwise distance of the inboards engines is less than half of the outboard engine. Thus, only the outboard engine inoperative condition was considered.

$$l_{vt} \cdot F_{vtmc} \geq y_{eng} \cdot T_{oei} \quad (13.53)$$

The vertical tail force F_{vt} can be represented by Equation (13.54).

$$F_{vt} = \frac{1}{2} \rho V_{mc}^2 S_{vt} C_{Lvt} \quad (13.54)$$

where C_{Lvt} is defined by Eq. (13.55).

$$C_{Lvt} = C_{Lvt0} + C_{L\alpha vt} \beta + C_{L\delta_r} \delta_{r_{max}} \quad (13.55)$$

The vertical tail lift curve slope $C_{L\alpha vt}$ were obtained from the DATCOM method. The rudder control power and the maximum deflection angle will be discussed subsequently in subsection 13.6.2. By adjusting the tail arm and rudder design parameters, the minimum required vertical tail surface area was obtained.

Another critical condition that constrained the sizing of the vertical tail is the crosswind landing. The aircraft shall be able to remain the desired flight path during landing with full flaps at a wind of 15 m/s, 90° to the aircraft velocity. The vertical tail shall be able to balance the yawing moment generated by the side force due to the wind with the crosswind side slip angle and the maximum rudder deflection:

$$l_{vt} \cdot F_{vtcw} \geq x_{ca} \cdot F_w, \quad (13.56)$$

where the wind force F_w is a function of the wind speed, side area of the aircraft, and the aircraft side drag coefficient, which is 0.5 to 0.8 for conventional aircraft. From Eq. (13.56), another minimum required tail surface area was obtained.

Another potential critical condition for the Ceres aircraft is at half of the climb time, when the density is low due to the altitude with the thrust remaining relatively high. Thus, one engine inoperative was evaluated at this condition in addition to the requirements from CS25.

According to the flight profile, at half of the climb, the altitude is 90% of the cruise altitude with a thrust of around 22 kN, the low density and relatively high thrust can reduce the stability of the aircraft.

The required vertical tail surface area for each conditions are listed in Table 13.16.

Table 13.16: Required Vertical Tail Surface Area

	Take-off OEI	Climb OEI	Crosswind Landing
Required S_v [m ²]	23.64	4.67	9.82

As can be noticed, the take-off OEI condition is the most critical condition for the lateral stability and controllability. A safety margin of 1.1 was applied, which resulted in a vertical tail surface area of 26 m².

13.6.2. Control Surface

In this section, the control surfaces - aileron, elevator, and rudder are designed and sized based on the aircraft stability and controllability requirements. The aircraft is equipped with spoilers for descend control, ground spoilers and assistance of roll control. The CTRL requirements impose constraints on the control surfaces design limiting the design space. With preliminary design parameters generated within the design space, the resulted control effectiveness can be verified with the DATCOM output.

Aileron The function of an aileron is to provide roll control for the aircraft. Two critical design points for ailerons are responsiveness at low speed with large deflections and high speed with small deflections in the worst case scenario of a full hydraulic loss. Typically, roll spoilers would assist with rolling. Based on this, two design constraints were generated: the dimensionless roll rate shall be larger than 0.07 during the cruise phase (phase B) and the aircraft shall be able to bank to 30° in 2.5 seconds¹⁸[77].

The same design parameters are usually used for ailerons on both sides of the wing for a symmetric aerodynamic behaviour. The design of the aileron consists of selecting the aileron type and determining the wing spanwise location, chord length, and the maximum deflection angle. Since the roll control requirements of Ceres aircraft is not harsh, plain flap ailerons were chosen to limit the cost. A first estimation of the design parameters was chosen based on statistics to compute the aileron roll control power ($C_{l_{\delta A}}$), which is a function of the aileron inboard and outboard edge location, chord fraction, and the main wing design.

$$C_{l_{\delta A}} = \frac{2C_{L_{\alpha w}}\tau}{Sb} \int_{y_i}^{y_o} C_r [1 + 2(\frac{\lambda - 1}{b})y] y dy \quad (13.57)$$

Preliminary values were chosen based on statistics to compute the steady-state roll rate and the time taken to achieve the required bank angle. These values were modified and iterated until the requirement was met.

Elevator The main function of the elevator is the longitudinal control and trim. With the aid of the elevator deflection, the tail lift coefficient can be changed which affects the aircraft pitching moment. The sizing of the elevator is limited by the take-off rotation and the longitudinal trim requirement. The take-off rotation will determine the maximum allowable up deflection of the elevator ($-\delta_{e_{max}}$) as the maximum positive pitching moment is needed and was analysed at the most forward cg position. This requirement is also dependent on the location of the landing gear because it is the rotation point at take-off. The latter requirement is for the sizing of the maximum allowable down deflection ($+\delta_{e_{max}}$).

The maximum allowable up deflection was set to 15° and subsequently, the elevator characteristic τ_e in Equation (13.58) was determined to satisfy the requirement for take-off from [72]. With this deflection, the

¹⁸ <http://www.flightlevelengineering.com/downloads/ProAdvice20320-20AILERON20SIZING.pdf>

elevator contribution of the horizontal tail lift is sufficient to produce a take-off pitch angular rotation of 5°/s.

$$C_{L_h} = C_{L_{\alpha_h}} (\alpha_h + \tau_e \delta_e) \quad [77] \quad (13.58) \quad \delta_e = - \frac{(\frac{T \cdot z_T}{\bar{q} \cdot S \cdot \bar{c}} + C_{m_0}) C_{L_{\alpha}} + (C_{L_1} - C_{L_0}) C_{m_{\alpha}}}{C_{L_{\alpha}} C_{m_{\delta_e}} - C_{m_{\alpha}} C_{L_{\delta_e}}} \quad [77] \quad (13.59)$$

$$C_{m_{\delta_e}} = -C_{L_{\alpha_h}} \eta_h \bar{V}_h \frac{b_e}{b_h} \tau_e \quad [77] \quad (13.60) \quad C_{L_{\delta_e}} = C_{L_{\alpha_h}} \eta_h \frac{S_h}{S} \frac{b_e}{b_h} \tau_e \quad [77] \quad (13.61)$$

The maximum allowable down deflection of the elevator was computed using Equation (13.59) and was based on the longitudinal trim requirement. The rate of change of aircraft pitching moment with respect to elevator deflection and the rate of change of aircraft lift coefficient with respect to elevator deflection were calculated using Equation (13.61) and Equation (13.60), respectively. The lift slope curve for the horizontal tail was obtained from an analysis run in XFLR5¹⁹. The corresponding elevator parameters are shown in Section 13.6.2.

Rudder The fundamental roles of the rudder are to provide yawing moment and lateral trim associated with the vertical tail. The most crucial control the rudder needs to function is when the aircraft take off with one engine inoperative or landing with crosswind, the rudder should aid the vertical tail to balance the yawing moment with the maximum deflection. Since the design requirements are identical to those of the vertical tail sizing, the rudder design was conducted concurrently with the vertical tail. Parameters that were determined for the rudder design were the rudder span, rudder chord length, and the maximum deflection angle.

There are commonly two types of rudder: swept rudder and rectangular rudder. The rectangular rudder was selected for the Ceres aircraft because of its low cost and ease of assembly. For a rectangular rudder, the rudder span is usually the same as the vertical tail span. The maximum deflection was set to be the same for both sides for similar aerodynamic behaviour, which was determined based on the calculated rudder control power $C_{L\delta_r}$, and lateral force coefficient from Equation 13.62 and Equation 13.55.

$$C_{L\delta_r} = C_{L\alpha_{vt}} \frac{b_r}{b_{vt}} \frac{c_r}{c_{vt}} \quad (13.62)$$

The optimal combination of deflection angle and chord fraction was determined for larger lateral force coefficient and lower vertical tail weight.

Table 13.17: Control Surfaces Parameters

Ailerons		Elevator		Rudder	
c_a/c [-]	0.2	c_e/c_h [-]	0.1	c_r/c_v [-]	0.2
$\delta_{a,up}$ [°]	15	b_e/b_h [-]	0.9	b_r/b_v [-]	1
$\delta_{a,down}$ [°]	15	$\delta_{e,up}$ [°]	15	δ_r [°]	25
$y_{a,in}$ [-]	75%	$\delta_{e,down}$ [°]	21		
$y_{a,out}$ [-]	90%				

Verification and Validation The tail parameters including the control surfaces were verified by looking at the trend of the surface areas and the fuselage length as a result of varying the tail arm. Moreover, the magnitude of the parameters were similar to existing aircraft, which validated the models. From [77], the range of deflection values of the control surfaces are shown in Table 13.18.

Table 13.18: Range of Deflection Angles for the Control Surfaces

	Aileron	Elevator	Rudder
δ [°]	10-30	10-25	15-32

¹⁹<http://www.xflr5.com/xflr5.htm>

Additionally, the lateral stability requirement was verified by computing the maximum rudder force. According to the mission requirement in [32], the rudder force shall not be larger than 667 N with maximum rudder deflection at minimum control speed. With the previously designed rudder parameters, the maximum rudder force is 612 N. Thus, the lateral stability requirement is verified.

As the computation of the control surfaces parameters require aerodynamic derivatives such as $C_{l_{\delta_A}}$, $C_{m_{\delta_e}}$ etc., the validation of the data is complicated without the aid of actual data from either CFD analysis or wind tunnel testing.

13.6.3. Dynamic Stability Coefficient Determination

To analyse the dynamic stability of the aircraft in Section 13.6.4, the aircraft stability derivatives have to be determined. These derivatives were obtained from the USAF Digital DATCOM method. The input of the program is the aircraft geometry and the program returns the stability derivatives and other flight coefficients of the aircraft for the requested flight conditions by the user. The method applied by this program is described by Roskam [72].

The basic wing and tail parameters were used as input based on the empennage design. The fuselage dimensions were also used since they also affect the aerodynamics of the aircraft.

Airfoil coordinates of the selected NASA SC(2)-0712 airfoil (applied to the wing) and the NASA SC(2)-0610 (applied to the horizontal tail) need to be inputted manually since DATCOM only provides automated functionality for NACA airfoils.

Finally the required flight conditions for which the program runs are specified. A range of angles of attack, altitudes and Mach numbers was analysed in one operation. The method was applied for the flight condition given by the cruise altitude, MTOW as well as at a Mach number of 0.2 at sea level. The inputs and outputs of the Digital DATCOM method can be found in Appendix B. These outputs were considered in the methods discussed below.

Twist & Dihedral The program also requires inputs for twist and dihedral (Γ) of the wing and horizontal tail. These have not previously been discussed but do play a significant role in the aerodynamics of the wing and horizontal stabiliser. Having a negative angle of twist, otherwise defined as washout has a decreasing effect on the wing weight but is also needed for the aircraft stall characteristics [72]. Wing tip stall must be prevented in all situations since it usually occurs asymmetrically resulting in a significant rolling moment. So, the root of the wing needs to stall first to ensure safe flight close to stall. This is achieved by setting the local incidence angle of the wing lower at the tip with a negative angle of twist.

Dutch roll and spiral stability of the aircraft need to be ensured for safe flight and low effort for the pilot. These dynamic modes are dominated by $C_{l_{\beta}}$. This derivative is required to be negative for spiral stability where a larger magnitude is associated to a more stable aircraft. It is affected mostly by the wing position (high or low wing), the angle of dihedral and sweep of the wing. The selected high wing and sweep mean that $C_{l_{\beta}}$ is already negative with sufficient magnitude. Furthermore, a too large magnitude of $C_{l_{\beta}}$ can cause Dutch roll which must be avoided. As a result, (as is usual for high-wing aircraft) a negative dihedral (=anhedral) will likely be selected.

Initially, the tail twist and Γ_{tail} were set to zero and a sensitivity analysis of the derivatives in Section 13.6.3 to wing twist and Γ_{wing} was performed. The results in this table all have magnitudes and signs according to expectations except for C_{L_q} and C_{m_q} . These are suspiciously large in magnitude and could be due to the rather unconventional ratio of dimensions of the Ceres aircraft. The fuselage is very small whilst the aspect ratio, span and tail arm are quite large. Another explanation for the unexpected numbers could be that the applied method for these two coefficients is not suitable for an aircraft geometry such as Ceres' and its given cruise flight conditions.

Based on the sensitivity analysis of the stability derivatives in Section 13.6.3 using figures such as Figure 13.26 and reference data from the airbus A310 [91], an angle of wing twist of -4.5° was selected. The A310 wing planform has a twist of -6° . Figure 13.26 shows that more than 5° of washout will drastically increase the parasite drag, thus a number just below this threshold is selected.

Due to a relatively small vertical tail, $C_{l_{\beta}}$ is negative but not very large in magnitude. In Figure 13.27 it can be seen that too much anhedral will even cause a positive $C_{l_{\beta}}$ which must be avoided. Since Γ does not affect other parameters as much as $C_{l_{\beta}}$ this is considered the driving criterion and an anhedral of 1

degree was selected. This may be tweaked after stability analysis since $C_{Y\beta}$, C_{Yp} , $C_{L\dot{\alpha}}$ and $C_{m\dot{\alpha}}$ do change with anhedral.

Table 13.19: DATCOM Results

Coefficient	C_{D_0} [-]	$C_{D_{cruise}}$ [-]	$C_{L\alpha}$ [1/rad]	$C_{l\beta}$ [1/rad]	$C_{m\alpha}$ [1/rad]	$C_{Y\beta}$ [1/rad]	$C_{n\beta}$ [1/rad]	$C_{L\dot{\alpha}}$ [1/rad]
Value	0.017	0.035	5.4	-0.031	-3.5	-0.50	0.030	2.5
Coefficient	$C_{m\dot{\alpha}}$ [1/rad]	C_{l_p} [1/rad]	C_{Y_p} [1/rad]	C_{n_p} [1/rad]	C_{n_r} [1/rad]	C_{l_r} [1/rad]	C_{L_q} [1/rad]	C_{m_q} [1/rad]
Value	-17.0	-0.48	0.054	-0.020	-0.052	0.016	17.8	-101.4

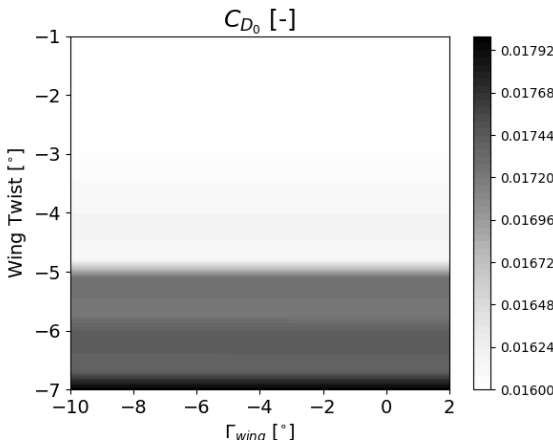


Figure 13.26: Zero-Lift Drag versus Wing Twist and Dihedral.

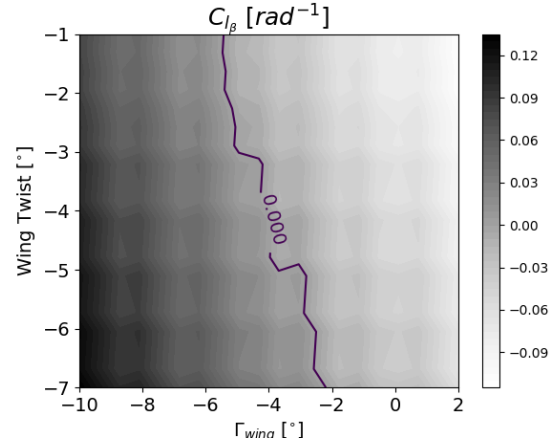


Figure 13.27: $C_{l\beta}$ versus Wing Twist and Dihedral.

With these selected values for wing twist and dihedral a similar sensitivity analysis was performed with varying horizontal twist and dihedral. From the associated plots of this analysis in Figure 13.28 and Figure 13.29 it can be seen that a change in tail twist or dihedral produces a smaller change in the coefficients than changes in the tail twist or Γ_{tail} . The drag is increased at zero twist and will be lower with a twist angle of -2 degrees which is thus selected. This is also necessary to prevent tip stall which is also preferably avoided for the tail. Additionally, a tail anhedral of 1° is selected to ensure positive $C_{l\beta}$. Γ_{tail} and tail twist do have an effect on most coefficients. These effects can be used if after the stability analysis in Section 13.6.4 any 'tweaking' of coefficients is necessary.

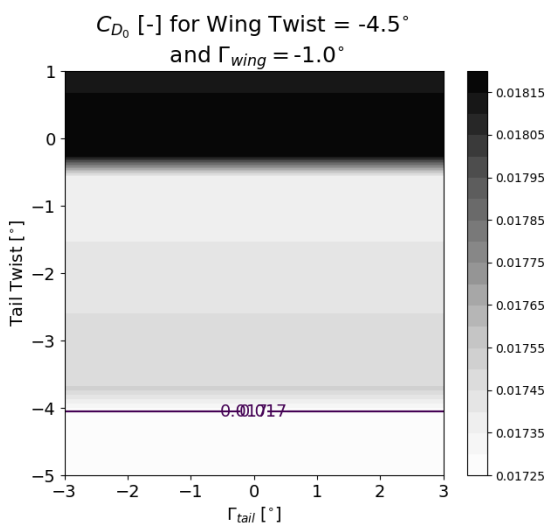


Figure 13.28: Zero-Lift Drag versus Tail Twist and Dihedral.

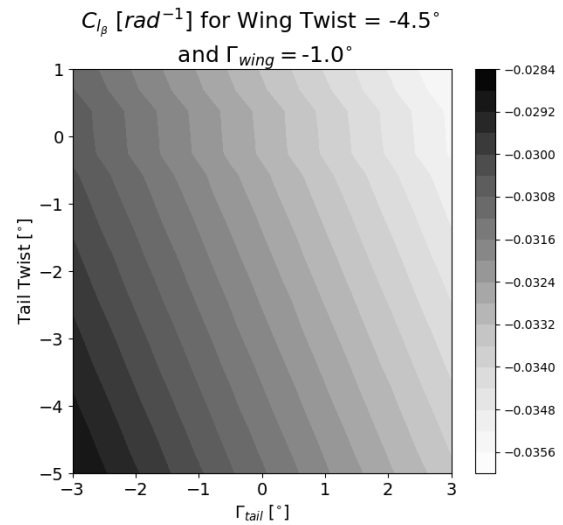


Figure 13.29: $C_{l\beta}$ versus Tail Twist and Dihedral.

Verification In order to verify that the DATCOM program produces correct results it must be verified and validated for the selected use case.

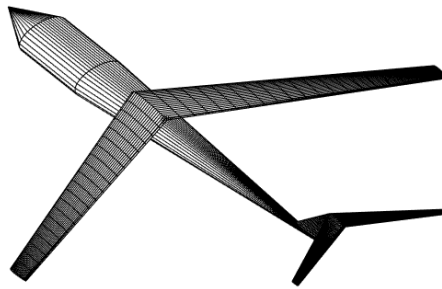


Figure 13.30: Rendering of Modelled Ceres Aircraft.

The first step in verification of the input parameters is based on a graphical representation of the aircraft to ensure it was inputted correctly. This is displayed in Figure 13.30.

Stability derivatives of an aircraft are defined such that they represent the same behaviour if their magnitudes are the same for different aircraft. As a result, it would make sense to ensure that the program produces the same results when the aircraft is scaled down or up. This was performed by scaling the aircraft up and down by a factor of two. The results from the scaled models can be considered equal up to round-off errors.

Validation In order to validate the Digital DATCOM method, it was applied for reference aircraft similar to the Ceres aircraft. Large transport aircraft and aircraft with high aspect ratio were selected and modelled at the same flight condition (altitude and Mach number) and compared to the results from the Ceres aircraft. The variation between results per aircraft for different flight conditions (Ceres cruise conditions and sea level conditions at Mach = 0.2) was also determined for these aircraft and compared to the Ceres aircraft. These comparisons were initially made with the Airbus A380, Boeing 737 and Lockheed U-2. Only the U-2 appeared to be a valid comparison to Ceres at the given flight conditions since it is designed for the same flight condition. When directly comparing Ceres' results to the U-2, the order of magnitude and signs of the coefficients are corresponding. Moreover, the variation of parameters per aircraft for low altitude and speed compared to cruise condition for the U-2 was proportionate. The output coefficients all generally increase by 5–10 % when increasing the altitude and speed as described both for Ceres and the U-2.

In addition, the specific results of Ceres aircraft were validated against reference numbers. For this process it must be noted that the stability characteristics and coefficients of the aircraft are previously unknown and hard to estimate. Reference values for stability coefficients belonging to stable aircraft were gathered from a previous academic project [42]. When comparing Ceres' results the order of magnitude and signs were checked. This comparison of the sign of the coefficients was done using knowledge from the AE3202-I Flight Dynamics course[44]. This provided insight in which coefficients require which signs and what can be expected for the Ceres aircraft. For example, the high aspect ratio, very small (narrow) fuselage and moderate sweep could cause either a negative or positive C_{Y_r} .

For validation purposes the drag polar from the DATCOM results is also plotted in Figure 13.31. The drag polar can easily be validated and compared to previous results so it can be used to validate the model inputs for the Digital DATCOM method.

C_{D_0} is determined to be significantly lower than the actual design value of ≈ 0.28 . This discrepancy is also found for the SUAVE method as described in Section 13.5. The Oswald efficiency factor is calculated based on the known aspect ratio and is found to have a lower magnitude than expected. DATCOM likely estimates the Ceres wing planform to be less efficient than the other used methods during the design. The shape of the polar itself is very natural and does not include any outliers with a threshold of 3 standard deviations.

The Digital DATCOM method applies the analytical method described by Roskam [72]. Roskam's meth-

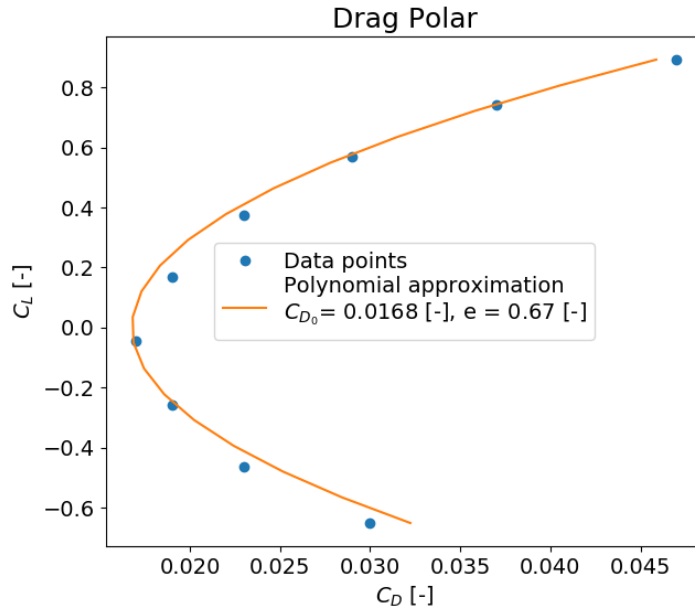


Figure 13.31: Drag Polar from Digital DATCOM.

ods have been found to be applicable for the Ceres aircraft and have been used throughout its design. This should thus provide consistent results. This will be verified in Section 13.6.4.

Final validation of the results from this method will be performed by determining the actual lateral and longitudinal dynamic stability behaviour of the aircraft with these parameters. These results are discussed in Section 13.6.4.

13.6.4. Dynamic Stability Analysis

In this section, the dynamic stability characteristics of the Ceres aircraft will be analysed for five eigenmotions. The stability derivatives are obtained from the DATCOM method described by Roskam [72] and will be verified using the digital DATCOM method [17] mentioned in the previous subsection. Recommendations for a further design iteration will be proposed based on the discrepancy analysis.

Analytical Model The dynamic stability analysis of Ceres aircraft was conducted at two critical flight conditions. One is the cruise phase (phase B) before payload dispersion when the aircraft is flying with a high weight at high altitude. The resulting large moment of inertia and low air density are unfavourable for the motion damping. The other critical condition is the take-off airborne phase (phase C). Besides from the large weight, the relatively low velocity and large angle of attack also increase the damping time.

The longitudinal and lateral dynamic stability analysis consists of the stability derivatives derivation and the eigenmotion characteristics analysis. In addition to flight conditions, the stability derivatives also depend on the geometric and aerodynamic properties of the main wing and tails, which was derived according to Roskam flight dynamics[72]. For the longitudinal stability derivatives, significant design parameters involved are wing surface area, MAC, wing lift slope, aspect ratio, horizontal tail lift slope, and horizontal tail volume. For the lateral stability derivatives, the significant design parameters involved are wing surface area, wingspan, wing lift slope, aspect ratio, vertical tail lift slope, vertical tail span, and vertical tail volume.

$$\begin{bmatrix} C_{X_u} - 2\mu_c \lambda_c & C_{X_\alpha} & C_{Z_0} & C_{X_q} \\ C_{Z_u} & C_{Z_\alpha} + (C_{Z_\alpha} - 2\mu_c) \lambda_c & -C_{X_0} & C_{Z_q} + 2\mu_c \\ 0 & 0 & -\lambda_c & 1 \\ C_{m_u} & C_{m_\alpha} + C_{m_\alpha} \lambda_c & 0 & C_{m_q} - 2\mu_c K_y^2 \lambda_c \end{bmatrix} \begin{bmatrix} A_u \\ A_\alpha \\ A_\theta \\ A_q \end{bmatrix} e^{\lambda_c s_c} = \begin{bmatrix} 0 \\ 0 \\ 0 \\ 0 \end{bmatrix} \quad (13.63)$$

$$\begin{bmatrix} C_{Y\beta} + (-2\mu_b)\lambda_b & C_L & C_{Y_p} & C_{Y_r} - 4\mu_b \\ 0 & -\frac{1}{2}\lambda_b & 1 & 0 \\ C_{l\beta} & 0 & C_{l_p} - 4\mu_b K_{XZ}^2 \lambda_b & C_{l_r} + 4\mu_b K_{XZ} \lambda_b \\ C_{n\beta} + C_{n\beta} \lambda_b & 0 & C_{n_p} + 4\mu_b K_{XZ} \lambda_b & C_{n_r} - 4\mu_b K_{Z}^2 \lambda_b \end{bmatrix} \begin{bmatrix} A_\beta \\ A_\phi \\ A_p \\ A_r \end{bmatrix} e^{\lambda_b s_b} = \begin{bmatrix} 0 \\ 0 \\ 0 \\ 0 \end{bmatrix} \quad (13.64)$$

The equations of motion for symmetric and asymmetric are shown in Equation (13.63) and Equation (13.64), respectively. The stability derivatives mentioned in the equations were obtained by analytical computation. A further derivation of the equations of motion was performed for each eigenmotion based on the motion characteristics. A code was written to compute the dimensionless eigenvalues, damping ratio, period and time to half amplitude for each eigenmotion. Based on the computed damping ratio and the time to half amplitude, the level of flying quality for each flight phase was determined [60]. The results obtained from the analytical model are listed in Table 13.20.

Table 13.20: Characteristics of the Eigenmotions

Eigenmotion	Eigenvalue	Damping Ratio	Period [s]	$T_{1/2}$ [s]	Quality Level
Short Period	-0.005±0.06j	0.088	2.417	3.024	3
	-0.055±0.187j	0.283	1.995	0.747	2
Phugoid	-2.842·10 ⁻⁵ ±0.001j	0.026	134.9	572.6	2
	-6.82·10 ⁻⁶ ±0.002j	0.004	204.1	6033.5	2
Aperiodic	-0.128±0j	-	-	1.57	2
	-1.509±0j	-	-	0.337	1
Dutch Roll	-0.018±0.17j	0.105	10.695	11.212	1
	-0.207±0.57j	0.343	7.664	2.466	1
Spiral	-0.0004±0j	-	-	556.3	1
	-0.002±0j	-	-	235.3	1

As can be noticed from the table, the stability characteristics at the cruise phase are more critical than those at the take-off phase. The damping ratio at the cruise phase is generally small compared to statistics. Design recommendations will be proposed to improve the damping behaviour.

Verification & Validation The output values can be verified by comparing the input stability derivatives with the ones obtained from the digital DATCOM method.

Table 13.21: Verification of Eigenmotion Parameters

Eigenmotion	Damping			Period [s]			$T_{1/2}$ [s]		
	Real	Ver.	Diff. [%]	Real	Ver.	Diff. [%]	Real	Ver.	Diff. [%]
Short period	0.088	0.084	-4.5	2.417	2.628	8.7	3.024	3.435	13.6
Phugoid	0.026	0.028	7.7	134.9	160.3	18.8	572.60	642.01	12.1
Aperiodic	-	-	-	-	-	-	1.57	1.39	-11.5
Dutch roll	0.076	0.059	-22.4	7.698	10.706	39	11.212	19.974	78.1
Spiral	-	-	-	-	-	-	556.3	-	-

The digital DATCOM parameters are inputted in the same program and the output values are shown in Table 13.21. The differences in the values can be explained by the assumptions made during the calculations of the derivatives as most of the intermediate parameters used in the computation of the derivatives were extrapolated from relevant graphs provided by Roskam [72]. Moreover, the time to half amplitude for the spiral eigenmotion is not included for the verification column in Table 13.21 because of its unstable nature as a result of running the code with the verification parameters.

Validation of the stability derivatives and the eigenmotion is beyond the scope of the project. However, it can be established by conducting wind tunnel tests and running a CFD analysis.

Recommendation for Future Design As can be seen from Table 13.20, the motion damping behaviour is poor compared to conventional aircraft especially the short period motion, which results in an uncomfortable flight for the pilot. In the future design, the horizontal wing parameters can be adjusted to obtain a higher lift curve slope. It is favourable for the longitudinal stability derivatives, whilst the fuselage length can be shortened to reduce the moment of inertia.

13.7. Payload Optimisation and Layout

The payload mass per aircraft is one of the most important parameters of the mission, it determines the number of aircraft needed and the frequency of flights, which are key components to the total costs. Furthermore, it determines the amount of fuel burn per aircraft, as well as the total weight of the aircraft. The payload is optimised for both environmental impact and cost, with it being constrained by the feasibility of the design. The optimisation was done with respect to the first year, as there is a possibility that Project Ceres can be cancelled within the initial stage. The range for which the payload was analysed, was from 4000 kg to 15 000 kg. This is because from analysis of the Class II sizing of the aircraft, it followed that for values slightly above 15 000 kg and more, the aircraft becomes unfeasible.

13.7.1. Environmental Impact

The environmental impact was quantified by the fuel burnt to inject the 0.2 Tg of SO₂ in the first year of mission, as it was determined that this was found to be the largest influence on the environmental impact [33]. The fuel burn was calculated by the methods explained in Section 13.5. From the total amount of aircraft and number of flights per year, an estimate of the total used fuel in the first year was made. The fuel burn versus payload shows a function with local minima at around 4400 kg, 8000 kg, and 9250 kg as illustrated in Figure 13.33. There is a slight peak in the fuel burned at around 8500 kg, this is due to the fact that the number of engines were minimised. Because of this, at this weight, the climb takes longer, and the total amount of fuel burned at this weight is higher. For a slightly higher payload, more engines were selected, and the fuel burned was lowered.

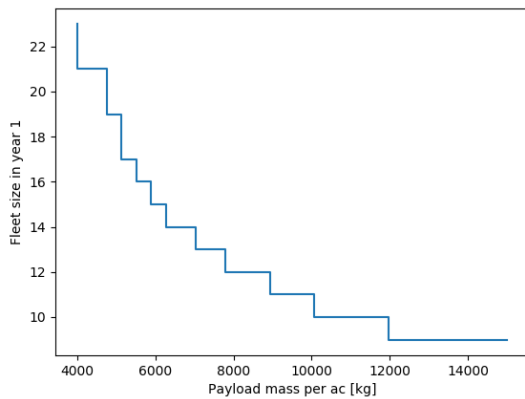


Figure 13.32: Fleet Size in Year 1 versus the Payload Mass per Aircraft.

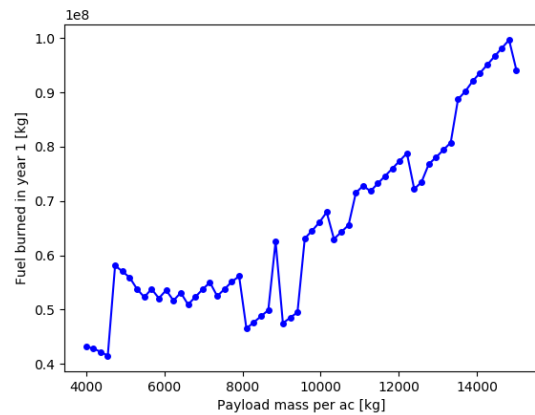


Figure 13.33: Total Fuel Burned after one Year versus the Payload Mass per Aircraft.

13.7.2. Costs

The costs were quantified by the number of aircraft needed in the first year in order to deliver the required sulphur in the stratosphere. Only the number of aircraft were taken into account, as this parameter had the largest influence on both the manufacturing cost and operational cost, according to the cost model from [33]. The given payload mass must be injected in 250 days and the number of aircraft is inversely related with the payload mass each aircraft has. However, the flight time increases with increasing payload mass. The cycle time was calculated using methods explained in Section 13.5, which was verified with SUAVE. The overall number of aircraft decreased non-linearly with increasing payload, due to increasing flight times. Figure 13.32 shows a step function, where each step indicates the number of aircraft used in the first year with its possible range of payload.

13.7.3. Optimal Payload

The payload must be optimised for minimal cost and environmental impact. This Multi-Objective Optimisation problem is solved using a Weighted Sum of Objectives approach. Both functions are normalised with respect to their minima, as shown in Eq. (13.65).

$$\overline{f_i(x)} = \frac{f_i(x)}{\min(f_i)} \quad (13.65)$$

The normalised functions were weighted and added together, creating a new function, as shown in Equation (13.66). Here, $\overline{f_1(x)}$ is the normalised total fuel burn for year 1, and $\overline{f_2(x)}$ is the normalised size of the fleet. This function was used in order to find the optimal payload. Due to the normalising method used, the absolute optimal solution would have a value of 1, which would only happen if the minimum for cost and the minimum for environmental impact would be at the same payload mass.

$$f_3(x) = w_1 \overline{f_1(x)} + w_2 \overline{f_2(x)} \quad (13.66)$$

To determine the weights of the functions $\overline{f_1(x)}$ and $\overline{f_2(x)}$, a sensitivity analysis has been performed to see how much the weights influence the final payload mass per aircraft and fleet size for year 1. In Figure 13.34, the combined function $f_3(x)$ can be seen for varying weights. From this graph, it can be seen that for weight ranging from 0.4 to 0.6, the optimum is the same, namely 9250 kg, with a score of 1.22. When the cost is weighted with a 0.7, the optimum changes, to a score of 1.20 and a payload of 10 900 kg. However, the score at 9250 kg is only slightly above this minimum. Furthermore, for other extremes such as weights of 0.7 and 0.8 for fuel burn the optimum does change significantly. As both factors are important, extremes of the weight variation will not be used, this results in a payload mass of 9250 kg and a minimum fleet of eleven aircraft in the first year. Including a margin of 5 %, the aircraft is designed to be able to hold and disperse a payload of 9700 kg.

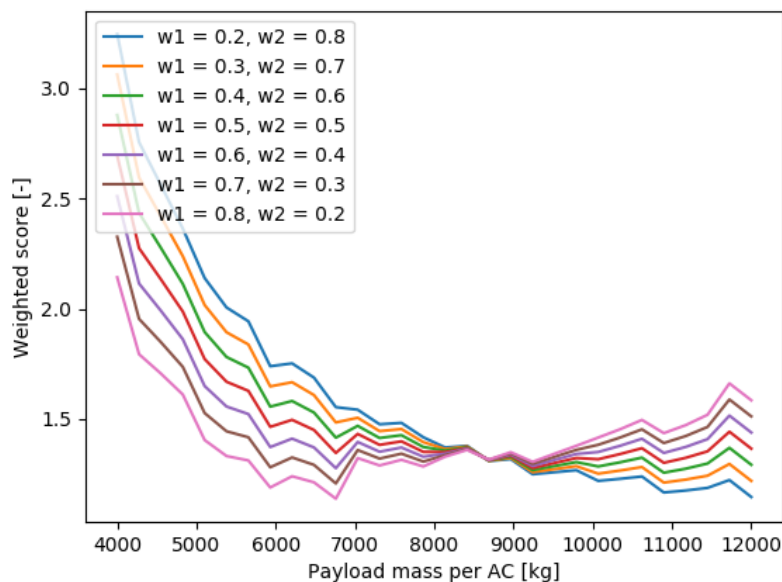


Figure 13.34: $f_3(x)$ with varying Weights.

13.7.4. Payload Burner

The payload of the Ceres mission consists of solid elemental sulphur pellets and a burner. This elemental sulphur needs to be melted and combusted with oxygen to get sulphur dioxide. The payload mass is quantified by optimising it for environmental impact and costs. The most important parameters next to the payload mass are the dimensions and the mass of the sulphur burner, the required inlet area for the air and the sulphur storage volume.

The principle of an open Brayton cycle is used to burn the sulphur to SO_2 . An existing jet engine is chosen and modified to burn sulphur. The atmospheric air is compressed to 1 bar, reacts with the sulphur and is ejected with the hot air. The option to use afterburners to eject the sulphur is also considered but rejected due to lack of literature [84]. The effectiveness of the aerosol particles is a measure of how much sunlight the particles reflect. This effectiveness depends on the size of the particles. There is an optimal particle size for the aerosols for multiple reasons. The settling speed of the particles increases with increasing radius and the amount of reflected solar radiation is also dependent on the aerosol size. The size of the particles is dependent on the dispersion rate of the sulphur dioxide. A dispersion rate of 8 g/m is the most effective

according to [84]. The combustor burns the sulphur with oxygen to form SO_2 . The molar masses of oxygen and elemental sulphur are 16 g/mol and 32 g/mol. The mass of one SO_2 particle is therefore 64 g/mol, with equal mass fractions of the sulphur and oxygen. This implies that the maximum payload mass of 9,700 kg of elemental sulphur needs to be combusted with 9,700 kg of oxygen. Therefore, the maximum total dispersed mass of aerosols is 19,400 kg per flight. The dispersion rate is 8 g/m, the required cruise can be calculated as in Equation (13.67) and using the cruise speed the required cruise time is calculated with Equation (13.68).

$$s_{cruise} = \frac{m_{sulphur}}{r_{\text{SO}_2}} = \frac{19400}{8} = 2425 \text{ km} \quad (13.67)$$

$$t_{cruise} = \frac{s_{cruise}}{Ma} = \frac{2425000}{0.72 \cdot \sqrt{1.4 \cdot 287 \cdot 216.65}} = 5885 \text{ s} = 3.26 \text{ hours} \quad (13.68)$$

9,700 kg of oxygen is needed to combust the sulphur. This sulphur could be taken in a pressurised oxygen tank onboard, but to reduce mass the oxygen is taken from the atmosphere. The cruise time and required oxygen mass are both known, and the oxygen mass flow is taken from these values. Smith et al. indicate an air to fuel ratio of 6:1 taking into account the efficiency of the burning process. 0.138 kg/s is the required air mass flow. The continuity equation is rewritten to get the required air inlet area in Equation (13.69) and plotted for different Mach numbers in Figure 13.35. The mass of the burner is estimated using Equation (13.36) to be 462 kg.

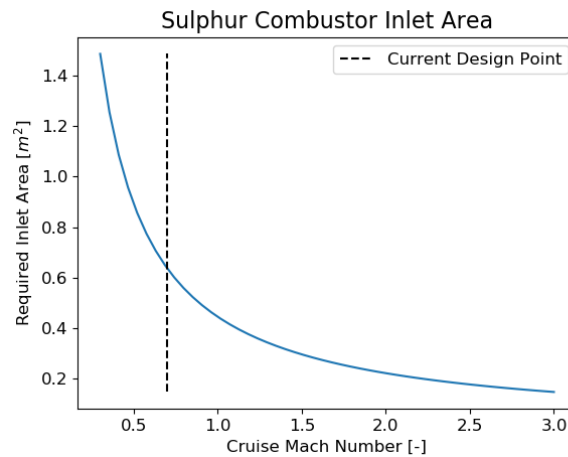


Figure 13.35: Required Combustor Inlet Area versus Mach Number.

$$A_{inlet} = \frac{\dot{m}}{\rho v} = \frac{\dot{m}}{\rho Ma} = 0.638 \text{ m}^2 \quad (13.69)$$

The inlet was integrated in the fuselage aft section. In order to minimise the increase of C_{D_0} due to the increased cross sectional area, various duct shapes were considered. The NACA ducts, see example below in Figure 13.36, provide aerodynamic advantages however in compressible flow such as the high subsonic speeds reached during the mission, their performance is less consistent. Nonetheless, this can be changed by the addition of a delta wing vortex generator. This is a configuration which is currently used in the APU inlet of the Boeing 737-800 for example. Due to the inlet area being quite large, it is here decided that 2 ducts will be used.[12, 39]

The outlet is also integrated in similar fashion as to what exists for APUs. This has many aerodynamic advantages when compared to podded APUs but the main pro in using this configuration is that the exhaust of SO_2 does not enter in contact with the rest of the aircraft. This is desired as the exhaust is corrosive and could potentially endanger the structural integrity of the aircraft.[59]



Figure 13.36: Example of a NACA Duct from the Boeing 737-800²⁰

13.7.5. Payload Power

The conversion of solid, granular sulphur to a liquid state requires the sulphur to be heated to 115°C or higher. During the melting process, the solid sulphur will first absorb a significant amount of energy to heat up from its confinement temperature to its fusion temperature. This involves the sulphur specific heat coefficient C , with enthalpy calculated using Equation (13.70).

Table 13.22: Specific Values for Sulphur Melting

Specific Heat (C)	0.710 kJ/(kg K)
Enthalpy of Fusion (L_F)	1.72 kJ/mol
Molar Mass (M)	0.0321 kg/mol
Heater Efficiency (η)	0.98

$$P = \frac{\dot{m} \left(C\Delta T + \frac{L_F}{M} \right)}{\eta} \quad (13.70)$$

The mass flow used is obtained in Section 13.7.4, and is equal to 0.826 for the sulphur. The sulphur must be heated to at least 115°C, but a margin is given for losses whilst travelling to the burner. An outlet temperature of 130°C is selected. In addition, the solid sulphur cools down whilst in flight. In a worst case scenario, the fuel will have cooled to ambient temperature at the 20 000 m cruise altitude. The starting temperature will be -56.5 °C. ΔT is equal to 186.5°K. Using a heater efficiency of 0.98, the required power goes up to 157 kW. In addition a margin of 10 % is added in case values change, yielding a final value of 172.7 kW.

13.8. Structural Design

The structural analysis of the Ceres aircraft analyses the loads acting on the surfaces. The structural design creates a structure that can withstand these loads. Due to the high aspect ratio, the wing is the most critical part of the design. The fuselage is non-pressurised, so no emphasis is put on this component in the structural analysis. The structural analysis consists of calculating the bending stiffness and torsional rigidity of the wing at each section of the wing, as this is constrained by aeroelasticity. The moment of inertia and torsional rigidity need to have a minimum value required to have aeroelastic speeds outside of the flight envelope. The wing section with the NASA SC(2)-0712 airfoil consist of three cells with spars to separate them at 20 % and 60 % of the chord. As visualised in Figure 13.37.

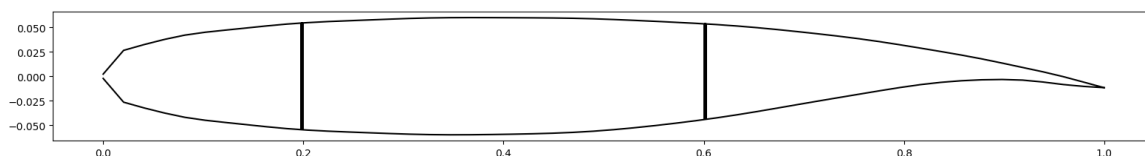


Figure 13.37: Airfoil with Spars.

Structural Rigidity The required structural rigidity was determined by doing a torsional analysis of the wing. The total torque in a wing section was calculated by summing the torques in each individual cell as in Equation (13.71). The rate of twist in each of the cells was determined by using Equation (13.72). The torsional rigidity is a structural property and therefore not dependent on the loads. Therefore a unit torque

²⁰<http://www.b737.org.uk/apu.htm>

is used in Equation (13.71). Combining this with the Equation (13.72) for each cell gives four equations for the unknown shear flows in each cell and the twist rate for each cell. The twist rate is equal in each cell, therefore a system with 4 equations and 4 unknowns was found, as in Equation (13.74). The torsional rigidity is defined as the ratio between the torque and rate of twist as in Equation (13.73).

$$T = 2A_1 q_1 + 2A_2 q_2 + 2A_3 q_3 \quad (13.71)$$

$$\frac{d\theta}{dy} = \frac{1}{2A_i} \oint \frac{q ds}{Gt} \quad (13.72)$$

$$GJ = \frac{T}{\frac{d\theta}{dy}} \quad (13.73)$$

$$\begin{bmatrix} 0 & 2A_1 & 2A_2 & 2A_3 \\ -1 & \frac{1}{2A_1} \frac{S_1}{G_{alu} t_{skin}} + \frac{h_{spar,1}}{G_{comp} t_{spar}} & \frac{-1}{2A_1} \frac{h_{spar,1}}{G_{comp} t_{spar}} & 0 \\ -1 & \frac{-1}{2A_2} \frac{h_{spar,1}}{G_{comp} t_{spar}} & \frac{1}{2A_2} \frac{S_2 + h_{spar,1} + h_{spar,2}}{G_{comp} t_{spar}} & \frac{-1}{2A_1} \frac{h_{spar,2}}{G_{comp} t_{spar}} \\ -1 & 0 & \frac{-1}{2A_3} \frac{h_{spar,2}}{G_{comp} t_{spar}} & \frac{1}{2A_3} \frac{S_3}{G_{alu} t_{skin}} + \frac{h_{spar,2}}{G_{comp} t_{spar}} \end{bmatrix} \begin{bmatrix} \frac{d\theta}{dy} \\ q_1 \\ q_2 \\ q_3 \end{bmatrix} = \begin{bmatrix} T \\ 0 \\ 0 \\ 0 \end{bmatrix} \quad (13.74)$$

The thickness of the spars and skin was determined based on the requirement for minimum aeroelastic speeds for torsional divergence, control reversal and flutter. Torsional divergence occurs when the wing twists further than allowed, because the torques created by the airflow are larger than the wing can handle. The aeroelastic speed at which this occurs must be outside of the flight envelope. To prevent aeroelastic phenomena a torsional rigidity of 25 MN m²/rad is required, as can be read in Section 13.2.3. The torsional stiffness is mainly sensitive to the skin thickness and the spar thickness. This is visualised in the sensitivity plot in Figure 13.38. A skin thickness of 1 mm and a spar thickness of 3 mm were chosen to prevent aeroelasticity in the flight envelope.

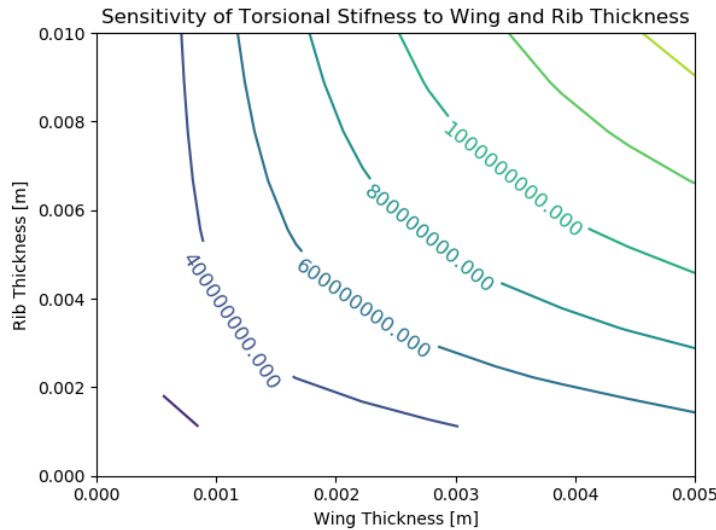


Figure 13.38: Sensitivity of Torsional Stiffness to Wing and Spar Thickness.

Bending Stiffness The wing area is fixed by the wing loading and take-off weight. The effects of bending due to the aerodynamic load and bending relief by the engines, fuel tanks and wing weight were analysed. The bending stiffness and flexural rigidity need to be calculated. The bending stiffness consists of the bending moments of the different structural components: the skin, the spars and the stringers. The skin thickness and spar thickness were already determined by the constraint for aeroelasticity, but the bending moment is still to be determined by the number of used stringers. The wing needs a certain bending stiffness

to prevent excessive bending in the flight envelope. The bending of the wing was analysed in the next paragraphs with the loads that act on the wing. But first the flight envelope was created with the maximum loads factors.

Flight Envelope With a first stage aircraft and an estimation of flight profiles, it is also necessary to construct the flight envelope to investigate the limit of Ceres aircraft in terms of load factor and flight performance. The cruise speed was obtained from the flight profile, and the stall speed can be computed with the maximum lift coefficient. Other velocity and load factor limits were computed using equations in [75] as shown in Figure 13.39 and Table 13.23.

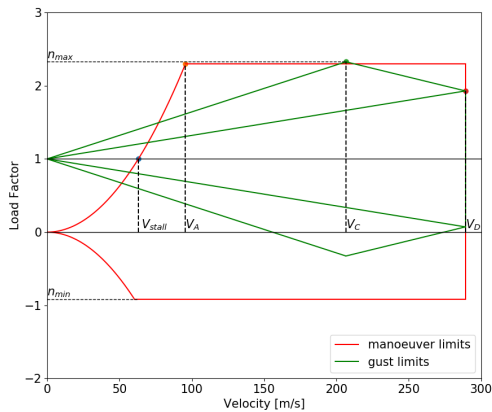


Table 13.23: Velocity and Load Factor Limits

Velocity [m/s]		Load Factor	
V_{stall}	63.08	n_{min}	-0.92
V_A	95.61	n_{maxm}	2.30
V_C	206.53	n_{maxg}	2.33
V_D	289.14	n_{ult}	3.48

Figure 13.39: Flight Envelope

Loading Diagrams For the modelling of the maximum shear, it was assumed that the lift distribution is elliptic, and the maximum load possible in the flight envelope was taken. Furthermore, the wing and fuel weights were modelled as distributed loads and the engines were modelled as point loads. From this model, the following shear force diagram of the wing Figure 13.40 was obtained. The shear force diagram is point symmetric which prevents the aircraft from rolling. The moment diagram with the internal moments of the wing was constructed by integrating the shear force diagram. Moreover, knowing that the internal moments at the wing tips would be zero also results in a boundary condition for the integration constant, which combined, results in Figure 13.41.

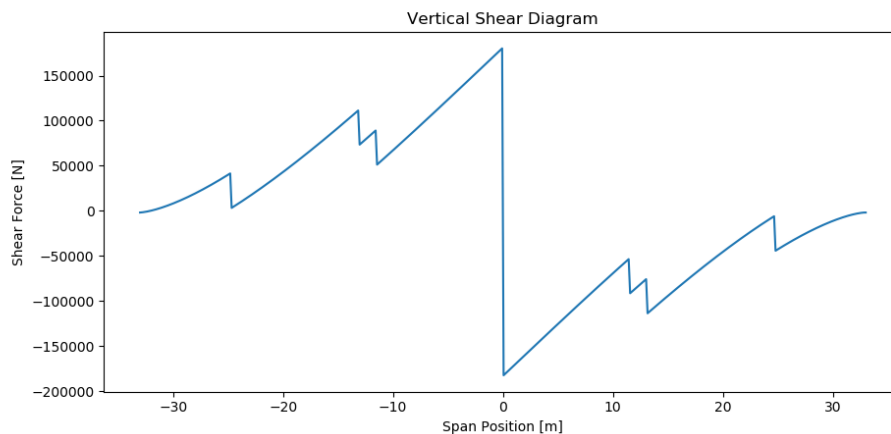


Figure 13.40: Vertical Shear Diagram.

Stringer Selection Standard L-shaped stringers with a surface area of 110 mm^2 were selected to reinforce the wing. The number of stringers needed was determined by a stress analysis of the wing. The stress in the wingbox cannot exceed the yield strength of the composite wingbox. The maximum stress in the upper and

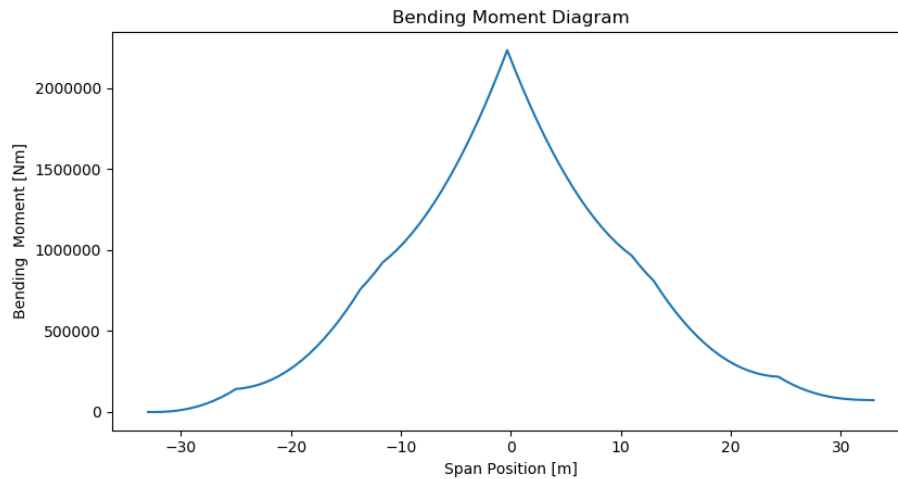


Figure 13.41: Bending Moment Diagram.

lower side of the wingbox as a function of the span is visualised in Figure 13.42. The black horizontal line indicates the yield stress and the coloured lines are the maximum stresses in at each position of the wing for the number of stringers indicated. The number of stringers goes in steps of 10. With 6 stringers in the wingbox and 4 on the spars. From this analysis 40 stringers are needed at the root of the wing to prevent yielding in any point of the wing. The number of stringers decreases step wise towards the wing tip.

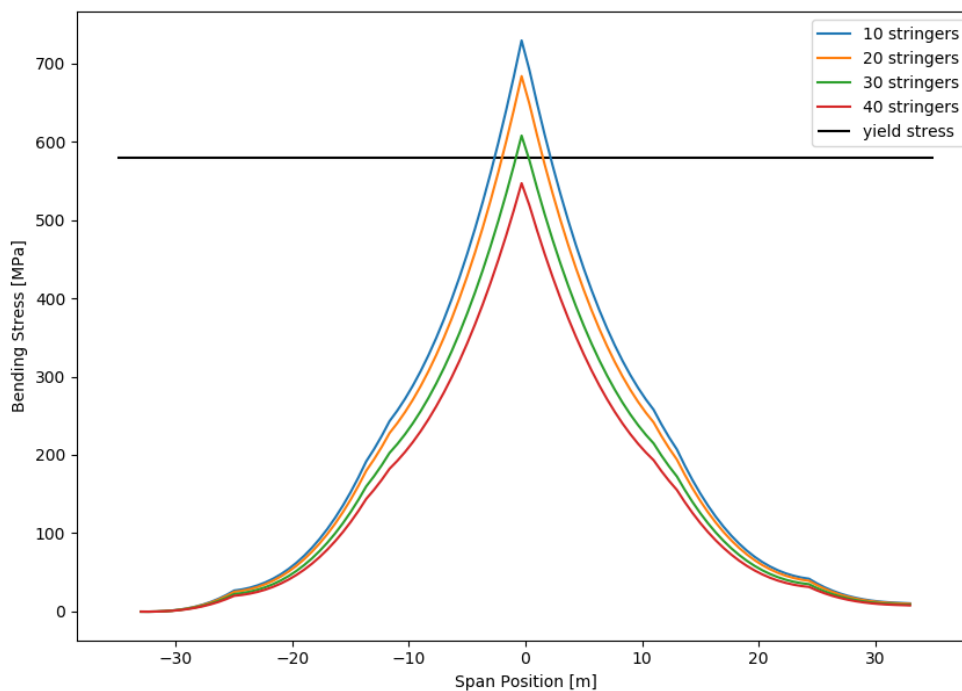


Figure 13.42: Bending Stress over the Wing Span.

Stress and Bending Analysis Using the diagrams, stress and deflection diagrams were plotted. The axial load of the wing due to axial forces was ignored. This is due to a majority of the axial load being caused by the internal bending moment. With the internal moment distribution given in Figure 13.41, the slope of the wing deflection can be found by integrating the moment diagram and dividing it by the flexural rigidity

(EI), shown in Equation (13.75). The deflection of the wing was found by integrating the slope as in Equation (13.76). The beam has no deflection at the midpoint where it is attached to the fuselage. The total bending of the wing in the ultimate load case is shown in Figure 13.43.

$$u' = \frac{-1}{EI} \int M(y) dy \quad (13.75)$$

$$u = \int u' dy = \frac{-1}{EI} \int \int M(y) dy dy \quad (13.76)$$

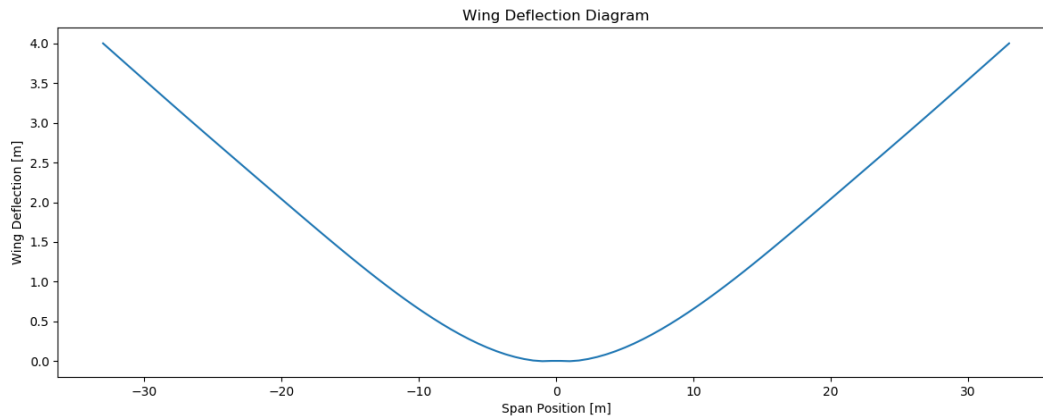


Figure 13.43: Wing Deflection Diagram.

Verification Structures The structural analysis consists of two parts, firstly the structural properties were analysed followed by the stresses and deflections making use of the loading diagrams. The structural properties were calculated with a numerical algorithm for idealised boom structures. The stress and bending analysis make use of these structural properties. The stresses were evaluated with simple analytical formulas once the structure and loads were known. This emphasises the need to verify the structural properties. The numerical program to calculate bending stiffness and torsional stiffness was verified for simple geometric shapes with dimensions for which the analytical solution was known. The results are shown in Table 13.24 and the numerical errors are acceptable small.

Table 13.24: Verification Bending Stiffness and Torsional Stiffness

Shape	Analytical Bending Stiffness	Numerical Bending Stiffness	Error
Rectangle	0.666667	0.66667	0%
Circle	0.785398	0.785398	+1.3%
Triangle	0.222222	0.21221324	-2.1%
Shape	Analytical Tors. Stiffness	Numerical Tors. Stiffness	Error
Rectangle	0.75	0.74999	+0.1%
Circle	1.57012	1.42871	-0.9%
Triangle	0.45100	0.462275	+2.2%

The structures of the wing are further verified by using Matlab beam bending software [7]. The results are plotted in Figure 13.44 with the original deflection in orange and the validation deflection in the dashed blue line. The software gave the same bending shape, but the wing tip deflection was a bit less with the Matlab software. This is probably due to the numerical integration error of the script. Less wingtip deflection is beneficial for the structure, therefore the structure is verified for wing bending. Validation can be done by use of numeral tests, however for this the structure needs to be build as well, which is beyond the scope of the DSE.

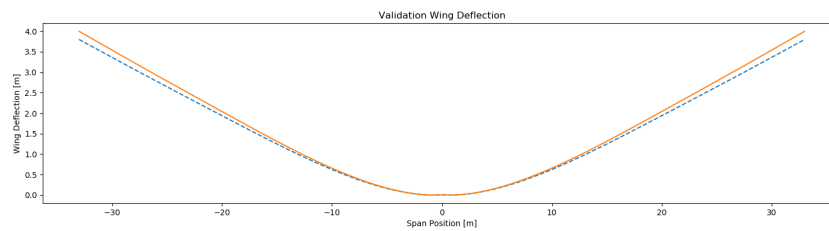


Figure 13.44: Validation of the Wing Deflection.

Material Selection and Structural Wing Weight The materials used in each structural component of the aircraft were chosen based on several factors. The material selection was made independently of the concepts, but based on the structural philosophy. The most important factor in the design is the strength to weight. Other factors of importance for specific parts of the aircraft are stiffness, resistance to corrosion, fatigue, ease of fabrication, manufacturability, sustainability and costs. The objective of this section is to perform a trade-off between these factors while complying to certain standards with respect to environmental impacts.

There are six commonly used materials in aircraft design: aluminium, steel, titanium, plastics, glass, and Carbon Fibre Reinforced Polymers (CFRP). Aluminium alloys are the standard materials for large thin sheets like the fuselage structure. Steel is also commonly used, but only for parts that need a high strength. The disadvantage of steel is the high density. Titanium alloys are used for the inlet and outlet section of the engine, and the compressor stage is usually made of steel. Plastics are used for parts that do not require high specific strengths and parts that need to be electrically insulating. Glass was selected for the cabin window. Composite materials consist of stronger fibres, usually carbon, set in a matrix of plastic resin. Use of composites is increasingly more frequent for structural components of aircraft as it is lightweight and stiff. [58]

Due to the strict cost requirements and the environmental constraints, it was decided to only consider the use of aluminium alloys and CFRP for the structural components. This choice was based on the possible end-of-life scenarios in which there is a non-negligible chance of the aircraft operations being stopped after its initial phase. For this reason, it is very important that the re-usability of the aircraft is maximised.

CFRP allow for tailoring of parts which can lead to a great weight decrease, this is due to the very high specific properties of the material and the nature of its use which derives from layering of sheets providing only a certain directional property. However, this comes at a certain cost both financially and environmentally [79].

It must first be noted that two main types of matrices CFRP exist: thermosets and thermoplastics. Both have a great environmental and financial impact as the process of production of the carbon fibres is extremely energy consuming and very costly to put in place [79]. In addition, using these materials with metals for example induces a great weight penalty, which can limit the benefits obtained. Curing thermosets requires an autoclave for high quality finishes, which means that for large parts, an extremely large autoclave is required for optimal results. Moreover, this oven requires very high amount of energy to operate as curing times can extend beyond a dozen of hours.

On the other hand, thermoplastics have lower specific properties but allow for a similar degree of tailoring with the benefit of being reusable to a certain degree.

Aluminium alloys on the other hand, have a higher use rate and have been used for a longer amount of time. This results in a greater number of models being available about the design of parts with these isotropic materials. Moreover, due to the development of additive manufacturing, the tailoring possibilities with metals have greatly increased, mostly reducing the weight penalty with respect to the use of composites. In addition to this new production method, metals can be easily be recycled. Nevertheless, the production of these materials requires a high amount of energy due to the mining of the ores and the processing of the latter. This can however be equated to the environmental impact of the production of carbon fibres.

Thus, it can be concluded that based on material performance and experience of the industry with certain materials, thermoplastics will not be used. Because of the long term impact of using low re-usability

materials such as thermosets and prepregs, it was decided to minimise the use of these materials. Moreover, due to the high manufacturing costs as well as the environmental impact of CFRP, it was decided to not use CFRP in the fuselage but solely consider using it in the wings as it is only in this location that the high aspect ratio leads to the structural weight outweighing the costs, both environmentally and financially. [79]

Lastly, most material is used for the fuselage and the wing. Therefore, the materials for the fuselage and wing were selected in this preliminary phase of the design. The fuselage will be made of aluminium alloys. An overview of the materials used in each subsystem is presented in Table 13.25, where EI is Environmental Impact and is quantified using a single score in mPts which is then converted to equivalent CO₂²¹. Aluminium 7075 was chosen out of the different aluminium alloys as it has the best strength over weight performance.

Table 13.25: Recapitulative table of the materials and properties which can be used

Material	Part	Density [kg/m ³]	Tensile strength [MPa]	E [GPa]	EI [CO ₂ t/kg]
Aluminium 6061	Fuselage, wing	2700	324	68.9	340 [37]
Aluminium 7050	Fuselage, wing	2830	552	71.7	310 [37]
Aluminium 7075	Fuselage, wing	2810	572	71.7	330 [37]
Titanium 5553	Fuselage	4650	1159	85	460 [61]
CFRP	Wing	1600	480	30	400 ²²

13.9. Systems and Internal Layout

This section details the various subsystems ranging from the communication to the electrical systems as well as the hydraulic system and the fuel systems. It then presents the current internal layout of the Ceres aircraft.

13.9.1. Communication System

This section focuses on describing the necessary communication interfaces for the successful mission execution. The necessary aircraft communication systems, benefits of downlinks and uplinks for the mission execution and the necessary interface by ATC are discussed in the subsequent sections. The flow diagram in Figure 13.45 aids the representation of the communication systems. Acronyms used in the diagram are explained in the following section.

Aircraft

The cockpit requires interfaces for the flight crew to be able to interpret the situation their aircraft is in. Thus, a series of displays are required to represent the state of the aircraft. Some displays serve the purpose of displaying the aircraft's flight parameters, state and horizontal situation, whilst others will allow for the configuration of flight profiles. These displays will be driven by a pair of flight computers to ensure sufficient redundancy. A set of standby instruments may be equipped in the case AC/DC power is lost. An autopilot interface will help programme the flight computer to execute actions commanded by the flight crew for the safe and successful execution of the mission.

The flight computers will gather environmental and system data from the aircraft to process and create appropriate flight profiles. Flight profile constraints will be input by the flight crew, with the flight management system calculating the appropriate lateral and vertical profiles. To allow for departures and approaches from airports without area navigation departures or approaches, a pair of navigation radios and Automatic Direction Finders (ADFs) will allow to perform Instrument Landing System (ILS), ILS CATII, Very High Frequency Omnidirectional Distance Measuring Equipment (VOR-DME), VOR and Non Directional Beacon (NDB) approaches. Other flight instruments will gather the necessary information used to aid the aircraft flight. The flight computer will communicate with the appropriate trim bundles for autopilot functionality and optimisation of flight profiles.

Due to the aircraft operating from existing aerodromes and airports, it must meet the regulations required for the visual flight rules and instrument flight rules as specified by International Civil Aviation Organization (ICAO) and the local regulators. Due to most airports having either Class A or Class C airspace around their aerodrome terminal zone or terminal manoeuvring area, in addition to Class A airspace in

²¹URL <https://www.sustainableminds.com/showroom/shared/learn-single-score.html>

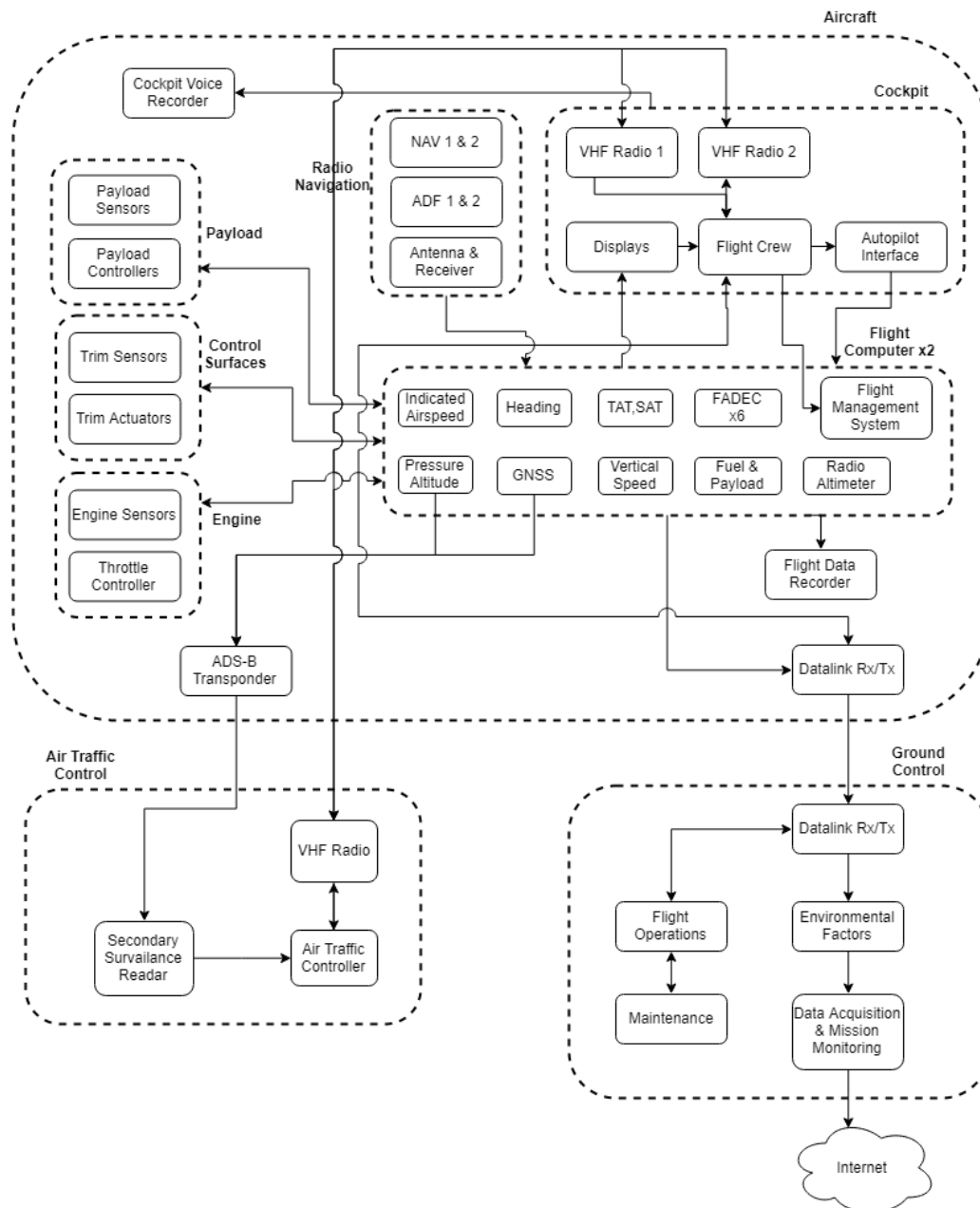


Figure 13.45: Communication Flow Diagram for the Aerosol Injection System to meet Specifications.

the mid-flight levels, the aircraft must be equipped with a transponder compliant with the latest regulations. Recent trends have proven the widespread adoption of Automatic Dependent Surveillance-Broadcast (ADS-B) out transponders, especially in the US. In addition, two Very High Frequency (VHF) radios will be required for redundancy and avoiding unnecessary abnormal operations in the case a radio fails.

A cockpit voice recorder and flight data recorder are included for to find the cause of any catastrophic situations if they occur and aim to mitigate it.

Ground Control

Ground control needs to receive a variety of data to help execute the aerosol injection mission successfully. Therefore, the flight parameters from the flight computer will be broadcasted via a datalink service. This datalink system will most likely be based on an existing Aircraft Communications Addressing and Reporting System (ACARS) system to help reduce costs. This will allow ground control to receive information about each operating aircraft and optimise the mission profile depending on flight conditions. The data received by the ACARS system will also aid fault resolution by maintenance, and help speed up any ground services required. The data from each mission will be broadcasted over the internet to help communicate between

the various operating bases and to release public information about the project status and milestones. Additionally, a two-way text communication link between the flight crew and ground crew will aid for efficient communication.

Air Traffic Control

Air Traffic Control must be able to pick up the ADS-B data on their secondary surveillance radar. This kind of radar is used worldwide for major air traffic regulators, and thus must not be provided to achieve the mission. In addition, to allow for communication with the aircraft, a VHF radio is required. Once again, this is standard equipment for all air traffic control stations. Adhering to the current standards of air traffic control procedures is considered important for reducing the costs of the mission.

13.9.2. Electrical System

The electrical systems within the aircraft have the function to distribute sufficient power from the EJ200 to all the necessary systems. The system must be designed such as to provide sufficient redundancy as to not impair mission capabilities in the case of one or multiple failures. The electrical system diagram is given in Figure 13.46.

The EJ200 generates electrical power with the use of an Integrated Drive Generator (IDG). It is the sole user of such electrical generation equipment within the military field. The IDG output is 115 VAC/400 Hz, with an unknown power generation at the time of this report writing. Military engines similar to the EJ200 normally provide a power of 40-65 kVA [71]. Six IDG will be present, as all engines will be equipped with generators. In the case that the generators do not come equipped on new engines, then the layout of 4 IDGs may also be adequate and helps minimise maintenance tasks.

Each IDG has its own appropriate generator bus tie. These ties may be controlled manually in the case that the generator load must be taken off. Each IDG also has the capability to be disconnected in the case of oil lubrication malfunctions. This system is widely used amongst Airbus airliners. AC power can also be provided through the use of the on-board Auxiliary power unit (APU) or external power. These sources provide both buses with AC power.

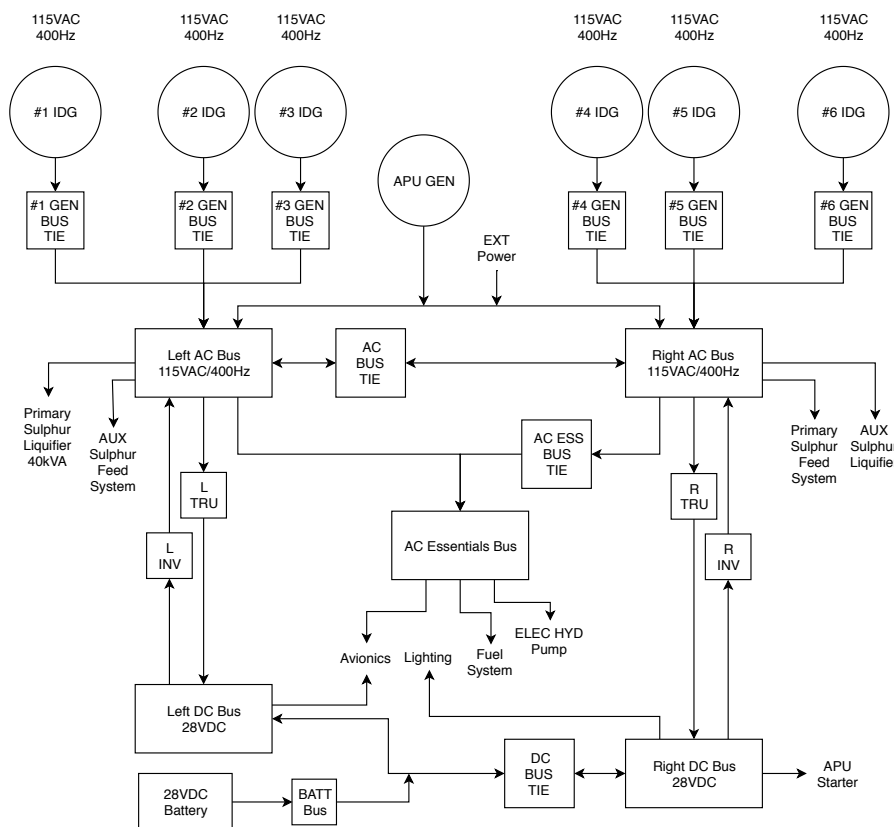


Figure 13.46: Diagram for the Electrical System On-board of Ceres Mission Aircraft.

Each generator bus tie leads to an appropriate AC bus for each side of the aircraft. This allows the sepa-

ration of the left and right buses for AC power. Additionally, this reduces the number of AC buses compared to the number required if individual buses were to be provided for each engine. This, in turn, provides lower costs and more centralised maintenance whilst prioritising safety. In the case an AC bus loses power from one side of the engines, the opposite AC bus is able to provide the bus with power through the use of an AC bus tie. The AC buses power the sulphur related systems and does not go through the AC essentials bus to reduce weight and circuit resistance due to their large power inputs.

The AC essentials bus powers all the necessary flight instruments for the safety of the mission. These include fuel pumps and hydraulic pumps which require significant amount of power, in the magnitude of 6-8 kVA. The essentials bus is thus powered mainly by the left AC bus, with the ability to use the right AC bus to alleviate load from the left system. The use of the right bus is done through an AC essentials bus tie. Activation is done automatically, with a manual use possible through the use of a push-button.

DC power is supplied by rectified power from each of the AC buses. This is done through the use of Transformer Rectifier Units (TRU), allowing for a step down from 115 VAC to 28 VDC. This allows for power to be given to all the avionics as well as the lighting systems and other smaller systems with smaller power inputs. The DC bus is also responsible for providing the necessary power for an APU start. The battery on board the aircraft can provide 28 VDC for the avionics and other systems for APU starts and standby avionics operations. In addition, the battery can be charged through the DC system. The DC bus can provide the AC bus with power by the use of an inverter. This can be used to transfer power in the case AC bus ties are not working or are overloaded, as well as allowing to power some AC systems at a low power regime when AC power is not available.

13.9.3. Hydraulic System

The hydraulic system has the primary function of augmenting flight control forces during pilot inputs. Additionally, it is used for secondary functions such as landing gear extension, nose wheel steering, converging-diverging nozzles, stabiliser trim, elevators, rudder and spoilers as well as wheel brake systems. The aircraft is assumed to have manual reversion cable controls throughout, running to the ailerons, elevator and rudder, as a mechanical backup for the latter two and a primary control for the ailerons. The hydraulic system diagram is shown in Figure 13.47.

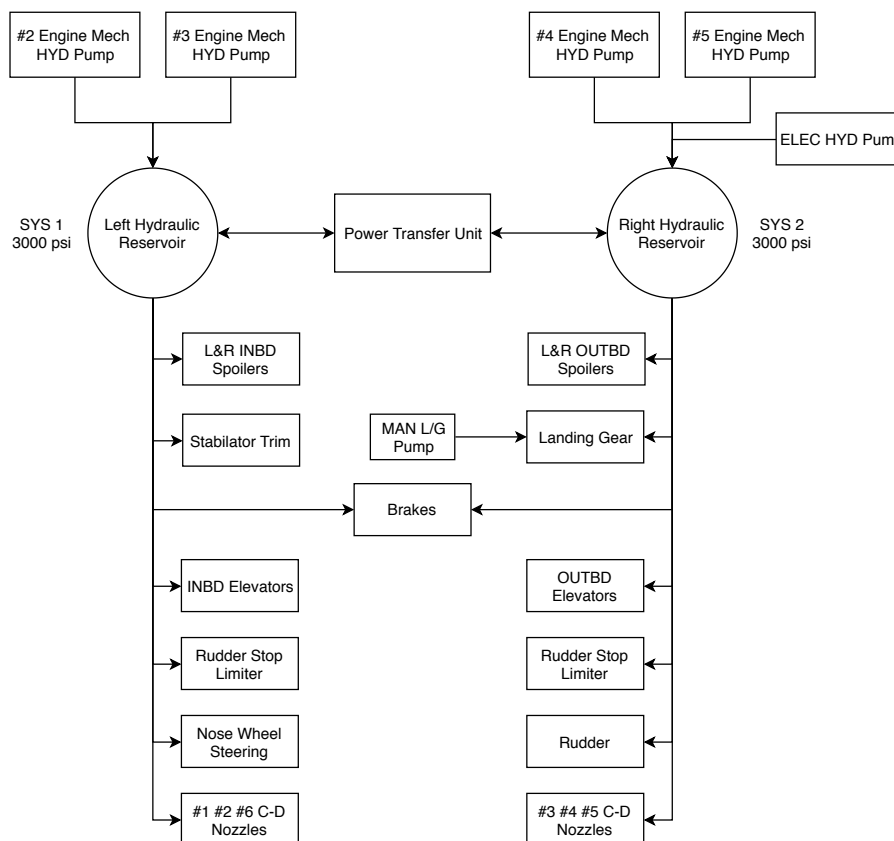


Figure 13.47: Diagram for the Hydraulic System On-board of Ceres Mission Aircraft.

Hydraulic pressure is provided by engine-driven pumps. Two engine-driven pumps drive each of the two hydraulic systems. System number 2 is driven by two engine pumps, as well as one electric pump. The electric pump helps provide hydraulic pressure during high demand situations, as well as providing pressure in the case of failure of any of the engine-driven hydraulic pumps. The electric pump is to be operated automatically, with a manual shut off when no hydraulic power is required, such as on the ground. Mechanical engine-driven pumps have their hydraulic system shutoff during the activation of the fire shutoff handles.

Hydraulic pressure is kept in hydraulic reservoirs. These reservoirs provide hydraulic fluid when demanded with the additional function of storing hydraulic fluid when it cannot be used within a hydraulic actuator. These vessels hold a standard pressure of 3000psi, as per aviation standards. Hydraulic pressure can be exchanged between the vessels through a Power Transfer Unit (PTU). The PTU does not communicate the pressure vessels together, thus a leak in one system will not drain the adjacent system. The PTU can be manually shut off in the case of overheating or any other malfunctions that require such action.

A total of two hydraulic systems are chosen due to the mechanical backup of the controls. This allows for a reduction in weight, as well as a simplification of maintenance procedures. Four engine-driven hydraulic pumps are chosen to provide sufficient redundancy whilst keeping plumbing to a minimum. This can be done due to the shared pylon of engines 2,3 and 4,5, respectively.

System number 1 is responsible for the inboard spoilers, stabiliser trim actuator, inboard elevator actuators, one of the rudder stop limiters, nose wheel steering and the converging-diverging nozzles for engines 1,2 and 6. In the case of a system number 1 pressure loss, all these systems will have limited or no use. Controllability of the aircraft is retained, with the most critical failure being the thrust loss on engines 1,2 and 6 due to the nozzles no longer providing proper expansion. Thrust asymmetry will be experienced solely due to engine number 2 having a lower thrust value than engine number 5. These are the inboard engines, and thus yawing moments will be kept below the critical yawing moments for which the vertical tail is designed for at the minimum control speed. Nose wheel steering would not be operational but only affects the aircraft at speeds below 50 knots on a roll out. Differential braking may be used to maintain directional controllability at low speeds and to help vacate the runway.

System number 2 is responsible for the outboard spoilers, landing gear actuators, outboard elevator actuators, the second rudder stop limiter, the rudder and the engine number 3,4 and 5 converging diverging nozzles. In the case of a system 2 pressure loss, the most critical systems are the landing gear, as well as the loss of the rudder hydraulic augmentation coupled with asymmetric thrust. The rudder retains controllability due to the mechanical backup. This implies higher control forces, but thrust asymmetries are kept to a minimum and may be reduced by the reduction in the thrust of engine number 2.

Wheel brakes operate with both systems, without mixing different system fluids. This allows for double redundancy and ensures that the aircraft may be stopped in the case of the lost of one system. The landing gear has a manual landing gear pump in the case of the lost of all hydraulic power on system number 2. An additional reserve brake accumulator may be required to guarantee to stop power under a full hydraulic failure or under prolonged parking brake use.

13.9.4. Fuel Systems

The aircraft will have an inner and outer tanks as well as vent tanks. The outer tank is beneficial for the bending relief of the wing. The layout of the fuel system can be seen in Figure 13.48 and is mirrored for the right wing.

There is an abundant amount of space for the fuel tanks since the wing of the Ceres aircraft is extremely large, therefore, space is not a constraint. As seen in the fuel system layout, the cross-feed pump is needed for balancing the fuel load for lateral stability of the aircraft. The cross-feed pump is also beneficial for the mitigation of any severe consequences as a result of engine failure or leakage of the fuel tank. Intermediate flow valves and pumps will be included between the tanks for easy transfer of fuel between tanks and allowing the tanks to feed all the engines instead of having individual tanks for each engine. As fuel is burned, the vent tank is essential for replacing the used fuel to keep the tank pressurised. It should be noted that architecture is only a simplification of the fuel system.

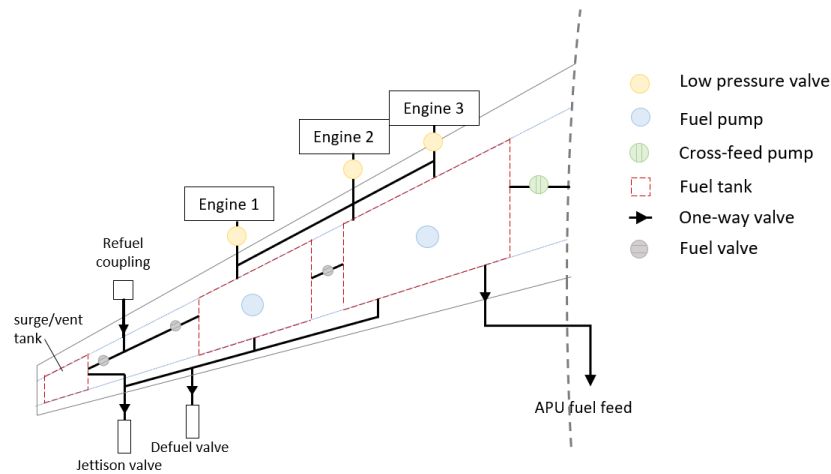


Figure 13.48: Fuel System Layout.

13.9.5. Internal Layout

The internal layout of Ceres aircraft is designed for the placement of payload. As mentioned in section 13.7, the payload consists of a sulphur tank and a combustion system. The sulphur tank was designed based on the payload weight per flight, while the longitudinal position was determined for static stability. A sketch of the internal layout of the aircraft is shown below, followed by a description of the payload system.

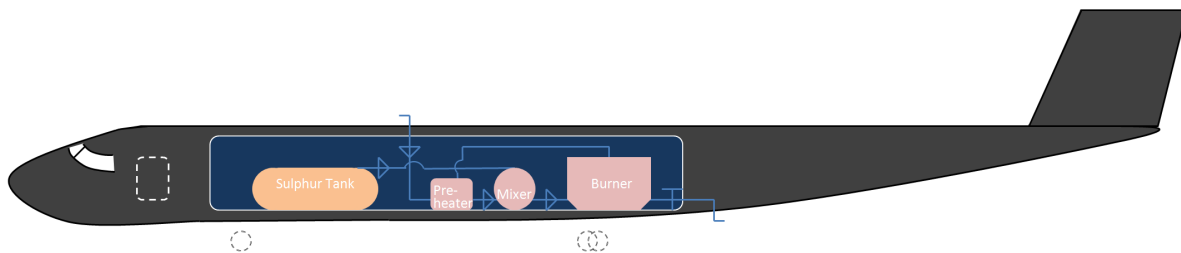


Figure 13.49: Visualisation of the Internal Layout of Ceres Aircraft.

Air is taken from the atmosphere through an air inlet, followed by a pre-heating treatment. Sulphur is pumped from the tank and mixed with the pre-heated air in the mixer at a pre-determined volume fraction. The sulphur air mixture will be combusted in the combustion chamber to generate SO_2 . The dispersion ratio can be adjusted by an adjustable valve. It should be noted that the figure only indicates a simplified payload system layout. A more detailed demonstration should be made with further investigation on the payload system in future research.

13.10. Final Design Characteristics

After all the design steps and decisions described previously in this chapter have been conducted and integrated, the final design parameters of Ceres can now be presented in Table 13.26. First, the wing and empennage are described, followed by the layout of the fuselage. Then, the flight performance parameters are listed. First, the aerodynamic parameters and then, propulsion. Finally, the parameters regarding the operations are shown.

Figure 13.50 shows the final layout of the Ceres aircraft. A high wing is selected with six underslung EJ200 engines of which the inboard two are double podded. A T-tail is selected thus only the vertical tail location needs to be specified in Table 13.26. The horizontal tail location is defined based on the vertical location and geometry.

A technical illustration of the design of Ceres is given in Figure 13.50 where it can be seen that a tricycle landing gear is selected.

Table 13.26: Final Design Parameters

Wing Parameters	S	A	MAC	b	x_{apex}^a	$\Lambda_{0.25c}$	λ	Twist	Anhedral	Airfoil
Values	277.5 m ²	13.0	4.85 m	60.1 m	21.4 m	27.3°	0.442	-4.5°	-1°	NASA SC(2)-0712
Horizontal Tail Parameters	S	A	MAC	b	$\Lambda_{0.25c}$	λ	Twist	Anhedral	Airfoil	
Values	49.3 m ²	8.67	2.54 m	20.7 m	31.4°	0.348	-2°	-1°	NASA SC(2)-0610	
Vertical Tail Parameters	S	A	MAC	b	x_{apex}	$\Lambda_{0.25c}$	λ	Airfoil		
Values	26.0 m ²	1.3	4.54 m	5.82 m	46.9 m	50.7°	0.646	NACA 0009		
Layout Parameters	l_{fus}	w_{fus}	h_{fus}	x_{cg}	Landing Gear Track					
Values [m]	52.4	6.13	3.5	24.1–24.7 (15–35 %MAC)	4.39					
Flight Performance Parameters	$C_{L_{cruise}}$	$C_{L_{max}}$	C_{D_0}	e	V_{cruise}	s_{cruise}	T_{SL}	T_{cruise}	SFC_{cruise}	$n_{engines}$
Values	0.54–0.83	1.0	0.0287	0.814	206.5 m/s	2425 km	360 000 N	22 086 N	2.64×10^{-5} kg/(N s)	6
Operations Parameters	$m_{payload}$	Dispersion Rate	Fleet Size _{y1}	Fleet Size _{y15}	Cycle Time	# Operational Days				
Values	9700 kg	0.008 kg/m	12	180	5.83 h	250/yr				

^aThe apex is defined as the leading edge of the root chord

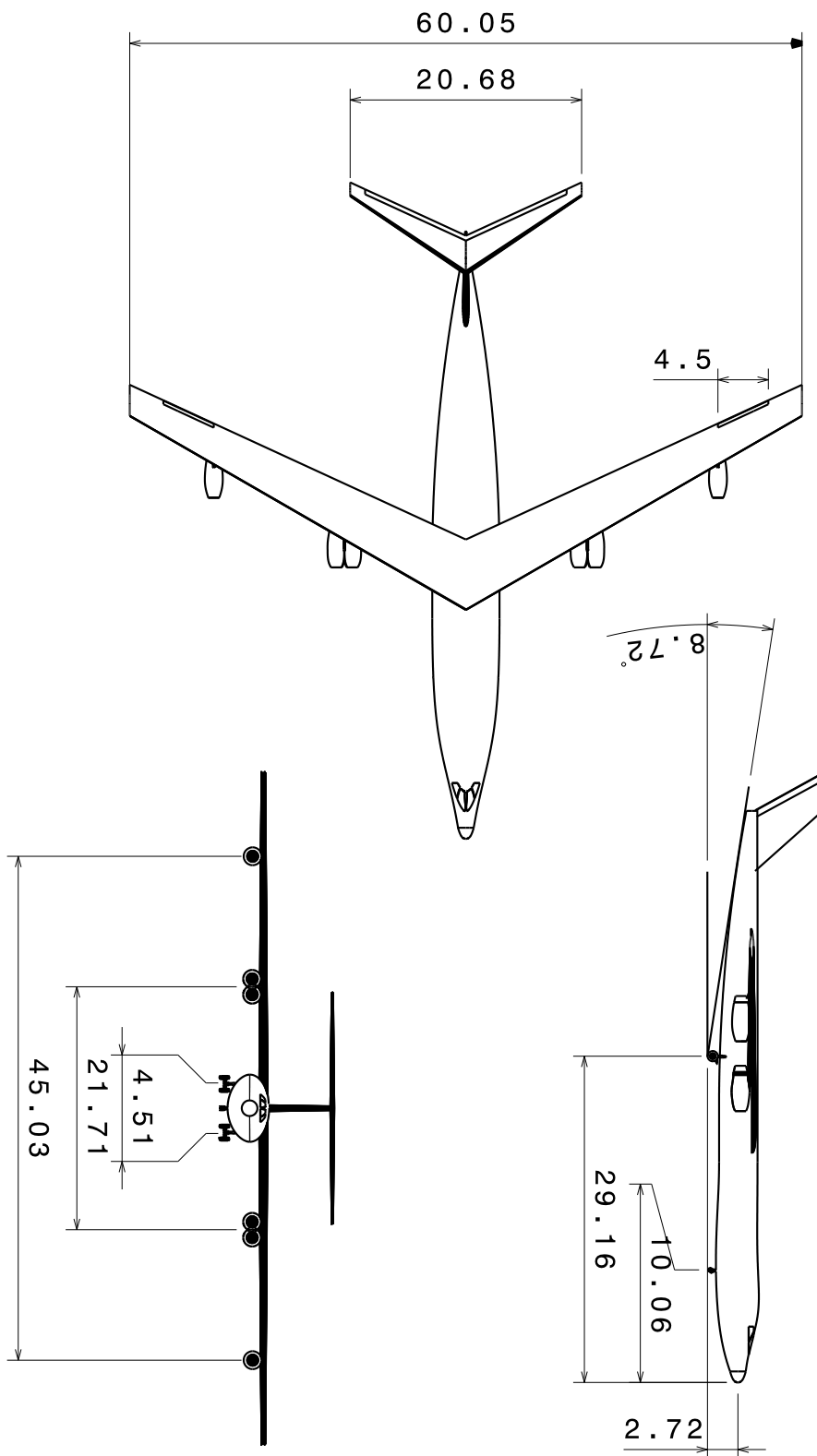


Figure 13.50: Three View Drawing of the Ceres Aircraft (Dimensions in m).

Impact Assessment

14.1. Financial Impact Assessment

After the aircraft specifications and operations are established, a detailed cost analysis was conducted. A model to approximate the costs was constructed based on Roskam's cost method from his book *Airplane Design* volume 8 [74]. The method allows for the computation of the cost of the three most important aspects of an aircraft life cycle: Research and Development (R&D), Manufacturing and Acquisition (M&A) and Maintenance and Operations (M&O). For verification and validation, a section model was used provided by W. Smith [85].

The outline of this section is as follows, first the method from Roskam is explained in more detail, in which its assumptions and constants are discussed. After that, the costs are discussed and summarised for R&D, M&A and M&O. Lastly, the total costs are summarised.

14.1.1. Method

Despite the age of the book of Roskam, it is still considered an appropriate method since it is widely used in the aerospace industry and accounts for time-varying variables. In this approach, the costs of the three components are treated separately. A Python script was written to automate the computations. The model requires basic aircraft and operations specifications as inputs. Examples of these inputs are maximum take-off weight, engine weight, cruise velocity, block time etc. As mentioned previously, the model from W. Smith was also used to obtain values for the costs. These were compared to the values from Roskam. While the second model gives values for all three aspects of the costs, it only goes into detail for the operations part. All cost outputs are converted to 2019 USD.

The model based on Roskam's cost method depends on numerous assumptions and parameters either computed or retrieved from volume 8 of [74]. The list of data retrieved from Roskam is shown in Table 14.1 which will be elaborated next.

Since the method originates from 1989, inflation had to be taken into account. This was done by using the Cost Expansion Factor CEF as seen in Table 14.1. As such, using the labour rates in 1989 retrieved in volume 8 of Roskam [74] the CEF from 1989 to 2019, which is based on the production price index (PPI),¹ was used. Additionally, the CEF between 1970 and 1989 was found in Roskam's work and amounts to 3.02.[74] Note that for correcting the material and equipment costs, the CEF value between 1970 and 1989 and CEF value based on the PPI values have to be super-imposed which results in the value shown in the table.

Furthermore, the assumption was made that 2 static and 4 operational test aircraft are needed, which is within the range of conventional numbers as stated in volume 8 of Roskam [74].

Next, different parts of the model scale with the difficulty of the design, F_{diff} . Volume 8 of Roskam states this to be between 1 for a conventional design with common technology, 1.5 for a design which requires moderate use of more advanced technology and a factor 2 for designs that rely on aggressive use of advanced technologies.[74] Ceres' design relies on relatively conventional technology, however, the way it is brought to use is advanced. Furthermore, Roskam mentions that the difficulty of the design is often underestimated and because of this a factor of 1.5 is selected.

Moreover, F_{CAD} is the factor which accounts for the proficiency of computer-aided design software of the manufacturer, which ranges between 1.2 and 0.8 and where a higher value means that the manufacturer is not adequate in using CAD. It was assumed that the manufacturer is proficient in the use of computer-aided programs to support the manufacturing and design, as such a value of 0.8 is assumed.

¹ <https://fred.stlouisfed.org/series/PCU3364113364113>

Additionally, F_{obs} considers the importance of low observability for the design, where the value can either be 3.0 or 1.0 (higher means more important). Since no requirements requires a 'stealthy' aircraft, the value was set as 1.0.

The factor which adjusts the cost due to the required test facilities (F_{tsf}) can either be 0.00 or 0.20, where the latter means the use of extensive test and simulation facilities are required. Considering the high altitude of Ceres, the dispersal operation and the effect of the payload itself, the use of testing and simulation facilities was predicted to be extensive. As such, the value was set to= 0.20.

Lastly, all remaining parameters are not discussed, e.g. the number of engines N_e is not discussed as this decision was based on the design concept and performance requirements.

Table 14.1: Chosen Parameters in the Preliminary Cost Model Based on Roskam's Method

Parameter	Description	Value	Unit
CEF19	Cost Expansion Factor of 2019 (base = 1970)	5.55	[\$/hr]
CEF90	Cost Expansion Factor of 1990 (base = 1970)	3.02	[\$/hr]
R_{e_r}	Engineering labour rate	62	[\$/hr]
R_{m_r}	Manufacturing labour rate	34	[\$/hr]
R_{t_r}	Tooling labour rate	43	[\$/hr]
F_{mat}	Correction factor for type of material	2.25	[-]
F_{diff}	Difficulty of airplane program	1.5	[-]
F_{CAD}	Effect of computer-aided design on cost	0.8	[-]
F_{obs}	Importance on low-observability	1	[-]
F_{tsf}	Cost adjustment factor due to additional test facilities	0.20	[-]
N_{rdte}	Number of test aircraft	6	[-]
N_{st}	Number of static test aircraft	2	[-]
N_e	Number of engines per aircraft	2	[-]
N_{rr}	Production rate of test aircraft	0.33	[aircraft/month]
N_{rm}	Production rate of aircraft produced to production standard	11/12	[aircraft/month]
F_{pro_r}	Profit percentage reserved for RDTE	0.10	[-]
F_{fin_r}	Interest rate for RDTE	0.05	[-]
F_{fin_m}	Interest rate for acquisition and manufacturing	0.05	[-]
F_{pro_m}	Profit percentage reserved for manufacturing activities	0.10	[-]

Research & Development

The R&D costs are composed of seven different costs segments. These are the airframe engineering and design costs, development of the supporting and testing facilities, the building of the facilities, the flight test airplane development and operation costs and the costs to finance the program. The last part is the costs due to the profit of the organisations involved. Since it is likely that a government will be the main funder of the project and profit is not an aim of the Ceres mission it was assumed to be a relatively low value of 5 % of the total R&D costs. Another assumption is that the profit of companies involved during the R&D phase is 10 %, which is the recommended value stated in volume 8 of Roskam[74]. The total costs are found by adding all the values. The engine costs for the EJ200 used is \$5M. The specified budget for R&D is set at \$4.48B. From the Roskam model, a value of \$1.92B was obtained, around 55 % below the maximum budget. Possible reasons for this low value are that the labour cost or profit margin are underestimated. When additional factors were added for increasing these costs, a high estimated value of \$3.32B was found. The model provided by W. Smith gave an estimate of \$3.3B, just above the high estimate value. In Table 14.2 the division of the R&D cost over the different segments is shown.

14.1.2. Manufacturing & Acquisition

According to Roskam, the *acquisition cost* (C_{ACQ}) is composed of the manufacturing cost and profit made by the manufacturer (C_{PRO}), see Equation (14.1).

$$C_{ACQ} = C_{MAN} + C_{PRO} \quad (14.1)$$

The total manufacturing costs consist of the following components: the *airframe engineering and design cost* (C_{aed_m}), *airplane program production cost* (C_{apc_m}), *production flight test operations cost* (C_{fto_m}) and the cost to finance the manufacturing (C_{fin_m}). Initially, it was assumed that 180 aircraft were going to be manufactured, 163 for operations and 17 for spares. Moreover, a 10 % profit margin was taken for C_{PRO} as

Table 14.2: R&D Costs of the Ceres Aircraft

Parameter	Ceres Aircraft R&D Costs [\$M]	Percentage of Total [%]
Airframe Engineering & Design	136.97	7.13
Development Support & Testing	27.84	1.45
Flight Test Airplane	1067.47	55.53
Flight Test Operations	17.09	0.89
Test & Simulations Facilities	384.42	20
Profit	192.21	10
Financing	96.09	5
Total	1922.09	100

suggested by Roskam in volume 8. [74]. Lastly, an interest rate of 5 % was set to finance the manufacturing of the aircraft design.

The cost of each individual term for the Ceres aircraft concepts is summarised in Table 14.3. This resulted in a manufacturing cost of \$107.45M. For manufacturing, a limit of \$112.9M per aircraft was given as a requirement. It was concluded that the requirement for the M&A costs is just met and only a small increase would deem it unacceptable. Roskam's method takes into account that the R&D have to be earned back during manufacturing and splits these additional costs over the 180 aircraft, resulting in a unit cost of \$118.13M. Since the Ceres system does not aim to make profit, this higher value for the unit cost was not considered as part of the manufacturing cost. The M&A cost breakdown is shown in Table 14.3. Here the costs are indicated per aircraft. Resulting in a total acquisition cost of \$19.34B for the 180 aircraft.

The model from W. Smith estimated a unit cost of \$113.01M. This takes into account aircraft production, airframe certification and engine modification R&D. Resulting in \$20.34B total cost for M&A.

Table 14.3: Breakdown of the Manufacturing and Acquisition Costs for the Ceres Aircraft Per Unit

Parameter	Ceres Aircraft M&A Cost [\$M]	Percentage of Total [%]
Airframe Engineering & Design	26.95	25.08
Airplane Production Cost	61.85	57.56
Flight Test Operations	0	0
Financing	8.88	8.23
Manufacturing Profit Margin	9.77	9.09
Unit Manufacturing Cost	107.45	100
Fleet Manufacturing Cost	19341	-

As remarked in Table 14.3, the cost for the production flight test operation is zero. As usual, these costs were neglected during the first preliminary cost estimation according to volume 8 of Roskam [74]. As mentioned before, F_{diff} was set to 1.5.

14.1.3. Maintenance & Operations

The M&O costs can be split up in two parts: direct and indirect operational costs. For simplicity, the indirect operational costs (IOC) were assumed to be 0.6 times the direct operational costs (DOC), [74]. Examples of IOC are depreciation of the ground equipment and facilities or administrative expenses. These costs are harder to predict individually, so a fixed percentage of DOC was chosen for it. The breakdown of the DOC and a value for the total operating costs can be found in Table 14.4. Flight operating costs mostly depend on the crew costs, fuel and oil costs and insurance costs. Maintenance includes the costs of the maintenance crew equipment and materials needed. The depreciation takes into account the costs due to the depreciation of the individual aircraft components and systems used during operations. The costs of fees and taxes include, for example, registering at airports in different countries. Finally, the financing of manufacturing was taken into account. A detailed breakdown of the operation costs for the Ceres aircraft is found in Table 14.4. The total M&O costs are given for an active fleet of 180 aircraft.

A total M&O cost of \$86.61B was obtained. This resulted in \$69.62M per aircraft per year. The requirement was given as a maximum of \$44.8M direct operating costs (DOC). As can be seen from Table 14.4, this requirement is just met for the Ceres aircraft design. Initially, an estimated DOC of \$43.52M per aircraft per year was obtained, which is 2.86 % below the requirement. Furthermore, for the DOC there is not a part that

is significantly larger than the other aspects. Since the IOC is harder to predict it was estimated at 60 %. From Roskam's method this is a usual value based on the aircraft MTOW. However, since Ceres is no ordinary mission it could be the case that it is either under- or overestimated. This can only be determined more accurately if a detailed look is taken into this topic. This was considered outside the scope of the DSE. Furthermore, it was noticed that the flight, maintenance and depreciation of components costs are all fairly close together and there is not an identifiable outlier. The fuel is the biggest influencing factor for the flight costs, with a chosen fuel cost of \$3 per gallon. Apart from the economical regression in 2008 and the after-effects, the price of JA-1 fuel has not been above the above mentioned level. Furthermore, it was assumed that the costs of the sulphur are included in the flight segment. The total M&O costs were based on the acquisition scheme of the aircraft as discussed in Section 8.1.

The model from W. Smith resulted in a total operation cost of \$53.12B resulting in an average of \$44.34M per aircraft per year. This was obtained from a detailed estimate including maintenance, fuel, crew, cargo handling, fees and taxes, insurances and payload costs etc. Since both models only differ by 1.04 %, it was assumed that the final value for DOC is relatively accurate. To conclude this part of the cost a short overview is given for the total estimations in the next section.

Table 14.4: Operating Costs Roskam Method for the Ceres Aircraft

Parameter	Ceres Aircraft Operations Cost	
	[\$M]	Percentage of total [%]
Direct Operating	43.52	62.50
<i>Flight</i>	13.35	30.68
<i>Maintenance</i>	12.52	28.77
<i>Depreciation of Components</i>	14.22	32.67
<i>Fees and Taxes</i>	0.38	0.87
<i>Financing</i>	3.05	7.00
Indirect Operating	26.10	37.50
Annual per aircraft	69.62	100
Total Operation (15 years)	86607.28	-

14.1.4. Total Program Costs

The costs acquired from the previous sections result in a total lifetime cost of \$107.87B. This value, the distribution over the three different segments, and the contingency value at this stage of the design are shown in Table 14.5. To conclude, the R&D costs are below the given requirement, while the M&A and M&O are above. Since cost estimation always goes hand in hand with relatively large uncertainties, no absolute conclusion should be drawn. However, it was concluded that a mission such as the Ceres system would have extensive operational costs, mostly due to the fleet size and amount of flight hours made each year. One point that was taken into account is that the program can be performed in such a manner that the initial costs are kept to a minimum in the starting phase. The total costs will increase gradually over the 15 years as the fleet size increases.

Table 14.5: Breakdown of the Total Costs for the Ceres Aircraft

Parameter	Ceres Aircraft Cost		Contingency [%]
	[\$B]	Percentage of Total [%]	
Research & Development	1.92	1.78	15
Manufacturing & Acquisition	19.34	17.93	5
Maintenance & Operations	86.61	80.29	15
Total	107.87	100	-

14.1.5. Verification & Validation

Since Roskam's method is used widely in the aerospace industry, it was deemed a viable method to approach the costs. The cost output for all three components is in the expected order of magnitude. By using examples from the book, the output of the cost model was compared to those values to verify if the model works correctly. By further comparing the individual components of the cost, it was concluded that no unexpected outliers are present. The composition of the costs was finally also compared to the values from the model made by W. Smith [85]. Especially for the operations, the two models approached the same value, which indicates that the estimate is accurate.

14.2. Environmental Impact Assessment

The EI assessment was divided into two categories. The first is the quantification of the emissions and the second is the noise.

14.2.1. Emissions Quantification

Many units to measure emissions are used throughout literature. For reproducibility as well as completeness, it was chosen to take the units used by the Intergovernmental Panel on Climate Change (IPCC) which is considered to be the governing body on environmental impact. The units chosen here are Radiative Forcing (RF) and Global Warming Potential (GWP). To these, the fuel burned was added so that the uncertainties due to the individual of GWP and RF for specific chemicals is limited and can be inputs for other methods.

Stratospheric Injection: The cost of stratospheric aerosol injection is not only financial but also environmental. To make the delivery of sulphur dioxide in the stratosphere possible, it is necessary to first transport the sulphur to this altitude, followed by the combustion of the substance to transform it into SO₂ in order to fulfil the mission. The environmental impact was divided into two different effects. On the one hand, part of the impact result from the dispersion of aerosols. These will be called primary environmental impacts, as they form part of the desired outcome of the mission. They fall beyond the scope of the research for this Design Synthesis Exercise (DSE), which will focus on the aircraft design as well as the system integration [40].

On the other hand, the quantification of the secondary environmental impact of the system is one of the primary objectives of the DSE. This consists of building a model for the expected environmental cost of such a system i.e. continuously operating aircraft at high altitudes. This model takes into account the impact of not only running a fleet of aircraft but also the construction of required infrastructure in relation to it, the impact of the ground operations enabling the deployment of the aircraft, the manufacturing of the fleet of aircraft and the end-of-life impact of the system.

Global Warming Potential and Radiative Forcing Global Warming Potential (GWP) is a coefficient applicable to all greenhouse gases which enables the comparison of the effect of specific greenhouse gas in relation to the impact of carbon dioxide. By multiplying the amount of greenhouse gases by this coefficient, a carbon dioxide equivalent (CO₂e) was obtained. All the emissions in CO₂ equivalent were then added. Radiative forcing relates the emissions of greenhouse gases to their impact regarding solar flux, its reflection or increase in intensity which is directly related to the surface temperature as well as global temperature. From literature, the following GWP and RF values were found and used for quantification of the equivalent CO₂ emissions of one flight, see Table 14.6.

Time-Frame for Impact Qualification Based on the work of J. Borken et al. [10], it was clear that the various parameters - GWP, GTP, radiative forcing - must be fixed in a time context. This was backed up in the paper by a comparison between air transport versus rail or road transport. As such, since the aircraft was predicted to operate as a short term measure, its effect after 5 years were considered primarily. As a result, the flight profile was optimised for a short term environmental impact minimisation. For the environmental impact quantification of the reaction products, GWP values for 20 years and 100 years were used as these are the most common ones (and found) from literature.[3, 15, 81, 98]

Table 14.6: GWP and RF Values for Each Pollutant in the Chemical Equations

Chemical	GWP20	GWP100	RF [W/m ² /ppm]
CO ₂ [28, 98]	1	1	1.985
CO[16]	14	4.4	0.024
H ₂ O[81]	-0.001	.0005	0.024
N ₂ O[28, 98]	268	298	0.193

Altitude Sensitivity The altitude of operation of the fleet of aircraft determines that the combustion must occur at an optimal air to fuel ratio (AFR) in order to minimise the impact of the emissions based on the

GWP, GTP and radiative forcing. However, since the fuel-to-air ratio was determined from SUAVE and left untouched, the effect of pre-fixing the AFR was not considered. As a result, during the flight, the aircraft mostly used rich-burn of the fuel for maximum power. A side effect of combusting rich is the higher emission of carbon monoxide. However, less NO_x is produced. As these reaction products are not shown in the chemical reactions² and literature did not provide sufficient data to quantify the NO_x and CO emissions, these fall beyond the scope of the DSE. However, accurate quantification of these resulting products is crucial to estimate the emissions of the Ceres operation in more detail.

Infrastructure Environmental Cost In order to minimise cost, it was decided to operate from existing airports. This in turn reduces the environmental footprint of the system compared to building airports [13]. Nonetheless, the strain to be expected from the system on an airport with multiple flights a day is comparable to regional airliners (here a Boeing 737). The recapitulation of the environmental impact of creating a new airport or operating from an existing airport is shown in Table 14.7. It was taken that the GGE produces 9 kg of equivalent CO_2 and that each kWh of energy required produces 0.28 kg of equivalent CO_2 . This shows that choosing to operate from an existing airport cuts the environmental footprint in half which is not negligible. As a result, the system will only be operated from existing airports. Further analysis of the environmental impact of operating an airport is beyond the scope of the DSE and this report and thus is not discussed.

Table 14.7: Computation of CO_2 Equivalent for the Infrastructure of the System [13]

Parameters per AC life	With new airport		Without new airport	
	Energy [GJ]	GHG [ton]	Energy [GJ]	GHG [ton]
Airport Construction	5800	450	-	-
Runway Construction	80000	7400	-	-
Tarmac Construction	210000	19000	-	-
Operation Runway Lighting	13000	2800	13000	2800
Operation Deicing production	21000	1500	21000	1500
Operation GSE	170000	13000	170000	13000
Maintenance Airport	290	23	290	23
Maintenance Runway	6400	910	6400	910
Maintenance Tarmac	17000	2400	17000	2400
Parking	71000	6800	71000	6800
Insurance Non operator	12000	1000	12000	1000
Insurance Liability	1400	110	1400	110
Total	170209200	55393	312090	28543
CO_2 equivalent [kg]	4.82E+07	4.99E+08	88410.76	2.57E+08
Total in CO_2 Eq. [kg]	5.47E+08		2.57E+08	

Manufacturing Environmental Cost The method used was based on the work presented in [5]. In this article, the authors evaluate the environmental impact of the manufacturing of an Airbus A320 aircraft. A similar study was conducted on an A330 which enables to contrast the points made above [21]. From this work, it was observed that the use of Carbon Fibre Reinforced Polymers greatly increases the Environmental Impact (EI) of the manufacturing phase as well as the production phase. This is confirmed in the paper studying the EI of composites [101]. From the latter study, it is shown that most of the footprint is from the carbon fibre production which requires 155 kWh/kg. This is, however, partly outweighed by the gains made regarding weight savings. This can be up to 25% [54] and leads to great reductions in fuel consumption which is responsible for about 99.5% of all CO_2 emissions during the life of an aircraft [51]. For this reason, during the design of the aircraft, it was of greatest priority to minimise fuel consumption.

Nonetheless, the EI of an aircraft of similar weight to the A320 has a quantifiable EI as shown in literature [5, 54]. The impact of manufacturing an aircraft suited for a lifetime of 20 years, to fly approximately

²<https://suw.biblos.pk.edu.pl/downloadResource&mId=152405>

2000 km 5 times per day, yields a CO₂ equivalent of roughly 356 t of carbon dioxide equivalent using [21] which was scaled from a structural fuselage weight of 4547 kg. As this emission was determined to be 22% of the total manufacturing CO₂e-emission[5] The total equivalent carbon dioxide emitted was determined to be roughly 1618 t. Using only the numbers of Lopes [5] which used the ReCiPe method and was scaled from a MTOW of 229.8 t, yields a total equivalent carbon dioxide of 410 t as per the Life Cycle Assessment (LCA). This needs to be put in perspective of the rest of the emissions where this is near to negligible.

A mitigation to reduce such an estimate is to change the method of production as this was taken from the model of Airbus where various components are manufactured across Europe and finally shipped to the final assembly line in Toulouse or Hamburg. The production should thus occur at the same location in order to limit the EI. However, this is greatly outweighed by the operational emissions and as such it is of lesser priority, especially once the landmass used and other factors are taken into account.

Operational EI Based on the work of Achternbosch [54] and the LCA done by Lopes 2010 [21], it was observed that the emissions due to the operation of a transport aircraft represent 99.9 % of the lifetime emissions of the aircraft. As such, the fuel burned was quantified to determine the operational environmental impact. Additionally, as mentioned before, fuel burnt was also considered and added such that uncertainties of RF and GWP values were taken into account. Thus, for the fuel burn, the chemical equations of kerosene for varying fuel-to-air ratio (FAR) was used. However the equations shown were limited to $0.50 < FAR < 1.55$. As such, the quantification of the fuel burnt only covers 84% of the burnt fuel during flight. As a result, the uncertainty of the fuel burnt due to incomplete coverage was taken to be 25%. Table 14.8 shows the fuel burnt per aircraft per flight.

For the computation of the total emissions, data of the mass fuel flow, height, density, and velocity were acquired at each given time step using the SUAVE module. As such, the fuel-to-air ratio was determined using Equation (14.2), where the denominator is the mass air flow at a given time step.

$$FAR = \frac{\dot{m}_{fuel}}{\rho AV} \quad (14.2)$$

From the known chemical equations³, the reaction products were computed for each given time steps for a range of FAR values. As the time steps were not unit, the resulting GWP values were multiplied by the time difference between the time steps to acquire the resulting CO₂e of the reaction products between the time steps. Finally, the CO₂e values of the individual products were summed for the total flight time to get the total CO₂e produced per flight. Alternatively, the emissions were computed using Table 2.1 of [20], where a lower and upper bound of the total CO₂e emission was found by using the given ranges of emissions in the table. The results of the two approaches are summarised in Table 14.8.

Table 14.8: Summary of the Total Emission and Environmental Impact due to Fuel Burnt During Operations

		Method using Lopes [20]	Method using Mzad ⁴
GWP20	CO ₂ e upper-bound [Mt]	1001	-
	CO ₂ e lower-bound [Mt]	827	232
GWP100	CO ₂ e upper-bound [Mt]	1065	-
	CO ₂ e lower-bound [Mt]	872	233
RF [W/m ²]		$3.69 \cdot 10^{-8}$	$6.07 \cdot 10^{-13}$

From Table 14.8 it was concluded that the total operational CO₂e emissions due to fuel burnt is between 0.66 and 0.88 Tg in 15 years with a total of 250 operational days per year and four flights a day per aircraft. Additionally, the radiative forcing due to Ceres range from $5.36 \cdot 10^{-13}$ to $2.94 \cdot 10^{-8}$ W/m². For these values, it was assumed that the operations starts with 12 aircraft with an increase of 8 aircraft a year. After 7 years, the fleet increment would be doubled. As mentioned in Chapter 8.

³<https://suw.biblos.pk.edu.pl/downloadResource&mId=152405>

End-of-Life Scenario and Impact The results of the end-of-life scenario and impact are shown in Table 14.9. The computations use the percentages for the disposal scenarios shown in Table 4.8 of [20] whose numbers are based on the PAMELA project. The breakdown does not add up to the full MZFW of the aircraft as the mass of secondary structural items were still unknown. Moreover, for simplicity, it was assumed that the aircraft is made of only aluminium and composite material. As a result, the total waste of aircraft is approximately 70% of the OEW. From separating the reusable material and incineration or dumping of the non-reusable material a CO_2e of 9.2 t is emitted to the environment. This waste percentage will change throughout the design phase as the design mature and different type of materials were taken into account. However, this is very conservative as the amount of waste is ever decreasing as part of PAMELA[1] and recycling technology was considered to be carbon neutral due to the value created.

Table 14.9: Breakdown of the Waste and Recycling Percentage of Large Sections of the Aircraft

Section	Recycled [kg]	Waste [kg]	% of Total Waste
Aircraft	16869	7159	70.20
<i>Fuselage</i>	4319	762	62.4
<i>Wing</i>	5330	4467	10.6
<i>Vertical Tail</i>	793	140	4.5
<i>Horizontal Tail</i>	1814	320	2.0
<i>Main Gear</i>	667	167	2.3
<i>Nose Gear</i>	148	37	.5
<i>Engine</i>	3798	1266	17.7

Comparison of impact From this it is clear that the impact of the Ceres mission forms a non negligible part of the overall footprint of human activities. Based on the values of Jet-A fuel consumption worldwide⁵ and the worldwide fuel consumption⁶, the impact of the fleet of aircraft would be about 0.43% of worldwide Jet-A consumption and 0.029% of worldwide oil consumption.

14.2.2. Noise Assessment

Noise regulations are becoming increasingly strict. Recently, the ICAO standard decreased to a maximum noise level of 265 EPNdB (Effective Perceived Noise Level) based on Ceres' current MTOW⁷. Noise levels are measured at three points during the flight, namely at 2000 m approach to landing, at sideline during take-off, and at flyover cutback 6500 m after take-off. Contributions of each of the aircraft's components to the total noise level differ at each of these points. During approach, the airframe dominates the total noise level generating almost 52% of the total noise. After take-off at sideline and flyover cutback, fan and jet noise dominate the total noise level [47].

Several computational tools exist to predict aircraft noise (e.g. PANAM by DLR and ANOPP2 by NASA), most of them are too detailed for conceptual design. These tools separate the contributions of the airframe and the engines. While scaling laws exist for engine noise, little literature on airframe noise scaling laws is available, therefore, it can only be discussed in a qualitative way.

Research indicates that several components of the airframe specifically contribute to the generated noise. In order of magnitude, the biggest contributors to the airframe noise are the landing gear (1), leading edge high lift devices (2), and flaps or rudder side edges (3) [8], together with other disturbances in the smooth airframe. Those of Ceres aircraft will generate relatively less noise than other airframes as it has no high lift devices and small control surfaces. Additionally, the frame has no windows other than the cockpit. The noise is significantly less for the landing gear because it is mounted on the fuselage compared to it being mounted on the wing. However, during detailed design of the landing gear, noise can be further decreased by preventing flow separation from components and lowering the complexity of the landing gear.

The current engine, the EJ200, produces more noise than other engines. This is, among other effects, due to the unfavourable configuration of the engine to noise shielding as the engines are mounted below the

⁵<https://www.statista.com/statistics/655057/fuel-consumption-of-airlines-worldwide/>

⁶<http://www.eia.gov/totalenergy/data/annual/archive/038409.pdf>

⁷<https://www.icao.int/environmental-protection/pages/reduction-of-noise-at-source.aspx>

wing. Furthermore, the engine has a low bypass ratio as well as an above average specific fuel consumption. Both these characteristics are unfavourable to noise generation.

It is recommended to further assess the noise of the engine by using noise scaling laws. These laws estimate the sound pressure produced by the engine, Equation (14.3) presents the scaling law as proposed by M. Kandula [48]. G_1 and G_2 refer to functions of the jet Mach number and K_1 is a proportionality constant. The pressure can be converted to Sound Pressure Level using Equation (14.4) and subsequently, the noise level on the ground can be determined and converted to EPNL. This data will be relevant to take-off as jet noise dominates in this condition. Moreover, take-off is the most critical condition for noise generation [22].

$$\frac{\bar{p}^2(\theta, f)}{(\rho_j u_j^2)^2} = K_1 \left(\frac{\rho_\infty}{\rho_j} \right) \left(\frac{u_j}{c_j} \right)^{3.5} \left(\frac{c_j}{c_\infty} \right)^{3.5} \left(\frac{d_j}{r} \right)^2 G_1(M_c, \theta) G_2\left(\frac{f}{f_p}, M_c, \theta\right) \quad (14.3)$$

$$SPL = 10 \log \left(\frac{p_e^2}{p_{e0}^2} \right), \quad p_{e0}^2 = 2 \cdot 10^{-5} \quad (14.4)$$

Resource Allocation

In this chapter, resource allocation is elaborated upon. This includes the contingency management of both the mass and the cost. After this, the budget of mass and costs are explained in more detail. Finally, all the requirements are stated, and whether or not they are complied to.

The contingency management is limited to the mass of the aircraft and the costs of Project Ceres. Other TPM parameters could have been used for contingency management. However, the chosen parameters encapture both the feasibility and the cost of the project, which is deemed sufficient at this stage of design. For future development, several other parameters can be used for TPM as well, as now a more accurate baseline for all parameters is established.

15.1. Contingency Management

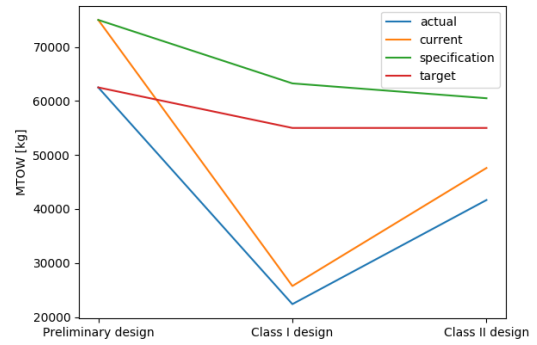
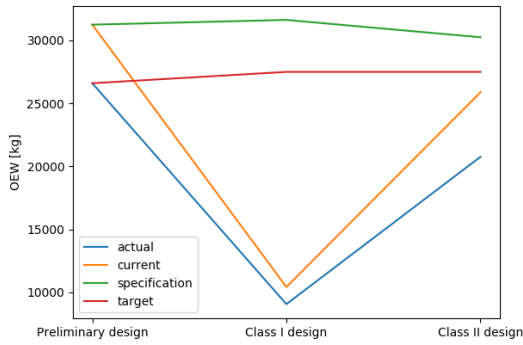
In the Baseline Report [32], the contingency values for each phase of the design were established. In this section, the results of the contingency management and the Technical Performance Measurement (TPM) procedures are elaborated upon.

Mass Contingency Previous aircraft designs show that from the uncertainties in the design, the mass will always grow in an undesired direction [38]. To prevent the design from exceeding the goal MTOW, appropriate contingencies were used. For the OEW, the contingency values were 20 %, 15 % and 10 % for the conceptual design, Class I design and detailed design, respectively. For the payload mass, the contingency values were 15 %, 10 % and 5 %, respectively. The contingency values for the conceptual design and the Class I design were equal due to the fact that no payload optimisation was carried out yet. The margin for the payload mass at the end is relatively small, to allow for a slight increase in required SO₂ injection. If it is necessary to increase the amount of SO₂ injected per year after conducting further research, the fleet size should be increased instead of increasing the payload per aircraft.

During different design phases, the design changed significantly. This is partly due to the fact that initial phases rely heavily on statistics. As project Ceres has a unique characteristics than other aircraft, statistics showed flaws. Another flaw was that there were only three measurement points, consisting of the conceptual design, the Class I estimate, and the detailed design. This caused the TPM procedures to be limited.

Project Ceres used TPM to make sure that the MTOW and the OEW do not exceed their set maxima. During the design process, these maxima changed according to what was thought to be a feasible end goal at the time. Initially, the target value was set at 62.5 t, with an OEW ratio of 40 %. After the preliminary sizing, it was decided that the initial goal was too conservative and that a lighter aircraft was possible. Additionally, the OEW ratio was set at a more realistic goal, resulting in a target value of 55 t for MTOW, and a 50 % OEW ratio. During the Class I design, it was decided to not decrease the maxima, as there were already signs of an increase in MTOW from the sizing of the wings and the engine weight. Following TPM procedures, the maximum OEW and MTOW including contingency, are called specification values. At each measurement point, the actual and current value are calculated. The actual value is the actual value of the MTOW and OEW at that time. The current value is equal to the actual value plus contingency. These values are shown in Figure 15.1. It can be seen that the current values are still below the specifications values, which shows that the design is still within its bounds. Furthermore, it can be seen that the target value of OEW was slightly raised during Class I design, as more realistic OEW over MTOW ratios were determined.

Contingency of the Cost The contingency of the cost was constructed in the same way as the weights. This means that for each design step, the values obtained for the research and development costs, the manufacturing and acquisition costs and the maintenance and operations costs were compared to the specification

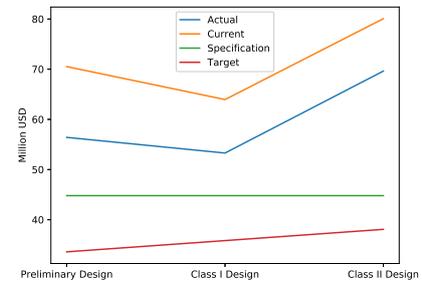
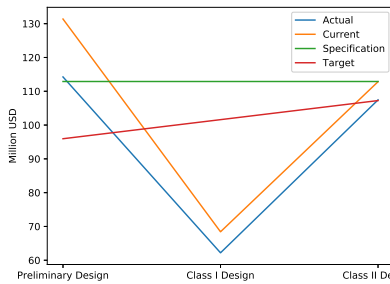
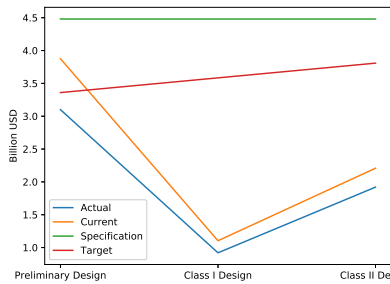


(a) TPM Values of the OEW at Different Design Points.

(b) TPM Values of the MTOW at Different Design Points.

Figure 15.1: Mass Contingency Management.

and target values. Here, the specification values were set to the requirements as the objective is to not surpass this value. From there, it is possible to compute the target value using the respective contingency margins for the R&D, M&A and M&O. These are 25%, 20% and 15% for the R&D and M&O and 15%, 10%, 5% for M&A. From Figure 15.2, it is possible to observe that all requirements are met. This is due to the fact that the operating cost requirement only covers direct operating costs which fall at a value of 38.52M€ as stated in Section 14.1.3.



(a) TPM Values of the Research and Development Costs

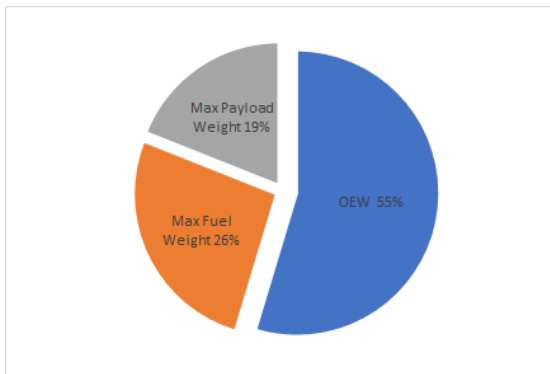
(b) TPM Values of the Manufacturing and Acquisition Costs

(c) TPM Values of the Maintenance and Operation Costs

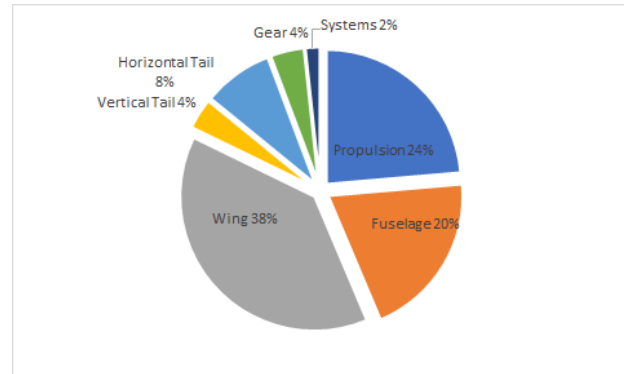
Figure 15.2: Cost Contingency Management.

15.2. Mass and Balance Budget and Breakdown

This section presents the mass breakdown for the aircraft. First, the proportions of the various aircraft items are presented in a pie chart, as shown below. This is then complemented by a table which summarises in more detail the weight and location of every component.



(a) Breakdown of the Maximum Take-off Weight.



(b) Breakdown of the Operational Empty Weight.

Figure 15.3: Mass Breakdowns.

Table 15.1: Mass and Balance Recapitulative Table

Parameter	Value [kg]	x cg location from nose [m]
Fuel	13468	28.96
Payload	9700	18
OEW	27928	28.95
<i>Propulsion</i>	<i>6000</i>	<i>26.34</i>
<i>Fuselage</i>	<i>5079</i>	<i>20.59</i>
<i>Wing</i>	<i>9793</i>	<i>28.96</i>
<i>Vertical Tail</i>	<i>933</i>	<i>39.52</i>
<i>Horizontal Tail</i>	<i>2133</i>	<i>39.52</i>
<i>Gear</i>	<i>1018</i>	<i>25.51</i>
<i>Systems</i>	<i>433</i>	<i>18.0</i>
MTOW	51096	26.9

Table 15.2: Recapitulative Table of the Costs

Parameter	Total Cost [\$B]	Total Cost [%]	Contingency [%]
R & D	1.92	1.78	15
M & A	19.34	17.93	5
M & O	86.61	80.29	15
Total	107.87	100	-

It must be noted that although the payload and fuel weight are taken to be 9.7 t and 13.5 t, respectively, these constitute maximum values. The aircraft is optimised for values which are beyond the required values to fulfil the mission. This means that the aircraft is not required to fly with these values. Furthermore, there is a 10 % safety margin on OEW, which is why the weights of the components do not add up to the total OEW. The maximum landing weight is 46 t and zero fuel weight equals 38 t.

15.3. Cost Budget and Breakdown

The cost budget and breakdown are detailed in Section 14.1. The section explains the methods used to determine the various costs as well as a more detailed breakdown of each cost segment. Table 15.2 summarises the overview of the costs. The costs are dominated by the maintenance and operations costs as is expected of an aircraft which goes through multiple cycles daily.

15.4. Power Budget and Breakdown

An electrical load analysis is performed in Table 15.3 and Table 15.4 for the take-off and cruise conditions. These numbers are derived from the electrical system sizing in Roskam [74]. The sulphur heating system requires large amounts of power, and thus six generators are deemed feasible for this design. If the generators output 40 kW, the load factor on these is 85% during cruise, which is considered standard in the aviation industry [80].

Table 15.3: Electrical System Power Budget Breakdown in the Take-off Condition

	Input [kVA]	Output [kVA]
#1-6 IDG	(40-65) · 6	-
Avionics	-	8
Ext. Lighting	-	0.8
Int. Lighting	-	1.2
ECS	-	0.32
Windshield	-	6.1
Hydraulics	-	10
Fuel	-	8.5
DC Power	-	7.9
sulphur Heater	-	0
sulphur Feed	-	0
Total	240-390	42.82

Table 15.4: Electrical System Power Budget Breakdown in the Cruise Condition

	Input [kVA]	Output [kVA]
#1-6 IDG	(40-65) · 6	
Avionics	-	8
Ext. Lighting	-	0.8
Int. Lighting	-	1.2
ECS	-	0.32
Windshield	-	6.1
Hydraulics	-	2
Fuel	-	8.5
DC Power	-	6.0
sulphur Heater	-	172.7
sulphur Feed	-	1
Total	240-390	205.62

15.5. Compliance to requirements

In the Baseline Report [32], all the necessary requirements were established. During the design process, it turned out that several requirements were not suitable for the current level of design. In this section, all the relevant requirements are stated, whether or not they have been met or if they still need to be verified, with a reference to the relevant section. After this, an explanation is given for the requirements that haven't been met. All the system requirements have been met. There are some subsystem requirements that have not been met, this is because these requirements were based on the design that was presented in the Midterm Report [33]. However, the design has changed severely after this point. For the subsystem requirements, it is also shown if it is a key requirement. Requirements with no identifier are non-driving requirements.

Table 15.5: System Requirements

Requirement	Statement	Complied	Reference
REQ-SYS-01	The SAI system shall be deployed in the form of a fleet.	✓	Section 8.1
REQ-SYS-02	The SAI system shall be able to deliver the payload at a minimum of 20 km.	✓	Section 8.1
REQ-SYS-03	The aircraft shall deploy 0.2 Tg of SO ₂ in the first year, based on 250 operational days.	✓	Section 8.1
REQ-SYS-04	The aircraft shall deploy 3 Tg of SO ₂ in Year 15.	✓	Section 8.1
REQ-SYS-05	The aircraft shall operate from existing airports using runways of 2500 m or less.	✓	Section 8.1
REQ-SYS-06	The aircraft shall be to operate in crosswinds of at least 20 kts.	✓	Section 13.6
REQ-SYS-07	The aircraft shall be able to operate in all weather, incl. CAT II landings.	✓	Section 13.9
REQ-SYS-08	The aircraft shall have diversion capabilities.	✓	Section 13.5
REQ-SYS-09	The aircraft fleet should include spares for aircraft maintenance.	✓	Section 8.1
REQ-SYS-10	The development costs shall be less than €4B if existing engines are used.	✓	Section 14.1.1
REQ-SYS-11	The development cost shall be less than €7B if new engines are to be developed.	N.A.	
REQ-SYS-12	The manufacturing costs of the aircraft shall be less than €100M.	✓	Section 14.1.2
REQ-SYS-13	Annual direct operating cost per aircraft shall be less than €40M.	✓	Section 14.1.3

Table 15.6: Aerodynamics and Flight Performance Requirements

Requirement	Statement	Type	Complied	Reference
REQ-AC-ANFP-01	The aircraft shall be optimised for REQ-OP-FP mission profile.		✓	Section 13.5
REQ-AC-ANFP-07	The aircraft shall be able to take off in less than 2500 m.	key	✓	Section 13.5
REQ-AC-ANFP-10	The steady gradient of the aircraft shall not be less than 3.2 % with all engines operating.	key	✓	Section 13.5
REQ-AC-ANFP-16	With 1 engine failure, in case of a 4-engined aircraft or more with landing gears retracted., the steady gradient shall be larger than 3.0 %.		To be verified	
REQ-AC-ANFP-19	With enroute configuration, in case of a 4-engined or more aircraft with landing gears retracted., the steady gradient shall be larger than 1.7 %.		To be verified	
REQ-AC-ANFP-20	The aircraft shall have a Go-around climb rate of at least 3.2 %.		To be verified	
REQ-AC-ANFP-21	The aircraft shall cruise with speed stability at 20 km altitude.		✓	[33]
REQ-AC-ANFP-22	The aircraft shall have a cruise speed below the Mach divergence velocity at 20 km.	key	✓	Section 13.5
REQ-AC-ANFP-24	The aircraft shall have a <0.72 cruise speed for the release of payload.	key	✓	Section 8.1
REQ-AC-ANFP-26	The aircraft shall have a <0.79 maximum cruise Mach for the release of payload.	key	✓	Section 8.1
REQ-AC-ANFP-27	The aircraft shall have a <0.82 Mach divergence.	key	✓	Section 13.2

Table 15.7: Payload Requirements

Requirement	Statement		Complied	Reference
REQ-SAI-POPS-01	The injection system, referred hereafter as payload, shall have a mass lower than 550 kg.	key	✓	Section 13.7
REQ-SAI-POPS-02	The payload shall not need an additional power input.		✓	Section 13.7
REQ-SAI-POPS-03	The Sulphur storage solution shall have a mass lower than 250 kg.	key	✓	Section 13.7
REQ-SAI-POPS-05	The amount of sulphur stored shall be equal to or greater than 10 t.	key	✗9.7 t	Section 13.7
REQ-SAI-POPS-07	The sulphur storage solution shall be capable of venting.		✓	Section 13.7
REQ-SAI-POPS-09	The combustion process shall be controlled during operation.	key	✓	Section 13.7
REQ-SAI-POPS-10	The combustion process shall produce more than 1.5 kg/s of SO ₂ .		✓	Section 13.7

Table 15.8: Flight Profile Requirements

Requirement	Statement	Type	Complied	Reference
REQ-OP-FP-01	The turnaround time shall be less than 2 h.	key	✓	Section 8.1
REQ-OP-FP-03	The on ramp time shall account for a crew change of 0.16 h.		✓	Section 8.1
REQ-OP-FP-07	The taxi and takeoff time shall account for the impact of meteorological conditions.		✓	Section 8.1
REQ-OP-FP-08	The taxi and takeoff time shall account for runway conditions.		✓	Section 8.1
REQ-OP-FP-11	The fuel burn for the entire cycle shall not exceed 2260 kg.	key	✗13 t	Section 13.5

Table 15.9: Structural Requirements

Requirement	Statement	Type	Complied	Reference
REQ-AC-STRUC-01	The materials used in the structure shall be existing.	key	✓	Table 13.25
REQ-AC-STRUC-02	The materials used in the structure shall have known fatigue properties.		✓	Table 13.25
REQ-AC-STRUC-03	The materials used in the structure shall be aluminium alloys and CFRP.		✓	Table 13.25
REQ-AC-STRUC-04	The aircraft structure shall be designed for 15000 cycles.	key	To be verified	
REQ-AC-STRUC-05	The aircraft structure shall be designed for 75 000 h.		To be verified	
REQ-AC-STRUC-06	The aircraft structure shall be designed for a c.g. shift in accordance to REQ-AC-CTRL-04.	key	✓	Section 13.8
REQ-AC-STRUC-07	The aircraft structure shall be designed to withstand the flight loads.	key	✓	Section 13.8
REQ-AC-STRUC-08	The aircraft structure shall be designed for a total lifespan of 15 years.		To be verified	
REQ-AC-STRUC-09	The aircraft structure shall be designed with a safety factor of 1.5.	key	✓	Section 13.8
REQ-AC-STRUC-10	The aircraft structure shall be designed to support limit loads without detrimental permanent deformation.	key	✓	Section 13.8
REQ-AC-STRUC-12	The aircraft structure shall be designed for meeting all load factors within the manoeuvring envelope.	key	✓	Section 13.8
REQ-AC-STRUC-23	The aircraft fuel tanks shall be designed to be isolated from personnel compartments.		✓	Section 13.9.5
REQ-AC-STRUC-32	The aircraft structure shall be designed such as to allow manufacturing using well documented methods.		✓	Section 13.8
REQ-AC-STRUC-33	The aircraft structure shall be designed taking into account manufacturing implications.		✓	Section 13.8

Table 15.10: Propulsion Requirements

Requirement	Statement	Type	Complied	Reference
REQ-AC-PROP-01	The propulsion system shall provide enough thrust to maintain a velocity of V_{cruise} at 20 km altitude.	key	✓	Section 13.3
REQ-AC-PROP-02	The propulsion system shall provide enough thrust in order to achieve a velocity of V_{lof} within 2500 m, at sea level.	key	✓	Section 13.3
REQ-AC-PROP-03	The propulsion system shall have a maximum of 4 engines.		✗6	Section 13.3
REQ-AC-PROP-04	The total mass of the propulsion system shall not exceed 5500 kg.	key	✗6000 kg	Section 13.3
REQ-AC-PROP-07	The nominal lifetime of a single engine shall be at minimum 7 years.		To be verified	
REQ-AC-PROP-09	The engine(s) shall be able to restart in flight, within the altitude envelope.		To be verified	
REQ-AC-PROP-10	The engine(s) shall be able to restart in flight, within the velocity envelope.		To be verified	

Table 15.11: Control Requirements

Requirement	Statement		Complied	Reference
REQ-AC-CTRL-01	The aircraft shall not encounter pitch-up tendencies during a stall condition.	key	✓	Section 13.6.2
REQ-AC-CTRL-03	The aircraft shall have convergent dynamic stabilities.	key	✓	Section 13.6.4
REQ-AC-CTRL-04	The aircraft shall be statically stable.	key	✓	Section 13.6.1
REQ-AC-CTRL-05	The aircraft shall be able to recover from a crosswind component greater than 20 kts.	key	✓	Section 13.6.2
REQ-AC-CTRL-10	The aircraft shall be certified for CAT II landings.	key	✓	Section 13.9.1
REQ-AC-CTRL-11	The aircraft shall be controllable and manoeuvrable in all flight regimes.	key	✓	Section 13.6.2
REQ-AC-CTRL-13	Rudder forces shall not exceed 667 N with V_{mc} .	key	✓	Section 13.6.2
REQ-AC-CTRL-14	The average dF_e/dV should be at least 4 N every 11.2 km/h.	key	To be verified	

Requirements not met or verified Here, all requirements which were not met are elaborated upon. A short explanation is also given to justify why certain requirements have not been verified yet.

1. REQ-SAI-POPS-05: This requirement was taken from Aurora [56]. However, after optimising the payload, a value of 9250 kg was found, with a maximum payload of 9700 kg.
2. REQ-AC-STRUC-04, 05 and 08: At this point in the design, a fatigue analysis has not yet been conducted due to time constraint and prioritisation of different characteristics. It is recommended that for the next design phase, this will be conducted.
3. REQ-AC-PROP-03: After a more thorough analysis of thrust performance at high altitude, it was decided that the engines selected in the Midterm Report [33] are not feasible. Initially, a limit of 4 engines was decided upon, in order to comply with the manufacturing cost requirements. However, the EJ200 is a smaller engine and significantly cheaper than the initial estimated cost per engine, and thus with 6 EJ200's, the manufacturing cost requirement is still met.
4. REQ-AC-PROP-04: Again, this requirement was set based on the Midterm Report, but due to the increase of the number of engines, the weight was also increased. It was favoured to have higher feasibility, than a lower engine weight.
5. REQ-AC-PROP-07, 08 and 09: These requirements could not be verified due to the lack of information available on the EJ200. However, the engine has a sufficient surge margin which reduces the importance of these requirements. In a more detailed design phase, these requirements will be verified as there will be more information available of the engines.
6. REQ-AC-CTRL-14: This requirement is not verified yet as only a preliminary layout of the hydraulics system has been determined yet. In the next design phase, the hydraulic system can be designed such that it meets this requirement.

III

Design Integration in Society

Part Introduction

This part expands on the steps taken following the main design phase. These include a more general verification and validation chapter in which details the method how these two aspects were conducted and integrated in the design exercise. This chapter is concluded by a recapitulative table of the requirements and the associated compliance matrix.

16

Reliability, Availability, Maintainability and Safety Analysis

For the purpose of gaining certainty that Ceres will complete its mission, reliability, availability, maintainability, and safety of the system must be assessed. This chapter performs an analysis on the previously mentioned items and proposes measures as to improve the performance of the system.

16.1. Reliability

The reliability of Ceres is defined as the ability of the system to deliver its payload to the stratosphere during its fifteen-year service life. The level of reliability is assessed using the Mean Time Between Failures (MTBF) as a quantification measure. Subsequently, the reliability can be expressed as a function of the MTBF as shown in Equation (16.1) [43]. In this report, failures are interpreted as parts of the aircraft that cannot adequately perform their function anymore due to impairments rendering the aircraft unable to provide service.

$$R = e^{-\frac{1}{MTBF} t} \quad (16.1)$$

At this stage of the design, it is still impossible to make a detailed estimation of the reliability of the system, since the subsystems have not been fully designed yet. To make an initial estimate of Ceres' reliability, the reliability of each of the subsystems of one individual aircraft were observed. Subsequently, the total reliability was estimated using the cumulative product of each of the individual subsystems. The total service life of an individual aircraft was set to be the total amount of working hours of the system divided by its fleet size.

16.2. Maintainability

The maintainability of Ceres reflects the accuracy, ease, safety, and costs of maintenance. Maintenance actions can be divided into preventive and corrective maintenance actions. Preventive maintenance actions refer to regularly scheduled checks of the aircraft; inspections are conducted to ensure the airworthiness of the aircraft. Corrective maintenance actions refer to the repair of broken parts as reported by the aircraft health system.

During transit checks parts such as wheels, brakes, and fluid levels are inspected, additionally, minor broken parts are repaired. Transit checks take approximately 12 hours a week. Besides transit checks, other checks are scheduled as well. Subsequently, each of the checks shall shortly be explained.

One of the lighter checks is the A check, which is performed every 8 to 10 weeks. During this check filters are changed, key systems such as control surfaces are lubricated and all emergency equipment is inspected. This check takes 20 to 60 man-hours and lasts approximately a day.

Heavier maintenance checks include the C check and the D check. The preceding takes place every 1.5 to 2 years and requires a majority of the aircraft's components to be inspected, resulting in over 6,000 necessary man-hours and the aircraft being out of service for 1-2 weeks. The last and most extensive check is the D check, which occurs every six years. For the purpose of inspection of the overhaul, the entire aircraft

is taken apart, resulting in checks of up to 50,000 man-hours and puts the aircraft out of service for nearly 2 months.

Finally, some unscheduled maintenance is required as well. Maintenance of this kind is perceived to be a part of the reliability of the aircraft.

The maintainability of an aircraft can be expressed by the Mean Time Between Maintenance (MTBM), which can be calculated using Equation (16.2) [43]. Here MTBPM represents the Mean Time Between Preventive Maintenance¹.

$$MTBM = \frac{1}{\frac{1}{MTBF} + \frac{1}{MTBPM}} \quad (16.2)$$

16.3. Availability

Availability is perceived as the readiness of Ceres to perform her mission. It represents the probability that the system will be available when required to. It is a result of reliability and maintainability. Several forms of availability can be distinguished such as inherent availability, achieved availability, and operational availability. The team chose to express the availability in terms of the achieved availability as scheduled maintenance will occur regularly over the course of the mission and will dominate unscheduled maintenance. The equation to calculate the achieved availability is given in Equation (16.3) [43]. In this equation, MTTM refers to the Mean Time To Maintain, which is the time required to perform both preventive and corrective maintenance actions.

$$A_a = \frac{MTBM}{MTBM + MTTM} \quad (16.3)$$

16.4. Safety

Safety is defined as the freedom from hazards to humans and equipment. An operational safety hazard analysis was performed as to ensure all hazards are properly mitigated. The following safety hazards were identified and mitigated.

Sulphur Handling Sulphur is stored outside or inside closed warehouses. These sulphur granules may cause dust which when put in contact with skin may cause irritation². LD50 values for dermal contact are >2000 mg/kg, as are oral. The risk is negligible, but in the case of visible dust in the air, dust masks shall be employed. Additionally, gloves shall be used when handling sulphur with bare hands, to avoid irritation.

Failure of One or More Engines Failure of the engines is caused by either malfunction of the engine itself or fuel system, or by external damage such as due to bird strikes, volcanic ash, or weather conditions. The consequences of engine failure differ per case.

In case of one engine out the risk is marginal, as the aircraft is designed to be stable even with one engine out. However, the probability of the aircraft reaching 20 km is decreased and the mission should be aborted. When more engines fail, the risk becomes critical or even catastrophic depending on which engines fail and the mission should be aborted immediately.

To avoid engine malfunction, regular checks should be performed. Furthermore, external damage due to weather conditions can be avoided by careful flight planning. As for bird strikes, monitoring bird activity and taking appropriate measures will help minimise bird strikes³.

Failure of the Sulphur Combustion Engine Failure of the combustion engine can either be caused by wear, tear, technical defects, or operating errors. Consequences of failure include damage to the fuselage and its structural integrity due to the engine catching on fire. Furthermore, undesirable products such as sulphur trioxide can be created by the engine which damages the environment. Additionally, sulphur trioxide is highly corrosive and is able to cause serious burns when inhaled, therefore it is dangerous to

¹<https://www.weibull.com/hotwire/issue147/hottopics147.htm>

² https://www.nis.eu/en/wp-content/uploads/sites/3/2016/09/EN_SDS_Granular_Sulphur___SDS_GHS_ANNEXII_CLP_2016912-35_NIS_Novi-Sad.pdf

³https://www.boeing.com/commercial/aeromagazine/articles/2011_q3/4/

humans⁴. Regarding what has been stated before, this safety hazard is considered critical. The hazard can be mitigated by regular inspection and maintenance.

Corrosion of the Fuselage Corrosion is caused by sulphur leakage from the storage tanks and can affect material properties of the fuselage and therefore its structural integrity. In addition, sulphur - when in contact with air - can react to sulphur dioxide or hydrogen sulphide, both poisonous gases to humans, therefore it is seen as a critical safety hazard. Sulphur leakage occurrence during flight can be mitigated by maintaining low temperatures within the cabin, hence slowing down reactions, as well as selecting corrosion-resistant alloys.

Failure of the Fuel System The biggest threats from the fuel system are caused by mechanical pump failure, fuel leak or fuel freezing. Any of these failures can result in partial or complete loss of thrust. The latter has caused severe accidents in the past. A complete loss of thrust due to fuel system failure would be catastrophic but is less likely due to the high number of engines. As a result, the fuel system can be separated in compartments making it redundant.⁵

Structural Failure Depending on the exact nature and location of a possible failure, structural failure can be considered to have a very high impact. Structural failures are mainly caused by poor maintenance, fatigue, corrosion, poor design or overloading of the airframe. Failure of redundant aircraft components will not necessarily result in a crash. However, catastrophic failure of a major aircraft component will in most cases lead to a severe accident. Recently, structural failure is not the biggest contributor to aviation accidents. Still, degradation of material properties due to fatigue or corrosion can pose a significant failure threat. Structural failures are in most cases directly related to the design of the aircraft, maintenance procedures or operation. Consequently, by correctly designing and maintaining the aircraft, as well as operating it strictly within its qualified flight envelope, these risks can be mitigated.

Failure of Avionics The threat related to avionics failure is heavily dependent on the scope of its application in the aircraft. If a fly-by-wire system is used, an avionics failure could directly affect the flight controls causing a loss of control. As a result, redundancy in avionics is needed for these aircraft. In other cases a complete failure of avionics would mean the pilot would lose all instruments, making controlling the aircraft much more difficult. Avionics failures can be caused by any kind of electrical failure, e.g. short-circuits. Also, failure of the power system of the aircraft could render the avionics inoperable. The odds of an avionics failure is lower than some other failures. This is heavily dependent on the amount of complexity and redundancy integrated into the avionics components. The threat of an avionics failure can be mitigated by reducing the reliability of the aircraft on it and improving the redundancy of the avionics system itself.

⁴ <https://pubchem.ncbi.nlm.nih.gov/compound/Sulfur-trioxide>

⁵ https://www.skybrary.aero/index.php/Aircraft_Fuel_Systems#Threats

Production Plan

Ceres aircraft will be produced in different production facilities for different components of the aircraft. The parts will be manufactured in batches and will be transferred to the production line for assembly of the components and lastly to the final assembly. The different systems such as the avionics, environmental control, communications will be integrated into the aircraft structure. Due to the engine's added value, it will be added last. Before the operation of the mission, the fleet has to be rigorously tested for the pressurisation of the cockpit, engine run-up, flight testing etc. for aircraft acceptance.

The materials used for the aircraft are shown in Table 13.25. The wingbox is one of the critical components of the aircraft and will be made out of composites. The structure of the wingbox can be established by manual lay-up or AFP (automated fibre placement) and will be cured in an autoclave. There are several advantages associated with AFP such that it offers precise ply thickness control, quality is consistent, low void content etc. However, as it is a complex tool the manufacturing costs will increase drastically. The many advantages outweigh the cost penalty, therefore, the manufacturing of the wingbox will make use of the AFP method. Conventional manufacturing methods can be used for the remaining parts of the aircraft structure. By using conventional methods, it will minimise the costs. The manufacturing costs should still comply with the requirement that each aircraft shall have a manufacturing cost of less than 100 Million Euros. A visual representation is given in Figure 17.1.

The assembly of each Ceres aircraft will follow the sequence depicted in Figure 17.2. Firstly, the cabin will be assembled along with the installation of the electrics, insulation, piping and valves for the dispersion and combustion system. Subsequently, the nose and the tail cone will be attached. The vertical tail, main wing and landing gear will be attached simultaneously to the fuselage structure. This is followed by the attachment of the horizontal tail to the vertical tail, finalising the T-tail configuration. The internal layout for the cockpit and the wiring for the flight control are then installed along with the systems for payload delivery. The aircraft must undergo large scale testing such as but not limited to the retraction and extraction of landing gear before the fitting of the engines. After the engines are fitted to the wings, systems are checked and flight control surfaces are tested. The flight control surfaces will initially be tested in isolation and checked when the control surfaces are integrated.

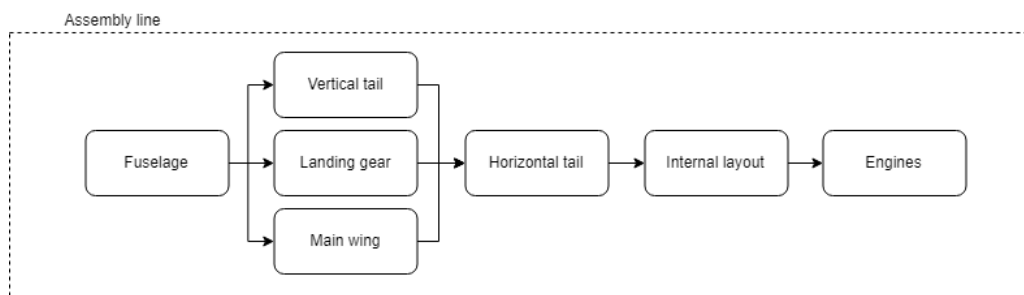


Figure 17.2: Assembly of Ceres Aircraft.

Lastly, the principle of lean manufacturing will be used in the production of the Ceres aircraft to be more sustainable by minimising waste such as:

- Overproduction
- Waiting time
- Transportation
- Work in progress
- Processing waste
- Movement
- Rework
- Under-utilising people

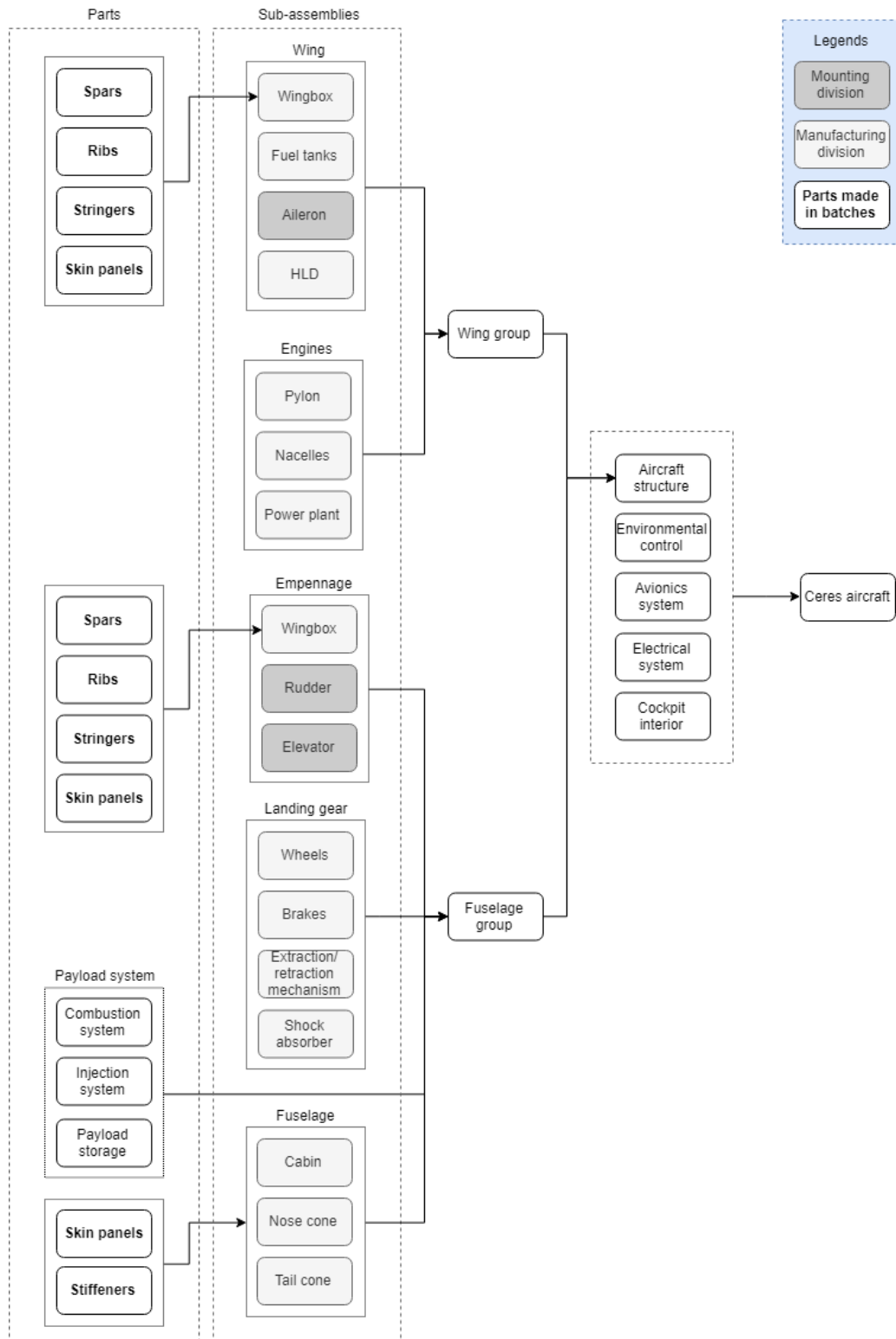


Figure 17.1: Parts and Sub-Assemblies of Ceres Aircraft.

Project Design and Development Logic

Between DSE and the start of operations, there are three important parts in the further development of project Ceres. The first two parts must be done consecutively, whereas the third part can be done in parallel. The first part is the more detailed design and optimisation phase, the second part is the manufacturing and testing phase, and the third phase is further research on the effects of the injection of aerosols, the optimal altitude for injection and effectiveness at varying altitudes. The first two parts are relevant for project Ceres, whereas the third part is outside of the scope the engineers working at project Ceres. Future research concerning this topic is recommended to be done by university institutes by funding from government bodies such as the UN and EU. As the third part is outside the scope of Project Ceres, there will not be a section detailing this further development phase.

All three parts are in a feedback loop. The design may need to be adjusted if testing confirms the presence of the feedback loop. As per the requirements, the aircraft from project Ceres were designed to operate at an altitude of 20 km. If further research points out that another altitude is better for the injection of aerosols, this will feed back into project Ceres. Project Ceres must assign a new team which will adjust the current design, in order to be able to fly optimally at the new altitude.

This chapter focuses on the Design and Development Logic up until when Ceres is ready for operation. Project Ceres should only be deployed as an emergency measure if effects of climate change are worse than expected, and the reductions of GHG are not enough to counter this. Due to this, it is not known if Project Ceres will be used, and if so, when it will be used. As the start of operations is not known, the operations as well as the end of life are not detailed in this chapter. However, the end of life is detailed in Section 14.2. Furthermore, the organisational and financial aspect of the next design phases were deemed to be beyond the scope of the DSE.

18.1. Detailed Design and Optimisation

The goal of DSE is to deliver a proof of concept, and is only eleven weeks long. Due to this, the level of detail to which the aircraft is designed, is not enough to be able to enter the manufacturing and testing phase. After DSE, the design needs to be updated with results from more in-depth analyses. This includes weight estimations based on the components in each subsystem, as well as a more detailed internal layout. More advanced models should be used to analyse the aerodynamic and stability characteristics, as well as the structural integrity. From these analyses, with component based weight estimation, new masses are found which need to be iterated again. With this more detailed design, the aircraft can go into the manufacturing and testing phase. In the next paragraphs, a more detailed description is given for each department. In Figure 18.1, the development logic of the detailed design phase is shown.

In the current phase, a detailed structural model is made for the wing, as this was the most critical part considering structural loads, due to the high span, this should also be applied to other wing-like surfaces. The next step is to use this for the weight estimation of the wing-like surfaces, as right now parametric relations are used from Torenbeek[91]. Next to this, the structural model of the fuselage needs to be refined, as well as the internal layout. Similarly, a more detailed model for the landing gear needs to be made, as well as a weight estimation based on the number of side braces, etc. After this, FEM simulations need to be used for the final design.

Regarding the propulsion department, an in-depth analysis was done for the engine selection. For further design development, it can be further optimised by removing the afterburner. Doing this, requires further research on how this affects the thrust levels and the weight of the aircraft as a whole. Regarding the stability and control department, already an in-depth analysis was conducted regarding the static and dynamic controllability and stability of the aircraft. However, stability were estimated using the DATCOM method[17, 27] and several assumptions were made in order to simulate the stability characteristics of the aircraft. Lastly, the aerodynamic and performance department had used mainly simplified theoretical and

parametric relations to estimate the aerodynamic characteristics. While these relations showed great accuracy, it can be improved upon by using CFD, and it needs to be validated with wind tunnel testing. The small scale tests in Figure 18.2 refer to the wind tunnel tests of a scale model.

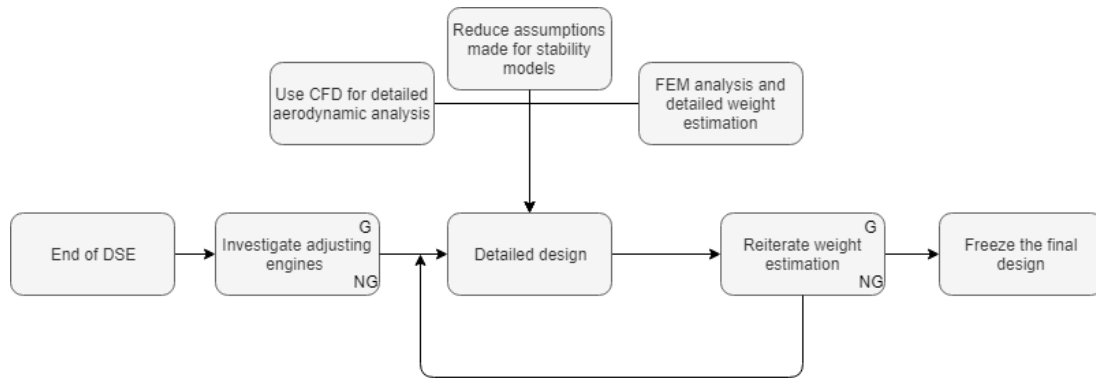


Figure 18.1: Development Logic of the Detailed Design Phase.

18.2. Manufacturing and Testing

It is of utmost importance to keep in mind that this project runs the risk of being cut short if it is observed that the climate control method has too many primary and secondary environmental impact. Another aspect to keep in mind, is the fact that not many aircraft have flown at an altitude of 20 km. As such, great importance should be put on preliminary testing, including flight testing of the system on other aircraft. This will lead to higher development costs in the short term but can potentially save a large amount of money, preventing other costs going into the development of the production methods. Furthermore, it is necessary to prove the feasibility of the design. In addition to this, to minimise the costs, throughout the design, development, and operation, the aircraft shall be comprised to a great extent of off-the-shelf components.

As a result from this design philosophy, the group decided to focus on the following steps as presented in Fig. 18.2 for the post DSE phases. This highlights the primary objective of the project which is cost-effectiveness of implementation.

The design and development is thus intertwined with the cost analysis which ensures that along the process of creating the aircraft, the various objectives as stated in the requirements are met. Moreover, these should be cross checked with a compliance matrix for fulfilling the technical requirements.

The tests include flight tests and ground tests which involve specific systems and subsystems in the aircraft and their integration according to the certification and permit to fly obtained from the authorities. Here, the certification and permit are assumed to be from EASA, CS-25. Various 'GO - NO GO' (in Figure 18.2 as G and NG, respectively) phases can be observed throughout these phases, for example, the testing phase of the injection system can lead to the project being brought to a halt if the adverse effects of SAI are shown to outweigh the temperature control capabilities.

18.3. Timeline

In this section, a short description of the timeline of project Ceres after DSE is presented, it is visually presented in Figure 18.3, in this timeline, it is assumed that project Ceres is continued immediately after DSE. It is estimated that the drawings for production will be finished in July 2024, whereas the detailed design report will be delivered in December 2024. The designing for manufacturing methods and planning will start in 2021, and is estimated to take roughly 3 years. From preliminary manufacturing methods, designs of tooling will start, and thus will start one year later than the manufacturing method design, at 2022. All manufacturing and tooling plans are estimated to be finished in 2025. Manufacturing of the prototype is estimated to start at this time as well. The prototype is estimated to be finished in 2026. After initial testing of the prototype, the production for the fleet of year 1 begins. Testing and certifications are estimated to take 5 years, and start to take place shortly after the start of production. It is estimated that if necessary, the operation could start in July 2031. However, Project Ceres should only be implemented if the global temperature increased further than expected, and emergency measures need to be undertaken.

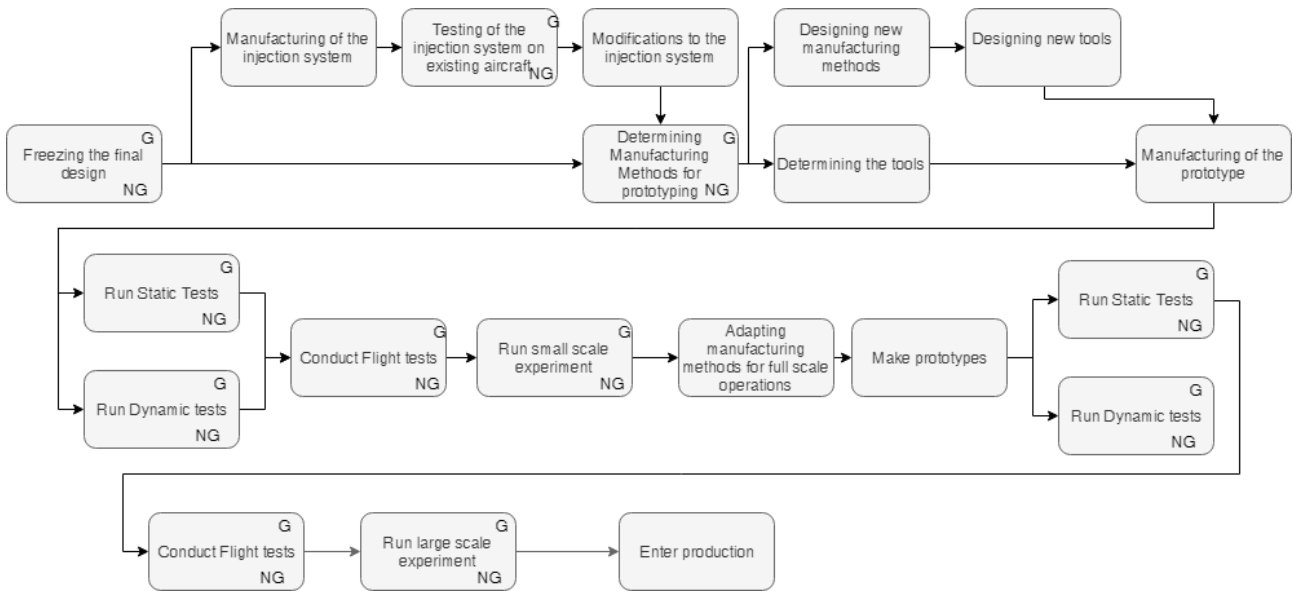


Figure 18.2: Development Logic of the Manufacturing and Testing Phase.

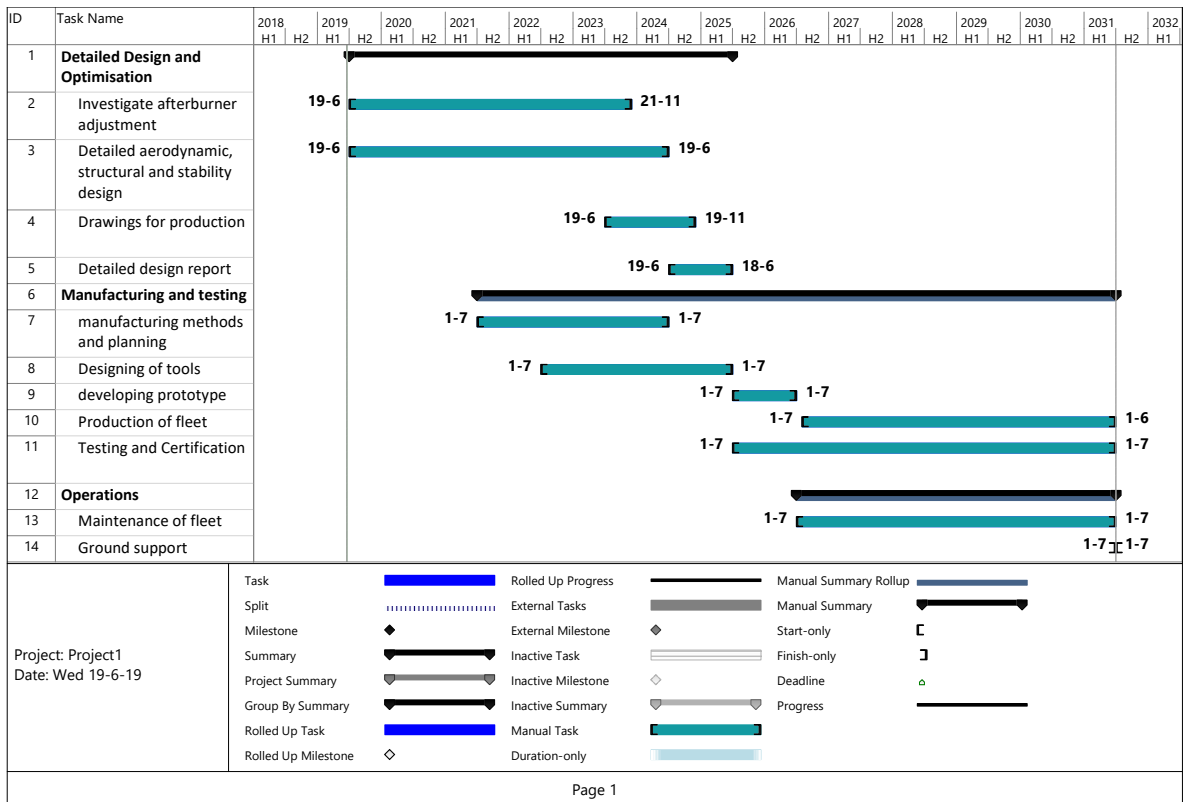


Figure 18.3: Post DSE Gantt-Chart.

Conclusion and Recommendations

19.1. Conclusion

Current climate models show a clear trend regarding the rise of temperatures which will exceed all set objectives, most noticeably the imposed limit of 1.5 °C, by between 2030 and 2052 (high confidence) as per the Paris agreement. Stratospheric geo-engineering presents a temporary emergency measure to reduce the heat absorption by the Earth. It must be strongly emphasised that stratospheric geo-engineering and other geo-engineering methods alone must not be used to combat climate change and ideally should not be used at all while greenhouse gas emissions are being reduced. However, due to the uncertainties in climate prediction models, stratospheric geo-engineering presents a possible but temporary emergency system to combat unexpectedly negative outcomes while greenhouse gas emissions are being reduced. One proposed geo-engineering measure involves the injection of aerosols into the stratosphere. These aerosols, based on sulphates, have the objective of mimicking volcanic eruptions inserting reflective crystalline particles into the stratosphere. These particles help reduce the solar flux received on Earth and consequently reduce the heat absorption. Many methods for aerosol injection are proposed, but few meet the feasibility and efficiency of stratospheric aircraft. The Ceres mission aims to reduce cost and increase dispersion efficiency by proposing a mission profile centred around 20 km altitude, based on eight airports around the Equator. These aircraft will deliver up to 3 Mt of sulphur dioxide each year at the peak of operations.

This report focuses on the proposal of a feasible aircraft system, capable of meeting the payload and altitude requirements. It is an expansion on previous design proposals for such a mission with the prime focus around the latest geo-engineering and stakeholder requirements.

The Ceres mission faces several challenges during its design. The requirements set to deliver up to 3 Mt of sulphur dioxide at 20 km on the fifteenth year. The initial delivery on year one starts at 0.2 Mt per year and ramps up until the fifteenth year. In order to meet the fifteenth year requirements, a fleet of 180 aircraft was determined to be necessary. Additionally, 250 operational days were selected, with round the clock operations. Each operation was estimated to take 4.6 hours of flight time, 1 hour of turnaround and 0.2 hours of taxiing. New aircraft would be added in an interval of 1.5 months on the first year, ramping up to 23 days intervals by the fifteenth year. The aircraft was designed as follows:

Firstly, to meet these operational demands, the aircraft was found to be most efficient for a conventional configuration. This was determined by means of an initial configuration trade off. This report further advances the design, by implementation of Class II weight estimates combined with zero lift coefficients. Sulphur is carried on board the aircraft, mixed and burnt with atmospheric oxygen through the use of a turbojet based sulphur burner. These parameters, combined with operational costs yielded an operational optimum for minimum cost at 9250 kg of payload.

In addition, final design of the aircraft yielded an estimated MTOW of 51 100 kg. Decomposition of the weights shows 9700 kg dedicated to the payload, with 13500 kg dedicated to the fuel and 28 000 kg dedicated to the OEW. All values have safety margins added due to the preliminary nature of the design. A wing with an aspect ratio of 13 was chosen, positioned as a high wing with six under slung engines to meet the necessary thrust requirements for a T/W ratio of 0.71. This arrangement provides a total thrust of 360 000 N with proven and available engines, the EJ200. A surface area of 277.5 m² is required for the wing with a 27.3° of sweep to allow for a mach drag divergence at Mach 0.78.

Finally, the cost of the Ceres mission is estimated at 107.9 billion dollars during the fifteen years of operation, including the development, manufacturing and maintenance costs. Development costs are estimated at 1.93 billion dollars for the financing of workers, facilities and test aircraft. Development profit was kept at 5% due to the public nature of the mission. Manufacturing and acquisition costs are around 107.5 million dollars per airframe, culminating to 19.3 billion dollars for the whole fleet. Finally, the operations and

maintenance will cost around 86.6 billion dollars, which is the biggest contributing cost. The annual cost per aircraft is of 69.62 million dollars. These numbers are comparable with large commercial airlines and thus allows to use financial models that are extensively developed. This finalises the report, which provides a feasible, high TRL and effective solution to the difficult aerosol geo-engineering challenges that lie ahead.

19.2. Recommendations

During the design phase, several points of improvement were noticed, but could not be integrated within the current design yet. In this section, these recommendations are stated.

Firstly, detailed aerodynamic and structural design needs to be continued in order to ensure the feasibility and that the performance level to fulfil the mission is reached. This will take various forms, the first of which will be a thorough CFD analysis coupled to wind tunnel testing of scaled models to determine more precisely the aerodynamic properties and characteristics of the aircraft. This will, in turn, enable a more detailed structural design to be done which will benefit the weight estimation, making it also more detailed and with less uncertainty. In addition, the coefficient of drag for zero lift should be agreed upon and fixed through verification and validation of the zero lift drag programme written using empirical formulas.

Moreover, in the future the buffet onset has to be taken into account in the complete design. Currently, the predicted cruise lift coefficient by SUAVE ranges from 0.83–0.545. This violates the buffeting onset margin of 30% which, if kept untouched, will result that the aircraft is unable to pass current standard civilian certification. Therefore, it is highly recommended in the future to determine the possibilities of flying below the C_L -buffet onset boundary constraint of 0.6 by the means of delaying the buffeting onset to pass certification during cruise. Since a lift coefficient of 0.6 is extremely difficult to combine with the mission profile required, it is of higher importance to attempt to develop models and systems to delay buffeting.

For further phases of the development of the aircraft engines it is advised to try and obtain verification and validation data on high altitude performance of engines. This data can then be applied to improve the accuracy of the engine model and that way reduce the uncertainties in it.

Additional refinement of the centre of gravity computation and its consequences is necessary as it was observed that the outputs of the CG range plots were excessively conservative. This will result in a change of location of the landing gear which has minimal repercussions on the performance of the aircraft. However, it will also result in a greater fuselage length due to the greater tail arm necessary to ensure stability and controllability. This can be partly mitigated with the use of a larger horizontal and vertical tail surface.

Additional recommendations include verification methods which include the crosschecking of different programs to ensure that the integration of the characteristics are reasonable. SUAVE should also be verified and validated for high altitude flight.

For further recommendations, the prediction of the T-tail flutter can be conducted to avoid any catastrophic accidents. The stability analysis can be done using the doublet lattice method (DLM) and/or the unsteady vortex lattice method (UVLM) in future design. This will enable a better quantification of the flutter exhibit by the empennage, especially during the critical phase of the mission at which the aircraft is near the transonic regime.

The aircraft exhibit poor motion damping behaviour compared to conventional aircraft. The poor damping behaviour is noticeable for the short period. For further recommendations and future design, the horizontal tail parameters can be iterated to ensure that the quality level of the eigenmotions behaviour is of an acceptable degree for both the take-off and cruise phase.

Lastly, it is recommended that further research should be conducted concerning the optimal dispersion height, as well as the effectiveness at lower altitudes. Subsequently, a trade-off study can be made which compares flying at a lower altitude with more payload, versus flying at the optimal altitude with less payload. This way, the cost can be minimised.

References

- [1] S.A.S. Airbus. Process for advanced management of end-of-life of aircraft, 2008.
- [2] Anderson. Fundamentals of aerodynamics, 2016.
- [3] AJ Apling, JP Blanchet, RJ Charlson, D Crommelynck, H Grassl, N Husson, GJ Jenkins, I Karol, MD King, V Ramanathan, et al. Radiative forcing of climate, 2018.
- [4] Normann Ashford and Paul H. Wright. *Airport engineering*. Wiley, 1992.
- [5] Nikolaos Asproulis Konstantinos Salonitis Athanasios Kolios, Stuart Howe. Environmental impact assessment of the manufacturing of a commercial aircraft. In *11th International Conference on Manufacturing Research (ICMR2013)*. Advances in Manufacturing Technology XXVII, 09 2013.
- [6] Robert Bartels. Flow and turbulence modeling and computation of shock buffet onset for conventional and supercritical airfoils, 04 1998.
- [7] Samit Basu. Fem: Beam freemat (matlab) code. <http://freemat.sourceforge.net/FreeMat-4.0.pdf>, 2009.
- [8] Lothar Bertsch. *Noise Prediction within Conceptual Aircraft Design*. PhD thesis, German Aerospace Center (DLR), 08 2013.
- [9] M. Cruellas Bordes, C.J.G. de Peter, M. Janssens, A.F. van Korlaar, L.P. Kulik, R. Maselis, L.H. Mulder, S. Stoev, K.J.E. van Vlijmen, I.E. de Vries, and et al. Final design report stratospheric aerosol geoengineering aircraft, 2016. Unpublished.
- [10] Jens Borken-Kleefeld, Terje Berntsen, and Jan Fuglestvedt. Specific climate impact of passenger and freight transport. *Environmental Science & Technology*, 44(15):5700–5706, 2010. doi: 10.1021/es9039693.
- [11] C. Carpenter. *Flightwise: Aircraft stability and control*. Flightwise. Airline, 1997. ISBN 9781853108709. URL <https://books.google.nl/books?id=1aNTAAAMAAJ>.
- [12] Cesar CELIS, Luís Fernando Figueira da Silva, Sandro Ferreira, Antonio Batista de Jesus, and Guilherme Lara Oliveira. Effective use of vortex generators to improve the performance of submerged air inlets for aircraft, 12 2006.
- [13] Mikhail Chester. Life-cycle environmental inventory of passenger transportation in the united states. *Institute of Transportation Studies, UC Berkeley, Institute of Transportation Studies, Research Reports, Working Papers, Proceedings*, 01 2008.
- [14] P. J. Crutzen. Albedo enhancement by stratospheric sulfur injections, 2006. URL http://faculty.washington.edu/stevehar/Geoengineering_packet.pdf.
- [15] John S Daniel and Susan Solomon. On the climate forcing of carbon monoxide. *Journal of Geophysical Research: Atmospheres*, 103(D11):13249–13260, 1998.
- [16] John S. Daniel and Susan Solomon. On the climate forcing of carbon monoxide. *Journal of Geophysical Research: Atmospheres*, 103(D11):13249–13260, 1998. doi: 10.1029/98jd00822.
- [17] DATCOMUSAF. The USAF stability and control DATCOM, 1999.
- [18] Ismail Daut, Mohd Yusoff, Safwati Ibrahim, Muhammad Irwanto, and Gomesh Nair. Relationship between the solar radiation and surface temperature in perlis. *Advanced Materials Research*, 512-515:143–147, 05 2012. doi: 10.4028/www.scientific.net/AMR.512-515.143.
- [19] P. Davidson, C. Burgoyne, H. Hunt, and M. Causier. Lifting options for stratospheric aerosol geoengineering: advantages of tethered balloon systems. *Philosophical Transactions of the Royal Society A: Mathematical, Physical and Engineering Sciences*, 370(1974):4263–4300, 2012. doi: 10.1098/rsta.2011.0639.
- [20] João Vasco de Oliveira Fernandes Lopes. Life cycle assessment of the airbus a330-200 aircraft, 11 2010. URL https://fenix.tecnico.ulisboa.pt/downloadFile/39514223995/Tese_JoaoVascoLopes.pdf.
- [21] João Vasco de Oliveira Fernandes Lopes. Life cycle assessment of the airbus a330-200 aircraft, 11 2010. URL https://fenix.tecnico.ulisboa.pt/downloadFile/39514223995/Tese_JoaoVascoLopes.pdf.
- [22] Professor dr. D.G. Simons. *Introduction to Aircraft Noise*. Faculty of Aerospace Engineering Delft University of Technology, 2018.
- [23] Mark Drela. Xfoil: An analysis and design system for low reynolds number airfoils. *Lecture Notes in Engineering Low Reynolds Number Aerodynamics*, page 1–12, 1989. doi: 10.1007/978-3-642-84010-4_1.
- [24] EUbudget. EU budget 2021-2027: Commission proposes to further strengthen climate action, 2018.
- [25] K. Richter F. Hörl. Monitoring the ej200 engine, 1995.
- [26] D. Ciliberti V. Cusati F. Nicolosi, P. Della Vecchia. Fuselage aerodynamic prediction methods. *Aerospace Science and Technology*, 55:332–343, 2016. doi: 10.1016/j.ast.2016.06.012. URL <https://doi.org/10.1016/j.ast.2016.06.012>.
- [27] R. D. Finck. USAF (United States Air Force) Stability and Control DATCOM (Data Compendium), 1978.
- [28] J. Fuglesvedt J. Huang D. Koch J.F. Lamarque D. Lee B. Mendoza T. Nakajima A. Robock G. Stephens T. Take-mura H. Zhang F.M. Bréon, W. Collins. Anthropogenic and natural radiative forcing, 2 2008.
- [29] James G. Coder and Mark Maughmer. Numerical validation of the squire-young formula for profile drag prediction, 01 2013.
- [30] Per K. Gegg. Factors affecting the emergence, development and uptake of aviation biofuels, 2014.
- [31] J. McArthur G.R. Spedding. Span efficiencies of wings at low reynolds numbers. *Journal of Aircraft*, 2010.
- [32] DSE group 22. Baseline report, 2019. Unpublished.
- [33] DSE group 22. Midterm report, 2019. Unpublished.
- [34] DSE group 22. Project plan, 2019. Unpublished.
- [35] Snorri Gudmundsson. *General Aviation Aircraft Design: Applied Methods and Procedures*. Butterworth-Heinemann, Aerospace Engineering, Embry-Riddle Aeronautical University, 2014. ISBN 978-0-12-397308-5.

- [36] Onur Gunel, Emre Koc, and Tahir Yavuz. Cfd vs. xfoil of airfoil analysis at low reynolds numbers. *2016 IEEE International Conference on Renewable Energy Research and Applications (ICRERA)*, 2016. doi: 10.1109/icrera.2016.7884411.
- [37] P. Gómez, D. Elduque, J. Sarasa, C. Pina, and C. Javierre. Influence of composition on the environmental impact of a cast aluminum alloy. *Materials (Basel)*, 9(6), 2016. ISSN 1996-1944 (Print) 1996-1944. doi: 10.3390/ma9060412.
- [38] Ir R. J. Hamann and Prof. dr. ir. M.J.L. van Tooren. *Systems Engineering & Technical Management Techniques Part I*. Delft University of Technology, Faculty of Aerospace Engineering, 2004.
- [39] Leticia Hime, Cesar CELIS, Luís Fernando Figueira da Silva, Sandro Ferreira, Antonio Batista de Jesus, Viviam Lawrence Takase, and Harry Tavares Maia Vinagre. A review of the characteristics of submerged air intakes, 11 2005.
- [40] Dr. Ir. S. Hulshoff and W. Smith. *Project Guide Design Synthesis Exercise: Low-cost System for Stratospheric Aerosol Injection*, 2019. Unpublished.
- [41] S. J. Hulshoff. Course AE4930 - Aeroelasticity. Technical report, Delft University of Technology, 2011.
- [42] A.C. in 't Veld and T.J. Mulder. Flight Dynamics Assignment AE3212-II, 2019.
- [43] Prof. dr. ir. M.J.L. van Tooren Ir. R.J. Hamann. Systems engineering & technical management techniques part ii, 2006. Unpublished.
- [44] J.A.Mulder. Flight dynamics lecture notes, 2013.
- [45] Johnson, W., Hill, A. and Eichmann, O. Pressure distributions from high reynolds number tests of a nasa sc(3)-0712(b) airfoil in the langley 0.3-meter transonic cryogenic tunnel, 1985.
- [46] Pearson Jr., E. O, A J. Evans, and West Jr, F. E. Effects of compressibility on the maximum lift characteristics and spanwise load distribution of a 12-foot-span fighter type wing of naca 230 series airfoil sections, 11 1945.
- [47] Stéphane Illa Jérôme Huber. Jet noise assessment and sensitivity at aircraft level, 2007.
- [48] Max Kandula. On the scaling laws and similarity spectra for jet noise in subsonic and supersonic flows. Technical report, Kennedy Space Center, 2008.
- [49] Gaetan Kenway and Joaquim Martins. Buffet-onset constraint formulation for aerodynamic shape optimization. *AIAA Journal*, 55:1–18, 04 2017. doi: 10.2514/1.J055172.
- [50] Gregg Kopp and Judith L. Lean. A new, lower value of total solar irradiance:evidence and climate significance. *GEOPHYSICAL RESEARCH LETTERS*, 01 2011. doi: 10.1029/2010GL045777. URL <https://agupubs.onlinelibrary.wiley.com/doi/epdf/10.1029/2010GL045777>.
- [51] Christopher Koroneos, Aris Dompros, George Roubas, and Nicolas Moussiopoulos. Life cycle assessment of kerosene used in aviation (8 pp). *The International Journal of Life Cycle Assessment*, 10(6):417–424, Nov 2005. ISSN 1614-7502. doi: 10.1065/lca2004.12.191. URL <https://doi.org/10.1065/lca2004.12.191>.
- [52] Ben Kravitz, Douglas G. Macmartin, Michael J. Mills, Jadwiga H. Richter, Simone Tilmes, Jean-Francois Lamarque, Joseph J. Tribbia, and Francis Vitt. First simulations of designing stratospheric sulfate aerosol geo-engineering to meet multiple simultaneous climate objectives. *Journal of Geophysical Research: Atmospheres*, 122(23), 2017. doi: 10.1002/2017jd026874.
- [53] Duane Kritzinger. *Aircraft System Safety: Military and Civil Aeronautical Applications*. Woodhead Publishing, 2006.
- [54] Chr. Kupsch B. Reßler G. Sardemann M. Achternbosch, K.-R. Bräutigam. Material flow analysis, a comparison of manufacturing, use and fate of cfrp - fuselage components versus aluminium components for commercial airliners. *Institut für Technikfolgenabschätzung und Systemanalyse*, 2002. URL https://www.dlr.de/fa/PortalData/17/Resources/dokumente/institut/srw_10.pdf.
- [55] D. Scholz M. Nita. Estimating the oswald factor from basic aircraft geometrical parameters. *Deutscher Luft- und Raumfahrtkongress 2012*, 2012.
- [56] Justin McClellan, James Sisco, Brandon Suarez, and Greg Keogh. Geoengineering cost analysis. *Geoengineering Cost Analysis*, 2011.
- [57] Justin McClellan, David W Keith, and Jay Apt. Cost analysis of stratospheric albedo modification delivery systems. *Environmental Research Letters*, 7(3):034019, 08 2012. doi: 10.1088/1748-9326/7/3/034019. URL <https://doi.org/10.1088/1748-9326/7/3/034019>.
- [58] T.H.G. Megson. *Aircraft Structures for engineering students*. Elsevier, 1999.
- [59] P.S. Mohan, M Sundaram, and S Guruviah. Corrosion of metals in sulphur dioxide atmosphere - a laboratory study. *Key Engineering Materials*, 20-28:179–184, 01 1991. doi: 10.4028/www.scientific.net/KEM.20-28.179.
- [60] NA. Military specification flying qualities of piloted airplane, 1991.
- [61] Terry Norgate, Sharif Jahanshahi, and William Rankin. Assessing the environmental impact of metal production processes. *Journal of Cleaner Production*, 15:838–848, 10 2006. doi: 10.1016/j.jclepro.2006.06.018.
- [62] Ed Obert. *Aerodynamic design of transport aircraft*. IOS Press, 2009.
- [63] International Civil Aviation Organization. Manual on civil aviation jet fuel supply, 2012.
- [64] M. Schraner P. Heckendorn, B. P. Luo and T. Peter. The impact of geoengineering aerosols on stratospheric temperature and ozone. *Environmental Research Letters*, 4((2009)045108):12, 2009.
- [65] Bill Palmer. *Understanding Air France 447*. William Palmer, 2013.
- [66] I L Pepler. *From The Ground Up*. Aviation Publishers Co. Limited, 27 edition, 1996.
- [67] Warren F. Phillips and Nicholas R. Alley. Predicting maximum lift coefficient for twisted wings using lifting-line theory. *Journal of Aircraft*, 44(3):898–910, 2007. doi: 10.2514/1.25640.
- [68] W. Verhage R. Curran. *AE3211-I Lecture 8 - Risk Management & Reliability Engineering*, 2019.

- [69] J. BEHENNA R. J. LANE. Ej200—the engine for the new european fighter aircraft, 1990.
- [70] Daniel P. Raymer. *Aircraft Design: A Conceptual Approach*. American Institute of Aeronautics and Astronautics, Inc., 1992.
- [71] Mazen Abdel-Salam Reyad Abdel-Fadil, Ahmad Eid. Electrical distribution power systems of modern civil aircrafts. *2nd International Conference on Energy Systems and Technologies*, 2013.
- [72] J. Roskam. *Airplane Flight Dynamics & Automatic Flight Controls: Part I (Volume 1)*. DARcorporation, 2001. ISBN 1884885179.
- [73] Ja Roskam. *Airplane Design Part V: Component Weight Estimation*. Design, Analysis and Research Corporation (DARcorporation), 1999. ISBN ISBN 978-18-8488-550-1.
- [74] Jan Roskam. *Airplane design*. Roskam Aviation and Engineering Corp., 1989.
- [75] Ger. J. J. Ruijgrok. *Elements of airplane performance*. Delft Academic Press, Faculty of Aerospace Engineering, Delft University of Technilogy, 2009. ISBN ISBN 978-90-6562-203-7. URL www.vssd.nl/hlf/ae02.htm.
- [76] S S. Dodbele, C P. Vandam, and P M. H. W. Vijgen. Design of fuselage shapes for natural laminar flow, 04 1986.
- [77] Mohammad H. Sadraey. *Aircraft design: a systems engineering approach*. Wiley, 2013.
- [78] Meinhard Schobeiri. *Fluid mechanics for engineers. a graduate textbook*, 01 2010.
- [79] Pascale Schwab Castella, Isabelle Blanc, Marcel Gomez Ferrer, Bastien Ecabert, Martyn Wakeman, Jan-Anders Manson, Daniel Emery, Seong-Ho Han, Jinglan Hong, and Olivier Jolliet. Integrating life cycle costs and environmental impacts of composite rail car-bodies for a korean train. *The International Journal of Life Cycle Assessment*, 14(5):429–442, Jul 2009. ISSN 1614-7502. doi: 10.1007/s11367-009-0096-2. URL <https://doi.org/10.1007/s11367-009-0096-2>.
- [80] Ravinka Seresinhe and Craig Lawson. Electrical load-sizing methodology to aid conceptual and preliminary design of large commercial aircraft, 2015.
- [81] Steven C Sherwood, Vishal Dixit, and Chryséis Salomez. The global warming potential of near-surface emitted water vapour. *Environmental Research Letters*, 13(10):104006, sep 2018. doi: 10.1088/1748-9326/aae018. URL <https://doi.org/10.1088/1748-9326/aae018>.
- [82] Rand Simberg. Near-term prospects for space tourism, 2000.
- [83] B. Singh. A Medium-Fidelity Method for Rapid Maximum Lift Estimation, 2017.
- [84] Jordan P. Smith, John A. Dykema, and David W. Keith. Production of sulfates onboard an aircraft: Implications for the cost and feasibility of stratospheric solar geoengineering. *Earth and Space Science*, 5(4): 150–162, 2018. doi: 10.1002/2018EA000370. URL <https://agupubs.onlinelibrary.wiley.com/doi/abs/10.1002/2018EA000370>.
- [85] W. Smith. Cost model for a stratospheric aerosol injection system, 2018. Unpublished.
- [86] Rayne Sung. A comparative study of the gas turbine simulation program (gsp) 11 and gasturb 11 on their respective simulations for a single-spool turbojet, 2013.
- [87] P. Sváček, M. Feistauer, and J. Horáček. Numerical simulation of flow induced airfoil vibrations with large amplitudes. *Journal of Fluids and Structures*, 23(3):391 – 411, 2007. ISSN 0889-9746. doi: <https://doi.org/10.1016/j.jfluidstructs.2006.10.005>. URL <http://www.sciencedirect.com/science/article/pii/S0889974606001253>.
- [88] Hai-Long Tang, Min Chen, Dong-hai Jin, and Zheng-ping Zou. High altitude low reynolds number effect on the matching performance of a turbofan engine, 2013. URL <https://journals.sagepub.com/doi/pdf/10.1177/0954410012437505>.
- [89] E. Torenbeek. Development and application of a comprehensive, design-sensitive weight prediction method for wing structures of transport category aircraft. Technical report, Delft University of Technology, 1992.
- [90] Egbert Torenbeek. Preliminary tailplane design. *Synthesis of Subsonic Airplane Design*, page 303–339, 1982. doi: 10.1007/978-94-017-3202-4_9.
- [91] Egbert Torenbeek. *Advanced Aircraft Design*. John Wiley and Sons, 2013.
- [92] Emilio Botero-Timothy MacDonald Timothy Momose Anil Variyar J. Michael Vekh Michael Colonno Thomas D. Economon Juan J. Alonso Tarik H. Orra Carlos Ilario da Silva Trent Lukaczyk, Andrew D. Wendorff. Suave: An open-source environment for multi-fidelity conceptual vehicle design. *54th AIAA Aerospace Sciences Meeting*, 2016. doi: DOI:10.2514/6.2016-1275. URL https://www.researchgate.net/publication/314090333_SUAVE_An_Open-Source_Environment_for_Conceptual_Vehicle_Design_and_Optimization.
- [93] E.G. Tulapurkara. *Airplane design*, 2013.
- [94] H. Schmidt U. Niemeier and C. Timmreck. The dependency of geoengineered sulfate aerosol on the emission strategy. *ATMOSPHERIC SCIENCE LETTERS*, 10 2011. doi: DOI:10.1002/asl.304. URL <https://rmets.onlinelibrary.wiley.com/doi/pdf/10.1002/asl.304>.
- [95] UNFCCC. 2018-2019 UNFCCC Budget Proposal, 2017.
- [96] Unknown. *Technology Readiness Levels Handbook for Space Applications*, 2008.
- [97] USbudget. US Office of Management and Budget, 2015.
- [98] J. Haigh D. Hauglustaine J. Haywood G. Myhre T. Nakajima G.Y. Shi S. Solomons V. Ramaswamy, O. Boucher. Radiative forcing of climate change, 2018.
- [99] Walter O. Valarezo and Vincent D. Chin. Method for the prediction of wing maximum lift. *Journal of Aircraft*, 31(1):103–109, 1994. doi: 10.2514/3.46461.
- [100] Gerard W. H. van Es. Rapid estimation of the zero-lift drag coefficient of transport aircraft. *Journal of Aircraft*, 39(4):597–599, 2002.
- [101] S. Vinodh, G. Sivaraj, S. Nithish, and R. Veeramanikandan. Life cycle assessment of an aircraft component: a case study. *International Journal of Industrial and Systems Engineering*, 27(4):485, 2017. doi: 10.1504/ijise.2017.10008235.
- [102] L. R. Wootton. The effect of compressibility on the maximum lift coefficient of aerofoils at subsonic airspeeds. *The Journal of the Royal Aeronautical Society*, 71(679): 476–486, 1967. doi: 10.1017/s000192400055263.
- [103] F. Yin and A. Gangoli Rao. Performance analysis of an aero engine with inter-stage turbine burner. *The Aeronautical Journal*, 121(1245):1605–1626, 2017. doi: 10.1017/aer.2017.93.

IV

Appendices

A

GasTurb Inputs

Station	W kg/s	T K	P kPa	WRstd kg/s	FN	=	59,91 kN
amb		288,15	101,325				
1	76,080	288,15	101,325		TSFC	=	20,5403 g/(kN*s)
2	76,080	288,15	100,312	76,849	WF Burner	=	1,23053 kg/s
13	21,737	451,00	421,309	6,540	s NOX	=	0,8478
21	54,343	451,00	421,309	16,351	BPR	=	0,4000
25	54,343	451,00	417,096	16,516	Core Eff	=	0,4591
3	52,713	781,81	2585,997	3,402	Prop Eff	=	0,0000
31	47,007	781,81	2585,997		P3/P2	=	25,780
4	48,237	1650,00	2508,417	4,663			
41	50,954	1607,79	2508,417	4,862	P16/P6	=	0,99384
43	50,954	1312,14	931,254		A63	=	0,27129 m ²
44	53,672	1287,27	931,254		A163	=	0,07477 m ²
45	53,672	1287,27	912,629	12,595	A64	=	0,34606 m ²
49	53,672	1093,73	423,922		XM63	=	0,24944
5	55,302	1081,60	423,922	25,609	XM163	=	0,22352
6	55,302	1081,60	415,444		XM64	=	0,25000
16	21,737	451,00	412,883		P63/P6	=	0,99000
64	77,039	915,96	410,009		P163/P16	=	0,99000
8	77,039	915,96	410,009	33,944	A8	=	0,15044 m ²
Bleed	0,272	781,81	2585,991		CD8	=	0,95000

Efficiencies:	isent	polytr	RNI	P/P	Ang8	=	25,00 °
Outer LPC	0,8900	0,9095	0,990	4,200	P8/Pamb	=	4,04648
Inner LPC	0,8900	0,9095	0,990	4,200	WLkBy/w25	=	0,00000
HP Compressor	0,8800	0,9050	2,413	6,200	WCHN/w25	=	0,05000
Burner	0,9950			0,970	WCHR/w25	=	0,05000
HP Turbine	0,9100	0,9001	3,324	2,694	Loading	=	100,00 %
LP Turbine	0,9100	0,9022	1,561	2,153	WCLN/w25	=	0,00000
Mixer	0,5000				WCLR/w25	=	0,03000

HP Spool mech Eff	0,9900	Nom Spd	20000 rpm		WBHD/w21	=	0,00000
LP Spool mech Eff	0,9900	Nom Spd	14600 rpm		far7	=	0,01623

P2/P1=	0,9900	P25/P21=	0,9900	P45/P44=	WBLD/w25	=	0,00500
Con-Di Nozzle:					PWX	=	50,0 kW
A9*(Ps9-Pamb)		-1,837			P16/P13	=	0,9800

hum [%]	war0	FHV	Fuel		P6/P5	=	0,9800
0,0	0,00000	43,124	Generic		A9/A8	=	1,30000

Figure A.1: GasTurb Inputs

B

DATCOM Input & Output

```

*****
* USAF STABILITY AND CONTROL DIGITAL DATCOM *
* PROGRAM REV. JAN 96 DIRECT INQUIRIES TO: *
* WRIGHT LABORATORY (WL/FIGC) ATTN: W. BLAKE *
* WRIGHT PATTERSON AFB, OHIO 45433 *
* PHONE (513) 255-6764, FAX (513) 258-4054 *
*****
1 CONERR - INPUT ERROR CHECKING
0 ERROR CODES - N* DENOTES THE NUMBER OF OCCURENCES OF EACH ERROR
0 A - UNKNOWN VARIABLE NAME
0 B - MISSING EQUAL SIGN FOLLOWING VARIABLE NAME
0 C - NON-ARRAY VARIABLE HAS AN ARRAY ELEMENT DESIGNATION - (N)
0 D - NON-ARRAY VARIABLE HAS MULTIPLE VALUES ASSIGNED

```

O E - ASSIGNED VALUES EXCEED ARRAY DIMENSION
O F - SYNTAX ERROR

O***** INPUT DATA CARDS *****

CASEID CERES

```
$FLTCON NMACH=2.0,MACH(1)=0.2,0.6$
$FLTCON NALT=2.0,ALT(1)=0.0,65617.0$
$FLTCON NALPHA=9.0,ALSCHD=-4.0,-2.0,0.0,2.0,4.0,6.0,8.0,10.0,12.0,
  GAMMA=0.0,WT=133762.59,LOOP=1.0$
$OPTINS SREF=3604.47,CBARR=17.48,BLREF=216.46$
$SYNTHS XCG=109.03,ZCG=2.77,XW=81.71,ZW=6.93,ALIW=0.0,XH=211.41,
  ZH=25.07,ALIH=0.0,XV=189.27,ZV=6.93,VERTUP=.TRUE.$
$BODY NX=4.0,ITYPE=1.0,
  X=0.,22.92,59.6,206.22,
  ZU=0.,6.93,6.93,6.93,
  ZL=0.,-6.93,-6.93,6.6,
  S=0.,264.11,264.11,0.34,
  P=0.,76.21,76.21,2.06,
  R=0.,12.13,12.13,0.33$
$WGSCHR TYPEIN=1.0, NPTS=31.0,
XCORD= 0.0, 0.002, 0.005, 0.01, 0.02, 0.03, 0.04,
0.08, 0.12, 0.16, 0.2, 0.24, 0.28,
0.32, 0.36, 0.4, 0.44, 0.48, 0.52,
0.56, 0.6, 0.64, 0.68, 0.72, 0.76,
0.8, 0.84, 0.88, 0.92, 0.96, 1.,
YUPPER= 0.0, 0.0092, 0.0141, 0.019, 0.0252,
0.0294, 0.0327, 0.0415, 0.0471,
0.0513, 0.0544, 0.0567, 0.0584,
0.0594, 0.06, 0.0601, 0.0598,
0.059, 0.0577, 0.0559, 0.0537,
0.0508, 0.0472, 0.0428, 0.0376,
0.0316, 0.0248, 0.0172, 0.0088,
-0.0007, -0.0117,
YLOWER= 0.0, -0.0092, -0.0141, -0.019, -0.0252,
-0.0294, -0.0327, -0.0414, -0.0472,
-0.0514, -0.0546, -0.0569, -0.0585,
-0.0595, -0.0598, -0.0596, -0.0586,
-0.0567, -0.0537, -0.0496, -0.0443,
-0.0382, -0.0315, -0.0244, -0.0174,
-0.011, -0.0059, -0.0035, -0.0041,
-0.0087, -0.0177$
$WGPLNF CHRDR=23.09,CHRDTP=10.21,SSPN=108.23,SSPNE=97.41,
  SAVSI=28.66,CHSTAT=0.0,TWISTA=-4.5,DHDADI=-1.0,TYPE=1.0$
$HTSCHR TYPEIN=1.0, NPTS=31.0,
XCORD= 0.0, 0.002, 0.005, 0.01, 0.02, 0.03, 0.04,
0.08, 0.12, 0.16, 0.2, 0.24, 0.28,
0.32, 0.36, 0.4, 0.44, 0.48, 0.52,
0.56, 0.6, 0.64, 0.68, 0.72, 0.76,
0.8, 0.84, 0.88, 0.92, 0.96, 1.,
YUPPER= 0.0, 0.0076, 0.0116, 0.0155, 0.0206,
0.0241, 0.0268, 0.0341, 0.0389,
0.0425, 0.0451, 0.047, 0.0484,
0.0493, 0.0498, 0.05, 0.0498,
0.0492, 0.0483, 0.047, 0.0453,
0.0432, 0.0405, 0.0372, 0.0332,
0.0285, 0.0231, 0.0169, 0.0101,
0.0025, -0.0067,
YLOWER= 0.0, -0.0076, -0.0116, -0.0155, -0.0206,
-0.0241, -0.0268, -0.0341, -0.039,
-0.0426, -0.0452, -0.0472, -0.0486,
-0.0495, -0.0498, -0.0496, -0.0489,
-0.0475, -0.0453, -0.0422, -0.0378,
-0.0327, -0.0269, -0.0206, -0.0142,
-0.0081, -0.0035, -0.0007, -0.0007,
-0.0042, -0.0116$
$HTPLNF CHRDR=10.93,CHRDTP=3.8,SSPN=38.33,SSPNE=34.5,
  SAVSI=31.38,CHSTAT=0.25,TWISTA=-2.0,DHDADI=-1.0,TYPE=1.0$
NACA-V-4-0009
$VTPLNF CHRDR=16.96,CHRDTP=10.95,SSPN=18.14,SSPNE=16.33,
  SAVSI=50.67,CHSTAT=0.0,TYPE=1.0$
DAMP
NEXT CASE
```

1 THE FOLLOWING IS A LIST OF ALL INPUT CARDS FOR THIS CASE.
0

CASEID CERES

```
$FLTCON NMACH=2.0,MACH(1)=0.2,0.6$
$FLTCON NALT=2.0,ALT(1)=0.0,65617.0$
$FLTCON NALPHA=9.0,ALSCHD=-4.0,-2.0,0.0,2.0,4.0,6.0,8.0,10.0,12.0,
  GAMMA=0.0,WT=133762.59,LOOP=1.0$
$OPTINS SREF=3604.47,CBARR=17.48,BLREF=216.46$
$SYNTHS XCG=109.03,ZCG=2.77,XW=81.71,ZW=6.93,ALIW=0.0,XH=211.41,
  ZH=25.07,ALIH=0.0,XV=189.27,ZV=6.93,VERTUP=.TRUE.$
$BODY NX=4.0,ITYPE=1.0,
  X=0.,22.92,59.6,206.22,
  ZU=0.,6.93,6.93,6.93,
  ZL=0.,-6.93,-6.93,6.6,
  S=0.,264.11,264.11,0.34,
  P=0.,76.21,76.21,2.06,
  R=0.,12.13,12.13,0.33$
$WGSCHR TYPEIN=1.0, NPTS=31.0,
XCORD= 0.0, 0.002, 0.005, 0.01, 0.02, 0.03, 0.04,
0.08, 0.12, 0.16, 0.2, 0.24, 0.28,
0.32, 0.36, 0.4, 0.44, 0.48, 0.52,
0.56, 0.6, 0.64, 0.68, 0.72, 0.76,
0.8, 0.84, 0.88, 0.92, 0.96, 1.,
YUPPER= 0.0, 0.0092, 0.0141, 0.019, 0.0252,
0.0294, 0.0327, 0.0415, 0.0471,
0.0513, 0.0544, 0.0567, 0.0584,
0.0594, 0.06, 0.0601, 0.0598,
0.059, 0.0577, 0.0559, 0.0537,
0.0508, 0.0472, 0.0428, 0.0376,
0.0316, 0.0248, 0.0172, 0.0088,
```

```

-0.0007, -0.0117,
YLOWER= 0.0, -0.0092, -0.0141, -0.019, -0.0252,
-0.0294, -0.0327, -0.0414, -0.0472,
-0.0514, -0.0546, -0.0569, -0.0585,
-0.0595, -0.0598, -0.0596, -0.0586,
-0.0567, -0.0537, -0.0496, -0.0443,
-0.0382, -0.0315, -0.0244, -0.0174,
-0.011, -0.0059, -0.0035, -0.0041,
-0.0087, -0.0177$
$WGPLNF CHRDR=23.09,CHRTP=10.21,SSPN=108.23,SSPNE=97.41,
SAVSI=28.66,CHSTAT=0.0,TWISTA=-4.5,DHDADI=-1.0,TYPE=1.0$
$HTSCHR TYPEIN=1.0, NPTS=31.0,
XCORD= 0.0, 0.002, 0.005, 0.01, 0.02, 0.03, 0.04,
0.08, 0.12, 0.16, 0.2, 0.24, 0.28,
0.32, 0.36, 0.4, 0.44, 0.48, 0.52,
0.56, 0.6, 0.64, 0.68, 0.72, 0.76,
0.8, 0.84, 0.88, 0.92, 0.96, 1.,
YUPPER= 0.0, 0.0076, 0.0116, 0.0155, 0.0206,
0.0241, 0.0268, 0.0341, 0.0389,
0.0425, 0.0451, 0.047, 0.0484,
0.0493, 0.0498, 0.05, 0.0498,
0.0492, 0.0483, 0.047, 0.0453,
0.0432, 0.0405, 0.0372, 0.0332,
0.0285, 0.0231, 0.0169, 0.0101,
0.0025, -0.0067,
YLOWER= 0.0, -0.0076, -0.0116, -0.0155, -0.0206,
-0.0241, -0.0268, -0.0341, -0.039,
-0.0426, -0.0452, -0.0472, -0.0486,
-0.0495, -0.0498, -0.0496, -0.0489,
-0.0475, -0.0453, -0.0422, -0.0378,
-0.0327, -0.0269, -0.0206, -0.0142,
-0.0081, -0.0035, -0.0007, -0.0007,
-0.0042, -0.0116$
$HTPLNF CHRDR=10.93,CHRTP=3.8,SSPN=38.33,SSPNE=34.5,
SAVSI=31.38,CHSTAT=0.25,TWISTA=-2.0,DHDADI=-1.0,TYPE=1.0$
NACA-V-4-0009
$VTPLNF CHRDR=16.96,CHRTP=10.95,SSPN=18.14,SSPNE=16.33,
SAVSI=50.67,CHSTAT=0.0,TYPE=1.0$
DAMP
NEXT CASE
0 INPUT DIMENSIONS ARE IN FT, SCALE FACTOR IS 1.0000

```

1 AUTOMATED STABILITY AND CONTROL METHODS PER APRIL 1976 VERSION OF DATCOM
USER DEFINED WING SECTION

UPPER ABCISSA	UPPER ORDINATE	LOWER ABCISSA	LOWER ORDINATE	X-FRACTION CHORD	MEAN LINE	THICKNESS
0.00000	0.00000	0.00000	0.00000	0.00000	0.00000	0.00000
0.00200	0.00920	0.00200	-0.00920	0.00200	0.00000	0.01840
0.00500	0.01410	0.00500	-0.01410	0.00500	0.00000	0.02820
0.01000	0.01900	0.01000	-0.01900	0.01000	0.00000	0.03800
0.02000	0.02520	0.02000	-0.02520	0.02000	0.00000	0.05040
0.03000	0.02940	0.03000	-0.02940	0.03000	0.00000	0.05880
0.03999	0.03270	0.04001	-0.03270	0.04000	0.00000	0.06540
0.08003	0.04150	0.07997	-0.04140	0.08000	0.00005	0.08290
0.12006	0.04710	0.11994	-0.04720	0.12000	-0.00005	0.09430
0.16003	0.05130	0.15997	-0.05140	0.16000	-0.00005	0.10270
0.20003	0.05440	0.19997	-0.05460	0.20000	-0.00010	0.10900
0.23996	0.05670	0.24004	-0.05690	0.24000	-0.00010	0.11360
0.27996	0.05840	0.28004	-0.05850	0.28000	-0.00005	0.11690
0.31989	0.05940	0.32011	-0.05950	0.32000	-0.00005	0.11890
0.35978	0.06000	0.36022	-0.05980	0.36000	0.00010	0.11980
0.39963	0.06010	0.40037	-0.05960	0.40000	0.00025	0.11970
0.43933	0.05980	0.44067	-0.05860	0.44000	0.00060	0.11840
0.47899	0.05899	0.48101	-0.05669	0.48000	0.00115	0.11570
0.51861	0.05768	0.52139	-0.05368	0.52000	0.00200	0.11140
0.55822	0.05587	0.56178	-0.04957	0.56000	0.00315	0.10550
0.59807	0.05366	0.60193	-0.04426	0.60000	0.00470	0.09800
0.63825	0.05077	0.64175	-0.03817	0.64000	0.00630	0.08900
0.67857	0.04717	0.68143	-0.03147	0.68000	0.00785	0.07870
0.71906	0.04279	0.72094	-0.02439	0.72000	0.00920	0.06720
0.75962	0.03760	0.76038	-0.01740	0.76000	0.01010	0.05500
0.80017	0.03160	0.79983	-0.01100	0.80000	0.01030	0.04260
0.84066	0.02479	0.83934	-0.00589	0.84000	0.00945	0.03070
0.88091	0.01716	0.87909	-0.00346	0.88000	0.00685	0.02070
0.92092	0.00873	0.91908	-0.00403	0.92000	0.00235	0.01290
0.96012	-0.00070	0.95988	-0.00870	0.96000	-0.00470	0.00800
1.00000	0.00000	1.00000	0.00000	1.00000	0.00000	0.00000

```

1 AUTOMATED STABILITY AND CONTROL METHODS PER APRIL 1976 VERSION OF DATCOM
WING SECTION DEFINITION
0 IDEAL ANGLE OF ATTACK = 0.62873 DEG.
ZERO LIFT ANGLE OF ATTACK = 0.97322 DEG.
IDEAL LIFT COEFFICIENT = -0.05182
ZERO LIFT PITCHING MOMENT COEFFICIENT = 0.02302
MACH ZERO LIFT-CURVE-SLOPE = 0.10374 /DEG.
LEADING EDGE RADIUS = 0.02216 FRACTION CHORD
MAXIMUM AIRFOIL THICKNESS = 0.11980 FRACTION CHORD
DELTA-Y = 3.01750 PERCENT CHORD

```

```

0 MACH= 0.2000 LIFT-CURVE-SLOPE = 0.10544 /DEG. XAC = 0.25409
0 MACH= 0.6000 LIFT-CURVE-SLOPE = 0.12467 /DEG. XAC = 0.25814
1 AUTOMATED STABILITY AND CONTROL METHODS PER APRIL 1976 VERSION OF DATCOM
USER DEFINED HORIZONTAL TAIL SECTION
UPPER ABCISSA UPPER ORDINATE LOWER ABCISSA LOWER ORDINATE X-FRACTION CHORD MEAN LINE THICKNESS
0.00000 0.00000 0.00000 0.00000 0.00000 0.00000 0.00000
0.00200 0.00760 0.00200 -0.00760 0.00200 0.00000 0.01520
0.00500 0.01160 0.00500 -0.01160 0.00500 0.00000 0.02320

```

0.01000	0.01550	0.01000	-0.01550	0.01000	0.00000	0.03100
0.02000	0.02060	0.02000	-0.02060	0.02000	0.00000	0.04120
0.03000	0.02410	0.03000	-0.02410	0.03000	0.00000	0.04820
0.04000	0.02680	0.04000	-0.02680	0.04000	0.00000	0.05360
0.08002	0.03410	0.07998	-0.03410	0.08000	0.00000	0.06820
0.12002	0.03890	0.11998	-0.03900	0.12000	-0.00005	0.07790
0.16000	0.04250	0.16000	-0.04260	0.16000	-0.00005	0.08510
0.20003	0.04510	0.19997	-0.04520	0.20000	-0.00005	0.09030
0.24003	0.04700	0.23997	-0.04720	0.24000	-0.00010	0.09420
0.28000	0.04840	0.28000	-0.04860	0.28000	-0.00010	0.09700
0.31994	0.04930	0.32006	-0.04950	0.32000	-0.00010	0.09880
0.35981	0.04980	0.36019	-0.04980	0.36000	0.00000	0.09960
0.39972	0.05000	0.40028	-0.04960	0.40000	0.00020	0.09960
0.43960	0.04980	0.44040	-0.04890	0.44000	0.00045	0.09870
0.47937	0.04920	0.48063	-0.04750	0.48000	0.00085	0.09670
0.51909	0.04829	0.52091	-0.04529	0.52000	0.00150	0.09360
0.55875	0.04698	0.56125	-0.04218	0.56000	0.00240	0.08920
0.59852	0.04527	0.60148	-0.03777	0.60000	0.00375	0.08310
0.63855	0.04317	0.64145	-0.03267	0.64000	0.00525	0.07590
0.67872	0.04048	0.68128	-0.02888	0.68000	0.00680	0.06740
0.71903	0.03718	0.72097	-0.02058	0.72000	0.00830	0.05780
0.75944	0.03319	0.76056	-0.01419	0.76000	0.00950	0.04740
0.79933	0.02850	0.80007	-0.00810	0.80000	0.01020	0.03660
0.84035	0.02310	0.83965	-0.00350	0.84000	0.00980	0.02660
0.88056	0.01688	0.87944	-0.00068	0.88000	0.00810	0.01760
0.92060	0.01007	0.91940	-0.00067	0.92000	0.00470	0.01080
0.96020	0.00249	0.95980	-0.00419	0.96000	-0.00085	0.00670
1.00000	0.00000	1.00000	0.00000	1.00000	0.00000	0.00000

1 AUTOMATED STABILITY AND CONTROL METHODS PER APRIL 1976 VERSION OF DATCOM
HORIZONTAL TAIL SECTION DEFINITION

0 IDEAL ANGLE OF ATTACK = 0.00385 DEG.
ZERO LIFT ANGLE OF ATTACK = -0.15924 DEG.
IDEAL LIFT COEFFICIENT = 0.01788
ZERO LIFT PITCHING MOMENT COEFFICIENT = -0.01197
MACH ZERO LIFT-CURVE-SLOPE = 0.10378 /DEG.
LEADING EDGE RADIUS = 0.01544 FRACTION CHORD
MAXIMUM AIRFOIL THICKNESS = 0.09960 FRACTION CHORD
DELTA-Y = 2.47500 PERCENT CHORD

0 MACH= 0.2000 LIFT-CURVE-SLOPE = 0.10559 /DEG. XAC = 0.25395
0 MACH= 0.6000 LIFT-CURVE-SLOPE = 0.12588 /DEG. XAC = 0.25703

1 AUTOMATED STABILITY AND CONTROL METHODS PER APRIL 1976 VERSION OF DATCOM
VERTICAL TAIL SECTION DEFINITION

0 IDEAL ANGLE OF ATTACK = 0.00000 DEG.
ZERO LIFT ANGLE OF ATTACK = 0.00000 DEG.
IDEAL LIFT COEFFICIENT = 0.00000
ZERO LIFT PITCHING MOMENT COEFFICIENT = 0.00000
MACH ZERO LIFT-CURVE-SLOPE = 0.09830 /DEG.
LEADING EDGE RADIUS = 0.00893 FRACTION CHORD
MAXIMUM AIRFOIL THICKNESS = 0.09000 FRACTION CHORD
DELTA-Y = 2.37673 PERCENT CHORD

0 MACH= 0.2000 LIFT-CURVE-SLOPE = 0.10007 /DEG. XAC = 0.25672
0 MACH= 0.6000 LIFT-CURVE-SLOPE = 0.12012 /DEG. XAC = 0.25923

1 AUTOMATED STABILITY AND CONTROL METHODS PER APRIL 1976 VERSION OF DATCOM
CHARACTERISTICS AT ANGLE OF ATTACK AND IN SIDESLIP
WING-BODY-VERTICAL TAIL-HORIZONTAL TAIL CONFIGURATION
CERES

FLIGHT CONDITIONS						REFERENCE DIMENSIONS						
MACH NUMBER	ALTITUDE FT	VELOCITY FT/SEC	PRESSURE LB/FT**2	TEMPERATURE DEG R	REYNOLDS NUMBER 1/FT	REF. AREA FT**2	REFERENCE LENGTH FT	REFERENCE LENGTH LAT. FT	MOMENT FT	REF. CENTER FT		
0	0.200	0.00	223.27	2.1162E+03	518.670	1.4136E+06	3604.470	17.480	216.460	109.030	2.770	
0	ALPHA	CD	CL	CM	CN	CA	XCP	CLA	CMA	CYB	CNB	CLB
0	-4.0	0.024	-0.613	0.3265	-0.613	-0.019	-0.532	9.166E-02	-5.851E-02	-8.700E-03	4.188E-04	1.475E-03
0	-2.0	0.018	-0.428	0.2088	-0.428	0.003	-0.487	9.425E-02	-6.030E-02			9.986E-04
0	0.0	0.014	-0.236	0.0853	-0.236	0.014	-0.361	9.691E-02	-6.254E-02			5.030E-04
0	2.0	0.013	-0.040	-0.0414	-0.040	0.014	1.041	9.807E-02	-6.252E-02			-5.585E-06
0	4.0	0.014	0.156	-0.1647	0.157	0.003	-1.051	9.690E-02	-5.993E-02			-5.173E-04
0	6.0	0.018	0.347	-0.2811	0.347	-0.019	-0.809	9.381E-02	-5.656E-02			-1.017E-03
0	8.0	0.024	0.531	-0.3910	0.529	-0.050	-0.738	8.913E-02	-4.915E-02			-1.497E-03
0	10.0	0.031	0.704	-0.4777	0.699	-0.091	-0.684	8.450E-02	-4.881E-02			-1.953E-03
0	12.0	0.041	0.869	-0.5862	0.859	-0.141	-0.683	8.099E-02	-5.971E-02			-2.379E-03
0				ALPHA	Q/QINF	EPSLON	D(EPSLON)/D(ALPHA)					
0				-4.0	1.000	-1.536	0.213					
0				-2.0	1.000	-1.111	0.219					
0				0.0	1.000	-0.660	0.231					
0				2.0	1.000	-0.187	0.241					
0				4.0	1.000	0.304	0.246					
0				6.0	1.000	0.798	0.246					
0				8.0	1.000	1.287	0.244					
0				10.0	0.975	1.772	0.240					
0				12.0	1.000	2.249	0.238					

1

AUTOMATED STABILITY AND CONTROL METHODS PER APRIL 1976 VERSION OF DATCOM
 DYNAMIC DERIVATIVES
 WING-BODY-VERTICAL TAIL-HORIZONTAL TAIL CONFIGURATION
 CERES

MACH NUMBER	FLIGHT CONDITIONS				TEMPERATURE DEG R	REYNOLDS NUMBER 1/FT	REFERENCE DIMENSIONS				
	ALTITUDE FT	VELOCITY FT/SEC	PRESSURE LB/FT**2				REF. AREA FT**2	REFERENCE LENGTH FT	LAT. FT	HORIZ FT	MOMENT REF. FT
0.200	0.00	223.27	2.1162E+03		518.670	1.4136E+06	3604.470	17.480	216.460	109.030	2.770
DYNAMIC DERIVATIVES (PER DEGREE)											
ALPHA	PITCHING			ACCELERATION			ROLLING			YAWING	
	CLQ	CMQ		CLAD	CMAD	CLP	CYP	CNP	CNR	CLR	
-4.00	2.813E-01	-1.645E+00		3.557E-02	-2.368E-01	-7.757E-03	-1.275E-03	1.081E-03	-8.399E-04	-3.044E-03	
-2.00				3.661E-02	-2.438E-01	-8.039E-03	-7.566E-04	7.369E-04	-8.633E-04	-2.263E-03	
0.00				3.861E-02	-2.571E-01	-8.281E-03	-2.193E-04	3.793E-04	-8.804E-04	-1.451E-03	
2.00				4.027E-02	-2.681E-01	-8.414E-03	3.284E-04	1.620E-05	-8.906E-04	-6.175E-04	
4.00				4.112E-02	-2.738E-01	-8.358E-03	8.800E-04	-3.491E-04	-8.935E-04	2.231E-04	
6.00				4.110E-02	-2.736E-01	-8.131E-03	1.422E-03	-7.090E-04	-8.894E-04	1.045E-03	
8.00				4.073E-02	-2.712E-01	-7.815E-03	1.951E-03	-1.061E-03	-8.787E-04	1.837E-03	
10.00				3.916E-02	-2.607E-01	-7.429E-03	2.461E-03	-1.404E-03	-8.621E-04	2.591E-03	
12.00				3.980E-02	-2.650E-01	-7.018E-03	2.946E-03	-1.729E-03	-8.403E-04	3.299E-03	

0*** VEHICLE WEIGHT = 133762.59 LB.

0*** LEVEL FLIGHT LIFT COEFFICIENT = 0.62628

1

AUTOMATED STABILITY AND CONTROL METHODS PER APRIL 1976 VERSION OF DATCOM
 CHARACTERISTICS AT ANGLE OF ATTACK AND IN SIDESLIP
 WING-BODY-VERTICAL TAIL-HORIZONTAL TAIL CONFIGURATION
 CERES

MACH NUMBER	FLIGHT CONDITIONS				TEMPERATURE DEG R	REYNOLDS NUMBER 1/FT	REFERENCE DIMENSIONS				
	ALTITUDE FT	VELOCITY FT/SEC	PRESSURE LB/FT**2				REF. AREA FT**2	REFERENCE LENGTH FT	LAT. FT	HORIZ FT	MOMENT REF. FT
0.600	65617.00	580.78	1.1548E+02		389.970	3.3591E+05	3604.470	17.480	216.460	109.030	2.770
DERIVATIVE (PER DEGREE)											
ALPHA	CD	CL	CM	CN	CA	XCP	CLA	DERIVATIVE			CLB
								CMA	CYB	CNB	
-4.0	0.030	-0.650	0.3610	-0.650	-0.016	-0.555	9.097E-02	-6.445E-02	-8.796E-03	5.275E-04	1.996E-03
-2.0	0.023	-0.462	0.2336	-0.462	0.007	-0.505	9.778E-02	-6.586E-02			1.407E-03
0.0	0.019	-0.258	0.0975	-0.258	0.019	-0.377	1.041E-01	-6.904E-02			7.613E-04
2.0	0.017	-0.045	-0.0426	-0.045	0.019	0.953	1.070E-01	-6.849E-02			7.890E-05
4.0	0.019	0.170	-0.1764	0.171	0.007	-1.034	1.053E-01	-6.437E-02			-6.136E-04
6.0	0.023	0.376	-0.3000	0.376	-0.017	-0.797	9.968E-02	-5.943E-02			-1.279E-03
8.0	0.029	0.568	-0.4141	0.567	-0.050	-0.730	9.129E-02	-4.954E-02			-1.897E-03
10.0	0.037	0.741	-0.4982	0.736	-0.092	-0.677	8.081E-02	-4.680E-02			-2.459E-03
12.0	0.047	0.892	-0.6013	0.882	-0.140	-0.682	6.963E-02	-5.633E-02			-2.927E-03

0

0

ALPHA	Q/QINF	EPSLON	D(EPSLON)/D(ALPHA)
-4.0	1.000	-1.616	0.217
-2.0	1.000	-1.181	0.227
0.0	1.000	-0.710	0.245
2.0	1.000	-0.202	0.260
4.0	1.000	0.330	0.266
6.0	1.000	0.860	0.260
8.0	1.000	1.369	0.249
10.0	0.971	1.857	0.234
12.0	1.000	2.304	0.223

1

AUTOMATED STABILITY AND CONTROL METHODS PER APRIL 1976 VERSION OF DATCOM
 DYNAMIC DERIVATIVES
 WING-BODY-VERTICAL TAIL-HORIZONTAL TAIL CONFIGURATION
 CERES

MACH NUMBER	FLIGHT CONDITIONS				TEMPERATURE DEG R	REYNOLDS NUMBER 1/FT	REFERENCE DIMENSIONS				
	ALTITUDE FT	VELOCITY FT/SEC	PRESSURE LB/FT**2				REF. AREA FT**2	REFERENCE LENGTH FT	LAT. FT	HORIZ FT	MOMENT REF. FT
0.600	65617.00	580.78	1.1548E+02		389.970	3.3591E+05	3604.470	17.480	216.460	109.030	2.770
DYNAMIC DERIVATIVES (PER DEGREE)											
ALPHA	PITCHING			ACCELERATION			ROLLING			YAWING	
	CLQ	CMQ		CLAD	CMAD	CLP	CYP	CNP	CNR	CLR	
-4.00	3.101E-01	-1.769E+00		4.002E-02	-2.666E-01	-7.884E-03	-1.274E-03	1.113E-03	-8.780E-04	-3.661E-03	
-2.00				4.173E-02	-2.779E-01	-8.632E-03	-7.587E-04	7.717E-04	-9.033E-04	-2.754E-03	
0.00				4.507E-02	-3.001E-01	-9.257E-03	-1.998E-04	4.009E-04	-9.224E-04	-1.759E-03	
2.00				4.785E-02	-3.187E-01	-9.591E-03	3.824E-04	1.900E-05	-9.337E-04	-7.050E-04	
4.00				4.889E-02	-3.256E-01	-9.501E-03	9.728E-04	-3.668E-04	-9.363E-04	3.687E-04	
6.00				4.782E-02	-3.185E-01	-9.018E-03	1.547E-03	-7.436E-04	-9.306E-04	1.402E-03	
8.00				4.587E-02	-3.055E-01	-8.335E-03	2.091E-03	-1.105E-03	-9.176E-04	2.364E-03	
10.00				4.175E-02	-2.781E-01	-7.353E-03	2.601E-03	-1.450E-03	-8.989E-04	3.237E-03	
12.00				4.114E-02	-2.740E-01	-6.133E-03	3.044E-03	-1.750E-03	-8.773E-04	3.968E-03	

0*** VEHICLE WEIGHT = 133762.59 LB.

0*** LEVEL FLIGHT LIFT COEFFICIENT = 1.27527

1

THE FOLLOWING IS A LIST OF ALL INPUT CARDS FOR THIS CASE.

0

1 END OF JOB.

Figure B.1: List of DATCOM Inputs and Outputs

C

Task Distribution

Table C.1: Task Distribution

Task	Item number	Group Member
Nomenclature		TH
Executive Overview	1	RT,TV
Introduction	2	TH
Mission Description	3	MB, RT
Requirements	4	NB
Sustainable Development Strategy	5	SL, TH
Functional Analysis	6	NK, SL
Market Analysis	7	MB, TV
Operations, Logistics Concept Description	8	NB, TV, TH, SL, MB, PD
Sensitivity Analysis	9	NB
Risk Assessment	10	AT, TV
Verification & Validation Procedures	11	NB, TH, NK
Concepts Trade Off	12	MB, JL, AT, NK
	13.1	TH, MB
Ceres Characterisation	13.2	NB, TH, RT, SL, NK
	13.3	NB, TV, PD
	13.4	NB, MB, RT, NK, AT
	13.5	PD,TH, TV
Ceres Characterisation	13.6	MB, AT, JL
	13.7	NB, RT, MB, TH, PD
	13.8	RT, JL
	13.9	PD, AT, JL
	13.10	MB, TH
Impact Assessment	14	TH, TV, SL, NK
Resource Allocation	15	NB, TH, PD
Reliability, Availability, Maintainability and Safety Analysis	16	NK, MB
Production Plan	17	AT
Project Design and Development Logic	18	NB, TH
Conclusion and Recommendations	19	PD, NB